THERMODYNAMIC MODEL FOR ASSOCIATING POLYMER SOLUTIONS

A Dissertation
Presented to
The Academic Faculty

By

Ibrahim Ali Ozkan

In Partial Fulfillment
Of the Requirements for the Degree
Doctor of Philosophy in Chemical and Biomolecular Engineering

Georgia Institute of Technology

July 2004

THERMODYNAMIC MODEL FOR ASSOCIATING POLYMER SOLUTIONS

Approved by:

Dr. Amyn S.Teja, Advisor

Dr. William J. Koros

Dr. Peter J. Ludovice

Dr. J. Carson Meredith

Dr. Thomas H. Sanders

Date Approved: 05 / 03 / 2004

ACKNOWLEDGEMENTS

I would like to express my deepest appreciation to my thesis advisor, Dr. Amyn S. Teja, for his wise guidance and advice throughout my years of graduate research. He is the most influential person behind my work, and I really appreciate him a lot for his assistance.

I would like to thank my parents, Vahdet and Fusun Ozkan, for their support and for being so patient and caring.

I would like to thank the members of my thesis committee for their input to my research: Dr. P.J. Ludovice, Dr. J.C. Meredith, Dr. W.J. Koros, and Dr. T. H. Sanders. Other research scientists to whom I am grateful are Dr. S. Michielsen, and Dr. J. Jones. I am especially thankful to Dr. Sun for the time and advice he has given me when I needed them.

I would like to express my gratitude to current and past graduate students, Dr. Linda Cote, Dr. Kim Abbett, Yalin Hao, Drs. Izumi and Shutaro Kurosawa, Chunbao Xu, Michael Beck, Kanrakot Thamanavat for the exchange of ideas and making it pleasurable to come to Bunger-Henry and ES&T. I would also like to thank several friends too numerous to name here who have made a social life and pleasurable.

Finally, I would like to express my deepest gratitude to my wife and best friend, Kerry Bullock-Ozkan, for sharing and enriching my life experiences for the past 3 years, and for her love, affection and support.

Support for this work is provided by School of Chemical and Biological Engineering at Georgia Institute of Technology and the Fluid Properties Research Institute.

TABLE OF CONTENTS

LIST OF FIGURES

LIST OF TABLES

LIST OF SYMBOLS

ΔG_m	Gibbs energy of mixing
v_m	Liquid molar volume of the mixture
Φ_i	Volume fraction of component i
δ_i	Solubility parameters of component i
n_i	mole number of component i
ΔH_m	Enthalpy of mixing
ΔG_m	Entropy of mixing
x_i	mole fraction of component *i*
r	average number of segments
z	lattice coordination number
χ	Interaction parameter between the solvent and solute
P	Pressure of the system
T	Temperature of the system
Q	partition function
k	Boltzmann's constant
v*	Characteristic volume
T*	Characteristic temperature
P*	Characteristic pressure
$\tilde{P}$	Reduced Pressure
$\tilde{v}$	Reduced Volume
$\tilde{T}$	Reduced Temperature
N	Number of molecules
R	Gas constant
Ω_i	Configuration of component i
Z_{comb}	Combinatorial factor
s	Number of intermolecular contact sites per segment
η	Constant characterizing the energy of interaction for a pair of neighboring sites
σ	"hard-sphere" radius
q	scaling factor for the hard-core cell volume in the free volume term
c	Segmental parameter
$\tilde{\rho}_i$	Reduced density of the component i
ρ_i *	Characteristic density of component i
ρ_i	Density of the component i
ε*	Interaction per segment
r	Number of segments on a polymer molecule
v*	Close-packed molecular volume of each segment
s	segmental chain length,
y	fraction of occupied sites

P	polymer segment
S	solvent
PS_μ	associated solvent-solute complex
μ	solute/solvent-binding ratio.
K	Equilibrium constant for association
α	Fraction of solute segments associated
x	number of segments in a polymer molecules
N_i	Number of molecules of component i
ν_i	Number of ways of arranging the i^{th} polymer molecule along with its associated solvent
Δu_i	Interaction energy of type i
T_0	Reference temperature
K_0	Reference equilibrium constant
u_{ij}	Energy of a particular ij pair
$g_{ij}(r)$	Pair correlation function at distance r
$n_{ij}(r)$	Number of ij kind of associated pairs at a distance r
r	Radius of first interaction shell.
δ^*_{solute}	Solubility parameter of solute in nonpolar analogue form
$\delta_{solvent}$	Solubility parameter of the solvent
ΔE_v	Enthalpy of vaporization
γ_i	Activity coefficient of component i
a_i	Activity of component i
μ_I	Chemical potential of component i
μ_i^0	Chemical potential of component i in pure form
α_i	polarizability of component i
μ_i	dipole moment of component i
Q_i	quadrupole moment of component i
r	distance between the molecules
$C_{1\text{-}5}$	fixed constants
$g_{ij}(r,T,\rho)$	radial distribution function,
A_0,A_1	constants
U_m	internal energy of a mixture
T_g	Glass transition temperature
ϕ_i	Fugacity coefficient of component i in the liquid phase
$\tilde{f}_i^j$	Fugacity of component i in the phase j
y_i	Mole fraction of the component i in the liquid phase
$\tilde{f}_i^{0j}$	Pure component fugacity of component i in the phase j
$\Delta_{fus}H_i$	Molar heat of fusion of component i
T_m	Melting temperature
ΔC_p	Molar heat capacity change
Δv_i	Molar volume change of component i
M_w	Molecular weight
ν	Band value on FT-IR Spectroscopy
b_m	“co-volume” or “excluded volume” of the mixture

a_m	"energy" or "attraction" constant of the mixture
b	"co-volume" or "excluded volume"
a	"energy" or "attraction" constant
Ω_a , Ω_b	Cubic EOS constants
Z	Compressibility
a_c	specific constant related to critical temperature and pressure
ω	Acentric factor
P^i_{vap}	Vapor pressure of component i
A_E	Molar excess Helmholtz energy
G_E	Molar excess Gibbs energy
k_{ij}	Interaction parameter between i-j pair
ζ_{ij},	Binary interaction parameter
w_i,	weight fraction of component i
C_i	molar concentration of component i
M_i	Molecular weight of the species
δ_{12}	Binary interaction parameter between component 1 and 2

Subscripts

c	*critical*
r	*reduced*
R	residual
C	combinatorial
1	solvent
2	solute
p	polymer
s	solvent
m	mixture
a	attraction
u	dispersion
cp	closed pack

SUMMARY

Polymer solutions in which there are strong specific interactions between the polymer and the solvent are of interest in a number of applications including drug delivery devices and biomembranes. Of particular interest are polymer solutions in which supercritical carbon dioxide (CO_2) is the solvent, because polymer processing with CO_2 is an important application of green chemistry. Unfortunately, experimental data on the phase behavior of polymer - CO_2 systems are relatively scarce, as are models that describe the phase behavior of such systems. The focus of this research is therefore on developing a thermodynamic model based on lattice theory for calculating phase behavior of polymer solutions with specific solute-solvent interactions at high pressures.

A new model, termed the LELAC (Lattice-based Extended Liquid Activity Coefficient) model is proposed based on the gART-L model of Sukhadia and Variankaval. The new model incorporates the compressibility effect at high pressures. The parameters of the model are (1) the equilibrium constant for association between a polymer segment and a solvent, (2) the specific interaction energy between a polymer segment and a solvent molecule, and (3) the dispersion interaction energy. The dispersion interaction energy is calculated using Regular Solution Theory and therefore depends on the pure component properties. One or both of the remaining parameters are obtained from independent measurements such as Fourier Transform Infra Red (FT-IR) spectra. Alternatively, the two parameters can be obtained by fitting data.

Cloud point curves of polymer - CO_2 systems have been successfully correlated (error of 1.3%) with the new model. Also, using fitted parameters from cloud point data, the sorption behavior of CO_2 in polymers has been predicted. The polymer investigated

include PBMA, PVAc and Polyacrylates. Comparison of cloud points with those obtained using the SAFT model revealed that the new model performs better than the SAFT model (3.6% error) with two adjustable parameters in each case. By contrast, the Sanchez-Lacombe equation of state is successful in correlating swelling behavior, but fails to adequately describe polymer solubilities in CO_2 even when its interaction parameter is allowed to vary with temperature.

The use of FT-IR spectroscopy to investigate interactions between CO_2 and a number of polymers has been investigated. The spectra confirm that complexes are formed between CO_2 and PMMA, PEMA, PBMA, PVMK, and PVAc. A complex of PVC and CO_2 is reported and a new mechanism involving a carbon – oxygen triple bond is postulated for this system.

CHAPTER 1

INTRODUCTION

Associating polymer solutions are an important class of systems in which strong specific interactions exist between the solvent and polymer molecules. These intermolecular interactions include dipole-dipole, acid-base, and hydrogen bonding interactions and lead to large deviations from ideal-solution behavior. In many cases, this results in liquid-liquid immiscibility at lower and/or upper critical solution temperatures.

The properties of associating polymer solutions have been exploited in drug delivery devices and bioactive sensors. Thus, aqueous solutions of poly (acrylamide), poly (ethylene glycol), poly (vinyl methyl ether) and polylactic acid, all of which associate with water, have been utilized in controlled-release drug delivery devices because temperature induced liquid-liquid phase separation facilitates the diffusion of drugs by increasing their diffusivity in such polymers. These devices are designed to inhibit severe medical conditions such as tumor-induced neovascularization (Langer, 1992).

Hydrogen bonding interactions are also responsible for the thermally reversible gelation of crosslinked poly (isopropylacrylamide)-water solutions that lead to unusual optical properties, in particular a visually perceptible color change. This phenomenon has been utilized in the production of “intelligent” colloidal crystals that act as bioactive sensors responding to a wide range of analytes, including viruses (Holtz and Asher, 1997).

Another example of the importance of specific strong interactions is in the application of polymeric membranes to the immunoisolation of islet cells (George and

Nair, 1999). The selective transport of insulin and glucose to albumin cells can be achieved using polymeric membranes produced from nonporous polyurethane. The transport depends to a large extent on the microstructure of the polymer, which in turn is dependent on the magnitude of specific interactions. It has been shown that insulin permeation is highly dependent on the degree of hydrogen bonding and hard segment content in nonporous polyurethane membranes (George and Nair, 1999).

As can be seen from the examples, an understanding of specific interactions and resulting liquid-liquid immiscibility is essential to the development and processing of many useful polymeric materials. Although there is considerable interest in the measurement of liquid-liquid behavior of associating polymer systems, experimental difficulties and lack of standardized techniques have resulted in very limited measurements related to the majority of systems of interest. Indeed, only a few partial phase diagrams have been published in the literature for polymer-solvent systems in general (Ehrlich, 1965; Zeman and Patterson, 1972). It is therefore important to develop models to correlate and extrapolate the limited amount of information that is available.

Thermodynamic models for the phase behavior of polymer solutions can be divided into two major classes: equation of state and activity coefficient models. Equation of state models take into account like-like molecular interactions in solution and manifest these properties in Pressure-Volume-Temperature (PVT) behavior. Mixture properties and unlike molecular interactions are accounted for by mixing rules. The best known examples of this class of models are the Sanchez-Lacombe equation of state (Sanchez and Lacombe, 1978) and the Statistical Associated Fluid Theory (SAFT) equation of state (Chapman *et al.,* 1990). These models have been successful in

incorporating the effect of pressure into the system. However, they either do not account for association or are too cumbersome to use, requiring a large number of parameters. Therefore, activity coefficient models are generally preferred when dealing with strongly associating systems. A few activity coefficient models such as the Painter- Coleman model (Painter *et al.*, 1990) have been successful in predicting phase behavior in strongly interacting systems, but these models do not account for the effect of pressure on phase behavior.

Associating polymer systems at high pressure are of recent interest because supercritical CO_2 has been proposed as an environmentally benign solvent for many polymer processes. Moreover, CO_2 has been known to exhibit specific interactions with a number of polymers (Kazarian *et al.,* 1996). Polymers are generally produced via solution processing techniques involving organic solvents that are toxic or otherwise environmentally harmful. There is therefore considerable interest in replacing these solvents with environmentally benign substances such as CO_2 (Liau and McHugh, 1985). Supercritical CO_2 is non-toxic, nonflammable, and offers higher mass transport rates than conventional solvents. There is also the possibility of *in situ* removal of small amounts of unreacted monomer and other impurities during processing. In addition, no separation steps are necessary after processing with supercritical CO_2, because the supercritical fluid dissipates upon depressurization. Finally, temperatures are generally lower than those employed in processes using conventional solvents. As a result, supercritical CO_2 has been employed as a solvent for polymerizations by a number of researchers (DeSimone *et al*., 1994; Pernecker and Kennedy, 1994). The phase behavior of polymer-supercritical

CO_2 solutions is therefore of interest in determining optimum conditions for these polymerization reactions.

As mentioned previously, some polymers are known to associate with supercritical CO_2 via Lewis acid-base interactions. A number of researchers have used spectroscopic methods to quantify such interactions (Kazarian *et al*., 1996). They have shown that CO_2 can participate in Lewis acid-base type interactions with polymers containing electron-donating groups. Such interactions increase the mobility of polymer segments and have a dramatic impact on the phase behavior of the solutions. Unfortunately, there are very few measurements of the phase behavior of associating polymer-CO_2 systems at high pressure. A need therefore exists for models that describe such phase behavior. The development of these models depends on an adequate description of non-idealities arising as a result of (1) size differences between the components in the solution, (2) molecular interactions due to association and dispersion. The effect of pressure on these interactions must also be considered when CO_2 is the solvent. Available models are generally able to describe size effects in polymer solutions. However, the effect of association is difficult to accommodate. Moreover, most of these models require a significant amount of experimental data for fitting parameters. Very few models can account for the effect of both pressure and specific interactions.

There are two basic types of approaches that can be followed in the development of models that account for both pressure and specific interactions. Equation of state models that take into consideration the effect of pressure can be modified to account for specific interactions. Alternatively, activity coefficient models that take into consideration specific interactions can be reformulated to incorporate the effect of

pressure. This work adopts the latter approach. In addition, an attempt is made to minimize the number of adjustable parameters in the model by making use of independent measurements such as FT-IR spectroscopy.

The organization of this thesis is as follows: the phase behavior of polymer solutions is reviewed in Chapter 2. Special attention is given to published models for the phase behavior of polymer solutions in Chapter 3. A new model is proposed for estimating the phase behavior of associating polymer solutions at high pressures in Chapter 4. This model is termed the Lattice-based Extended Liquid Activity Coefficient (LELAC) model. In Chapter 5, FT-IR spectroscopy is used to demonstrate the association between several polymers and supercritical CO_2 and to obtain the association parameter in the LELAC model. In Chapter 6, the LELAC model is applied to the calculation of solubility (cloud points) of polymers in supercritical CO_2. Also, the parameters fitted from the cloud point calculations are used to predict the sorption of CO_2 in the polymer. The estimation of swelling and solubility of polymers in supercritical CO_2 using the Sanchez-Lacombe Equation of State is described in Chapter 7. Conclusions and recommendations for future work are outlined in Chapter 8.

CHAPTER 2

PHASE DIAGRAMS OF BINARY MIXTURES OF SMALL AND LARGE MOLECULES

A brief overview of the phase behavior of binary solutions, with special emphasis on polymeric and associating systems, is given in the first section of this chapter. The next section describes the changes that occur in the phase behavior of polymer solutions when supercritical fluids, especially supercritical carbon dioxide (CO_2), are introduced into the system.

A proper description of phase behavior requires an understanding of the behavior of systems of small molecules. Therefore, it is convenient to begin the discussion with a review of phase behavior in binary systems of small molecules.

Phase Behavior of Binary Mixtures

Binary mixtures of small molecules exhibit a great variety of phase behavior. Scott and van Konynenburg (1970) and Van Pelt *et al.* (1991) have shown that all such behavior can be represented by eight types of phase diagrams, shown schematically in Figures 2- 1, 2- 2 and 2- 3. The following paragraphs will provide an explanation and examples of systems exhibiting these eight types of phase behavior. The behavior is described in terms of vapor-liquid critical loci and the loci of upper critical solution temperature (UCST) and lower critical solution temperature (LCST). All these phenomena (critical point, UCST, LCST) are characterized by temperatures, pressures, densities and compositions that are identical in two phases. The loci of UCST and LCST

may end at an upper critical end point (UCEP) or lower critical end point (LCEP) where a third, non-critical phase is in equilibrium with the two identical critical phases.

In order to understand the phase behavior of binary mixtures, it is necessary to become familiar with the definition of the terms of LCST, UCST and critical point. At a LCST, two liquid phases critically merge to form a single liquid phase as the system temperature is lowered. At a UCST, two liquids critically merge to form a single liquid phase as the system temperature is raised. At a critical point, two phases (vapor-liquid or two liquids) become indistinguishable in temperature, pressure, composition and density.

Type –I

Type–I systems are characterized by a continuous vapor-liquid critical curve from the critical point of the more volatile component to the critical point of the less volatile component. A continuous critical curve is obtained when the two components are of similar molecular size and their energies of interaction are similar, or when the components have critical properties of comparable magnitude (Rowlinson and Swinton, 1982). Two phases exist in the P-T region bounded by the critical mixture curve and the two pure component vapor pressure curves.

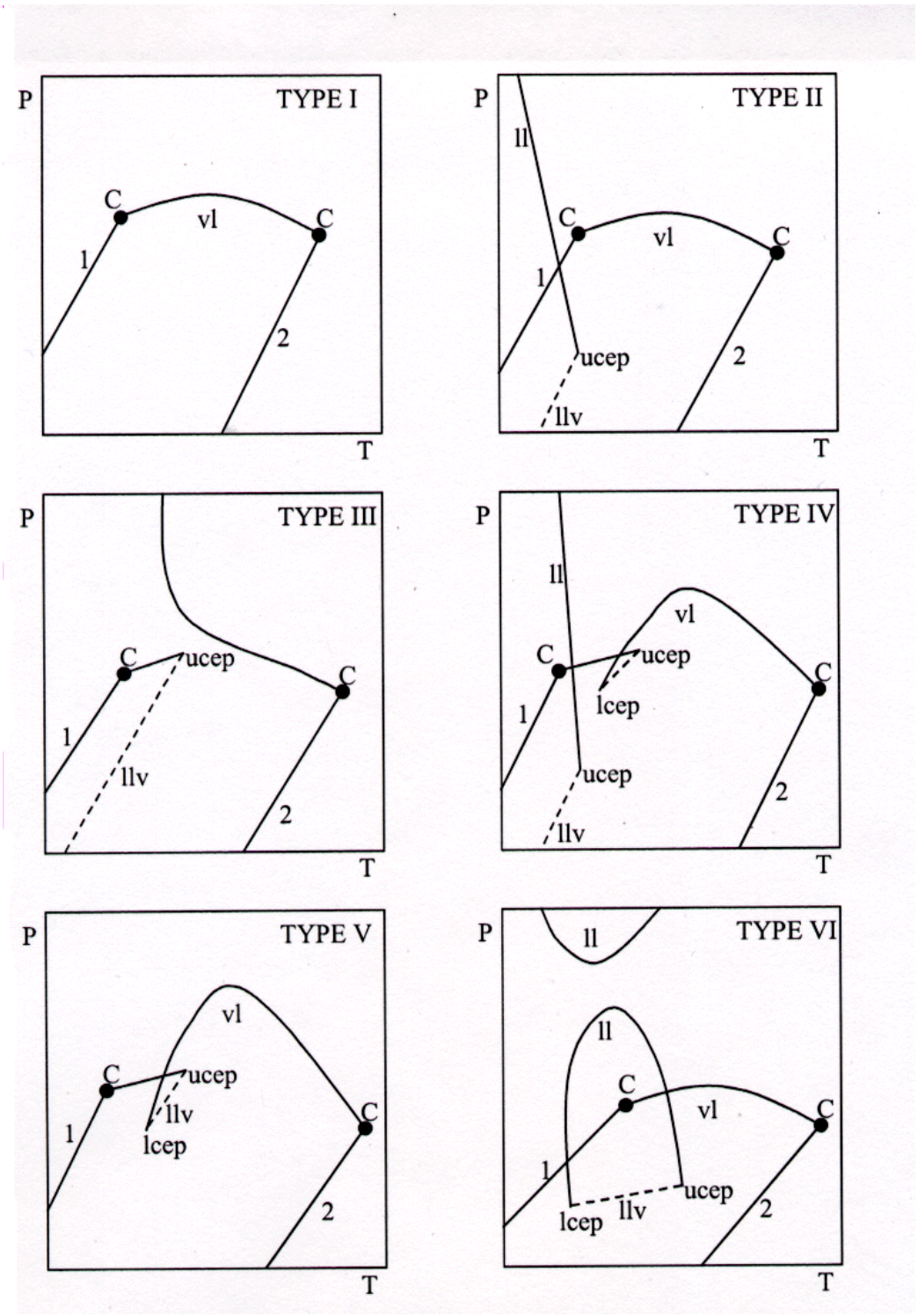

Figure 2-1 Classification of the six principal types of phase diagrams for binary mixtures. The lines denoted 1 and 2 are the vapor pressure curves of the two components. Points C are the pure component critical points of the two components. The remaining lines represent critical lines. Three phase equilibrium is denoted by a broken line.

It is important to remember that the behavior depicted in Figure 2- 1a is only one possible representation of a system with a continuous critical curve. Such curves can exhibit pressure minima or maxima with increasing temperature, or they can be essentially linear between the critical points of the components (Schneider, 1970). Critical azeotropy at some point along the curve is also possible. Numerous binary systems with type-I phase behavior have been reported in the literature, as discussed by Ng and Robinson (1978) and Van Pelt *et al*. (1991). Typical examples include methane / ethane, carbon dioxide / n-butane, and benzene / toluene.

Type-II

Type-II phase behavior is similar to Type-I in that the critical mixture curve is continuous between the critical points of the two pure components. However, there is also a liquid-liquid-vapor (LLV) line in the P-T diagram. The P-T locus of liquid-liquid critical points is termed a UCST line, and the line is generally very steep, indicating that liquid-liquid critical points are relatively insensitive to pressure. The carbon dioxide / n-octane system is an example of a binary mixture exhibiting this type of phase behavior (McHugh and Krukonis, 1994).

Type-III

Type-III phase behavior is shown in Figure 2- 1c. The distinguishing trait of this type is the occurrence of a LLV region located very close to the critical point of the more volatile component. The branch of the critical curve starting at the critical point of the less volatile component intersects the LLV line at the low temperature end, called the

lower critical end point. The other branch of the critical mixture curve, which starts at the critical point of the more volatile component, intersects the LLV line at the high-temperature end. At temperatures below the LCST, a region of LLV behavior appears similar to that found in type-II phase behavior (McHugh and Krukonis, 1994).

Type-III phase behavior is usually observed when the critical properties of the two components differ substantially. For binary mixtures comprised of normal hydrocarbons, type-III behavior occurs when the size difference between the components reaches a certain value. For example, LLV behavior near the critical point of methane occurs when the ratio of number of carbon atoms between methane and the second component exceeds 5.0; for binary ethane-hydrocarbon mixtures, LLV behavior occurs near the critical point of ethane when the ratio exceeds 9.5; for binary propane-hydrocarbon mixtures, LLV behavior occurs near the critical point of propane when the ratio exceeds 13.5 (Rowlinson and Swinton, 1982).

LLV behavior can also occur if the two species in the mixture differ considerably in the strength of their intermolecular potentials. In this case the occurrence of LLV behavior is an enthalpy driven process; examples are alcohol-supercritical fluid (SCF) mixtures where alcohol-alcohol hydrogen bonding interactions are much stronger than alcohol-SCF interactions (McHugh and Krukonis, 1994). Kuenen and Robson (1899) have presented a study of ethane-alcohol mixtures that provides insight into the trends observed in SCF-alcohol mixtures. They found that the solubility of an alcohol in a hydrocarbon solvent increases as the carbon number of the alcohol increases, or conversely, as the amount of alcohol-alcohol hydrogen bonding decreases. They showed that the temperature span of the LLV line is ~282 K for the ethane-ethanol system, ~276

K for the ethane-propanol system, and ~275 K for the ethane-butanol system. No LLV line is found in the ethane-isopentanol system. Other examples of type-III mixtures are the ethylene / n-propanol system and the ethylene/o-dichlorobenzene system, as discussed by Todd and Elgin (1955).

Type-IV

Type-IV phase behavior is shown in Figure 2- 1d. As the size and chemical nature of the mixture constituents become more dissimilar, the P-T trace of the UCST curve in type-III behavior shifts to higher temperatures, and the branch of the critical mixture curve that intersects the LLV line at the LCST shifts to lower temperatures. The two two-phase regions of the diagram now extend over wider ranges of temperature and pressure. Eventually, the UCST curve will superpose onto the critical mixture curve and give rise to a critical mixture curve which no longer intersects a region of LLV behavior, as shown in Figure 2-1d (McHugh and Krukonis, 1994).

It is not necessary for the critical mixture curve to exhibit a minimum in pressure. Many binary aqueous mixtures have critical mixture curves that start at the critical point of water with an initially negative slope, and then rise to higher pressures as the temperature decreases. These curves eventually reverse direction and show positive slopes at higher pressures (Yiling *et al.,* 1991). Examples of type-IV behavior include carbon dioxide / squalane (2,6,10,15,19,23- hexamethyltetracosane) system (Liphard and Schneider, 1975).

Type-V

Type-V behavior is shown in Figure 2- 1e. This type of phase behavior is very similar to type-III behavior. However, in type-V systems, there is no region of liquid-liquid immiscibility at temperatures below the LCST. The first branch of the critical line goes from the critical point of the first component to an UCST, but the second branch goes from the critical point of the second component to an LCST. Unlike type-IV systems, the liquids in type-V mixtures are completely miscible below the LCST. Two liquid phases exist only at temperatures between the UCST and LCST.

Mixtures of n-alkanes with large size differences show type-V phase behavior. While the binary methane / n-pentane system shows type-I phase behavior, type-V phase behavior occurs in the system methane / n-hexane. Type-V phase behavior is also found in binaries containing alcohols, exemplified by ethylene / methanol (Prausnitz *et al.,* 1986).

Type-VI

Binary mixtures showing type-VI phase behavior have two critical curves: one connects the critical points of the pure components while the other connects a UCST and a LCST. It is the presence of the LCST that distinguishes type-VI from type-II systems. A closed dome of immiscibility exists between the LCST and UCST. The two critical curves meet at an upper critical end point; at higher pressures two liquids are miscible. Examples of this complex behavior can be found in mixtures where one or both components associate or self-associate through hydrogen bonding, and include water / n-butanol and water / succinonitrile.

Type-VII and Type-VIII

Type VII behavior shown in Figure 2- 2, is similar to type V, but displays closed-loop immiscibility at low temperatures. Such behavior is thought to be caused by directional bonding between molecules such as hydrogen bonds in water / 2-butoxyethanol. Type-VIII behavior is shown in Figure 2- 3. This type of phase behavior has never been observed experimentally, but has been predicted using an equation of state. This behavior is similar to type-VI behavior with a closed dome of immiscibility and has been predicted to exist in the CF_4 / NH_3 system.

The above discussion of phase diagrams shows that systems in which there are large size differences between the components generally exhibit type-III or type-IV behavior unless there are strong interactions present, in which case type-VI or type VIII behavior may result.

Figure 2- 5 is an analog of Figure 2- 4, and shows the schematic P-T plot for a polymer-solvent mixture that has been observed in several polymer solutions such as Polystyrene (PS) in alkane solutions (Zeman and Patterson, 1972; McHugh and Guckes, 1985; McClellan and McHugh, 1985). Due to large differences in size between the components, many of the features of Figure 2- 1 are suppressed. A pure polymer does not have a critical point or a vapor pressure curve. Also, the high-temperature and low-temperature LLV lines in a polymer-solvent mixture superpose onto the vapor pressure curve of the pure solvent. UCST and LCST branches of the critical mixture curve are prominent on the phase diagram and are often referred to as cloud point curves (McHugh and Krukonis, 1994).

Figure 2- 6 shows a typical LCST cloud point behavior for a non-polar polymer, (polyisobutylene (PIB)), in a nonpolar hydrocarbon solvent (butane, pentane, or hexane) (Zeman and Patterson, 1972). The cloud point curve is shifted to higher temperatures (or the region of miscibility is increased), as the differences between the free volumes (related to the expansivity of the substance, or inversely, to its compressibility) of the solvent and PIB decrease with an increase in the molecular weight of the solvent.

Type-IV phase behavior is shown in Figure 2- 7. As mentioned previously, this behavior can occur when the disparity in the size and/or intermolecular potentials of the components becomes very large. In such cases, the temperature range between the UCST and the critical mixture curve becomes smaller and smaller. Eventually the difference in the properties of the components becomes so large that the UCST and the critical mixture curve merge into a single critical mixture curve (McHugh and Krukonis, 1994). Figure 2- 8 shows the transformed type-IV behavior for polymer-solvent systems (McHugh and Krukonis, 1994). The cloud point curve in Figure 2- 8 can be loosely interpreted as a combination of LCST-type transitions at higher temperatures and UCST-type transitions at lower temperatures.

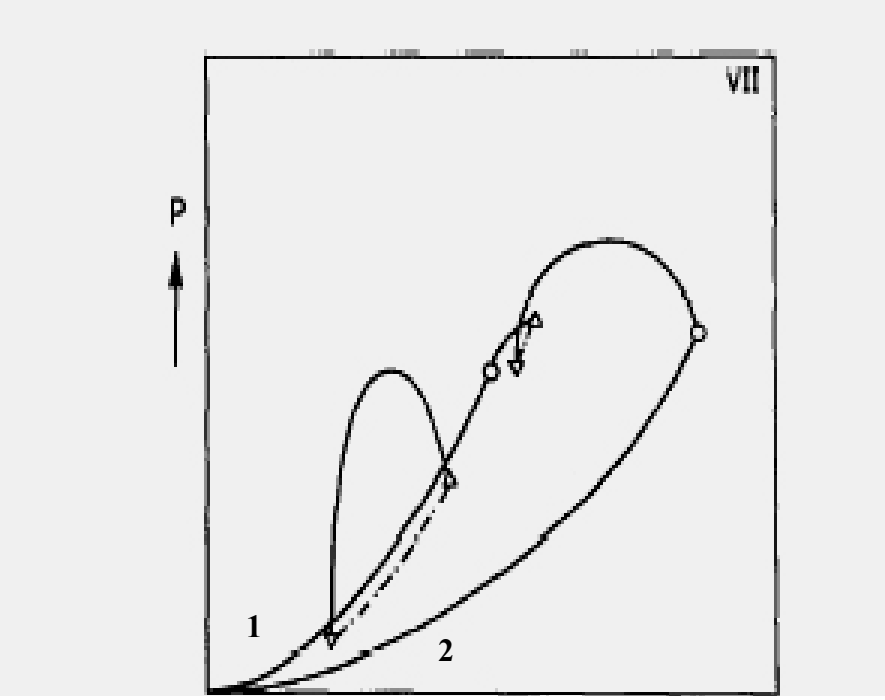

Figure 2-2 Pressure -Temperature projections for type VII mixtures. The hollow points are the pure component critical points of the two components. The lines denoted 1 and 2 are the vapor pressure curves of the two components. Three phase equilibrium is denoted by a broken line. Adapted from van Pelt *et al*., 1991.

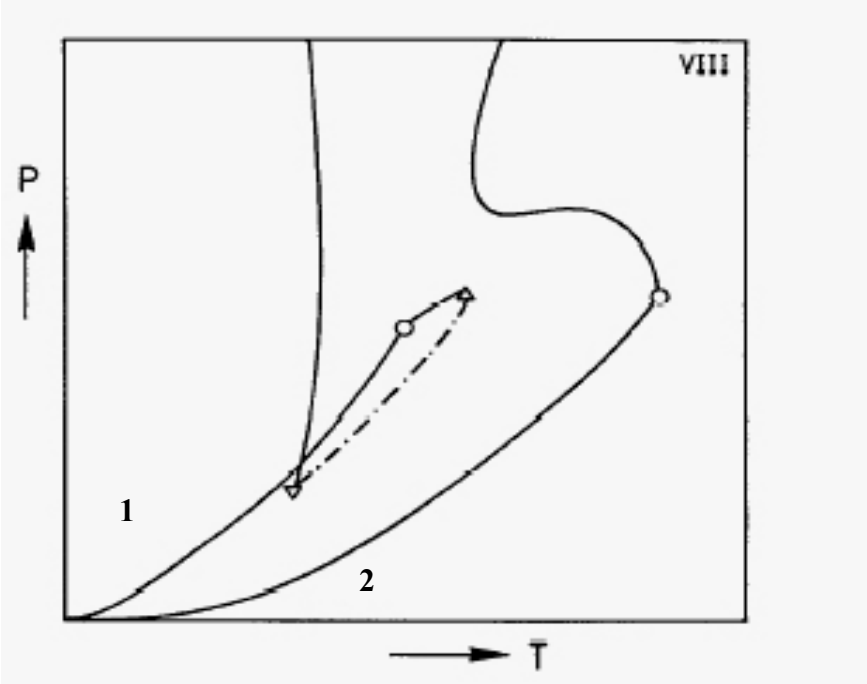

Figure 2-3 Pressure-Temperature projection for type VIII mixtures predicted with an equation of state. The hollow points are the pure component critical points of the two components. The lines denoted 1 and 2 are the vapor pressure curves of the two components. Three phase equilibrium is denoted by a broken line. Adapted from van Pelt *et al*., 1991.

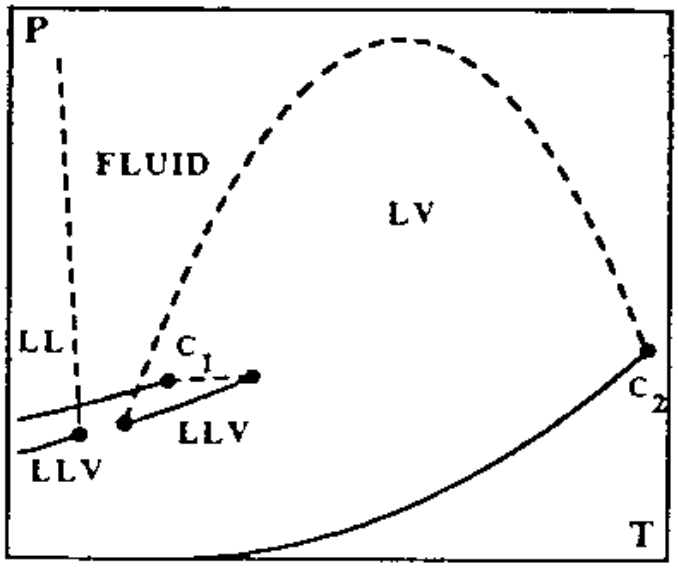

Figure 2-4 A type-III system for small molecules.

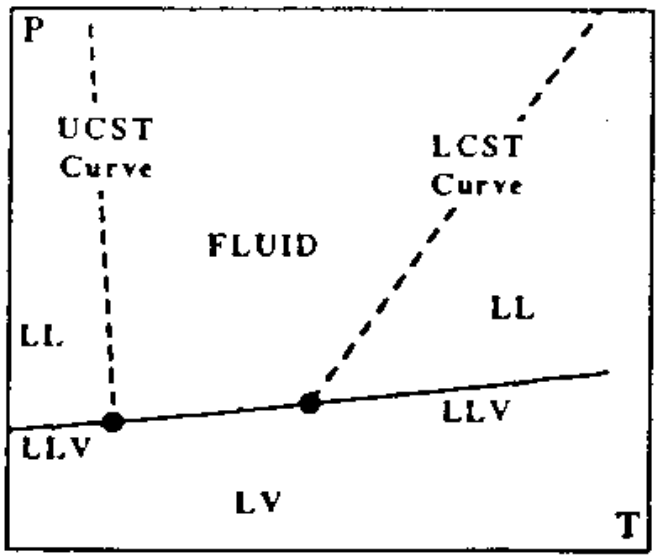

Figure 2-5 A polymer- solvent type-III system.

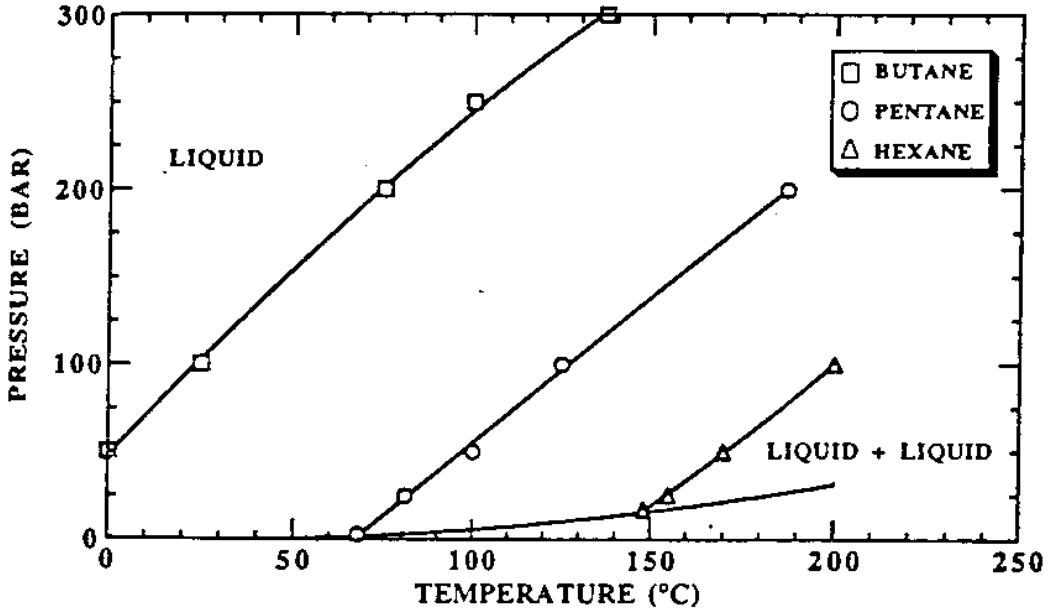

Figure 2-6 Effect of solvent quality on the location of the cloud point curve for PIB in butane, pentane, and hexane.

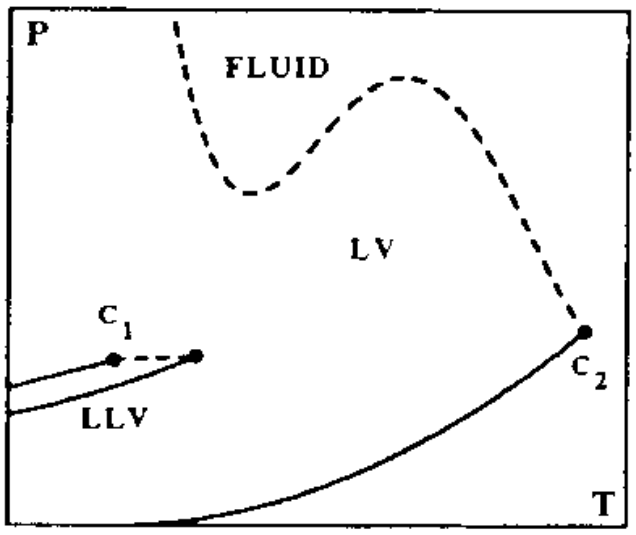

Figure 2-7 A type-IV system for small molecules.

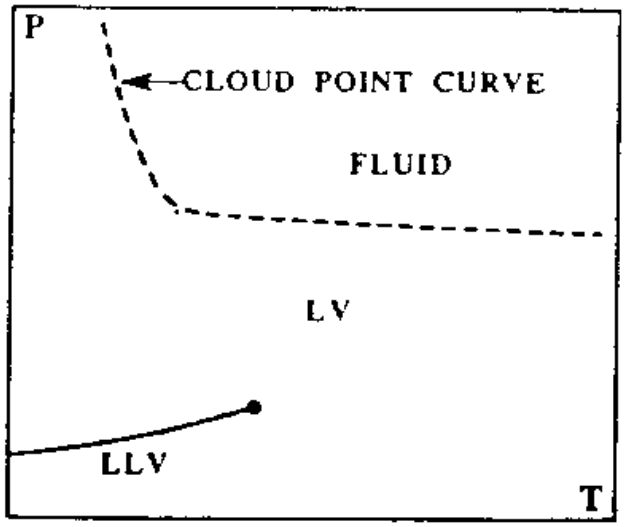

Figure 2- 8 A polymer-solvent type-IV system.

Phase Behavior of Polymer Solutions in Supercritical CO_2

Supercritical CO_2 has attracted a great deal of attention recently as a replacement for organic solvents in polymer processes. CO_2 is environmentally benign, inexpensive, nontoxic, non-flammable, fairly inert and has moderate critical temperature and pressure (T_c= 304.2 K, P_c=74 bar). Separation of supercritical CO_2 from a non-volatile substrate can be achieved simply by depressurizing the system, leaving no solvent residue at the end of the process. Relatively low temperatures can be used for CO_2 processing due to its critical properties. Also, the solvent strength of CO_2 can be easily changed by manipulating the system pressure and temperature or by adding a co-solvent, thus allowing processes to be easily "tuned". However, only a few polymers are soluble in CO_2. By contrast, CO_2 dissolves in many polymers and causes swelling and plasticization (glass transition temperature depression) of the polymer.

CO_2 is a good solvent for many non-polar (and some polar) molecules at low molecular weights (Hyatt, 1984). However, its dissolving power is limited for most high molecular weight polymers under readily achievable conditions (<400 K, <100 MPa). The only polymers that have good solubility in pure CO_2 under mild conditions are certain amorphous fluoropolymers and silicones (McHugh and Krukonis, 1994). The pressure and temperature needed to dissolve such polymers in CO_2 depends on solvent-solvent, solvent-segment, and segment-segment interactions and on the free volume difference between the polymer and CO_2. The physical properties of CO_2 are listed in Table 2- 1. Due to its structural symmetry, CO_2 does not have a dipole moment, but does have a substantial quadrupole moment that operates over a much shorter distance than dipolar interactions. Some polarity in the polymer chain tends to lead to enhanced

solubility, however high pressures and high temperatures are still needed in order to dissolve non-fluorinated polymers.

Table 2- 1 Physical properties of CO_2.

T_c(K)	P_c(bar)	ρ_c(g/cm^3)	$\alpha \times 10^{25}$(cm^3)	μ(D)	$Q \times 10^{26}$(erg$^{1/2}$cm$^{5/2}$)
304.2	73.8	0.468	27.6	0.0	-4.3

A number of studies in the literature have shown that supercritical CO_2 is a suitable solvent for some polymers and copolymers at high pressures and temperatures (McHugh and Krukonis, 1994). An example is given in Figure 2- 9 where the cloud point curves of PVAc and PMA in CO_2 have been plotted (McHugh *et al.,* 1996). It has been also demonstrated that CO_2 at ambient temperatures and at pressures around 60 MPa can be used to solubilize polymers such as poly (dimethyl silicone) and poly (phenyl methyl silicone)s (McHugh and Krukonis 1994; Yilgor *et al*., 1984; Krukonis 1985). Beckman *et al.* (1991), Barton and Dris (1996) and Xiong and Kiran (1995) have measured the solubility of poly (perfluoropropylene oxide) and poly (dimethylsiloxane) in CO_2 and also reported a high solubility of poly (dimethylsiloxane) in CO_2 at approximately 45 MPa. It is also possible to dissolve very low molecular weight ($\leq$ 1000 g/mol) slightly polar polymers such as polystyrene or polyisobutylene in supercritical CO_2 (Gregg *et al.,* 1994) as well as co-polymers, such as poly (tetrafluoroethylene-*co*-hexafluoropropylene) with 19 mol % hexafluoropropylene in CO_2 at temperatures above 458 K and pressures around 1000 bar (McHugh *et al*., 1996). In related work, DeSimone and co-workers (1992, 1994, 1995) have generated a large body of data demonstrating that CO_2 can dissolve hydrocarbon polymers that contain fluorinated octyl acrylates, and they have reported a

high solubility of poly (1,1-dihydroperfluorooctyl acrylate) (poly (FOA)) in supercritical CO_2 .

The above studies include most of the available experimental data on the solubility of polymers in CO_2. By comparison, there are numerous studies of swelling of polymers by CO_2. An example of such measurements is shown in Figure 2- 10 from the work of Liau and McHugh (1985) and Wissinger and Paulaitis (1987). Volume change of the polymer due to the amount of CO_2 soluble in the polymer is plotted versus the pressure of the system.

When a polymer is exposed to a liquid or gaseous solvent, the matrix swells. The extent of swelling depends on the type of polymer, the solvent used and the swelling conditions. The addition of the solvent leads to plasticization of the polymer, and a decrease in its glass transition temperature (Wissinger and Paulaitis, 1991; Condo and Johnston, 1992). It has been shown that CO_2 is a good plasticizing agent for a variety of polymeric materials such as polystyrene, polyethylene, poly (ethylene teraphthalate), polyisoprene, polymethylmethacrylates, polycarbonates, polyurethanes (Chiou *et al.*, 1985; Lee *et al.*, 1999; Zhang *et al*., 1997; Wissinger and Paulaitis, 1991; Wang *et al*., 1982; Shieh *et al.*, 1996; Hirose *et al.*, 1986). CO_2 also plasticizes crosslinked elastomers, some block copolymers and polymer blends (Goel and Beckman, 1992; 1993; Lee *et al.*, 1998; Kato *et al.*, 1997; Mokdad *et al.*, 1996).

Plasticization is a common phenomenon in polymer processing techniques. In heterogeneous polymerization, plasticization may facilitate diffusion of the monomer and initiator into the polymer phase. This has been utilized in processes such as polymer extraction, impregnation, and formation of microcellular foams, particulate polymers and

polymer coatings (Britto et al., 1996; Pratt and McHugh 1996; Yilgor and McGrath, 1984; Kim et al., 1998; Webb, 1998). While supercritical CO_2 is not unique in its ability to plasticize polymers, it does have unusual properties that are useful for polymer synthesis and processing. Thus, plasticization by supercritical CO_2 allows the processing to occur at low temperatures, which is important for the treatment of thermally sensitive materials.

In summary, two types of polymer phase diagrams are important in polymer processing- cloud point curves that describe the solubility of a polymer in the solvent, and swelling curves that describe the solubility of a gas ("solvent") in the polymer. Data on cloud point and swelling curves, especially when the solvent is CO_2, are scarce and it is particularly important to develop models that are able to extrapolate or predict cloud point curves at high pressures.

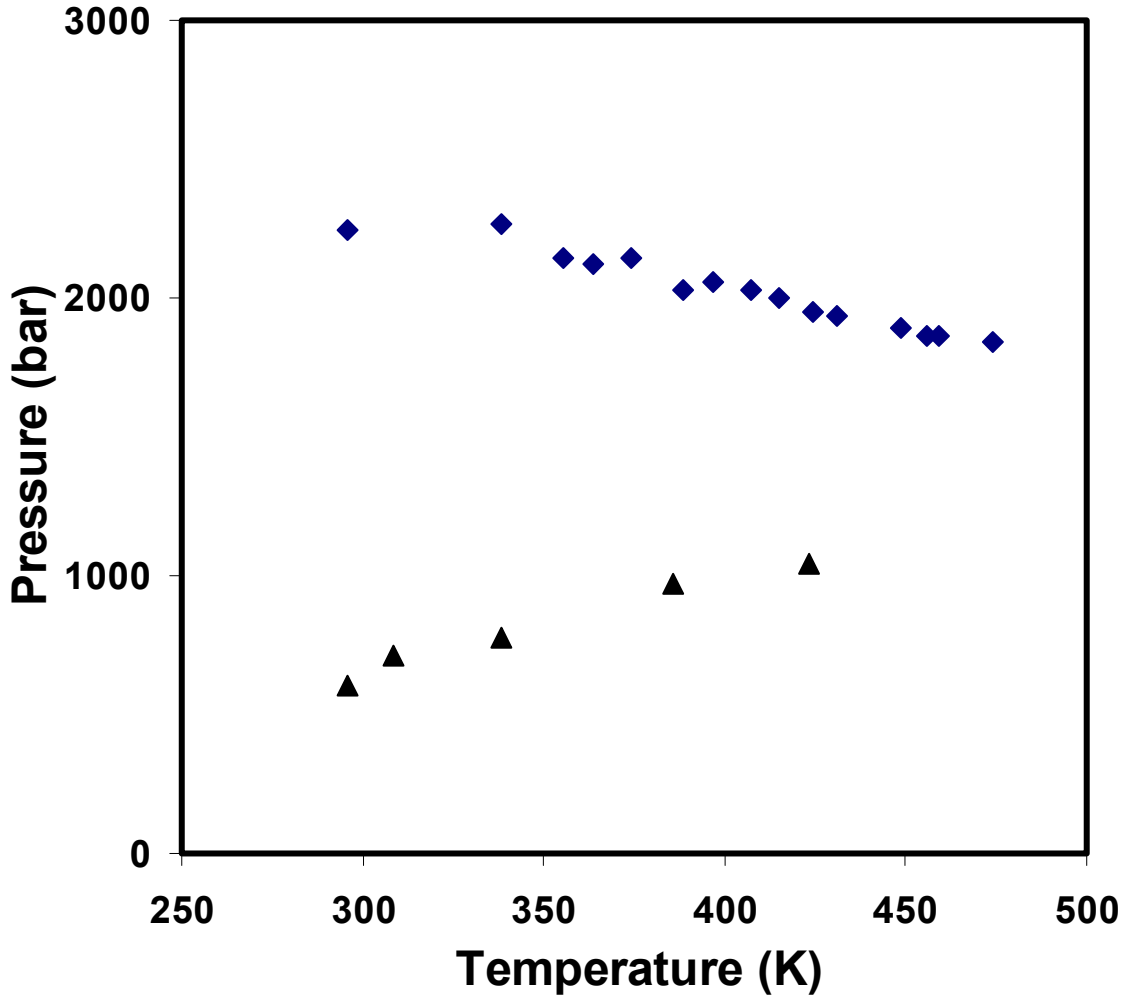

Figure 2- 9 Experimental data for CO_2-poly(methyl acrylate) (PMA) (squares)and CO_2-poly(vinyl acetate) (PVAc) (triangles) cloud-point curves from McHugh *et al.*, 1996. The weight average for PMA is 31,000 and for PVAc is 125,000. The polymer concentrations are ~5 wt. % in each case.

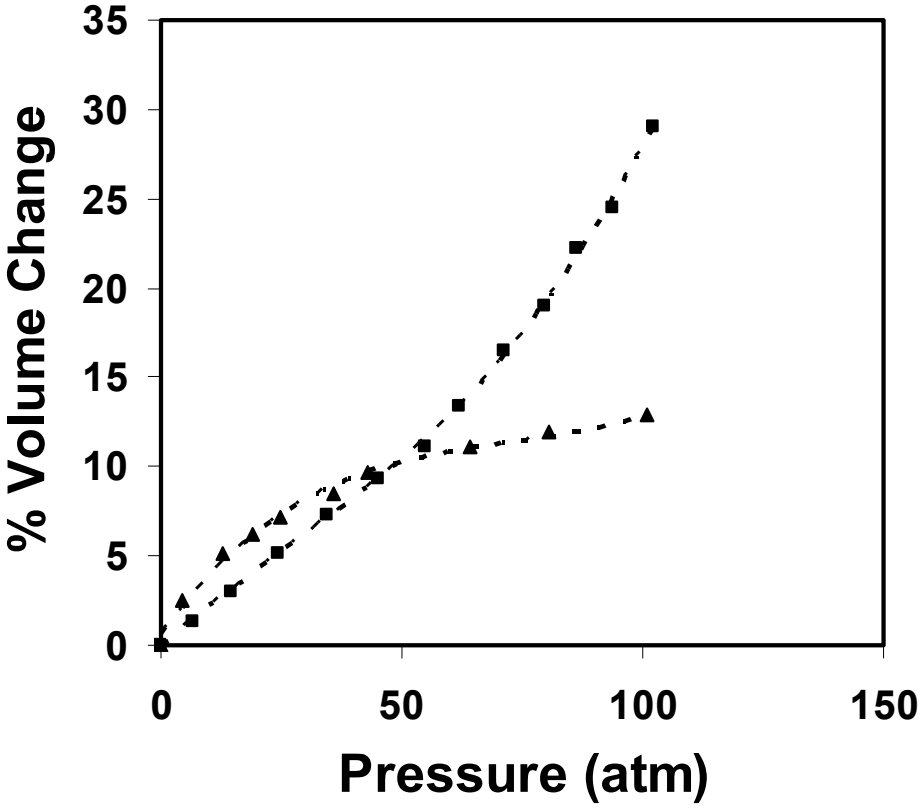

Figure 2- 10 Polymer swelling data (volume change of polymer versus pressure) for PMMA-CO_2 system at 315 K. Triangles represent the swelling data by Liau and McHugh, 1985 and squares represent the swelling data by Wissinger and Paulaitis, 1987.

CHAPTER 3

MODELING THE PHASE BEHAVIOR OF POLYMER SOLUTIONS

A review of thermodynamic models for the phase behavior of polymer solutions is presented in this chapter. These models can be divided into two classes: equations of state and activity coefficient models. Representative examples of these two classes of model are described and their advantages and disadvantages are outlined.

Equation of State (EOS) models for polymer solutions

In general, equation of state and activity coefficient models for polymer solutions are based on lattice theory, which attempts to describe the liquid state as a quasicrystalline state. This quasicrystalline picture of the liquid state supposes that molecules are arranged in a regular array in space, or in a *lattice*. Polymer segments are also arranged on a lattice, with connected segments lying on adjacent lattice sites.

Equation of state models have been formulated to take into account the fact that pure fluids have different free volumes, and therefore, different expansitivities. The models therefore incorporate additional properties of the pure components beyond those that reflect molecular size and potential energy.

Polymer equation of state models have been reviewed by Rodgers (1993) and can be broadly classified into three major categories: cell models, lattice-fluid models and perturbation models. The cell and lattice-fluid models provide different adaptations of the incompressible-lattice model to polymers; however, each incorporates compressibility in a different manner. Cell models such as the Flory-Orwoll-Vrij (FOV) equation of state (Flory *et al.*, 1964) restrict volumetric changes in the system to changes in the lattice cell

volume, i.e. the space surrounding a polymer segment placed on a lattice framework. In contrast, lattice-fluid models such as the Sanchez-Lacombe model (Sanchez and Lacombe, 1978) allow the inclusion of empty sites or lattice vacancies while keeping volume per cell constant. The Sanchez-Lacombe model has had some success in calculating the properties of polymer solutions (Rodgers, 1993) and is discussed below. Another type of equation of state model is based on the perturbation theory and is exemplified by Perturbed Hard-Sphere-Chain Theory which forms the basis for the SAFT (Statistical Associated Fluid Theory) equation of state. The SAFT equation uses a reference fluid that incorporates both molecular size and association as well as pressure effects and will be described in detail below.

Sanchez-Lacombe (SL) equation of state

The SL EOS is based on the incompressible-lattice model. The lattice is occupied by both r-mers and vacant lattice sites or 'holes' which are introduced in the lattice to obtain the correct system density. The lattice size is fixed so that changes in volume can only occur by the appearances of new holes. Using statistical mechanics, Sanchez and Lacombe (1976, 1977) derived the partition function for a system of N polymer molecules on a lattice with holes. The total number of lattice sites in the system, N_r, is

$$N_r = N_0 + rN \qquad \textbf{(3- 1)}$$

where N_0 is the number of vacancies and r is the number of segments in a polymer molecule. The close packed volume of a molecule, rv^*, is assumed to be independent of

temperature and pressure, v^* is the volume of a single mer and is equal to the volume per lattice site. The total volume of the system is then:

$$V = (N_0 + rN)v^* \tag{3- 2}$$

The energy of the lattice depends only on nearest-neighbor interactions. The SL EOS assumes random mixing of vacancies and mers; therefore, the number of mer-mer neighbors is proportional to the probability of finding two mers in the system. The lattice energy is then

$$E = -\frac{z}{2} N_r \varepsilon \left(\frac{rN}{N_0 + rN} \right)^2 \tag{3- 3}$$

where z is the lattice coordination number and ε is the mer-mer interaction energy. The configurational partition function for this system is given by;

$$Z = Z_{comb} \exp\left(-\frac{E}{kT} \right) \tag{3- 4}$$

and the combinatorial factor is given by:

$$Z_{comb} = \left(\frac{\delta}{\sigma} \right)^N \left(\frac{(N_0 + rN)!}{N_0! N!} \right) \frac{1}{(N_0 + rN)^{N(r-1)}} \tag{3- 5}$$

In equation 3-5, δ is the flexibility parameter of the r-mer and σ is a symmetry number. Both of these quantities are assumed to be constants. The Guggenheim-Miller approximation (Guggenheim, 1950) is used to calculate the number of configurations Ω available to a system of N_1r_1-mers, N_2r_2-mers… and N_o empty lattice sites. A random mixing expression was used for the energy term so that no local composition effects are included. The equation of state may be obtained from the partition function (Sanchez and Lacombe, 1976) and takes the form

$$\frac{\overline{P}\overline{v}}{\overline{T}} = -\overline{v}\left[\ln\left(1-\frac{1}{\overline{v}}\right)+\frac{1}{\overline{v}}\right]-\frac{1}{\overline{T}\overline{v}} \qquad \textbf{(3- 6)}$$

or equivalently,

$$\widetilde{\rho} = 1 - exp\left[-\frac{\left(\widetilde{\rho}^2+\widetilde{P}\right)}{\widetilde{T}}-\left(1-\frac{1}{r}\right)\widetilde{\rho}\right] \qquad \textbf{(3- 7)}$$

where $\overline{P}$, $\overline{v}$, and $\overline{T}$ are the reduced pressure, reduced volume and reduced temperature and $\widetilde{\rho} = \frac{1}{\widetilde{v}}$. These reduced variables are defined by the following expressions:

$$\overline{P} = \frac{P}{P^*} = \frac{Pv^*}{\varepsilon^*} \qquad \textbf{(3- 8)}$$

$$\overline{v} = \frac{V}{V^*} = \frac{V}{N_{Av} r v^*} \qquad \textbf{(3- 9)}$$

$$\overline{T} = \frac{T}{T^*} = \frac{Tk}{\varepsilon^*} \qquad \textbf{(3- 10)}$$

where ε^* is the interaction energy per segment, rv^* is the close-packed molecular volume, k is Boltzmann's constant, and N_{Av} is Avagadro's number.

To extend this equation to an n-component mixture, it is necessary to define a characteristic mixture temperature, pressure and close-packed molar volume. Different types of mixing rules can be employed. For example, the average chain length of the mixture can be given by

$$\frac{1}{r} = \sum_{i=1}^{n} \frac{\Phi_i}{r_i} \qquad \textbf{(3- 11)}$$

where Φ_i is the site fraction of component i. The characteristic segment is

$$v^* = \sum_{i=1}^{n} \sum_{j=1}^{n} \Phi_i \Phi_j v_{ij}^* \qquad \textbf{(3- 12)}$$

v_{ij}^* (when i≠j) is calculated by

$$v_{ij}^{*} = \left(\frac{v_{ii}^{*1/3} + v_{jj}^{*1/3}}{2} \right)^{3} \left(1 - \eta_{ij}\right) \qquad \textbf{(3- 13)}$$

where η_{ij} is a binary interaction parameter that accounts for the deviations from hard-sphere type behavior. The characteristic interaction energy between segments can be obtained from

$$\varepsilon^{*} = \sum_{i=1}^{n} \sum_{j=1}^{n} \Phi_i \Phi_j \varepsilon_{ij}^{*} \qquad \textbf{(3- 14)}$$

The Sanchez-Lacombe model uses a binary interaction parameter k_{ij} in the expression for ε_{ij}

$$\varepsilon_{ij}^{*} = \left(\varepsilon_{ii}^{*} \varepsilon_{jj}^{*}\right)^{1/2} \left(1 - k_{ij}\right) \qquad \textbf{(3- 15)}$$

where k_{ij} corrects for deviations from simple Lorentz-Berthelot type behavior. The adjustable binary interaction parameters, k_{ij} and η_{ij}, are generally determined by fitting experimental pressure-composition (P-x) isotherms.

Several assumptions were made in developing the SL equation of state. The flexibility parameter and close packed volume were assumed to be independent of temperature and pressure. Also, random mixing of holes and molecules was assumed (Sanchez and Lacombe, 1976). With these assumptions, the SL EOS has been used to model phase behavior of polymer solutions with varying degrees of success. Gas and

organic vapor solubilities in polymers such as polymethylmethacrylate, and polydimethylsiloxanes are well correlated by the equation (McHugh *et al.,* 1988; Wissinger and Paulaitis, 1987). The T_g depression associated with a compressed gas dissolving in the polymer matrix has also been determined by using the Gibbs-Di Marzio criterion, which states that at the glass transition the polymer is essentially frozen and has zero configurational entropy. The solubility of the gas by the polymer and its T_g have been calculated by simultaneously solving the EOS and the Gibbs-Di Marzio criterion. The SL EOS is able to correlate the T_g depression as a function of dissolved CO_2 concentration in polymers such as polymethylmethacrylate (Condo *et al.,* 1992).

Other types of phase behavior such as LCST and UCST have been correlated for polyisobutylene /solvent systems in good agreement with experimental data (Sanchez and Lacombe, 1976). Also, LCST behavior in polymer blends such as polyvinyl methyl ether / polystyrene and poly (tetramethyl carbonate) / polystyrene (Sanchez and Lacombe, 1977) can be successfully correlated. However, the correlation of UCST and LCST in systems such as polyethylene-ethylene systems requires adjustable parameters that change significantly with temperature to obtain a good representation of the phase behavior (Kiran *et al.,* 1993; Trumpi *et al*., 2003). Also, the fit is extremely sensitive to the parameters selected and the phase behavior can change dramatically from LCST to UCST behavior when the parameter values change only slightly.

Perturbed Hard-Chain Theory (PHCT)

The perturbed Hard-Chain Theory (PHCT) is based on the same fundamentals described in the generalized van der Waals partition function. For a binary mixture, the

partition function Q depends on the temperature T, total volume V, and the number of molecules N_1 and N_2 such as:

$$P = kT\left(\frac{\partial \ln Q}{\partial V}\right)_{T,N_1,N_2} \quad \textbf{(3- 16)}$$

where k is the Boltzmann's constant. The partition function for a pure simple fluid containing N molecules in total volume V is (Vera and Prausnitz, 1972; Hill, 1986):

$$Q(T,V,N) = \frac{1}{N!}\left(\frac{V}{\Lambda^3}\right)^N \left(q_{rep}\right)^N \left(q_{att}\right)^N \left(q_{r,v}\right)^N \quad \textbf{(3- 17)}$$

where Λ is the de Broglie wavelength that depends only on the temperature and molecular mass; q_{rep} and q_{att}, are the contributions from repulsive and attractive intermolecular forces experienced by each molecule and $q_{r,v}$ is the contribution per molecule from rotational and vibrational degrees of freedom. For a monatomic ideal gas, the last three contributions are unity. However, for real fluids each of the last three terms are functions of temperature and density such as:

$$\left(q_{rep}\right) = \frac{V_f}{V} \quad \textbf{(3- 18)}$$

and

$$\left(q_{att}\right) = \exp\left(\frac{-E_0}{2kT}\right) \quad \textbf{(3- 19)}$$

where the free volume V_f is the volume available to the center of mass of a molecule as it moves in the system, holding the positions of all other molecules fixed; E_0 is the intermolecular potential energy experienced by one molecule due to attractive forces. The inclusion of these expression leads to the generalized van der Waals partition function for a simple fluid:

$$Q(T,V,N) = \frac{1}{N!}\left(\frac{V}{\Lambda^3}\right)^N \left(\frac{V_f}{V}\right)^N \left(\exp\left(\frac{-E_0}{2kT}\right)\right)^N (q_{r,v})^N \qquad \textbf{(3- 20)}$$

For simple molecules, the final term that accounts for molecular rotations and vibrations is only a function of temperature, but for polymer molecules it also depends on density, especially when the molecules deviate from spherical shape. The expressions are available in Prigogine (1957).

Extension of the partition function to mixtures is possible using the idea of one fluid theory. According to this, a mixture can be considered as a hypothetical fluid where the characteristics are composition averages of its components. Using this approximation the generalized van der Waals partition function can be written as for a mixture containing N_1, N_2, ….. N_m molecules of components of 1,2, …..m :

$$Q(T,V,N_i) = \frac{1}{\prod_{i=1}^{m}(N_i!)}\left(\prod_{i=1}^{m}\left(\frac{V}{\Lambda_i^3}\right)^{N_i}\right)\left(\overline{\frac{V_f}{V}}\right)^N \left(\exp\left(\frac{-\overline{E_0}}{2kT}\right)\right)^N \prod_{i=1}^{m}\left(\overline{q_{r,v}}\right)^{N_i} \qquad \textbf{(3- 21)}$$

Functions Λ_i depend only on temperature and mass m_i. However, other properties are composition averages of the corresponding pure-component properties calculated by mixing rules. For mixtures that contain large polyatomic molecules, procedures are available to account for the effect of density on rotational and vibrational contributions to the partition function.

To reduce the partition function to practice, the expressions for free volume V_f and potential energy E_0 are required. Depending on the particular expression used for these properties, the generalized van der Waals partition function leads to a variety of models such as the *Perturbed- Hard- Chain- Theory (PHC*T). The PHCT equation makes use of V_f expression from the molecular simulation work of Percus and Yevick (1958),which leads to the Carnahan and Starling equation, (1972):

$$V_f = V \exp\left[\frac{\eta(3\eta - 4)}{(1-\eta)^2}\right] \qquad \textbf{(3- 22)}$$

where η is the reduced density, calculated by

$$\eta = \eta_{cp}\left(\frac{v_0}{v}\right) \quad \text{and} \quad v_0 = \left(\frac{\sigma^3}{\sqrt{2}}\right)N_{Av} \qquad \textbf{(3- 23)}$$

v_0 is the smallest possible closed packed volume that can be occupied by N hard spheres of diameter σ.

In the development of PHCT, Beret (1975) and Donohue (1978) used the above expression to account for molecular repulsion. For the potential energy which accounts for molecular attraction, an analytical expression is used that is obtained from molecular simulation studies of Alder *et al.* (1972) for molecules whose intermolecular forces are represented by a square well potential. Using these relationships the resulting equation of state is

$$\frac{\tilde{P}\tilde{v}}{\tilde{T}} = \frac{1}{c} + \frac{4\eta - 2\eta^2}{(1-\eta)^3} + \frac{1}{\tilde{T}\tilde{v}} \sum_{n=1}^{4} \sum_{m=1}^{M} \left(\frac{mA_{nm}}{\tilde{v}^{m-1}} \right) \left(\frac{1}{\tilde{T}^{n-1}} \right) \qquad \textbf{(3- 24)}$$

where A_{nm} 24 constants are obtained from molecular simulation data. The reduced parameters are:

$$\tilde{P} = \frac{P}{P^*} = \frac{P(rv^*)}{\varepsilon q} \qquad \textbf{(3- 25)}$$

and

$$\tilde{T} = \frac{T}{T^*} = \frac{ckT}{\varepsilon q} \qquad \textbf{(3- 26)}$$

and

$$\tilde{v} = \frac{v}{v^*} = \frac{v\sqrt{2}}{N_{Av} r \sigma^3} \qquad \textbf{(3- 27)}$$

where q is the non-dimensional external area of the molecule (q=1 for a single arbitrarily chosen reference segment), ε is the characteristic segment-segment potential energy, v^* is

the characteristic hard-core volume per segment and r is the number of segments per molecule and c can be calculated from the relationship

$$c = \frac{P^*(rv^*)}{kT^*} \qquad \textbf{(3- 28)}$$

For each fluid, PHCT contains three molecular parameters, εq, rv^*, and c obtained by fitting experimental data, usually volumetric and vapor-pressure data. As shown by Donohue (1978), Kaul *et al*. (1980) and Cotterman *et al.* (1986) the PHCT equation can be extended to mixtures using mixing rules, and Liu (1980) showed that it can be used for systems with large differences in molecular size and shape. It has been applied to different systems where Henry's constants for the volatile solute (1) in polymer (2) can be calculated, when the Henry's constant is defined by

$$H_{1,2} = \lim_{w_1 \to 0} \frac{f_1}{w_1} = \lim_{w_1 \to 0} \frac{RT}{M_1 v_2} \exp\left(\frac{\mu_1^{HC} + \mu_1^{att} + \mu_1^{SV}}{kT} \right) \qquad \textbf{(3- 29)}$$

where f_1 is the fugacity and w_1 is the weight fraction of the volatile solute; M_1 is the molar mass of the solute, R is the gas constant, and v_2 is the specific volume of the polymer. μ_1^{HC}, μ_1^{att} and μ_1^{SV} are the chemical potentials form the hard-chain part, attractive part, and second-virial-coefficient part as calculated from PHCT for mixtures (Kaul *et al.,* 1980).

Ohzono *et al.* (1984) and Iwai and Arai (1991) applied the PHCT to correlate weight fraction Henry's constants of nonpolar hydrocarbon vapors in molten polymers

such as n-alkanes in polypropylene with one adjustable parameter over a range of temperatures. However, the theory does not apply to associating polymer systems. For such systems, an extension known as Statistical Associated Fluid Theory (SAFT) has been proposed and will be described below.

Statistical Associated Fluid Theory (SAFT)

A recent extension of the PHCT, based on Wertheim's perturbation theory (Wertheim, 1984), is termed the Statistical Associating Fluid Theory (SAFT, Chapman *et al.,* 1990). This method uses a hard sphere chain reference in place of the much simpler hard sphere reference fluid used in PHCT (Beret, 1975; Donohue, 1978). Wertheim's theory was developed by expanding the Helmholtz energy in a series of integrals of molecular distribution functions and the association potential. He showed that many integrals in this series are zero which results in a simplified expression for the Helmholtz energy. He applied this theory to hard chain fluids and developed first order and second order thermodynamic perturbation theories applicable to flexible chain molecules and to other molecules that exhibit chain conformation and branch structure. SAFT represents molecules as covalently bonded chains of segments that may contain sites capable of forming associative complexes. A mean-field attractive term is used as a perturbation of the reference equation that consists of terms accounting for the connectivity of the hard segments in the main chain, the hard-sphere repulsion of the segments, and the energy of site-site specific interactions of the segments with themselves or other segments. With this approach, the hard sphere chain equation of state is

$$\left(\frac{P}{\rho kT}\right)_{HSC} = 1 + r^2 b\rho g\left(d^+\right) - \left(r-1\right)\left(\rho\frac{\partial \ln g\left(d^+\right)}{\partial\rho}\right) \qquad \textbf{(3- 30)}$$

where $g(d^+)$ is the radial distribution function of hard spheres at contact (calculated from the Carnahan- Starling equation), r is the number of tangent hard-spheres per molecule, and b is the second virial coefficient of hard spheres prior to bonding to form chains where

$$b = \frac{2\pi}{3}d^3 \qquad \textbf{(3- 31)}$$

In equation 3-30, the first two terms are the non-bonding contributions and the last term reflects chain connectivity. The equation obeys the ideal-gas law in the limit when $\rho \rightarrow 0$.

To model a real fluid, a perturbation term is added in order to include attractive forces. Chapman et al. (1990) adopted the dispersion term from molecular simulation data for Lennard- Jones fluids. On the other hand, Huang and Radosz (1990) used a series initially fitted by Alder *et al*.(1972) to molecular dynamics data for a square well fluid

$$\left(\frac{P}{\rho kT}\right)_{pert} = r\sum_{\alpha}\sum_{\beta}\beta D_{\alpha\beta}\left(\frac{u}{kT}\right)^{\alpha}\left(\frac{\eta}{\eta_{cp}}\right)^{\beta} \qquad \textbf{(3- 32)}$$

where η_{cp}=0.7405, is the packing fraction of hard spheres at the closest packing, and

$$u = \varepsilon\left(1 + \frac{e}{kT}\right) \qquad \textbf{(3- 33)}$$

where $\left(\frac{e}{kT}\right)$= 10 K, ε is the well depth of the potential. $D_{\alpha\beta}$ are universal constants which have been refitted to accurate PVT, internal energy and second virial coefficient data. The effective hard-sphere diameter *d* depends on temperature as suggested by the Barker- Henderson perturbation theory (1967)

$$d = \sigma\left[1 - 0.12\exp\left(\frac{-3\varepsilon}{kT}\right)\right] \qquad \textbf{(3- 34)}$$

where σ is the effective hard-sphere diameter at zero temperature; it is also the distance of separation at minimum potential energy.

The general form of the equation is

$$\left(\frac{P}{\rho kT}\right) = \left(\frac{P}{\rho kT}\right)_{HSC} + \left(\frac{P}{\rho kT}\right)_{pert} \qquad \textbf{(3- 35)}$$

There are five pure-component parameters in the SAFT equation: the temperature-independent volume of a segment v^{oo}, the temperature-independent, nonspecific energy of attraction between two segments u^{o}/k, the number of segments in a

molecule *m*, the energy of association between sites on a moleculeε/*k*, and the volume of association ν. Estimates for the energy of association can be obtained from spectroscopic measurements with liquids that have the same functional groups as the solvent or the polymer. Estimates for ν can be obtained from tables regressed from pure-component data (Huang and Radosz, 1991). The other two parameters can be estimated by regression of PVT data.

Different mixing rules (Chapman *et al.,* 1990) for the volume of the segment v^0 and the energy of interaction *u* and the number of the segments in the mixture *m* are used in order to extend the SAFT equation to mixtures.

$$v^0 = \sum_i \sum_j \Phi_i \Phi_j m_i m_j v_{ij}^0 \qquad \textbf{(3- 36)}$$

where

$$v_{ij}^0 = \frac{1}{8}\left[v_i^{0\,1/3} + v_j^{0\,1/3} \right]^3 \qquad \textbf{(3- 37)}$$

$$\frac{u}{kT} = \frac{1}{v^0} \sum_i \sum_j \Phi_i \Phi_j m_i m_j \left[\frac{u_{ij}}{kT} \right] v_{ij}^0 \qquad \textbf{(3- 38)}$$

$$u_{ij} = \left(u_{ii} u_{jj} \right)^{1/2} \left(1 - k_{ij} \right) \qquad \textbf{(3- 39)}$$

and

$$m = \sum_i \sum_j \Phi_i \Phi_j m_{ij} \qquad \textbf{(3- 40)}$$

where

$$m_{ij} = \frac{1}{2}\left[m_i + m_j\right]\left(1 - \eta_{ij}\right) \qquad \textbf{(3- 41)}$$

The mixing rule includes binary parameters k_{ij} and η_{ij} which are generally obtained by fitting experimental data.

A large number of SAFT pure-component parameters for small molecules have been reported in the literature (Chapman *et al.,* 1990). Regression of polymer PVT data, however, yields parameters that lead to poor phase equilibrium predictions (Hasch *et al.*, 1995; 1996). Values for v^{oo} and u^{o}/k are usually too large, whereas the values for m tend to be too small. The dilemma with SAFT is that calculated polymer densities are not very sensitive to variations in pure-component parameters, whereas phase equilibrium calculations are very sensitive to these parameters. Moreover, the predictive power of the equation is limited since a nonzero value of k_{ij} is needed to obtain a reasonable representation of the phase behavior of polymer solutions. As shown in Figure 3-1, cloud point curves for some systems such as PE-ethylene can be estimated using SAFT with reasonable success with two adjustable parameters. However, no systematic studies have been performed to provide general guidelines for estimating the parameters. Therefore, it is difficult to use this model for most systems.

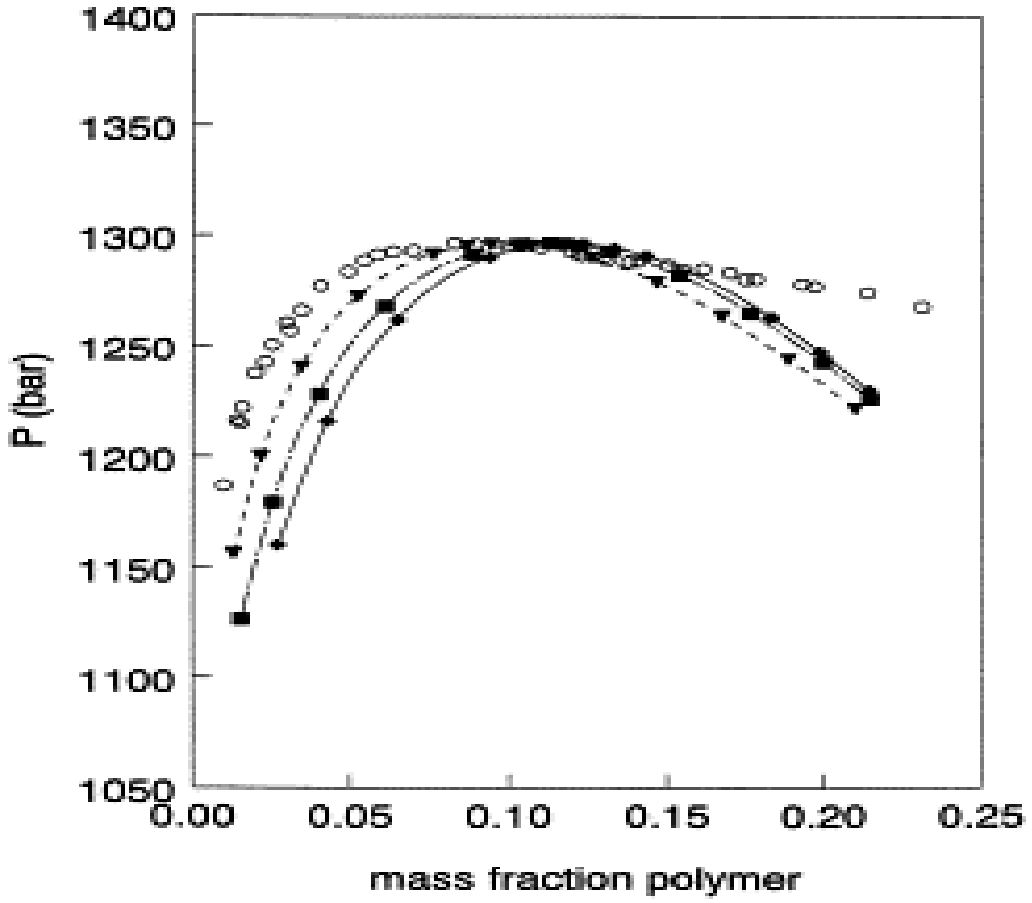

Figure 3- 1 SAFT EOS Calculation of Pressure-Composition cloud point curves for polyethylene-ethylene system at 423.15 K. Graph adapted from Noak *et al.,* 1999. Open circles represent the experimental data (Noak *et al.,* 1999). Lines with filled squares (♦) represent SAFT calculations (u_o/k=216.15 ,k_{12}=0.05776); Lines with filled triangles (▼) represent SAFT calculations with u_o/k=228.36, k_{12}=0.0369); Lines with filled squares (■) represent SAFT calculations with u_o/k=210, k_{12}=0.06793.

Activity Coefficient models

In an ideal solution, the sizes of the molecules of each component, as well as like and unlike molecular interactions between the molecules are equal. Thus, there is no volume change upon mixing (ΔV_m=0); and no enthalpy change upon mixing (ΔH_m=0). The entropy change upon mixing is equal to the entropy change due to random mixing. However, these considerations do not hold for polymer solutions. In such solutions, differences between molecular sizes lead to volume changes upon mixing, energetic differences affect the enthalpy of mixing, and differences in the configurations available to the molecules of each component in the mixture contribute to nonrandom entropy of mixing.

Lattice theories assume that the structure of a solution can be represented by an array of lattice sites that are occupied by molecules, and that these molecules experience only nearest neighbor interactions. Molecular considerations suggest that deviations from ideal solution behavior are primarily due to (i) forces of attraction between like molecules that are different from those between unlike molecules, leading to a nonzero enthalpy of mixing; (ii) differences in size or shape between unlike molecules that are significant, or the molecular arrangement in the mixture that is appreciably different from in the pure components, leading to a nonideal entropy of mixing. Most lattice models resort to mean-field approximations for calculating the entropy and enthalpy of mixing, so that the solvent distribution around the solute corresponds to its volume fraction. Although no exact solution to the lattice partition function exists, various approximate solutions have been proposed. The Flory-Huggins formulation (Huggins, 1941; Flory, 1942) is one such

approximation for mixing of long chain molecules with much smaller molecules or with other long chain molecules.

Flory- Huggins Theory

The Flory-Huggins theory considers the arrangement of molecules on a three dimensional lattice with a fixed coordination number, which is the number of nearest neighbor sites around a particular cell on the lattice. The polymer molecules are assumed to consist of segments of equal sizes with the average number of segments, *r,* in a chain generally given by the ratio of the molecular volume of the polymer to that of the solvent. Each lattice cell is occupied by either a solvent molecule or a chain segment, and each polymer molecule is placed in the lattice so that its chain segments occupy a sequence of *r* cells. The number of ways of arranging molecules on the lattice and the total number of nearest neighbor contacts can then be computed. The entropy of mixing can be calculated from

$$\Delta S_m = k \ln \Omega = k \ln \frac{N!}{N_s!(rN_p)!} \approx -k\left(N_s \ln \Phi_s + N_p \ln \Phi_p\right) \qquad \textbf{(3- 42)}$$

where N is the total number of molecules, N_s and N_p are the number of solvent and polymer molecules, r is the segment number, R is the gas constant and Φ_s and Φ_p are volume fractions of solvent and the polymer respectively, given by

$$\Phi_s = \frac{N_s}{N_s + rN_p} \qquad \Phi_p = \frac{rN_p}{N_s + rN_p} = 1 - \Phi_s \qquad \textbf{(3- 43)}$$

The application of the Flory-Huggins model to polymer solution requires the addition of an enthalpy change of mixing (ΔH_m) term to represent the residual contribution. If this contribution is assumed to be the same as that obtained from Regular Solution Theory, then the Flory-Huggins equation becomes

$$\frac{\Delta G_m}{RT} = \frac{\Delta G^R}{RT} + \frac{\Delta G^C}{RT} = \frac{\Delta H_m}{RT} - \frac{\Delta S_m}{R} = n_s \ln \Phi_s + n_p \ln \Phi_p + \chi n_s \Phi_p \qquad \textbf{(3- 44)}$$

where n_s, n_p are the moles and Φ_s and Φ_p are the volume fractions of solvent and polymer respectively. R is the gas constant. ΔG^R and ΔG^C are the residual and combinatorial parts of the Gibbs Energy of mixing, respectively, and χ is an interaction parameter. The activity of the solvent, a_s is given by

$$\ln(a_s) = \ln(1 - \Phi_p) + \left(1 - \frac{1}{r}\right)\Phi_p + \chi \Phi_p^2 \qquad \textbf{(3- 45)}$$

It should be noted that the Flory-Huggins theory has the following limitations:

- The segments are arranged on the lattice via a random walk. Thus, configurations where two polymer segments can occupy the same lattice cell are not excluded in a proper fashion.
- Strong polar interactions or specific interactions like hydrogen bonding, which affect the enthalpy of mixing but can also significantly influence the entropy of mixing, are not accounted for in the theory. These interactions can bias the

orientation of certain types of molecules and lead to a decrease in the entropy of mixing (Flory, 1941).

- The polymer molecules are constructed from freely jointed chains, and thus the conformational characteristics are not affected by solution concentration.
- The volume change upon mixing is assumed to be zero, which is a poor assumption when there are large differences in free volume between the polymer and the solvent (Flory, 1941; Huggins, 1942).

The second assumption is especially limiting when strong specific interactions exist between solvent molecules or between solvent molecules and a polymer segment. Such forces can lead to specific preferences for nearest–neighbors. Solvent molecules might associate with solute (polymer segments) in such a way that they preferentially occupy certain sites around a solute, while the remaining sites might not have any such preference. There have been many studies where preferential association (Moore, 1955, 1965, 1967) between two components has been found. This implies that the entropies computed by Flory-Huggins type lattice models over-estimate the entropy of mixing. The number of like and unlike pair interactions, and hence the enthalpy of mixing, may also be under-estimated. Hence the error in the Gibbs energy could be large. Mixtures exhibiting an UCST reflect the dominance of the entropy of mixing at high temperatures, resulting in a single phase. Upon cooling, unfavorable unlike pair interactions can lead to phase separation. However, if specific interactions exist amongst the components in solution, it is possible to expect favorable enthalpic effects at lower temperatures that result in phase mixing. A LCST can result from favorable interactions between the components due to an increase in temperature. Therefore, it is important to incorporate

specific interactions in activity coefficient models in order to provide a more complete description of phase behavior.

Models that explicitly account for association in solution have been proposed by Veystman (1990) and Painter *et al.,* (1989, 1990). Veystman's model includes an estimate of the number of ways that association could be distributed among the functional groups in a system. This formalism has been applied to linear polymers as well as network structures (Painter *et al.,* 1990). However, parameters of the model must be obtained by fitting experimental data (Panayiotou and Sanchez, 1991).

Another approach was followed by Painter *et al.* (1989, 1990) who developed a theory for estimating phase behavior in strongly interacting polymer blends. In this method, the Gibbs Energy is expressed in terms of an equilibrium distribution of the species present in solution. The functional groups in the system form a sequence of "chains", these species are termed the "monomers" (non-interacting species), "dimers"(associated species), "trimers", etc. The formation of these species is assumed to be due to chemical reactions, with equilibrium constants characterizing the amounts of species. The equilibrium constants were assumed to be temperature and composition dependent. The advantage of such a formulation over Veytsman's approach is that the association parameters of the model can be obtained from spectroscopy. However, the disadvantages of both approaches are that the models are very complicated and a number of parameters (more than ten) are needed.

UNIFAC-FV

A different approach was adopted by Oishi and Prausnitz (1978) who modified the highly successful UNIFAC (UNIversal Functional group Activity Coefficient) model (Fredenslund *et al.,* 1975) to include contributions of the free volumes of the polymer and the solvent. UNIFAC uses a combinatorial expression developed by Staverman (1950) and a residual term determined by Guggenheim's quasichemical theory (1952). Oishi and Prausnitz recognized that the UNIFAC combinatorial contribution does not account for free volume differences between the polymer and the solvent. They therefore added a free volume contribution to the original UNIFAC model to arrive at the following expression for the weight fraction activity coefficient of a solvent in a polymer solution

$$\ln \gamma_1 = \ln \frac{a_1}{w_1} = \ln \gamma_1^C + \ln \gamma_1^R + \ln \gamma_1^{FV} \qquad \textbf{(3- 46)}$$

The free volume contribution is given by

$$\ln \gamma_1^{FV} = 3C_1 \left[\frac{v_1^{1/3} - 1}{v_m^{1/3} - 1} \right] - C_1 \left[\frac{v_1}{v_m} - 1 \right] \left[\frac{v_1^{1/3} - 1}{v_1^{1/3} - 1} \right] \qquad \textbf{(3- 47)}$$

Here $3C_1$ represents the number of external degrees of freedom per solvent molecule (C_1 is usually set to 1.1), v_1 and v_m are the molar volumes of the solvent and the mixture, respectively. The combinatorial and residual contributions γ^C and $^{\gamma R}$ are identical to the original UNIFAC contributions.

This modification, termed UNIFAC-FV, is currently the most successful method available to predict solvent activities in a polymer solution. Only the densities of the pure polymer and solvent at the temperature of the mixture and the structure of the solvent and the polymer are required to obtain the parameter. Molecules that can be constructed from the groups and available from UNIFAC method can be treated. However, UNIFAC-FV has only been validated for the simplest of these structures and performs poorly with complex structures (Oishi and Prausnitz, 1978; Daubert and Danner, 1989).

The generalized associative reformulation of thermodynamics (gART-L) model

It is apparent from the above discussion that available thermodynamic models for polymer solutions generally do not take into account any association between the polymer and the solvent. In the few models that do consider specific interactions, the models require "fitting" to a significant amount of experimental phase equilibrium data to estimate the parameters. There is therefore a need for a model that accounts for association and requires only minimal amount of experimental data. Sukhadia and Variankaval (Sukhadia, 1999; Variankaval, 2001) proposed a lattice activity coefficient model that accounts for specific interactions between polymer segments and solvent molecules leading to the formation of complexes. The solution is assumed to consist of three types of molecules: complexes (associated polymer-solvent molecules), unassociated solvent and unassociated solute molecules. Their approach accounts for the presence of "associated" solute-solvent molecules and/or molecular segments. The model differs from other activity coefficient models in that the entropy of mixing is calculated by a direct filling of the associated complexes in the lattice, and not by placing the

equilibrium distribution of associated species on the lattice. This model is described in detail below.

In a solution in which specific (chemical) interactions exist between a solute molecule *P* and the solvent *S*, the following equilibrium reaction may be postulated:

$$P + \mu S \Leftrightarrow PS_{\mu} \qquad \textbf{(3- 48)}$$

where *P* is the solute (polymer segment in the discussion below), *S* is the solvent, and PS_{μ} is the associated solvent-solute complex with μ being the solute/solvent-binding ratio. The equilibrium constant K for association is then given by

$$K = \frac{\left[PS_{\mu}\right]}{\left[P\right]\left[S\right]^{\mu}} \qquad \textbf{(3- 49)}$$

where *[P], [S],* $[PS_{\mu}]$ are the concentrations of the solute, solvent and associated complex respectively.

For a solution containing N_1 solvent molecules and xN_2 molecules of solute (or N_2 polymer molecules, each of which consist of x segments), this relationship becomes:

$$K = \left(\frac{\alpha}{1-\alpha}\right)\left(\frac{1-\mu\alpha\Phi_2}{\Phi_1 - \mu\alpha\Phi_2}\right)^{\mu} \qquad \textbf{(3- 50)}$$

where Φ_1 and Φ_2 are the volume fractions of components 1 (solvent) and 2 (solute/ polymer segment) and α is the fraction of solute molecules involved in complex formation. At equilibrium, the system is composed of $\alpha x N_2$ associated solute molecules, $\mu\alpha x N_2$ associated solvent molecules, $(1-\alpha)x N_2$ unassociated solute molecules and $N_1 - \mu\alpha x N_2$ unassociated solvent molecules, all placed on the lattice. The value of x, which is the number of segments in each polymer molecule, is generally obtained from the ratio of volumes of the solute to the solvent. It is much larger than unity in polymer solutions.

The volume fractions can be calculated using:

$$N = N_1 + xN_2 \qquad \textbf{(3- 51)}$$

and

$$\Phi_1 = \frac{N_1}{N_1 + xN_2} \qquad \Phi_2 = \frac{xN_2}{N_1 + xN_2} = 1 - \Phi_1 \qquad \textbf{(3- 52)}$$

Entropy of Mixing

The entropy of mixing ΔS_m is obtained from the definition:

$$\Delta S_m = k\left(\Omega_{solution} - \Omega_{polymer} - \Omega_{solvent}\right) = k\, ln \frac{\Omega_{solution}}{\Omega_{polymer} * \Omega_{solvent}} \qquad \textbf{(3- 53)}$$

where $\Omega_{solution}$, $\Omega_{polymer}$, $\Omega_{solvent}$ are the number of configurations of associated complex, pure polymer, and pure solvent molecules respectively.

The number of configurations of the $(i+1)^{th}$ polymer molecule on a lattice along with the associated solvent, when there are i polymer complexes already on the lattice, is first calculated. It is assumed that the fraction of associated segments α per molecule is the same for all molecules and also that there is only one way of arranging the associated solvent around the corresponding polymer segments. This can also lead to a decrease in entropy and also avoid an overestimation of the solution entropy when the solvent molecules are very strongly associated to specific sites to form essentially permanent complexes.

The number of ways of arranging the $(i+1)^{th}$ polymer molecule on the lattice along with its associated solvent is given by

$$\nu_{i+1} = [N - ix(1+\mu\alpha)]\{(z-1)(1-f_i)\}^{x-1}\left(\frac{x!}{(x-\alpha x)!(\alpha x)!}\right) \qquad \textbf{(3- 54)}$$

where f_i is the probability that the lattice site is occupied by a segment of the previously placed i polymer molecules or one of their associated solvent molecules. f_i can be expressed as:

$$f_{i=}\frac{ix(1+\mu\alpha)}{N} \qquad \textbf{(3- 55)}$$

The term $\left(\frac{x!}{(x-\alpha x)!(\alpha x)!}\right)$ accounts for the number of ways of selecting αx associated segments from x segments in a polymer molecule. Substituting f_i into equation 3-54, we have

$$\nu_{i+1} = (z-1)^{x-1}\frac{[N-ix(1+\mu\alpha)]^x}{N^{x-1}}\left(\frac{x!}{(x-\alpha x)!(\alpha x)!}\right) \qquad \textbf{(3- 56)}$$

The total number of ways of arranging N_2 polymer-solvent complexes is given by

$$\Omega_{complex} = \left(\frac{\prod_{i=1}^{N_2}\nu_i}{N_2!}\right)\left(\frac{N_1!}{(\mu\alpha x N_2)!(N_1-\mu\alpha x N_2)!}\right) \qquad \textbf{(3- 57)}$$

Combining equation 3-56 and 3-57

$$\Omega_{complex} = \frac{1}{N_2!}\left(\frac{(z-1)^{N_2(x-1)}}{N^{N_2(x-1)}}\right)\left(\frac{x!}{(x-\alpha x)!(\alpha x)!}\right)^{N_2}(x(1+\alpha\mu))^{xN_2}$$
$$\left(\frac{\left(\frac{N}{x(1+\mu\alpha)}\right)!}{\left(\frac{N}{x(1+\mu\alpha)}-N_2\right)!}\right)\left(\frac{N_1!}{(\mu\mu\alpha x_2)!(N_1-\mu\alpha x N_2)!}\right) \qquad \textbf{(3- 58)}$$

The remaining unassociated solvent molecules can be inserted into the lattice only one way because all the other lattice cells are occupied by associated solvent and solute molecules. Hence:

$$\Omega_{unassoc} = 1 \qquad \textbf{(3- 59)}$$

In this way, the distributions of the polymer-solvent associated complex and the unassociated solvent are calculated. The total number of ways of forming the solution is

$$\Omega_{solution} = \Omega_{complex}\Omega_{unassoc} \qquad \textbf{(3- 60)}$$

For pure polymer, $\alpha = 0, \mu = 0, N_1 = 0 \; and \; N = xN_2$; thus

$$\Omega_{polymer} = \left[\frac{(z-1)^{(x-1)N_2}}{N_2!}\right]\left[\frac{x^{N_2 x}(N_2!)^x}{(xN_2)^{N_2(x-1)}}\right] * (1) = \left[\frac{(z-1)^{(x-1)N_2}}{N_2!}\right]\left[\frac{x^{N_2 x}(N_2!)^x}{(xN_2)^{N_2(x-1)}}\right] \qquad \textbf{(3- 61)}$$

For pure solvent, $\alpha = 0, \mu = 0, N_2 = 0 \; and \; N = N_1$, since all the solvent molecules in the pure and unassociated form are not different from each other, then the number of ways of arranging the pure solvent molecules into a lattice is only one. Thus:

$$\Omega_{solvent} = 1 \qquad \textbf{(3- 62)}$$

Using Sterling's approximation, ln N! = N ln N –N, we can calculate the entropy change of mixing by inserting these values into the equation for entropy. Thus:

$$\frac{\Delta S_m}{nR} = -\frac{\Phi_2}{x}\ln\Phi_2 - \left(\frac{1-\Phi_2(1+\mu\alpha)}{(1+\mu\alpha)}\right)\ln\{1-\Phi_2(1+\mu\alpha)\} + \Phi_1\ln\frac{\Phi_1}{\Phi_1-\mu\alpha\Phi_2} \\ -\mu\alpha\Phi_2\ln\frac{\mu\alpha\Phi_2}{\Phi_1-\mu\alpha\Phi_2} - \Phi_2(1-\alpha)\ln(1-\alpha) - \alpha\Phi_2\ln\alpha \qquad \textbf{(3- 63)}$$

Enthalpy of mixing

Enthalpy of mixing can be calculated from the total number of interactions in the lattice due to association and dispersion. For each polymer chain, there are αx associated segments and *(1-α) x* unassociated segments. The associated segments have *(z-2-μ)* neighbors of the unbound solvent and unassociated segments have *z-2* neighbors of the unbound solvent. Thus, the number of unassociated contacts for N_2 associated polymer molecules is:

$$xN_2\{1-\Phi_2(1+\alpha\mu)\}[(z-2-\mu)\alpha+(1-\alpha)(z-2)] \qquad \textbf{(3- 64)}$$

where $\{1-\Phi_2(1+\alpha\mu)\}$ is the volume fraction of the unassociated solvent. The volume fraction of the unbound solvent is used to account for the fact that a fraction of the neighboring sites is occupied by polymer segments. Also, the total number of associated contacts for N_2 polymer molecules is $\alpha\mu xN_2$.

The enthalpy change of mixing of polymer solutions can be calculated by multiplying the number of associated/unassociated contacts with their energies:

$$\Delta H_m = \alpha\mu x N_2 \Delta u_a + x N_2 \{1 - \Phi_2(1+\alpha\mu)\}[(z-2-\mu)\alpha + (1-\alpha)(z-2)]\Delta u_u \quad \textbf{(3- 65)}$$

and

$$\chi_a = \frac{\Delta u_a}{RT} \quad , \quad \chi_u = \frac{\Delta u_u}{RT} \quad \textbf{(3- 66)}$$

Then:

$$\frac{\Delta H_m}{RT} = \alpha\mu\Phi_2\chi_a + \Phi_2\{1-\Phi_2(1+\alpha\mu)\}[(z-2-\mu)\alpha + (1-\alpha)(z-2)]\chi_u \quad \textbf{(3- 67)}$$

Here Δu_a is the interaction energy per associated contact and Δu_u is the interaction energy per unassociated contact; χ_a and χ_u are interaction and dispersion parameters, respectively.

Gibbs Energy of mixing

Now that enthalpic and entropic changes for the solution have been obtained, the Gibbs energy of mixing can be obtained using the relation

$$\Delta G_m = \Delta H_m - T\Delta S_m \quad \textbf{(3- 68)}$$

Thus:

$$\frac{\Delta G_m}{nRT} = \alpha\mu\Phi_2\chi_a + \Phi_2\{1-\Phi_2(1+\alpha\mu)\}[(z-2-\mu)\alpha + (1-\alpha)(z-2)]\chi_u + \frac{\Phi_2}{x}\ln\Phi_2 + \left(\frac{1-\Phi_2(1+\mu\alpha)}{(1+\mu\alpha)}\right)\ln\{1-\Phi_2(1+\mu\alpha)\} - \Phi_1\ln\frac{\Phi_1}{\Phi_1-\mu\alpha\Phi_2} + \mu\alpha\Phi_2\ln\frac{\mu\alpha\Phi_2}{\Phi_1-\mu\alpha\Phi_2} + \Phi_2(1-\alpha)\ln(1-\alpha) + \alpha\Phi_2\ln\alpha \quad \textbf{(3- 69)}$$

Model parameters

The gART-L model requires knowledge of three parameters: the equilibrium constant K, and two interaction parameters related to association (χ_a) and dispersion (χ_u). The specific binding ratio μ is also a parameter but is assumed to be unity in this work because the systems that have been modeled contain molecules which are capable of associating only with a single functional group. The following sections describe the methods used by Sukhadia (1999) and Variankaval (2001) to show how these parameters may be obtained at a given temperature and composition of the solution.

Equilibrium Constant K and Specific Interaction parameter χ_a

The equilibrium constant K can be determined from the relative amounts of associated and unassociated species in a solution at different temperatures, obtained by spectroscopic measurements. This yields the equilibrium constant, which is related to the enthalpy of association via the van't Hoff equation:

$$K = A\,exp\left(\frac{-\Delta H_a}{RT}\right) \qquad \textbf{(3- 70)}$$

and

$$ln\frac{K}{K_0} = \frac{-\Delta H_a}{R}\left(\frac{1}{T} - \frac{1}{T_0}\right) \qquad \textbf{(3- 71)}$$

where K_0 is the equilibrium constant for association at a reference temperature T_0 (say, 300 K). Also, ΔH_a is assumed to be independent of T, based on spectroscopic evidence that the enthalpy of interaction does not change in the temperature range studied (Sukhadia, 1999). Thus, K can be calculated at any temperature using this relationship if the energy of interaction and equilibrium constant for association at a reference temperature are known.

Methods using IR, NMR, and Raman spectroscopy have been proposed for estimating the energy of interaction and equilibrium constant for association (Joesten and Schaad, 1974). Molecular simulations provide an alternative to spectroscopy in estimating these parameters; intermolecular interactions between molecules can be estimated through the use of established force fields. Sukhadia (1999) used the CVFF (Consistent Valence Force-Field) relationship, and simulated the solution by placing the solute and the solvent molecules in an amorphous cell with periodic boundary conditions. The relaxed structure was then used to calculate pair correlations and hence the equilibrium constant for association. This gives the number of interacting pairs. The pair correlation function is defined as

$$g_{ij}(r) = \frac{dn_{ij}(r)/dV}{N_{ij}/V} \qquad \textbf{(3- 72)}$$

where N_{ij} is the total number of *ij* pairs in the system, V is total volume of the amorphous cell and $n_{ij}(r)$ is the number of *ij* associated pairs at a distance r, the radius of the first interaction shell. After rearranging the relation above

$$n_{ij}(r) = \frac{N_{ij}(r)}{V}\int_0^r g_{ij}(r)4\pi r^2 dr \qquad \textbf{(3- 73)}$$

In a system containing xN_2 polymer segments, and N_1 solvent molecules of which $n_{ij}(r)$ are associated, the equilibrium constant can be calculated from

$$K = \frac{\left(\frac{n_{ij}(r)}{N_1 + xN_2 - n_{ij}(r)}\right)}{\left(\frac{xN_2 - n_{ij}(r)}{N_1 + xN_2 - n_{ij}(r)}\right)\left(\frac{N_1 - n_{ij}(r)}{N_1 + xN_2 - n_{ij}(r)}\right)} \qquad \textbf{(3- 74)}$$

This relationship was used by Sukhadia to obtain the equilibrium constant at several temperatures. The specific interaction energy was then estimated from the slope of ln K versus 1/T.

The equilibrium constant at a desired temperature can be used to calculate the association ratio at that temperature and concentration using

$$K = \left(\frac{\alpha}{1-\alpha} \right) \left(\frac{1-\mu\alpha\Phi_2}{\Phi_1 - \mu\alpha\Phi_2} \right)^{\mu} \qquad \textbf{(3- 75)}$$

where μ is assumed to be 1 (single association between solute molecule/segment and solvent). Hence:

$$\alpha = \frac{(1+K) - \sqrt{(1+K)^2 - 4\Phi_1\Phi_2 K(1+K)}}{2\Phi_2(1+K)} \qquad \textbf{(3- 76)}$$

Equilibrium constants and interaction enthalpies obtained by Sukhadia (1999) for several systems are given by in Table 3-1.

Dispersion Interaction Parameter χ_u:

The dispersion interaction parameter can be calculated using the regular solution theory of Hildebrand and Scott (1950). In order to use this concept for dispersion, the solute molecule is converted to a representative non-polar molecule through appropriate substitution for the group that provides the interaction with the solvent. The solubility parameter of this non-polar analog and the solvent are designated as δ^*_{solute}, and $\delta_{solvent}$, respectively. Replacing the enthalpy term with the dispersion interaction given in the model, we have

$$\chi_u = \frac{V_{solvent}(\delta_{solvent} - \delta^*_{solute})^2}{RT(z - \mu\alpha - 2)} \qquad \textbf{(3- 77)}$$

where z is the coordination number, α is the ratio of association and $V_{solvent}$ is the volume of the solvent.

The solubility parameters can be calculated using the group contribution method (Danner and Daubert, 1990), in which each group is assigned a molecular volume (V_i) and enthalpy of vaporization (ΔE_v) and

$$\delta_i = \left(\frac{\sum_i \Delta E_{iv}}{\sum_i V_i} \right)^{1/2} \qquad \textbf{(3- 78)}$$

The nonpolar analog and calculated dispersion parameters used for the systems investigated by Sukhadia (1999) are given in Table 3-2.

Gibbs Energy versus composition curves using the gART-L model at different temperatures were used to construct phase diagrams and obtain phase separation temperatures of several systems. Parameters used in these calculations are listed in Tables 3-1 and 3-2. A value of 10 for the coordination number and 1 for the binding ratio were used in all calculations.

Table 3- 1 Parameters obtained from MD simulation by Sukhadia (1999).

System	**Specific Interaction Energy** (ΔH_a)(kJ/mol)	**Equilibrium Constant (K_0) @ 300 K**
PIPA-Water	-14.686	0.97
PAN-Water	-8.410	3.49

Table 3- 2 Dispersion parameters and solute non-polar analog (Sukhadia, 1999).

System	Non-polar analog of the solute	Dispersion Interaction Parameter (χ_u) @ 300 K
PIPA-Water	$(-CH_2-CH_2-)_n$	1.16
PAN-Water	$(-CH_2-CH_2-)_n$	1.16

Liquid-liquid phase separation temperatures were predicted for systems such as poly (isopropylacrylamide) (PIPA) – water, shown in Figure 3-2. PIPA is fairly soluble in water at room temperature and atmospheric pressure. Interest from the scientific and industrial community in PIPA has been growing especially in the last decade, since it has a large number of potential applications, including mobilization of enzymes and protein separation (Shild *et al*., 1990, 1991, 1992). It has become the most popular member of a class of polymers that possesses inverse solubility in aqueous solutions upon heating, a property that it shares with some other polymers capable of interacting through hydrogen bonding with water. Despite current interest in PIPA, accurate data concerning its phase equilibria in water are still scarce. The PIPA -water system is expected to show a LCST (Shild, 1992). The gART-L model predicts a LCST in agreement with experiment. On the other hand, the UNIFAC-FV model failed to predict an LCST even at very high temperatures.

Results of gART-L calculations and experimental data for the poly (acrylonitrile)-water or PAN-water system are shown in Figure 3-3. It is known that a single phase exists in this system in the range 5-10 weight percent PAN at 500 K (Frushour, 1997). Predictions show a single phase in this concentration region, which is consistent with experimental observations. The same system has been modeled with UNIFAC-FV model

by Sukhadia, who showed that the gART-L approach performed adequately, but the UNIFAC-FV model did not. The gART-L model predicts UCST phase behavior in this system, although this cannot be verified because of a lack of experimental data.

It is clear from the above discussion that only one model (SAFT) is available that accounts for both strong interactions and compressibility effects in polymer solutions. This model is complex and requires at least two adjustable parameters. The primary objective of this work is therefore to develop a model that is relatively simple and requires few adjustable parameters. The model must be able to make use of spectroscopic or molecular modeling techniques to estimate required parameters independent of any phase equilibrium measurements. It must be validated on a number of systems characterized by UCST and LCST phase behavior. Finally, the model must not be limited to ambient pressures. An extension of the gART-L model that can also account for compressibility of the solution is described that meets all the criteria outlined above.

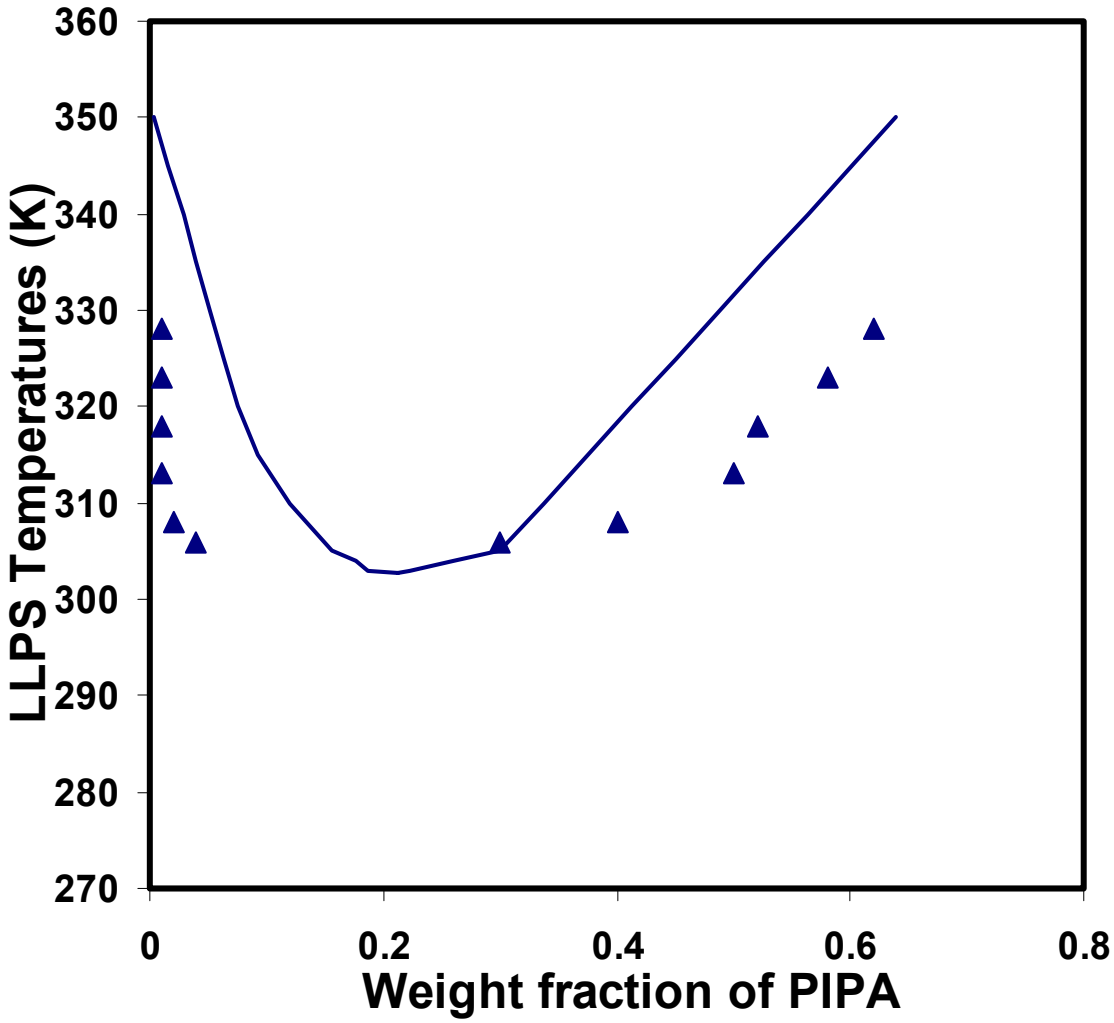

Figure 3- 2 Prediction of LCST of PIPA-water system. Experimental data taken from (Chee, 1997). The solid lines represent the calculation using the gART-L model. The triangles represent experimental values.

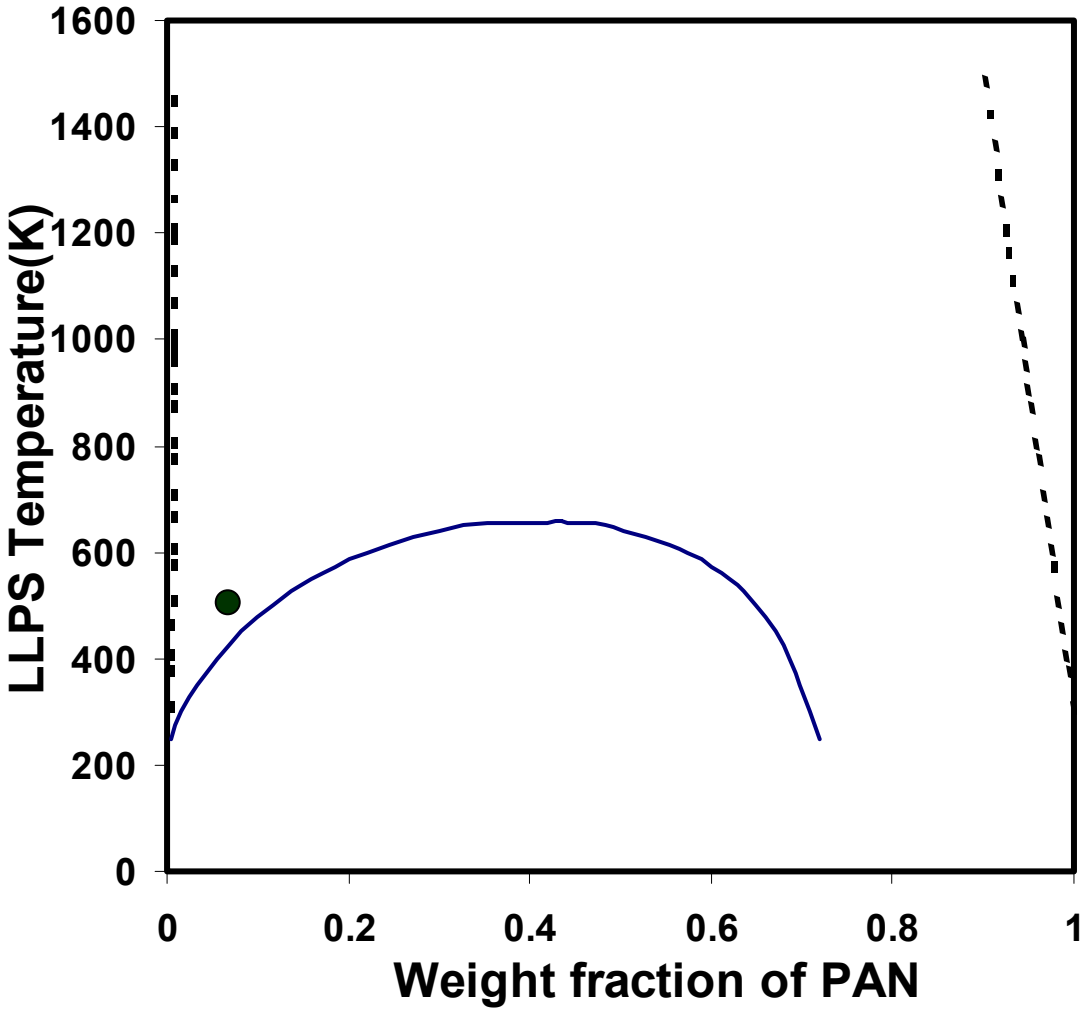

Figure 3- 3 Prediction of liquid-liquid phase separation temperatures of PAN-water system. Based on partial experimental data (Frushour, 1997), single phase exists at 500 K, ~5 wt%. The solid lines represent the calculations using the gART-L model. The dashes lines were calculated using the UNIFAC-FV model. The point is the experimental value.

CHAPTER 4

LATTICE-BASED EXTENDED LIQUID ACTIVITY COEFFICIENT (LELAC) MODEL

In this chapter, a new model is proposed to describe the phase behavior of associating polymer solutions at high pressures. This model extends the gART-L approach, which takes into account association between solute and solvent molecules, to solvents such as carbon dioxide that are compressible and can interact with the polymer.

A modified gART-L model

Application of gART-L model results in the following expression for the Gibbs energy of mixing:

$$\frac{\Delta G_m}{nRT} = \alpha\mu\Phi_2\chi_a + \Phi_2\{1-\Phi_2(1+\alpha\mu)\}[(z-2-\mu)\alpha + (1-\alpha)(z-2)]\chi_u + \frac{\Phi_2}{x}\ln\Phi_2 + \left(\frac{1-\Phi_2(1+\mu\alpha)}{(1+\mu\alpha)}\right)\ln\{1-\Phi_2(1+\mu\alpha)\} - \Phi_1\ln\frac{\Phi_1}{\Phi_1-\mu\alpha\Phi_2} + \mu\alpha\Phi_2\ln\frac{\mu\alpha\Phi_2}{\Phi_1-\mu\alpha\Phi_2} + \Phi_2(1-\alpha)\ln(1-\alpha) + \alpha\Phi_2\ln\alpha \quad \textbf{(4- 1)}$$

The expression incorporates five characteristic quantities: the solvent-solute binding ratio μ;, the association ratio α; the segment ratio x,; and the specific interaction parameters for association and dispersion, χ_a and χ_u.

The binding ratio is assumed to be 1 throughout this work because the polymers investigated have, at most, a single functional group that is able to interact with CO_2.

The association ratio α is related to the equilibrium constant K of the association reaction ($P + \mu S \Leftrightarrow PS_{\mu}$) as follows:

$$\alpha = \frac{(1+K) - \sqrt{(1+K)^2 - 4\Phi_1\Phi_2 K(1+K)}}{2\Phi_2(1+K)} \qquad \textbf{(4- 2)}$$

where Φ_1 and Φ_2 are volume fractions of the polymer and solvent, respectively. K may be determined from the relative amounts of associated and unassociated species present in a solution via spectroscopy. Alternatively, it may be determined as described below.

The specific interaction parameter for association χ_a (or equivalently, the enthalpy of association ΔH_a) is obtained from the shift of the peak ($\Delta\nu$) in the FTIR spectrum of the functional group of the polymer that occurs when it is subjected to CO_2 pressure. Thus:

$$\Delta H_a = 0.9874\Delta\nu = RT\chi_a \qquad \textbf{(4- 3)}$$

The enthalpy of association is related to the equilibrium constant for the association reaction K via the van't Hoff equation:

$$ln\frac{K}{K_0} = \frac{-\Delta H_a}{R}\left(\frac{1}{T} - \frac{1}{T_0}\right) \qquad \textbf{(4- 4)}$$

where K_0 is the equilibrium constant for association at a reference temperature T_0 (say, 300 K). In the above expression, ΔH_a has been assumed to be independent of T over the small range of temperature of many studies (Kazarian *et al.,* 1996). K can therefore be calculated at any temperature if ΔH_a and K_0 are known.

The dispersion parameter χ_u is calculated from group contributions to the solubility parameter of the non-polar analog of the polymer. When calculating the solubility parameter, appropriate substitution must be made for the functional group in the polymer molecule which provides the strong interaction with the solvent.

The segment ratio x is generally obtained from the ratio of the molar volumes of the solvent and the solute at ambient conditions (Huggins, 1941; Flory, 1942). This somewhat arbitrary ratio works well for liquids, since liquid volumes are not significantly affected by pressure. However, at supercritical conditions, the molar volume of the solvent changes dramatically with pressure.

In order to extend the gART-L approach to high pressures, two approaches can be followed. The first approach is to take the derivative of the Gibbs energy of mixing with respect to pressure and equate it to the volume of change upon mixing (ΔV_m) as follows:

$$\left(\frac{\partial \Delta G_m}{\partial P}\right)_{T,x} = \Delta V_m \qquad \textbf{(4- 5)}$$

Swelling data for the polymer – CO_2 system may then be integrated to obtain Gibbs Energy of mixing as a function of pressure. However, integration requires swelling data from zero pressure to the system pressure which is seldom, if ever, available. Thus, this approach is very difficult to accomplish for the incorporation of the pressure effect.

Another approach is to incorporate the pressure dependence into the model parameters. The association ratio, equilibrium constant and enthalpy of interaction are independent of pressure as can be seen from the corresponding expressions for these quantities. The dispersion interaction parameter is dependent on the pressure via the variation of the solubility parameter of CO_2 with pressure. However, the pressure dependence is not as strong as the parameter x. This can be seen in the cloud point curve for poly vinyl acetate (PVAc)-CO_2 in Figure 4-1. ΔH_a of 3.9003 kJ/mol from spectroscopic measurements and K_0 of 4.381 from the fitting of the model are used for the calculation for this system. Note that a value of x that is obtained from actual molar volumes (which depend on pressure and temperature) gives a much better fit of the cloud point curve than the value of x obtained from the ratio of molar volumes at fixed conditions. A fixed "liquid molar volume" of 55 cm^3/mol for CO_2 (Shair and Prausnitz, 1961) was used in these calculations. However, the calculated CO_2 volumes at high temperatures and pressures are much larger than this value. The change in molar volumes with T and P must therefore be taken into account in the calculations. If polymer properties are obtained from the Tait EOS (1888) and CO_2 properties from the Patel-Teja equation of state (Patel and Teja, 1982), the effective number of segments x changes with pressure and temperature as shown in Figure 4-2 for the system PVAc-CO_2. As the pressure increases, there is an increase in x since the density of CO_2 increases more rapidly than the density of the polymer. The effect of temperature is not as large as the effect of pressure and leads to only a modest increase in x. The modified gART-L model incorporating the "compressible solution" is termed the Lattice-Based Extended Liquid

Activity Coefficient (or LELAC) model in this work. The application of the LELAC model to the calculation of phase equilibria and swelling is discussed below.

In the application of the LELAC model to polymer – CO_2 systems discussed below, a knowledge of two characteristic parameters (ΔH_a and K_0) is required. The remaining characteristic quantities in the model either have fixed values or they can be calculated from ΔH_a and K_0. If ΔH_a is obtained via FTIR spectra, then the model can be applied with one adjustable parameter K_0. If FTIR spectra are not available, then the model must be applied with two adjustable parameters (ΔH_a and K_0).

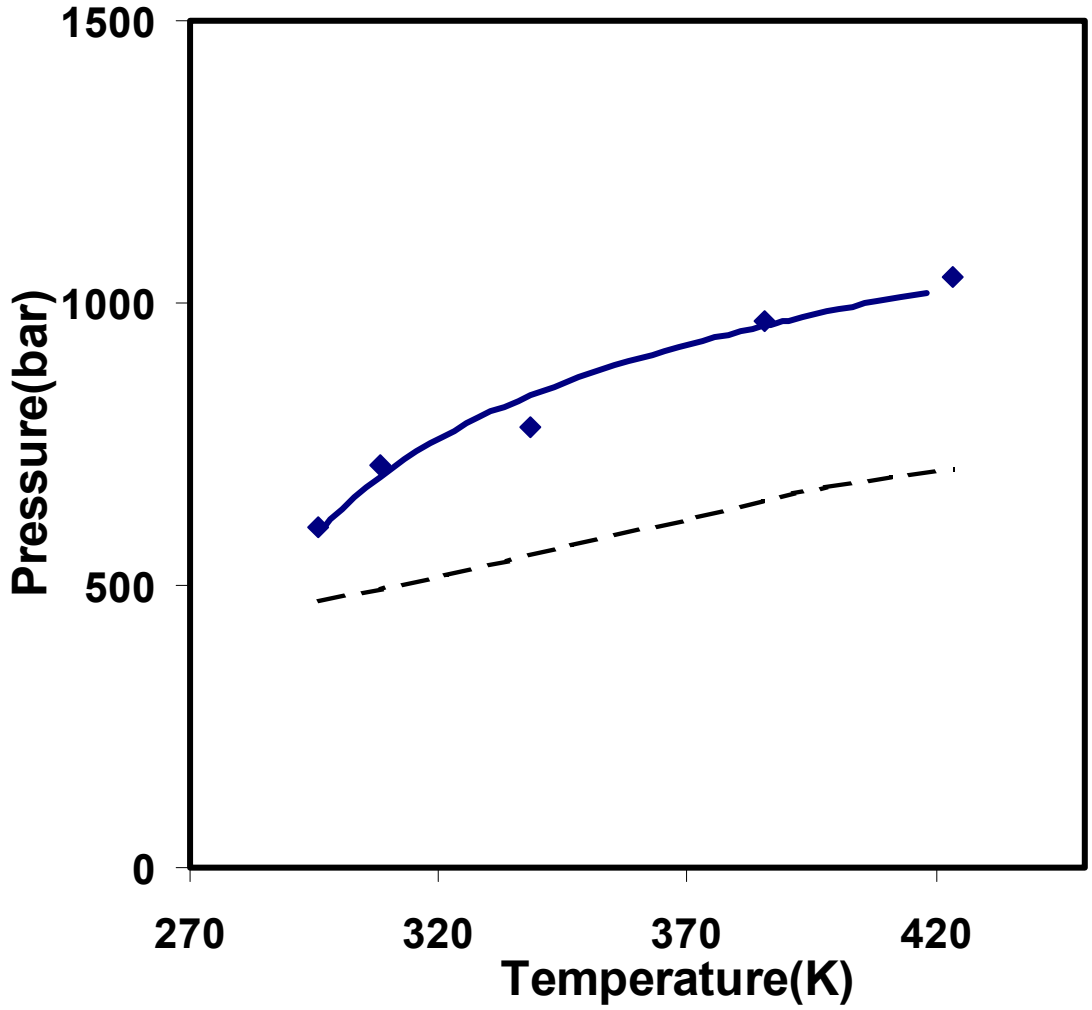

Figure 4- 1 Effect of the segment number x on calculated cloud points in PVAc – CO_2 . Points on the graph represent experimental values, whereas the solid lines represent LELAC calculations with x obtained from the actual molar volumes of the pure components. The dashed lines represent LELAC calculations with constant *x* (~1900) determined from the ratio of molar volumes of the components from Shair and Prausnitz, 1961.

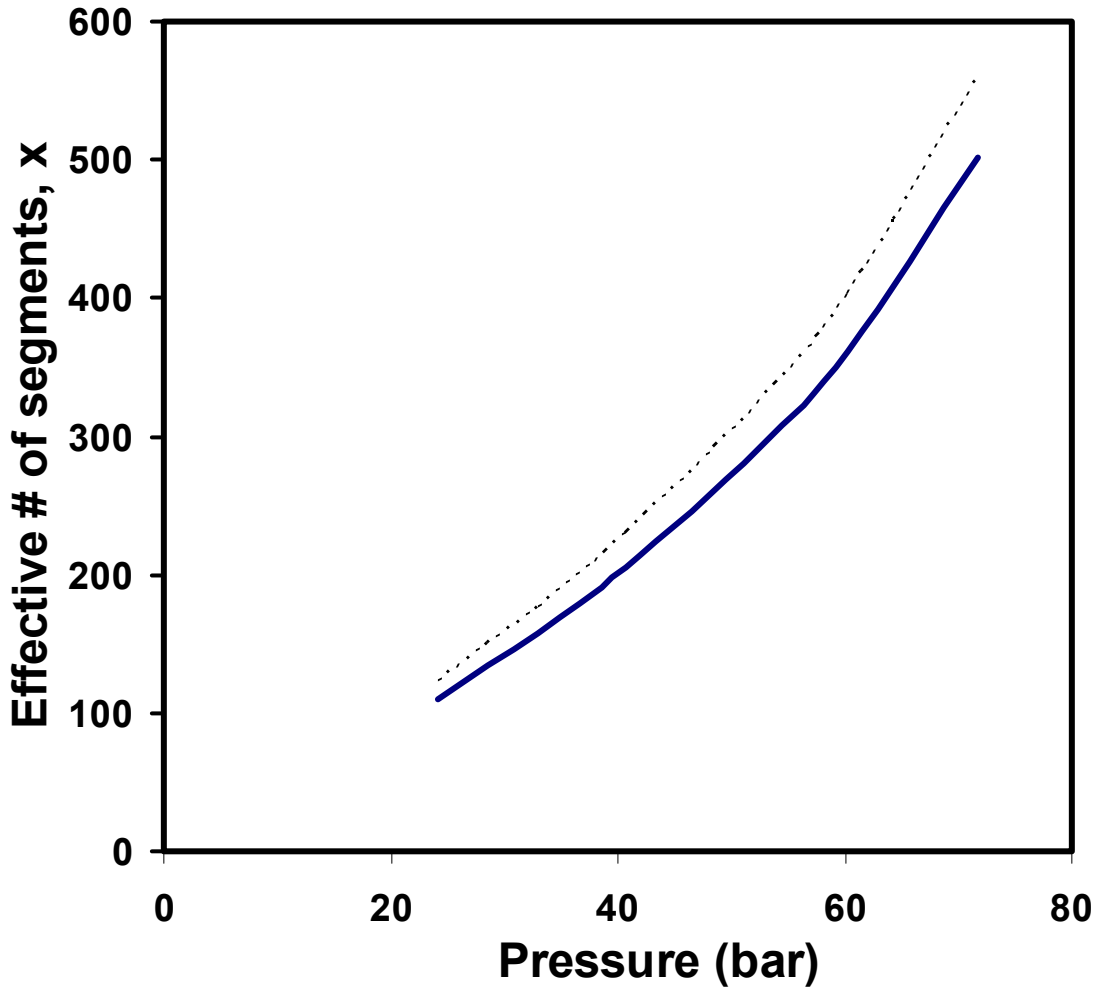

Figure 4- 2 The dependence of effective number of segments (for PVAc in PVAc-CO_2) on temperature and pressure. The solid lines represent x values at 313.15 K, and the dashed lines at 333.15 K.

Calculation of cloud point curves

A plot of the Gibbs Energy of mixing ΔG_m of a binary system as a function of composition at a fixed pressure and temperature is illustrated in Figure 4-3. At equilibrium, the Gibbs energy must be at a minimum, and hence $\Delta G_m < 0$. In addition, the Gibbs energy of mixing curve must be concave upwards at all compositions for the components to be completely miscible, and therefore $\frac{\partial^2 \Delta G_m}{\partial \Phi_p^{\,2}} > 0$. The system separates into two phases at temperatures where the curve exhibits two minima. Compositions of the two phases in equilibrium (B_1 and B_2 in Fig. 4-3) are obtained by drawing a tangent to the curve (Lupis, 1953), and applying the relation

$$\left[\frac{\partial \Delta G_m}{\partial \Phi_p}\right]_{B1} = \left[\frac{\partial \Delta G_m}{\partial \Phi_p}\right]_{B2} \qquad \textbf{(4- 6)}$$

Figure 4-4 illustrates the change in the ΔG_m vs composition behavior as the temperature is increased from T_1 to the upper critical solution temperature T_c. The system is completely miscible at temperatures above T_c and partially miscible from T_3 to T_1. The contact points of the common tangents to the minima in the ΔG_m vs composition curves are projected onto the temperature-concentration plane to form the binodal curve in Figure 4.4b. The projections of the inflection points form the spinodal curve, which defines the limit of the metastable region. For some systems, the binodal and spinodal curves can be concave upwards, which indicates LCST behavior. The phase diagram is obtained by plotting the phase separation temperatures versus the compositions of the two

phases in equilibrium. If the second derivative of the Gibbs energy with respect to the composition is calculated and equated to zero, the two spinodal compositions are obtained. Between these concentrations, the system is unstable to composition fluctuations and spontaneously separates into two phases (spinodal decomposition).

A similar procedure can be applied to generate pressure-composition curves at constant temperature, as illustrated in Figure 4-5. This figure shows a phase diagram that includes the binodal and spinodal boundaries. Stable, metastable, and unstable regions are also shown. The regions between the binodal and spinodal are metastable, where solutions are stable to small fluctuations in compositions, but undergo demixing in the case of large fluctuations. Inside the spinodal envelope, all fluctuations result in an increase in Gibbs energy. As a result, the solutions are unstable and demixing is spontaneous.

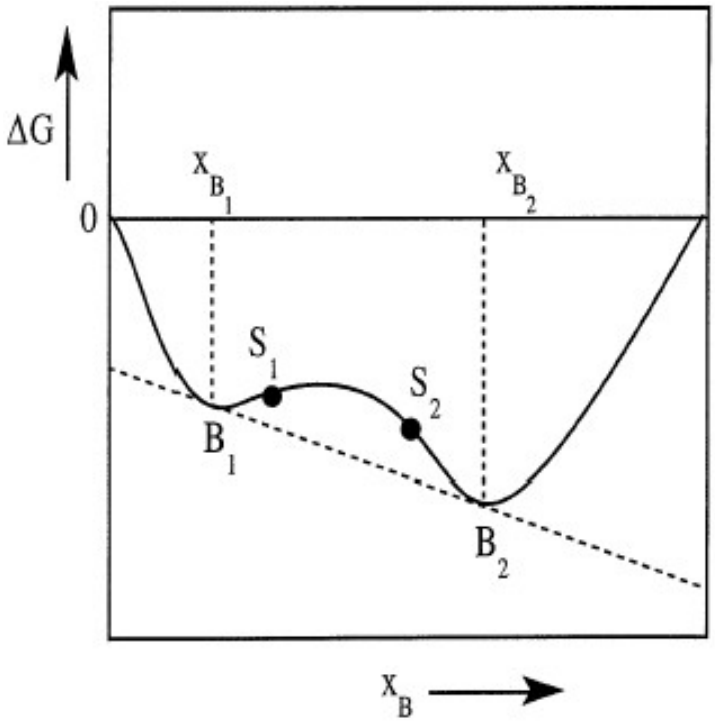

Figure 4- 3 The Gibbs energy of mixing as a function of composition at a temperature where the two phases with compositions x_{B1} and x_{B2} are in equilibrium.

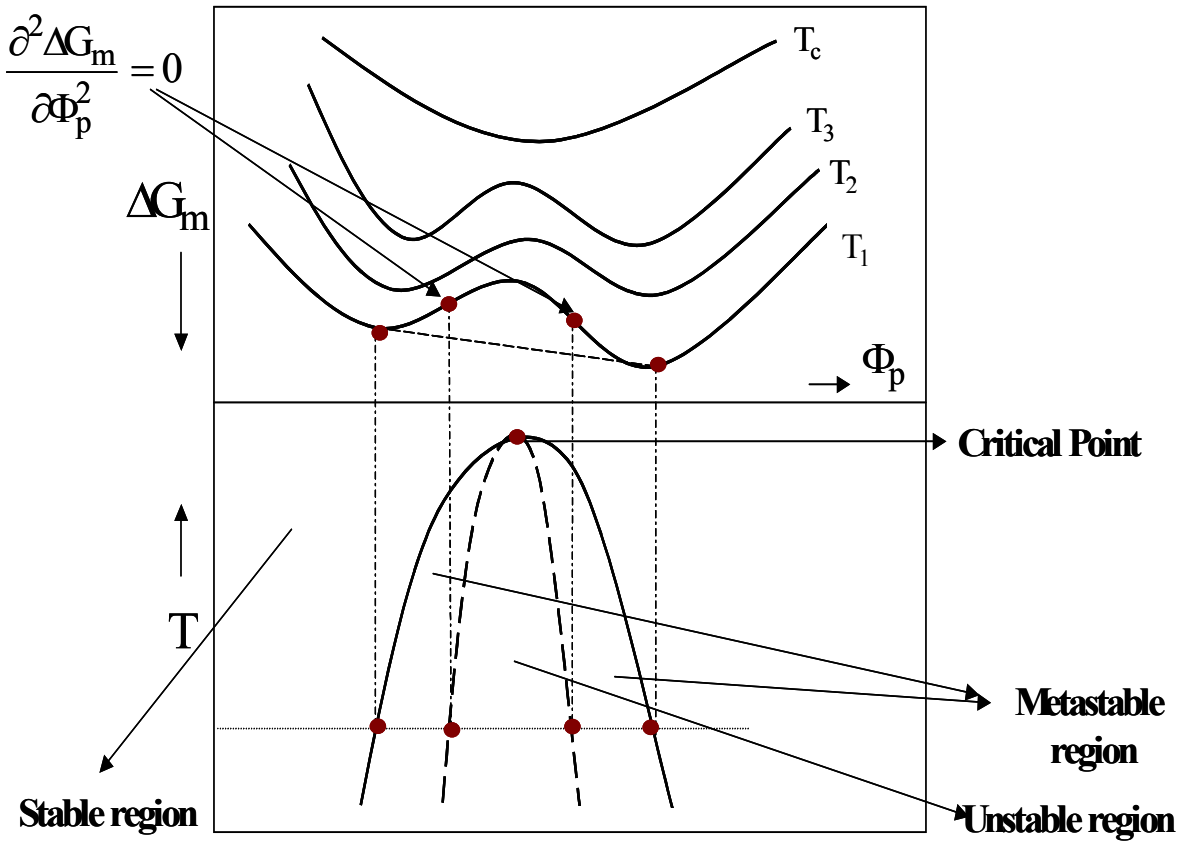

Figure 4- 4 The Gibbs Energy of mixing - composition behavior at increasing temperatures between T_1 and T_c (the Upper Critical Solution Temperature).

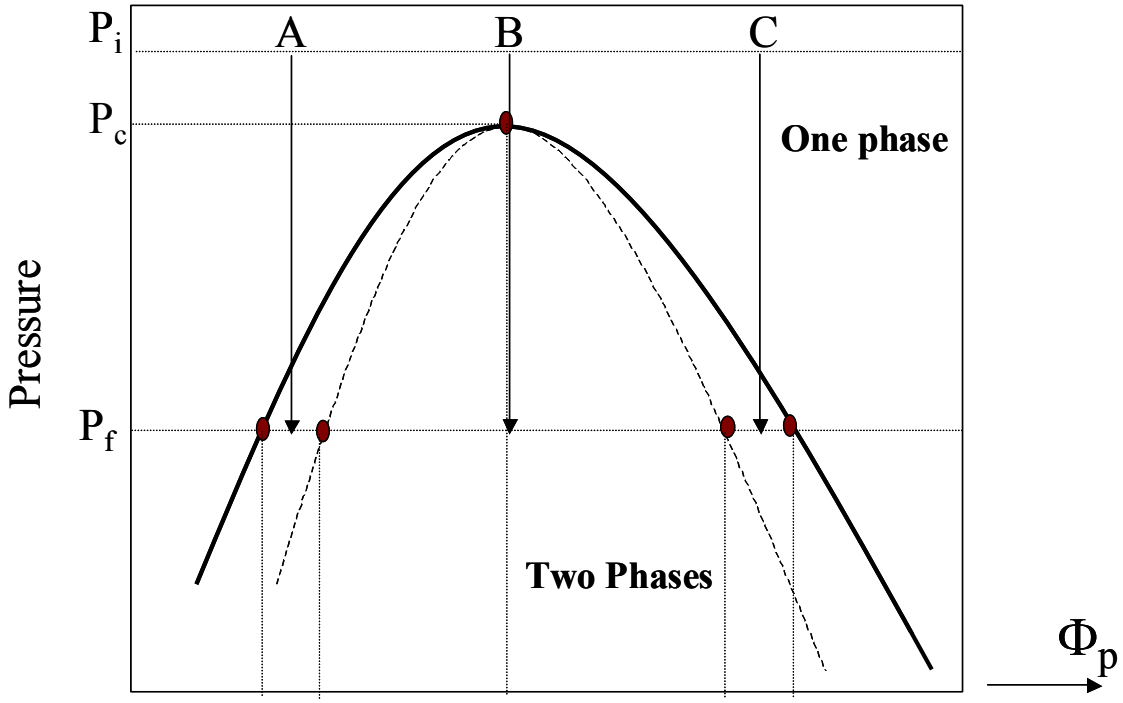

Figure 4- 5 Schematic illustration of pressure induced phase separation.

Equilibrium between two phases *L1* and *L2* requires that the fugacities of any component *i* be equal in the two phases , and therefore:

$$\hat{f}_i^{L1} = \hat{f}_i^{L2} \qquad \textbf{(4- 7)}$$

The fugacity of any component in a liquid phase (say *L1*) is related to its mole fraction x_i in that phase via:

$$\hat{f}_i^{L1} = \gamma_i x_i f_i^{L1(0)} \qquad \textbf{(4- 8)}$$

where γ_i is the activity coefficient of component *i* in that phase and $f_i^{L1(0)}$ is the fugacity of *i* at some arbitrary reference condition or standard state. Equation (4-7) can therefore be written as follows:

$$\gamma_i x_i^{L1} f_i^{L1(0)} = \gamma_i x_i^{L2} f_i^{L2(0)} \qquad \textbf{(4- 9)}$$

If the standard state is chosen to be the same in both phases, then the above equation for components 1 and 2 in the light (*l*) and heavy (*h*) phases reduces to:

$$\left[\gamma_1(x_1, T, P)x_1\right]^{(l)} = \left[\gamma_1(x_1, T, P)x_1\right]^{(h)} \qquad \textbf{(4- 10)}$$

and

$$\left[\gamma_2(x_2, T, P)x_2\right]^{(l)} = \left[\gamma_2(x_2, T, P)x_2\right]^{(h)} \qquad \textbf{(4- 11)}$$

in which the dependence of the activity coefficients on the temperature, pressure, and composition is indicated by the brackets. These equations may be solved for any two of the quantities T, P, $x_2^{(l)}$ and $x_2^{(h)}$. Note that this requires an expression for the activity coefficient of each component as a function of the temperature, pressure, and composition. The latter is provided by the LELAC model in this work.

Cloud point calculations using the LELAC model

If the composition in one of the phases (say the light phase $x_2^{(l)}$) is known, then the pressure and composition of the heavy phase ($x_2^{(h)}$) can be calculated at a given temperature using equations (4- 10) and (4- 11). Cloud point curves at constant concentration (isopleths) can therefore be calculated by repeating the calculations at different temperatures.

In the present work, the LELAC model is used to obtain activity coefficients, and experimental cloud point data are fitted using either K_0, or K_0 and ΔH_a as adjustable parameters depending on the availability of spectroscopic data (which yields ΔH_a) for the specific system. Values of the parameters obtained by such fitting are discussed in the next chapter. Note that the composition of the heavy phase is also obtained in these calculations, although this is rarely, if ever, reported in the literature.

Once K_0, or K_0 and ΔH_a are known, then cloud point behavior at compositions other than the composition used to obtain the parameters can be generated. In addition, UCST and LCST data can also be obtained. At a UCST or LCST, the binodal and spinodal curves merge into a single point defined by

$$\frac{\partial^2 \Delta G_m}{\partial \Phi_2^2} = 0 \qquad \textbf{(4- 12)}$$

and

$$\frac{\partial^3 \Delta G_m}{\partial \Phi_2^3} = 0 \qquad \textbf{(4-13)}$$

Hence, the pressure and composition at a UCST or LCST can be obtained by solving the above equations at a specified temperature. Thus the entire phase diagram can be obtained.

Calculation of the solubility of CO_2 in a polymer

For equilibrium between a fluid phase and a polymer phase, we may write:

$$\hat{f}_1^g(T,P,y) = \hat{f}_1^l(T,P,x) \qquad \textbf{(4- 14)}$$

where $\hat{f}_1^g$ is the fugacity of component *i* in the fluid phase and $\hat{f}_1^l$ is the fugacity *of i* in the polymer phase. In the case of CO_2 sorption in polymers at ambient conditions, it is appropriate to assume that the polymer does not dissolve in the CO_2 phase. Therefore, only the CO_2 partitions between the phases and the equality of fugacity condition can be written for CO_2 only. Since the fluid phase may be assumed to be pure CO_2, we may write:

$$\hat{f}_1^g(T,P) = \phi_1(T,P)P \qquad \textbf{(4- 15)}$$

and

$$\phi_1(T,P) = \frac{1}{RT}\int_0^P \left[v_1 - \frac{RT}{P} \right] dP \qquad \textbf{(4- 16)}$$

or

$$\phi_1(T,P) = \frac{1}{RT}\int_{v_1}^{\infty} \left[P - \frac{RT}{V} \right] dV - ln\left(\frac{Pv_1}{RT} \right) \qquad \textbf{(4- 17)}$$

An equation of state such as the Patel-Teja Equation of state (Patel and Teja, 1982) can now be used to obtain the fugacity coefficient.

The fugacity of CO_2 in the polymer phase can be determined using

$$\hat{f}_1^l(T,P,x) = x_1\gamma_1 f_1^{ol} \qquad \textbf{(4- 18)}$$

The liquid phase fugacity of CO_2, f_1^{ol} can be calculated using the correlation proposed by Prausnitz and Shair (1961). The expression for the activity $a_1 \left(= \gamma_1 x_1\right)$ of CO_2 can be obtained from the LELAC model and is given by

$$
\begin{aligned}
\ln a_1 &= \beta\mu\Phi_2\chi_a + \Phi_2\left[\left(-\Phi_2\beta\mu + \Phi_2(1+\mu\alpha)\right)(z-2-\mu) - \beta\mu\left(1-\Phi_2(1+\mu\alpha)\right)\right]\chi_u \\
&-\frac{\Phi_2}{x} + \left(\frac{1}{1+\mu\alpha} - \frac{\beta\mu}{(1+\mu\alpha)^2}\right)\ln\left(1-\Phi_2(1+\mu\alpha)\right) \\
&+\left(\frac{\left(1-\Phi_2(1+\mu\alpha)\right)}{(1+\mu\alpha)}\right)\left(\frac{1-\beta\mu\Phi_2}{1-\Phi_2(1+\mu\alpha)} - 1\right) - \ln\left(\frac{\Phi_1}{\Phi_1-\mu\alpha\Phi_2}\right) - 1 + \Phi_1\left(\frac{1-\beta\mu\Phi_2}{\Phi_1-\mu\alpha\Phi_2}\right) \\
&+\beta\mu\Phi_2\ln\left(\frac{\mu\alpha\Phi_2}{\Phi_1-\mu\alpha\Phi_2}\right) + \mu\alpha\Phi_2\left(\frac{\beta}{\alpha} - \frac{1-\beta\mu\Phi_2}{\Phi_1-\mu\alpha\Phi_2}\right) + \beta\Phi_2\ln\frac{\alpha}{1-\alpha}
\end{aligned}
\qquad \textbf{(4- 19)}
$$

where

$$
\beta = \frac{\alpha(K+1)-K}{(2\alpha\Phi_2-1)(K+1)} \qquad \textbf{(4- 20)}
$$

Therefore, the amount of CO_2 sorbed into a polymer can be calculated using the parameters K_0 and ΔH_a obtained by fitting cloud point data and/or spectroscopic measurements.

Conversely, these whole set of calculations can be done in an inverse way where sorption data are fitted using the equations above with the adjustable parameter(s) for the polymer system. Then, these adjusted parameters that are calculated using sorption data can be used predict cloud point data of these polymer systems. The results of such predictions are presented in Chapter 6. The use of FT-IR spectroscopy to obtain the enthalpy of interaction for several polymer-CO_2 systems is described in the next chapter. Then, the results of calculations of cloud point curves, pressure- composition and temperature- composition curves, as well as CO_2 solubility using the LELAC model are presented.

CHAPTER 5

IN SITU FT-IR SPECTROSCOPY OF POLYMER- SUPERCRITICAL CO_2 SYSTEMS

It has been suggested that CO_2 might serve as an electron donor (Hyatt, 1984) or as an electron acceptor (Hildebrand *et al*., 1970) in solution. The latter is consistent with the low basicity of CO_2 (Sigman *et al*., 1985); thus, one might expect Lewis acid-base interactions between CO_2 and other electron donors. Polymers containing basic groups represent excellent electron donor candidates and a series of polymers (basic and non-basic) subjected to CO_2 have been investigated in this work using FT-IR spectroscopy.

Fourier Transform Infrared (FT-IR) spectroscopy measures the dominant vibrations of functional groups and highly polar bonds. Thus these chemical 'fingerprints' are made up of the vibrational features of all the components in the sample. The spectrometer records the interaction of IR radiation with a sample, measuring the frequencies at which the sample absorbs the radiation and the intensities of the absorptions. Determination of these frequencies allows identification of the chemical makeup of the sample, since chemical functional groups are known to absorb light at specific frequencies. FT-IR experiments generally can be classified into the following two categories: Qualitative analysis- where the aim is to identify the sample and Quantitative analysis - where the intensity of absorption (or more commonly absorptions) is related to the concentration of the component.

Fourier Transform Infrared (FT-IR) spectroscopy is an excellent tool to probe the interaction between CO_2 and polymeric materials in terms of both qualitative and quantitative analysis due to the fact that it can be applied to high pressures as described by Gupta and Brinkley (1998), Berens *et al.* (1992), Chapman *et al.* (1996), and Vincent *et al.* (1997). The FT-IR method has some limitations because of absorptivity effects (Kazarian *et al.,* 1993), producing unpredictable changes in intensities. Also, the results from IR studies on specific interactions such as hydrogen bonding depend to a large extent on the type of system investigated. There are also some concerns with systems that have multiple associations (Coleman *et al*., 1996; Painter *et al.,* 1999). However, this problem should not occur in the systems investigated in the present study, because CO_2 and the polymers investigated do not self-associate to any appreciable extent (Kazarian *et al.,* 1996).

Experimental

Materials

Poly (methyl methacrylate) (PMMA), poly (2-vinyl pyridine) (P2VP), and polyvinyl chloride (PVC) were purchased as pellets from Polysciences, Inc.(Warrington, PA). Poly (vinyl acetate) (PVAc), poly(ethylene terephlate) (PET), poly(vinyl methyl ketone) (PVMK), low density poly(ethylene) (PE), poly(butylmethacrylate) (PBMA), and poly(ethylmethacrylate) (PEMA) were purchased from Aldrich Chemical Co. (St. Louis, MO). Poly(vinyl floride) (PVF) was supplied by Du Pont (Wilmington, DE) and Polystyrene (PS) by 3M (Minneapolis, MN). High-purity CO_2 (99.99 %) was purchased

from Matheson (Newark, NJ) and passed over molecular sieves to remove trace amounts of water and hydrocarbons.

Preparation of Films

The preparation of polymer films included compression molding (hot pressing), pretreatment, and CO_2 swelling. Since the diffusion process is sensitive to the thermal history of the polymer, great care was taken to ensure identical thermal histories for each film. The thermal profile utilized during compression molding of the polymers (in this example, PMMA) consisted of:

- Loading the mold with PMMA pellets and heating to 433.15 K;
- Pressing to 4000 psia after the polymer had melted;
- Holding the temperature constant for 5 minutes;
- Lowering the temperature to 378.15 K;
- Holding the temperature constant for 5 minutes;
- Lowering the temperature to 368.15 K;
- Holding the temperature constant for 5 minutes; and
- Quenching to room temperature.

Compression molding was performed using a Universal Film Maker (Spectra Tech, Madison, WI). The polymer films utilized in this work were 0.015, 0.035 and 0.077 cm thick.

Many polymers, such as PMMA, absorb significant quantities of water. Therefore, special attention was paid to the removal of water from the films. Pretreatment consisted of drying the polymer film and extracting residual monomer. The film was then sealed in an optical cell, dried by heating to 323 K and applying vacuum. The drying process took approximately 4 hours to eliminate all the water. Drying was followed by FT-IR spectroscopy to observe the disappearance modes of H_2O from the polymer film. Residual monomer was extracted by using carbon dioxide at 308 K and the pressure of the subsequent experiment. The extraction was also monitored by using FT-IR spectroscopy to observe the disappearance of the carbonyl of methyl methacrylate from the fluid phase as CO_2 was purged from the well mixed optical cell.

Transmission Spectra

A special high-pressure optical cell, described in the work of Kazarian *et al.* (1996) was constructed and is shown in Figure 5-1. The key feature of this cell is the use of two different paths for the IR beam through parallel pairs of IR windows. One path is used to measure the spectrum of the film subjected to CO_2, while the other is used to measure the spectrum of the fluid itself. The spectra of the fluid were subtracted from the spectra measured through the polymer and the fluid under identical high-pressure conditions to yield the required information on the gas absorbed by the polymer. Spectra could also be measured through each path separately by moving the cell within the spectrometer compartment. Additional details of this cell are presented in Appendix A. As noted in the Appendix, the cell is equipped with ZnSe and BaF_2 windows that allow observation of the ν_2 frequency spectral regions. It is very important to ensure that the

polymers of interest do not absorb strongly in the region of the CO_2 ν_2 mode. Fortunately, PMMA and all other polymers studied here exhibited little if any absorption in the region of interest. Finally, the path lengths were varied from 0.3 cm to 5.4 cm to suit the range of the measured polymer concentrations.

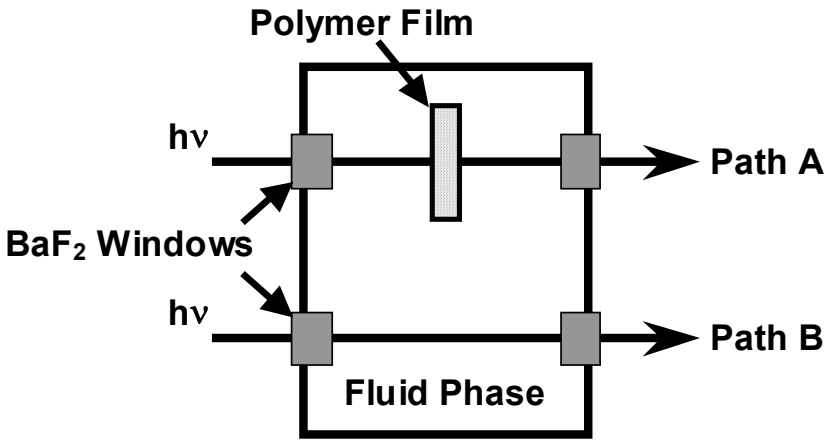

Figure 5- 1 Transmission FTIR cell used for studying specific interactions between polymers and supercritical CO_2. The polymer film is placed on one of the BaF_2 windows. The optical path length is ~ 4 mm.

In order to promote the diffusion of CO_2 into the polymer matrix, and to maintain uniform conditions inside the cell, the contents were stirred constantly during the experiment using two stir bars placed at the bottom of the cell. The temperature in the cell was measured using an Omega type- K thermocouple (Inxs Inc., Delray Beach, FL) in contact with the fluid. The pressure was read from a Druck pressure gauge DPI 260 and a Druck pressure transducer PCDR 4010 (Omega Engineering Co., Stamford, CT), connected to the cell via a short line of tubing. The temperature was controlled within 0.5

K by an Omega CN9000A temperature controller with six cartridge heaters (Omega Engineering Co., Stamford, CT). Carbon dioxide was introduced to the cell using an ISCO syringe pump, model 500D (Lincoln, NE).

Results

PMMA-CO_2

PMMA was chosen because its IR spectrum had been investigated in detail previously by many investigators (Kazarian *et al.,* 1993; Cooper *et al.*, 1993; Poliakoff *et al.,* 1995; Shim and Johnston*,* 1989; DeSimone *et al.,* 1994; Clark and DeSimone*,* 1995; Adamsky and Beckman, 1994). These investigators found that the most noticeable changes in the spectrum of PMMA were associated with the coupled vibration of the ester group when subjected to high-pressure CO_2. This produced two bands, ν_1 and ν_2, at 1270 cm^{-1} and 1240 cm^{-1}, respectively. The bands were also observed by Nagai (1963) and later confirmed by Havriliak and Roman (1966) who also showed that their origin lies in two rotational sites for the ester groups. The ratio of the magnitudes of heights of these two bands remains constant with changing temperature below the glass transition temperature (T_g) of the polymer, but varies at temperatures above T_g. The variation of the ratio results from changes in conformational energies, and thus provides evidence of polymer plasticization upon heating. Figure 5-2 shows the ν_1 and ν_2 bands of PMMA under vacuum, and after application of high-pressure CO_2. It can be seen clearly that CO_2 causes the ν_1 and ν_2 bands of the ester group of PMMA to change in relative intensity. The bands become narrower and a frequency shift occurs in the case of the ν_1 band. The changes observed in the spectra resemble changes seen when the polymer is heated in

vacuum and also when PMMA is dissolved in chloroform (Havriliak and Roman, 1966) indicating that the incorporation of CO_2 reduces non-specific intermolecular interactions between polymer chains. This result is consistent with previous findings that the CO_2 molecules interact with the oxygen atom of the carbonyl group in the form of a weak Lewis acid-base complex (Kazarian *et al.*, 1996). Such an interaction also reduces polar chain-chain interactions in which the ester group relaxes from its non-equilibrium state with a corresponding rotation around the C-C bond (see Figure 5-3).

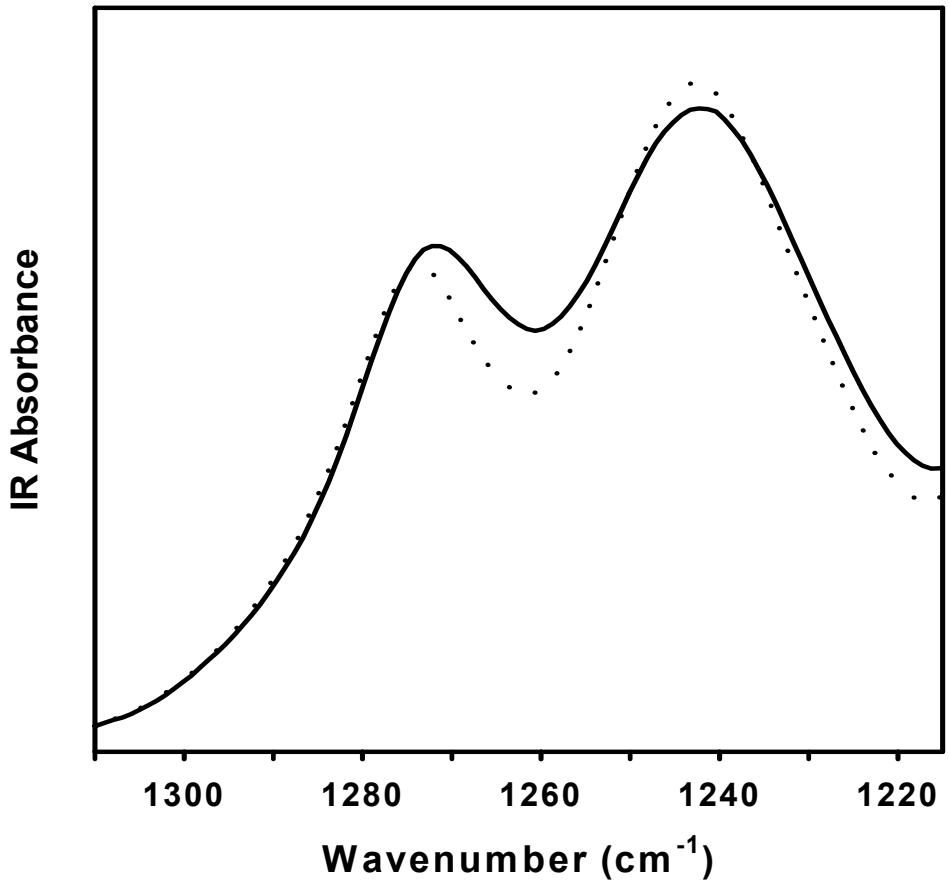

Figure 5- 2 The effect of added CO_2 (55.16 bar, 313 K) on the IR spectrum of PMMA film in the region of ester group vibrations. (i) PMMA film under vacuum (solid line), (ii) PMMA film subjected to CO_2 (dashed line).

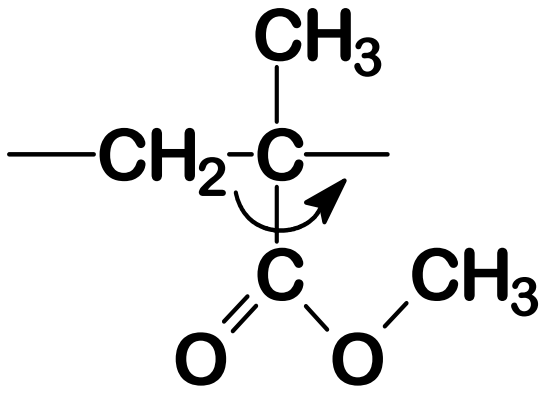

Figure 5- 3 Structure of repeating unit of PMMA. Plasticization allows the ester group to relax from its "frozen" non-equilibrium state with corresponding rotation around the C-C bond (proposed by Kazarian *et al*., 1997).

The spectral changes indicate that the effect of CO_2 on the vibration of the ester group is similar to that of conventional plasticizers, and is also similar to that observed on heating the polymer to its T_g, which increases the mobility of the ester group (Havriliak and Roman*.,* 1966, Briscoe and Thomas, 1995). By contrast, if CO_2 was to simply change the dielectric environment of the ester group, then a change in temperature would have much less effect on the relative intensities of the ν_1 and ν_2 bands even below the T_g of the polymer. Figure 5-4 shows the spectra of PMMA subjected to CO_2 at 313 K and 353 K. Increasing temperature causes an increase in the amount of the high-energy conformer, thus varying the ratio of band absorbances. This temperature dependence of the bands is strikingly similar to the spectral changes in PMMA above its T_g (Havriliak and Roman, 1966; Belopolskaya and Trapeznikova, 1971); however in this case, the presence of CO_2 allows the observation of plasticization at much lower temperatures. A blank experiment on the same film in the absence of CO_2 showed no temperature dependence for the bands within the range of 313 K - 353 K that provides the proof for molecular level interaction

of CO_2 with the polymer. The ν_2 mode splitting provides the only spectroscopic evidence of a specific CO_2-PMMA interaction. However, additional support for its characterization as a Lewis acid-base interaction has been obtained from experimental studies of several weak CO_2 complexes (Dobrowolski and Jamroz, 1992; Nxumalo *et al*., 1994).

These results indicate that the strength of the specific interaction of the carbonyl group of PMMA (electron donor) with CO_2 (electron acceptor) is not of the order of that of the hydrogen bond. It is difficult to obtain an exact measure of the strength in these experiments, although an estimate can be obtained. For example, since the ν (C=O) frequency of PMMA saturated with CO_2 is 1733 cm^{-1}, ν(C=O) is approximately 4 cm^{-1}. The interaction energy can be estimated from (Fowkes *et al.*, 1984):

$$\Delta H_a = 0.9874 \Delta \nu \qquad \textbf{(5- 1)}$$

where ΔH_a is in kJ/mol and ν is in cm^{-1}. This yields an enthalpy for the acid-base interaction of CO_2 with the PMMA carbonyl group of ~ 4 kJ / mol.

Similar arguments can be used to obtain the enthalpy for the acid-base interaction between CO_2 and other polymers. Table 5-1 presents the comparison of the experimental results in this work and Kazarian et al., 1996. The interaction energies calculated using equation 5-1 from the data are shown in Table 5-2. Also, the interaction parameters (χ_a) are shown in the same table at 353 K. The values of the interaction energy is within the same range of the energies tabulated for Lewis Acid- Base interactions by Joesten and Schaad (1974). When compared to the values of 7 -10 kJ/mol for typical hydrogen-

bonding systems, the magnitude of the calculated values are not as large as those values, however close for systems such as CO_2 with PMMA, PVMK,PVAc and PBMA.

Table 5- 1 Comparison of FT-IR frequency band shift results.

System	Frequency band shift (cm^{-1})(This work)	Frequency band shift (cm^{-1}) (Kazarian *et al.*, 1996)
PMMA- CO_2	4.02	4.00
PEMA- CO_2	4.13	4.15
PBMA- CO_2	3.86	3.85
PVMK- CO_2	4.54	4.55
PVC- CO_2	3.08	---
PVAc- CO_2	3.97	3.95
PVF- CO_2	2.34	2.35

Table 5- 2 Interaction Energies in Polymer-CO_2 systems via FT-IR spectroscopy.

System	Specific Interaction Energy (kJ/mol)	Specific Interaction Parameter (χ_a) at 353 K
PMMA- CO_2	-3.9496	-1.3457
PEMA- CO_2	-4.0977	-1.3962
PBMA- CO_2	-3.8015	-1.2953
PVMK- CO_2	-4.4927	-1.5308
PVAc- CO_2	-3.9003	-1.3289
PVF- CO_2	-2.3204	-0.7906

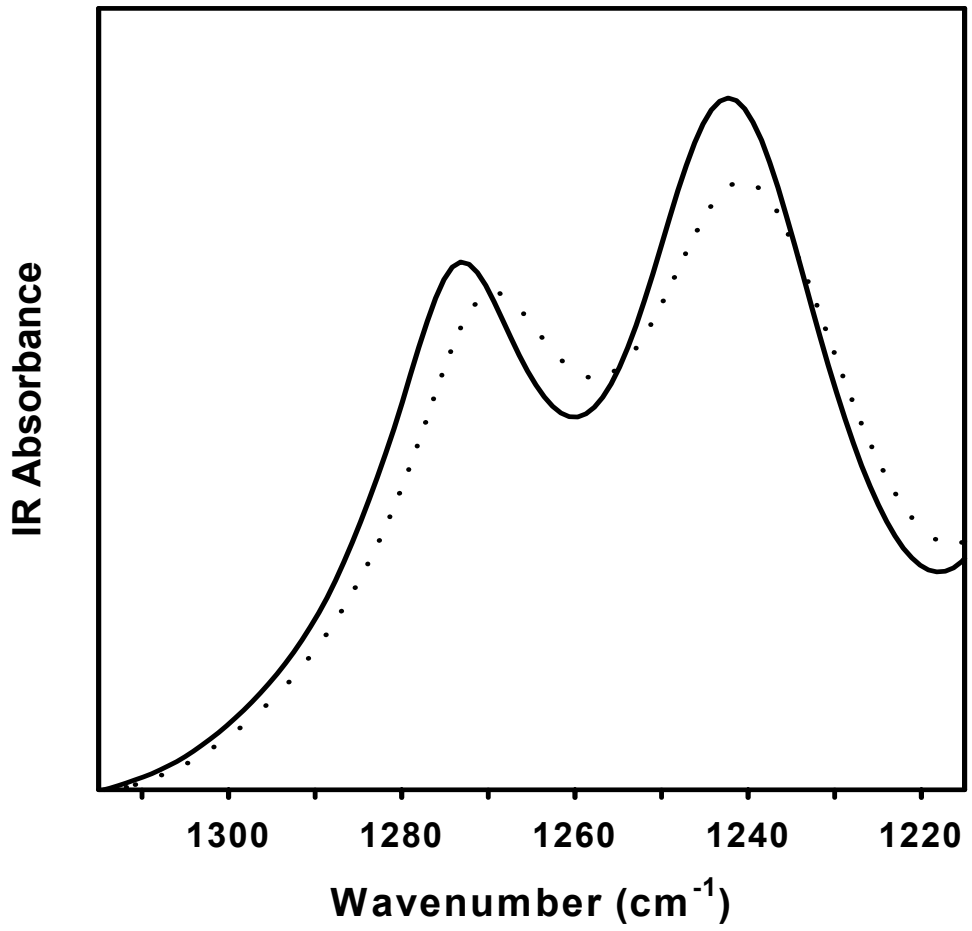

Figure 5- 4 The IR spectrum of PMMA exposed to CO_2 at 313 K (CO_2 pressure = 69 bar) (solid line); and 353 K (CO_2 pressure = 90 bar) (dashed line).

Poly (ethylmethacrylate)(PEMA)-CO_2 and Poly(butylmethacrylate)(PBMA)-CO_2

PEMA and PBMA are similar type of polymers which were found to interact with CO_2 (Kazarian *et al.,* 1996). The shift and splitting of the ν_2 bending mode of CO_2 trapped within these two polymers are almost identical to those seen in the case of PMMA. However, PEMA and PBMA have different glass transition temperatures (336 K and 300 K, respectively) so that PBMA was above its T_g at low CO_2 pressures, which led to significantly reduced rigidity of the polymer chains and thus faster desorption of CO_2. Nevertheless, the spectra of the incorporated CO_2 were similar to those observed in the case of PMMA and PEMA films.

Poly(vinylmethylketone)(PVMK)-CO_2

The degree of splitting of the ν_2 bending mode of CO_2 incorporated into PVMK films is nearly the same as in PMMA. The low-frequency shift of this doublet in comparison with the ν_2 mode of CO_2 was also similar. Thus, the suggestion that CO_2 interacts with the oxygen atom of the carbonyl group in PMMA (Kazarian *et al.,* 1996). is supported by this experiment, because there is no ester oxygen atom in PVMK.

Poly(vinylchloride)(PVC)-CO_2

A similar interaction was observed in the PVC–CO_2 system, in which there is no ester oxygen atom. A splitting of the band corresponding to the ν_2 bending mode was observed which increases with pressure, indicative of specific interactions between CO_2 and the basic vinyl groups (Figure 5-5). This interaction appears to be another Lewis

acid-base type in which the carbon atom of CO_2 acts as an electron acceptor, although the contribution of electrostatic forces cannot be excluded.

Figure 5-6 presents the temperature dependence of that interaction. As can be seen in the figure, the magnitude of the associated peak decreases with the temperature, which is typical of specific interactions such as H-bonding. The relative intensity of this frequency band also decreases with temperature, which means that the formation of this complex has an inverse dependence with temperature. Formation of this complex is responsible for the swelling and plasticization behavior of PVC (Chiou *et al.*, 1985, Shieh *et al.*, 1996) A possible mechanism for complex formation is depicted in Figure 5-7. It is postulated that the vinyl group first attracts an electron and forms a carbene complex that is very reactive. The carbene group then reacts with CO_2 to form another complex that, after rearrangement, results in a complex with a C≡O triple bond. The existence of this bond can be inferred from the 2070- 2100 cm^{-1} frequency band in the IR spectrum, as shown in reported spectra (Bell, 1972). Such a triple bond has not been observed in FT-IR spectra of the other polymer-CO_2 systems.

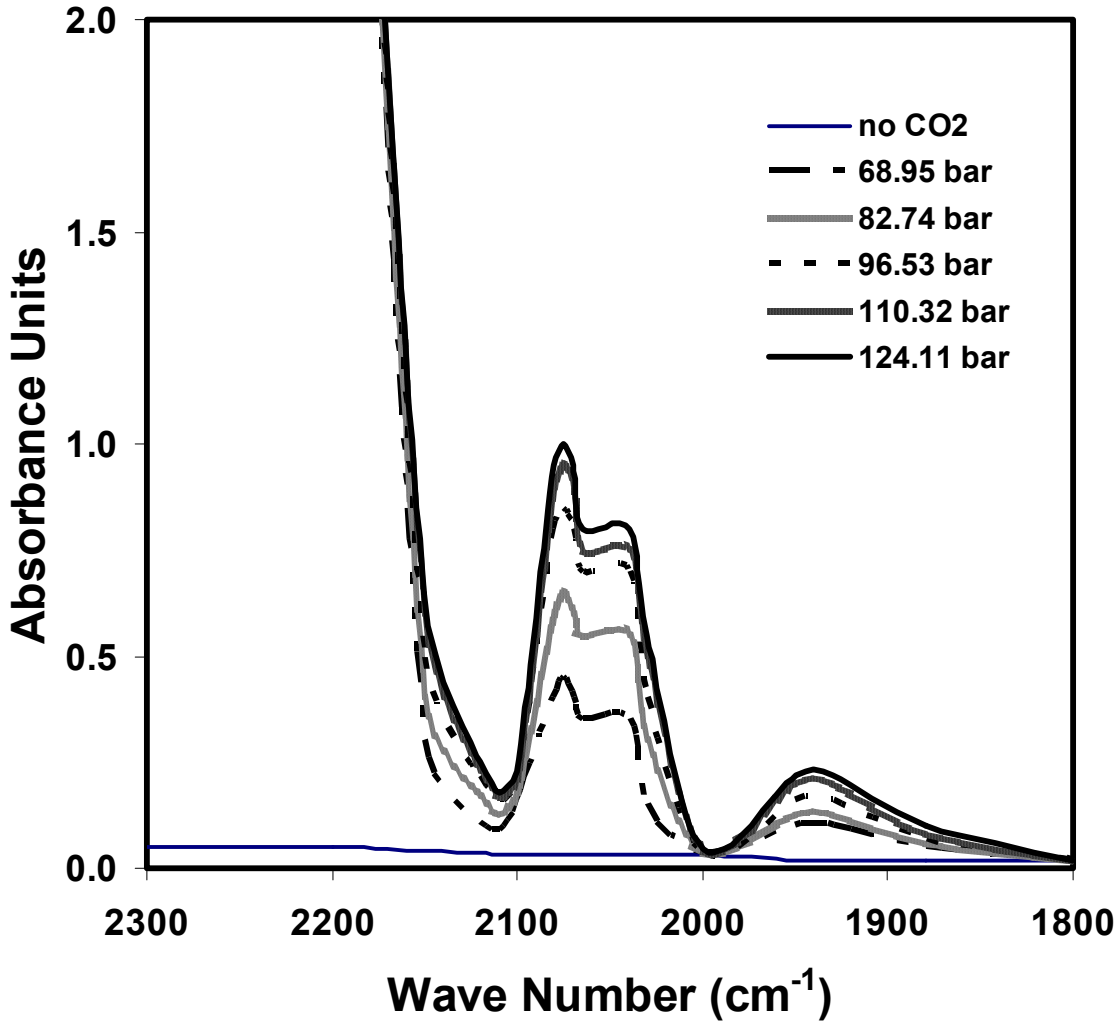

Figure 5- 5 FT-IR spectra of PVC-CO_2 system at pressures ranging from 69 bar to 125 bar.

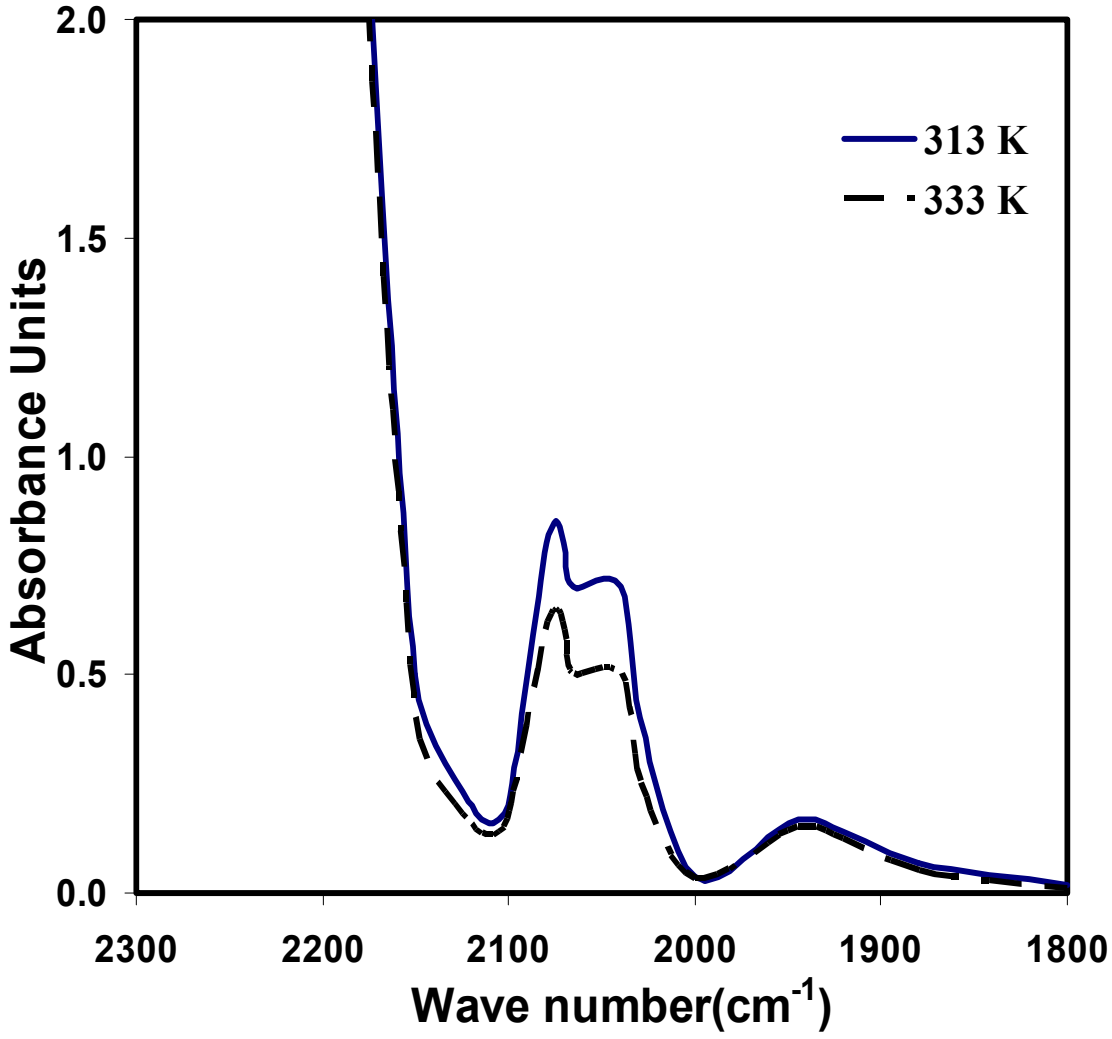

Figure 5- 6 FT-IR spectra of PVC-CO_2 systems at 313 K and 333 K.

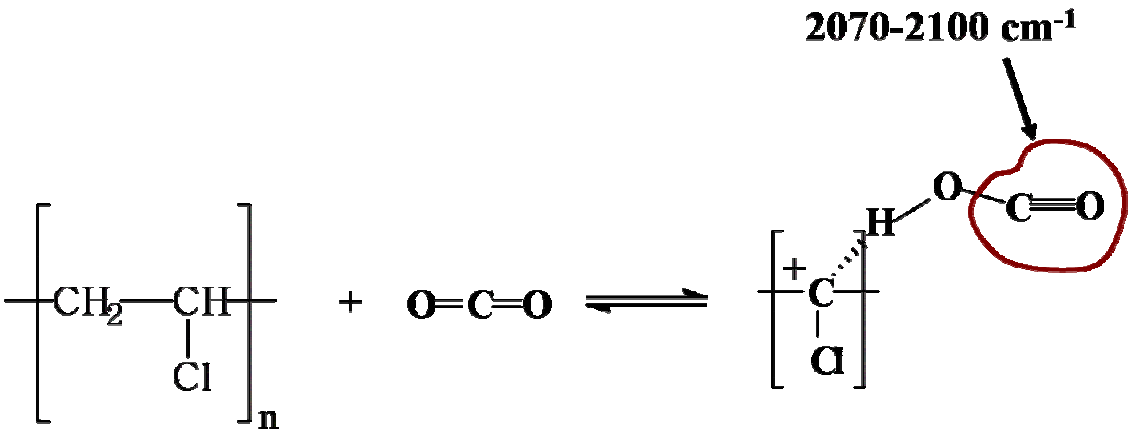

Figure 5- 7 Possible mechanism for complex formation in PVC-CO_2 systems.

Poly(vinylacetate)(PVAc)-CO_2

The splitting of the ν_2 mode was also observed in the case of PVAc. In this case, the amount of polymer-CO_2 species detected within the polymer film was rather small. This may be a result of inter- and intrapolymer interactions between carbonyl and amide groups (i.e., hydrogen bonding) that lead to a situation where neither of the basic sites in the polymer is readily available for specific interactions with CO_2. Apparently, H-bonding prevents the carbonyl groups from being available for interaction with CO_2. Nevertheless, the interaction between PVAc and CO_2 is comparable with the PMMA-CO_2 interaction.

Poly(vinylflouride)(PVF)-CO_2

The fluorine atoms in PVF constitute weak basic sites. Vincent *et al.* (1997) identified a difference in ν_2 modes of CO_2 incorporated into PE and PVF films. In the

case of PVF, only minor splitting of bands was observed in this work and confirmed by Kazarian *et al.* (1996). This result is properly due to weak electrostatic interaction of CO_2 with the C-F dipole in PVF. Very similar ν_2 band splitting of CO_2 (661 and 658 cm^{-1}) was observed for carbon dioxide clathrate hydrate at low temperature (Fleyfel and Devlin, 1991). However, different sites within the matrix were used to explain the splitting in that case.

Poly(ethylene terephthalate) (PET) - CO_2

PET is another polymer with at least two functional groups (the phenyl ring and the carbonyl group) that may interact with CO_2 (Vieth, 1991). The ν_2 band of CO_2 in PET film was indeed distorted and a doublet at 659 and 655 cm^{-1} was observed. The splitting of the band was somewhat smaller than in other carbonyl-containing polymers (e.g., PMMA or PVMK). Also, the presence of several basic sites in PET, together with its comprehensive microstructure and morphology (Vieth, 1991), makes assignment of the observed split a complicated task. Further studies are therefore necessary to resolve this matter.

Polyethylene (PE)- CO_2 and Polystyrene (PS) – CO_2

In the case of Polyethylene (PE) and Polystyrene, no ν_2 band splitting was observed consistent with the results from Kazarian *et al.* (1996). These polymers do not posses strong Lewis base sites. The ν_2 band of CO_2 in PS was broader than in the case of PE. This indicates some distortion of the bending mode consistent with weak electrostatic interactions of CO_2 with the π-system (phenyl ring) in PS (Nandel and Jain, 1984).

Discussion

The splitting of the ν_2 bending mode of CO_2 signifies interaction between the CO_2 and the polymers, and has been observed in a wide range of polymers in this work (Table 5-1) and by others. Analysis of the spectra reveals that mobility of the ester units increases with increasing pressure of CO_2. These results provide molecular level evidence for the CO_2-induced plasticization of polymers. The data measured in this work and the studies of Kazarian *et al.* provide strong evidence of the existence of specific intermolecular interactions between CO_2 and electron-donating polymer systems, in the form of an electron donor-acceptor complex. The results also suggest that CO_2 in most cases might act as an electron acceptor rather than as an electron donor (see also Quinn *et al.,* 1995). Finally, such interactions may increase the nucleophilicity of CO_2 oxygen atoms, which may have some relevance in catalysis if CO_2 is able to bind to metal centers (Jessop *et al*., 1995).

The view of CO_2 as an electron acceptor may provide additional insights into the behavior of solubility of polymers in supercritical CO_2. Although there are a limited number of polymers that are soluble in $scCO_2$ (fluoropolymers and dimethylsiloxane), few poly (acrylate)s do exhibit significant solubility (McHugh and Krukonis, 1989). Mawson and co-workers (Mawson *et al.,* 1995) have suggested that the interaction of CO_2 with polymers possessing acrylate groups may be of a Lewis acid-base nature and is related to the solubility. The interaction of CO_2 with dipoles of C-F bonds may play a role where poly (tetrafluoroethylene) can be soluble in $scCO_2$ at high enough pressures and temperatures (Tuminello *et al.*, 1993). Based on the solubility behavior of fluoropolymers, Shah and co-workers (1993) have also proposed specific CO_2-fluorine

interactions to explain the increased solubility of CO_2 in polymers containing fluorine groups.

CHAPTER 6

ESTIMATION OF POLYMER-SUPERCRITICAL CO_2 PHASE BEHAVIOR USING A LATTICE-BASED EXTENDED LIQUID ACTIVITY COEFFICIENT (LELAC) MODEL

This chapter presents results of phase equilibrium calculations involving binary polymer-CO_2 mixtures using the LELAC model. Cloud point curves have been calculated for systems that include PBMA - CO_2 and PVAc - CO_2, as well as CO_2 + a family of polyacrylates. The parameters obtained by fitting cloud point curves are then used to predict pressure- composition curves at different temperatures and temperature-composition curves at different pressures. Additionally, the solubility of CO_2 in these polymers is predicted using parameters obtained from cloud point curves at a single composition. Similar calculations are also performed for several other polymer systems that do not contain CO_2 as the solvent. Finally, an alternative procedure has been followed where sorption data have been correlated and the adjustable parameter obtained from this correlation has been used to predict the cloud point behavior of those solutions.

Correlation of cloud point behavior of polymer-CO_2 mixtures

Cloud point data of McHugh and co-workers (1996) for the systems PBMA-CO_2 and PVAc-CO_2 were correlated using ΔH_a values obtained from FTIR measurements described in Chapter 5. A single adjustable parameter K_0 was used to fit these data. Cloud point curves for a series of Polyacrylate – CO_2 systems were also correlated.

However, two adjustable parameters (ΔH_a and K_0) were used in these calculations because no spectroscopic measurements were available.

As outlined in Chapter 4, cloud point calculations involve equating the activities of the polymer and CO_2 in the two phases in equilibrium. Since experimental cloud point pressures and temperatures at a single concentration (5 wt % polymer in the "light" phase) have generally been reported in the literature, cloud point pressures and concentrations in the "heavy" phase were calculated at a series of temperatures by solving equations (4- 10) and (4- 11). As noted above, one or two adjustable parameters are required in the calculations, depending on the availability of spectroscopic data for the system. The calculations were repeated at different concentrations of the "light" phase, using the same values of the adjustable parameter(s).

Experimental and calculated cloud-point curves in the PBMA-CO_2 system are shown in Figure 6-1. The interaction energy ΔH_a in this system is estimated to have a value of ~ 4 kJ / mol from the peak shift in the FT-IR spectrum shown in Chapter 5. As can be seen in the figure, the data are fitted well using only one adjustable parameter. The two curves (for polymer M_W of 100,000 and 320,000) were calculated using the same value of the adjustable parameter, indicating that K_o does not apparently depend on the molecular weight. On the other hand, the molecular weight affects the segment fraction x via the molar volume of the polymer. As a result, the cloud-point curve for PBMA with M_w =100,000 is shifted by as much as 45 K relative to the cloud point curve of PBMA with a M_w = 320,000. This indicates that higher temperatures would be needed for CO_2 to solubilize the higher molecular weight PBMA.

Similar behavior is encountered in the PVAc - CO_2 system, as shown in Figure 6-2. Calculated results are in qualitative agreement with experimental data using one adjustable parameter, although the average error of 2.45 % is somewhat higher than the average errors in the previous system (0.47% and 0.88 %). In both systems, ΔH_a was obtained via FT-IR studies.

Cloud point curves in PBMA – CO_2, PVAc – CO_2 and other polymer – CO_2 systems were also calculated with the SAFT equation of state using two adjustable parameters. The results are given in Table 6-1 and plotted in Figures 6-1 and 6-2. The overall average deviation between experimental and calculated values was ~3.6%, whereas the corresponding deviation using the LELAC model was ~1.3%. Both these values are probably within experimental error, although it should be added that the LELAC model has one fewer adjustable parameter in the cases of PBMA-CO_2 and PVAC- CO_2 mixtures tabulated in Table 6-1.

Table 6- 1 Results of PBMA and PVAc-CO_2 systems using the LELAC and SAFT

Polymer	MW	T_g (K)	ΔH_a (kJ/mol)	K_0	LELAC AAD%	SAFT AAD%
PBMA	100,000	293	-3.8015	7.536	0.47	8.44
PBMA	320,000	293	-3.8015	7.536	0.88	4.83
PVAc	125,000	303	-3.9003	4.381	2.45	3.02

$$AAD\% = \frac{100}{NP}\sum abs\left(\frac{P_{calc} - P_{\exp}}{P_{\exp}}\right)$$

Table 6- 2 Results of Polymer-CO_2 systems using the LELAC and SAFT models.

Polymer	MW	T_g (K)	ΔH_a (kJ/mol)	K_0	LELAC AAD%	SAFT AAD%
PMA	31,000	282	-7.985	6.106	2.29	2.51
PBA	62,000	224	-5.624	5.088	0.59	2.66
PEA	120,000	250	-3.214	4.713	0.84	1.80
PEHA	113,000	218	-2.861	3.266	1.57	4.43
POA	23,000	NA	-2.413	2.745	1.21	1.47

The LELAC model was also used to calculate cloud points curves in poly (acrylate) – CO_2 systems. Two adjustable parameters were used in the calculations because spectroscopic data were not available for these systems. Figures 6-3, 6-4, 6-5, 6-6, and 6-7, along with Table 6-2 present comparisons between calculated and experimental cloud-point curves for poly (methyl acrylate) (PMA), polyethylacrylate (PEA), poly (butyl acrylate) (PBA), poly (ethylhexyl acrylate) (PEHA), and poly (octadecyl acrylate) (PODA) in CO_2. Also shown for comparison are SAFT calculations of McHugh *et al.*, (1999) for these systems. Both the models were able to correlate the data well, using the same number of adjustable parameters in each case. The fitted parameters are shown in Table 6-3 and are of the same magnitude as the parameters obtained for mixtures of PBMA or PVAc with CO_2. Moreover, the values of the interaction energy are similar to the energies tabulated for Lewis-Acid base interactions by Joesten and Schaad (1974). It is therefore possible to state that strong interactions between CO_2 and the polymer are likely to be found in polyacrylate – CO_2 systems.

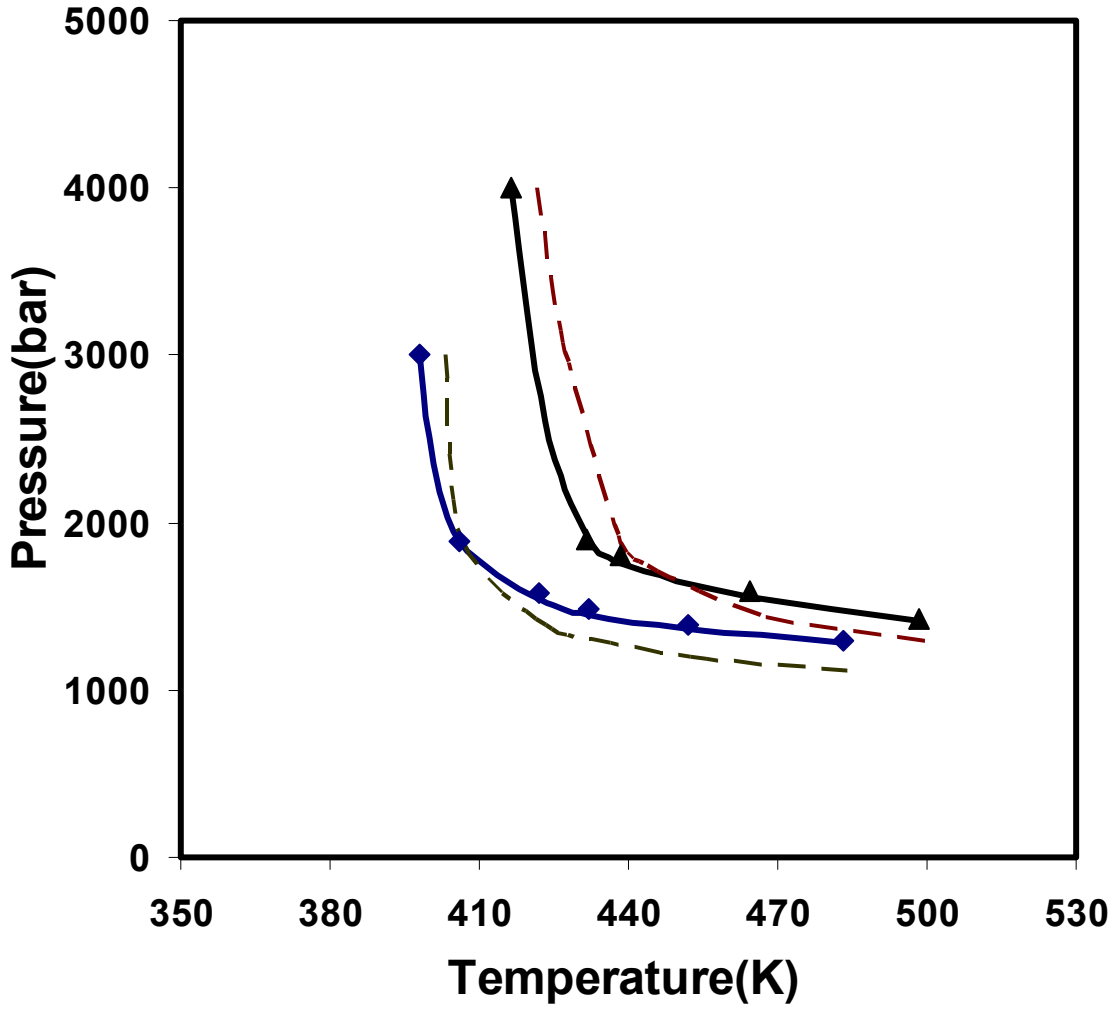

Figure 6- 1 Cloud point curves in the PBMA – CO_2 system. The solid lines represent LELAC calculations with ΔH_a=-3.8015 kJ/mol, and K_0=7.536. The dashed lines were calculated using the SAFT equation with u_0/k=202.0, k_{ij}=0.080 (MW= 100,000) and u_0/k=208.0, k_{ij}=0.074 (MW= 320,000). The points are the experimental values (Mc Hugh *et al.*, 1996).

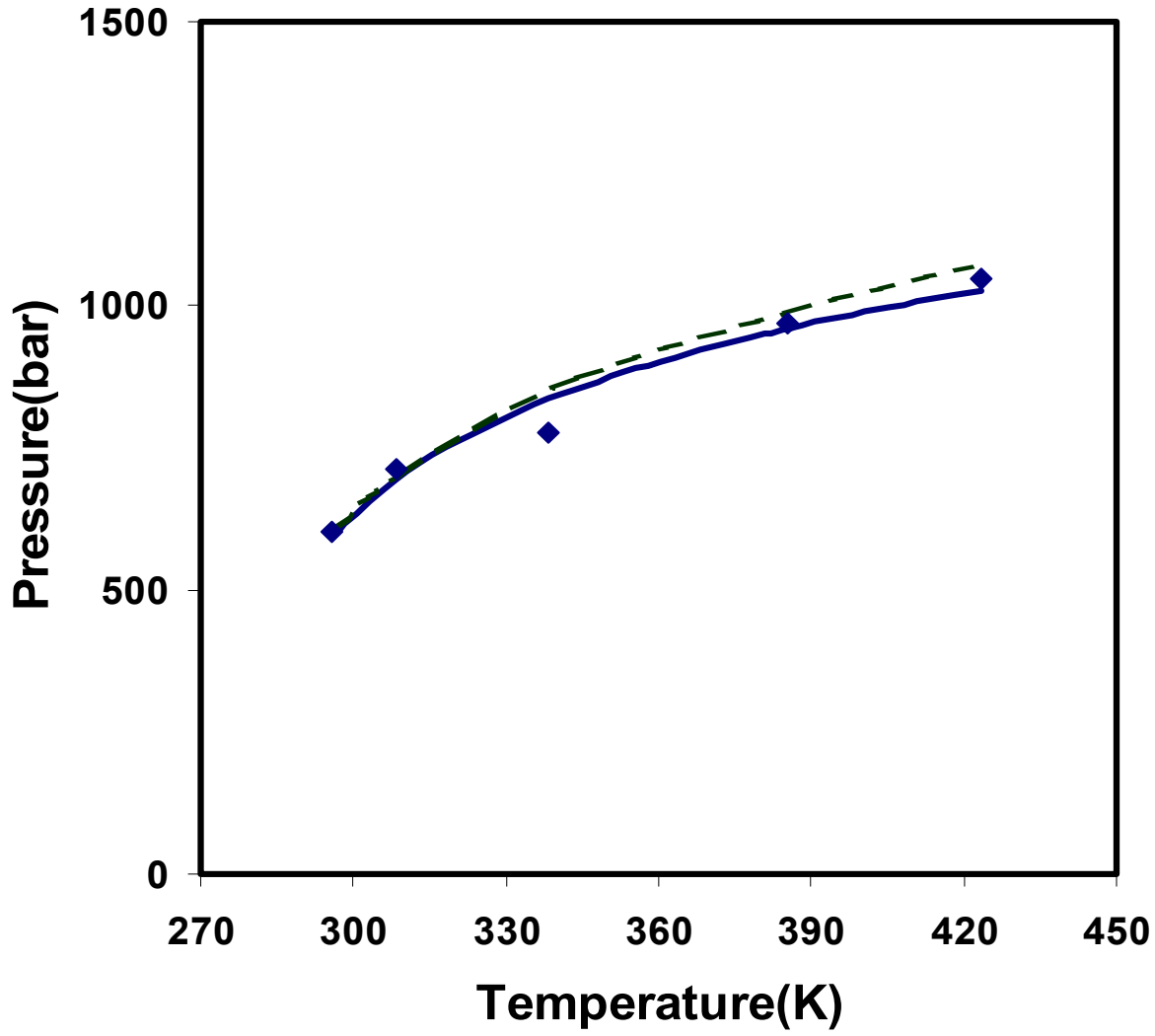

Figure 6- 2 Cloud point curves in the PVAc – CO_2 system. The solid lines represent LELAC calculations with ΔH_a=-3.9003 kJ/mol, and K_0=4.381. The dashed lines were calculated using the SAFT equation with u_0/k=225.0, k_{ij}=0.020 (MW= 125,000). The points are experimental values(Mc Hugh *et al.*, 1996).

Table 6- 3 Fitted Association energies (ΔH_a) and equilibrium constants (K_0).

System	ΔH_a(kJ/mol)	K_0	T_g(K)
PMA- CO_2	-7.985	6.106	282
PEA- CO_2	-5.624	5.088	224
PBA- CO_2	-3.214	4.713	250
PEHA- CO_2	-2.861	3.266	218
POA- CO_2	-2.413	2.745	NA

The magnitude of the fitted parameters decreases as the length of the alkyl tail on the acrylate increases. This is due to a decrease in effective polarity as a result of shielding of the molecule by the alkyl tail, which limits CO_2 access to the functional group on the polymer chain. This is clearly a function of the polymer architecture and the type of repeat unit in the polymer. Moreover, with the increasing alkyl tail length, the reduced dipole moment also decreases (Prausnitz et al., 1986), leading to a reduction in effective polarity. The results of these property changes are seen in Figure 6-8, which shows cloud point curves for a series of polyacrylate-CO_2 systems. It is readily apparent from the order of the curves in pressure-temperature space that the cloud-point behavior is not fixed by M_w or by T_g but by a combined effect. Thus, the PODA - CO_2 curve is not necessarily at the lowest temperature between these curves and the PODA - CO_2 curve turns dramatically with respect to pressure at ~ 500 K. This is surprising since it suggests that CO_2 is too polar to dissolve PODA even at this very high temperature. As the alkyl tail on the acrylate decreases in length, the polymer remains in solution at lower

temperatures, suggesting that interactions between the acrylate group and CO_2 are favorable and promote solubility.

Figure 6- 8 also shows that the cloud-point curve in the PMA-CO_2 system extends to lower temperatures than in the other poly (acrylate)-CO_2 systems. The PMA curve is shifted to higher pressures, and it does not exhibit a sharp increase in pressure that would be expected at very low temperatures. PMA has the highest T_g of all the polymers modeled in this study, suggesting that it has the lowest rotational flexibility of chain segments, which makes it difficult to dissolve in CO_2. However, PMA is also the most polar of the poly (acrylates), since its reduced dipole moment is scaled with the smallest molar volume, which enhances its solubility in CO_2 as the temperature is decreased. This might explain the cloud point behavior of PMA.

Additionally, another trend can be seen with the magnitudes of the parameters and the T_g of the polymer component in the system. Due to molecular architecture of the polymer, T_g values decreases with increasing alkyl tail length since the addition of longer alkyl chain affects the stiffness of the polymer significantly. On the other hand, as pointed above, the shielding of the functional group in the polymer by the alkyl chain decreases the magnitude of the interaction parameters. Thus, it is also possible to point out that the polymer component with the higher T_g has the higher value of the fitted parameters. It is perfectly reasonable to assume that within a family of polymer-CO_2 systems where the polymer component has a higher T_g, the fitted parameters will increase with T_g.

Also, if a comparison is made between the experimentally calculated values of interaction energies for the polymethacrylate – CO_2 systems in Chapter 5 and the

corresponding fitted values for the polyacrylate – CO_2 systems in this chapter, it is clear that the fitted values for the polyacrylates are higher, as shown in Table 6- 4. This might be due to shielding by the additional methyl group in the polymethylmethacrylate. Another possible reason might be the methyl group alters the dielectric environment of the polymer and thereby affecting the interaction capability of the functional group.

Table 6- 4 Comparison of fitted and experimental parameter values for polymer-CO_2 Systems

System	ΔH_a(kJ/mol)
(a)PMA- CO_2	-7.985
(b)PMMA- CO_2	-3.950
(a)PEA- CO_2	-5.624
(b)PEMA- CO_2	-4.908
(a)PBA- CO_2	-3.214
(b)POA- CO_2	-3.802

(a) from FT-IR spectra

(b) by fitting cloud point curves

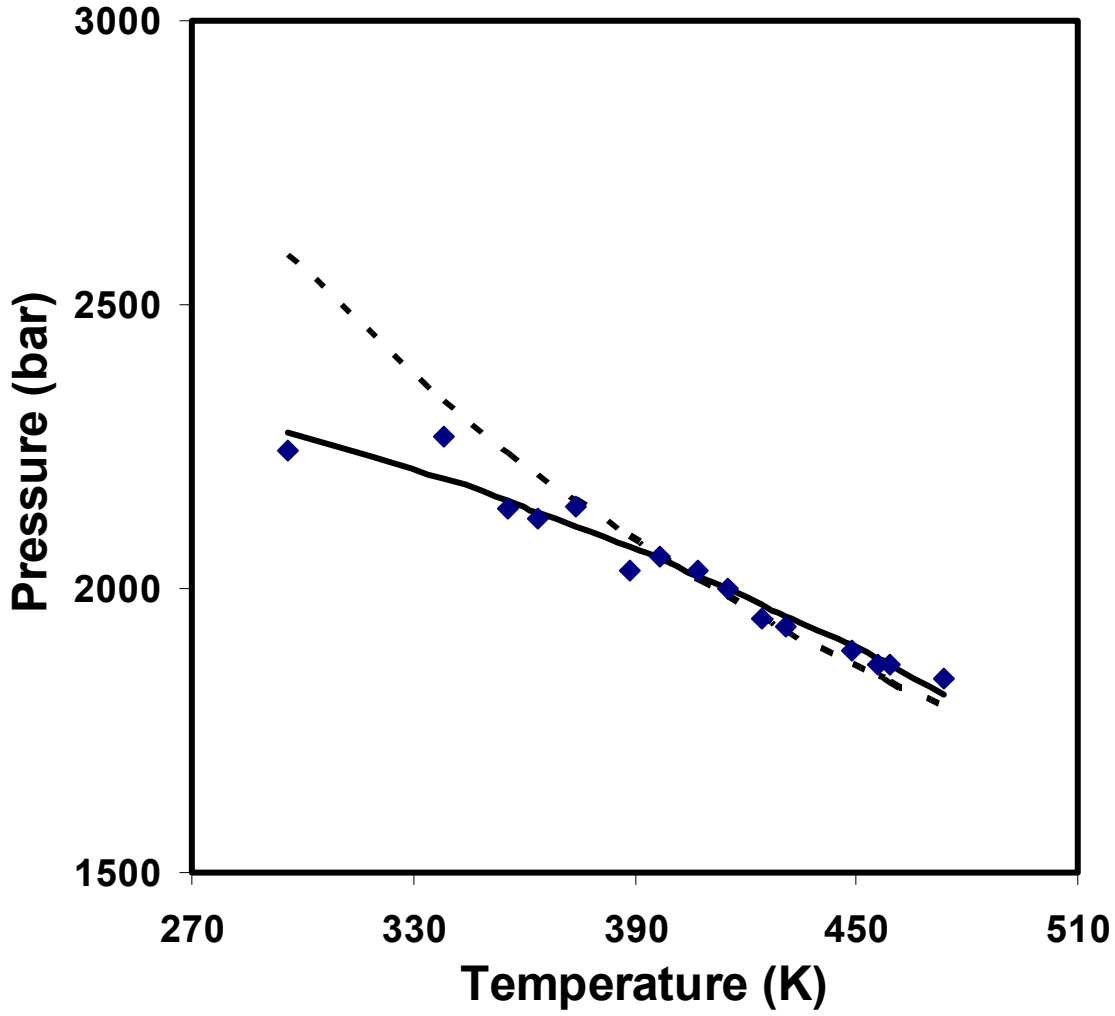

Figure 6- 3 Cloud point curves in the PMA – CO_2 system. The solid line represents LELAC calculations with ΔH_a=-7.985 kJ/mol, and K_0=6.106. The dashed line was calculated using the SAFT model with u_0/k=240.0, k_{ij}=0.043 (MW= 31,000). The points are experimental values(Mc Hugh *et al.,* 1996).

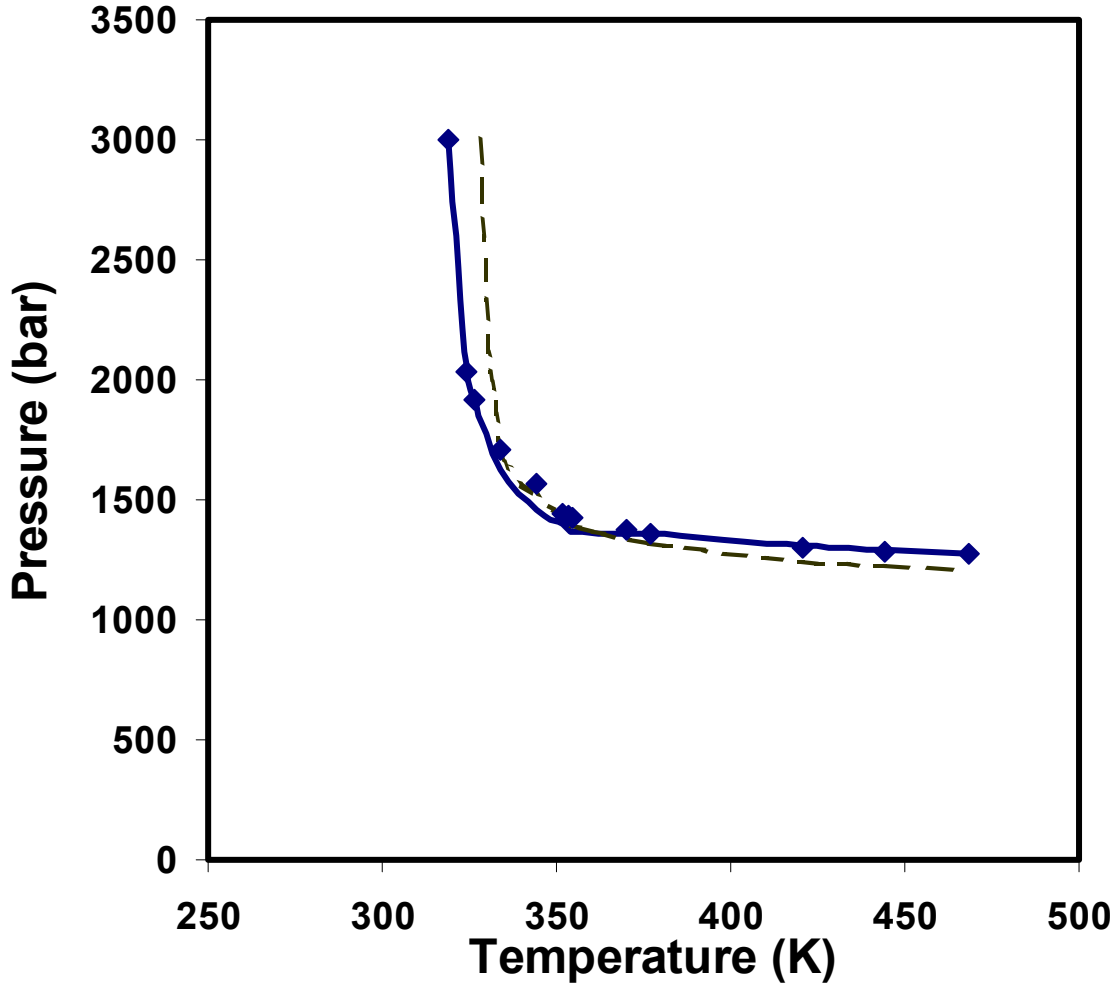

Figure 6- 4 Cloud point curves in the PEA – CO_2 system. The solid line represents LELAC calculations with ΔH_a=-5.624 kJ/mol, and K_0=5.088. The dashed line was calculated using the SAFT equation with u_0/k=215.0, k_{ij}=0.060 (MW= 120,000). The points are experimental values(Mc Hugh *et al.,* 1996).

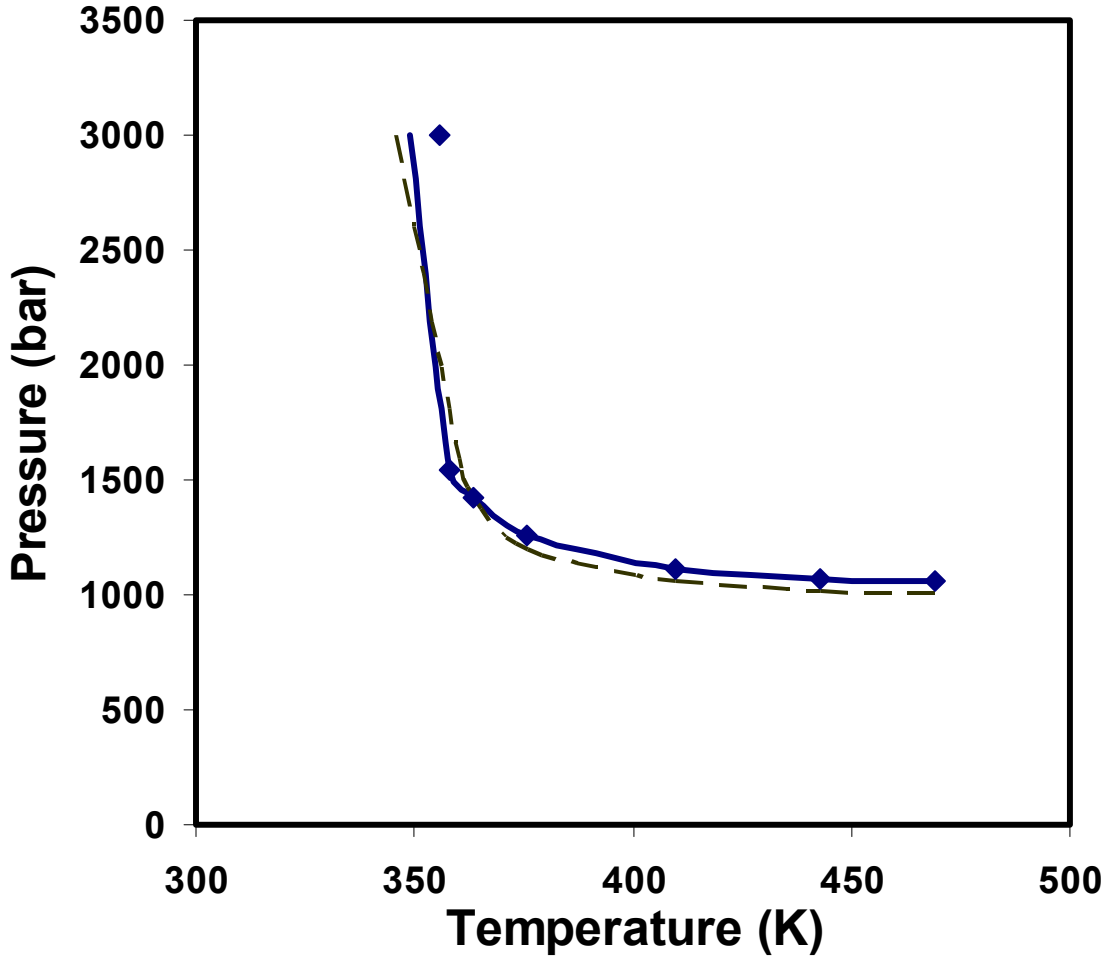

Figure 6- 5 Cloud point curves in the PBA – CO_2 system. The solid line represents LELAC calculations with ΔH_a=-3.214 kJ/mol, and K_0=4.713. The dashed line was calculated using the SAFT equation with u_0/k=205.0, k_{ij}=0.071 (MW= 62,000). The points are experimental values(Mc Hugh *et al.,* 1996).

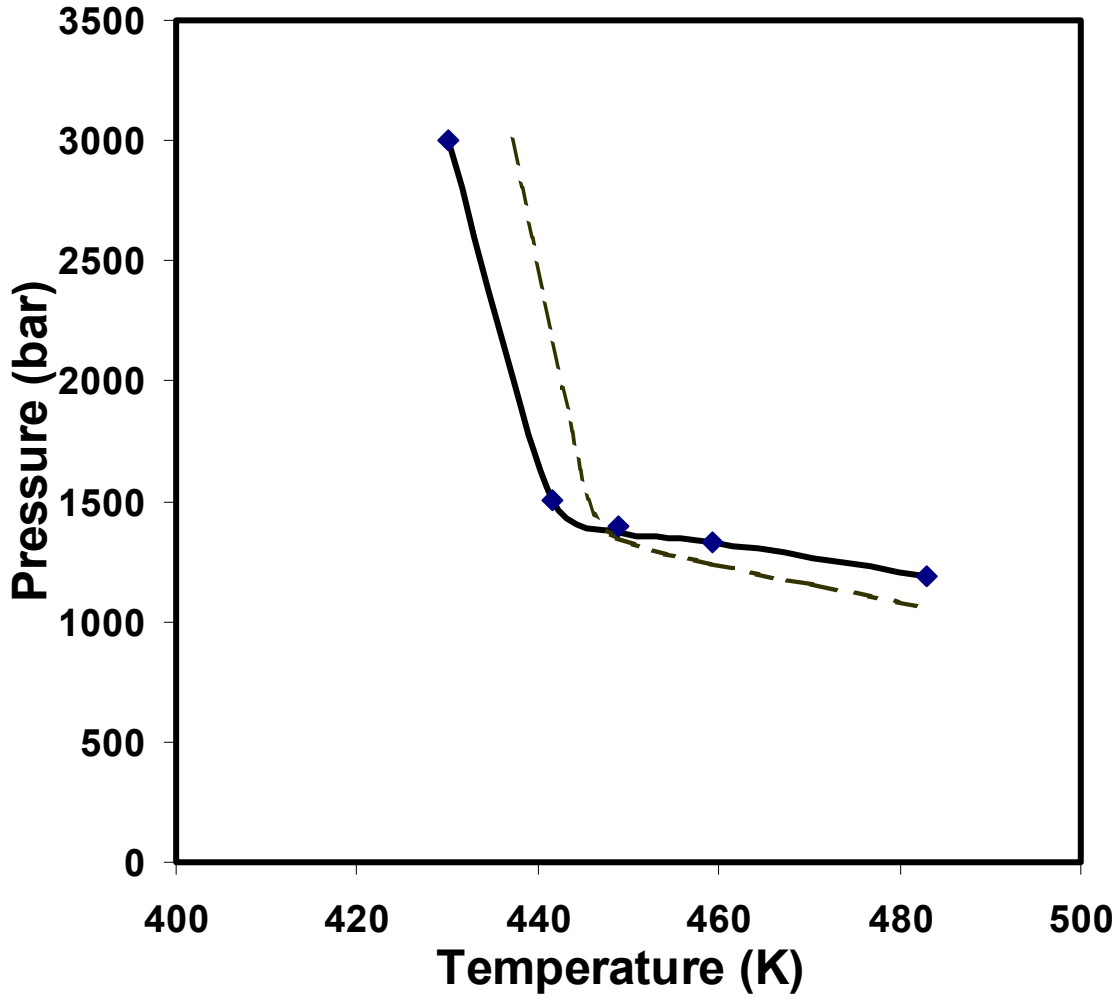

Figure 6- 6 Cloud point curves in the PEHA – CO_2 system. The solid line represents LELAC calculations with ΔH_a=-2.861 kJ/mol, and K_0=3.266. The dashed line was calculated using the SAFT equation with u_0/k=215.0, k_{ij}=0.093 (MW= 113,000). The points are experimental values(Mc Hugh *et al.,* 1996).

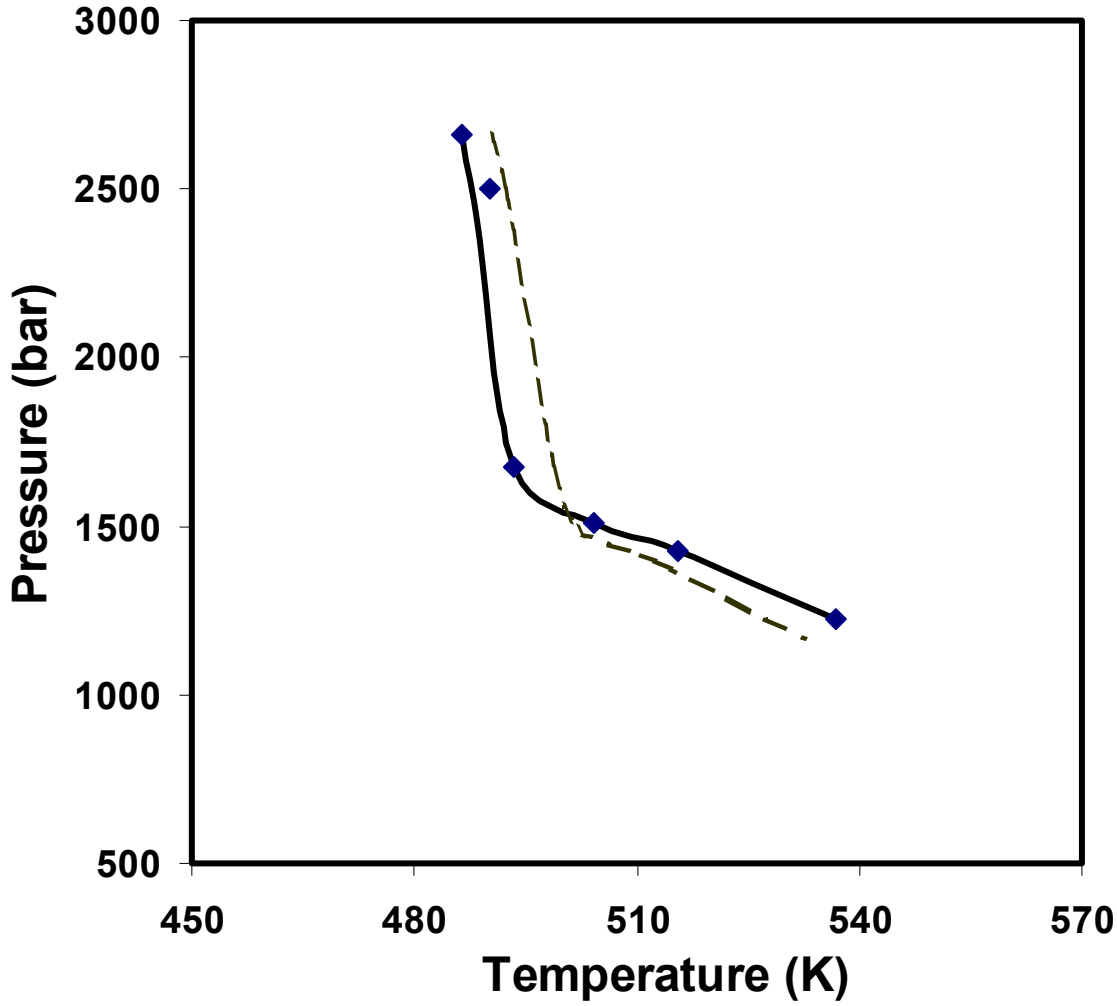

Figure 6- 7 Cloud point curves in the POA – CO_2 system. The solid line represents LELAC calculations with ΔH_a=-2.413 kJ/mol, and K_0=2.745. The dashed line was calculated using the SAFT equation with u_0/k=200.0, k_{ij}=0.053 (MW= 23,000). The points are experimental values(Mc Hugh *et al.,* 1996).

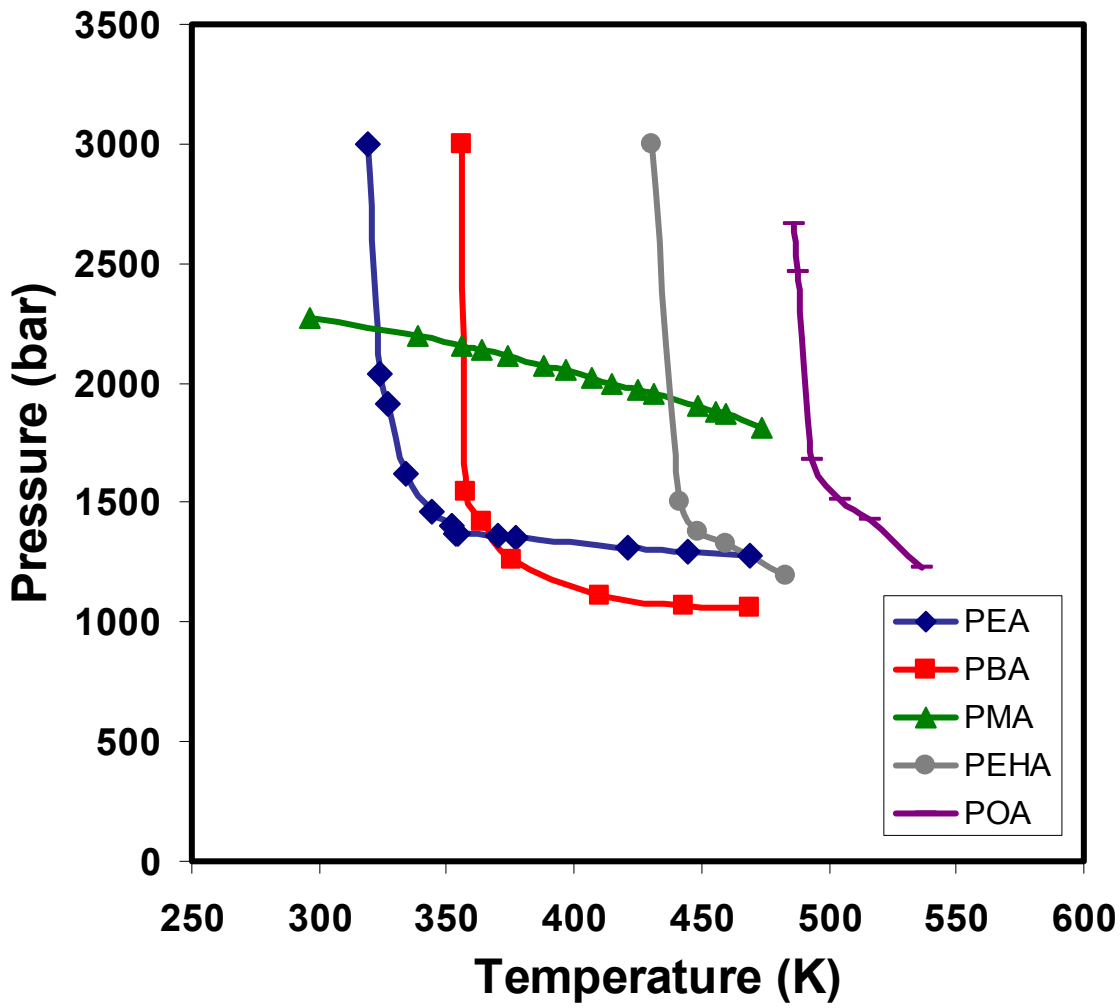

Figure 6- 8 Effect of the non-polar alkyl tail on the cloud point curves of a family of polyacrylates in supercritical CO_2. The alkyl chain length increases as follows PEA>PBA>PMA>PEHA>POA.

The LELAC model was also used to calculate cloud point curves in system which the solvent was not CO_2. The results for these systems are tabulated in table 6-5. Results for Polyisobutylene (PIB) – alkane systems are shown in Figure 6- 9. The values obtained for the fitted parameters in these systems were found to be much smaller than those seen in polymer-CO_2 systems, even though the systems were fitted equally well (average errors between 0.7% and 2.6%). These systems are known to demonstrate much less interaction between the polymer and the solvent due to their chemical structure, and the model is able to correlate these systems with errors lower than the previous systems which involves a stronger interaction between the components. The model was able to capture the effect of changing solvent quality on the cloud points. The cloud point curves shifted to higher temperatures as the free volume difference between the polymer and the solvent decreased with increasing molecular weight of the solvent.

Figure 6-10 shows the P-T curve for the systems containing polyethylene (PE) and low molecular weight hydrocarbons. The fitting of the experimental data yielded good results for both ethylene and propylene systems. The cloud point pressures decrease substantially with higher molecular weight solvent due to free volume differences and the increasing dispersive interactions between the polymer and the solvent. It has been noted before that the value of the variable x is directly related to the volume ratio of the components in the system and it is a function of the molecular weight of the polymer. Therefore it is related to the free volume differences between the polymer and the solvent in the system. It has been observed that cloud point pressure increases as x is increased due to this relation. A similar trend can be seen in Figure 6-11 where systems of

polystyrene (PS) with butane and pentane have been correlated. However, the magnitude of the parameters of this system reveals that PS tends to interact more with the solvent than the other systems since the interaction energy values are larger. It is clear that the quality of the solvent seems to play a big role in the miscibility of the mixture at high-pressure conditions and the value of one of the variables in the LELAC model seems to reflect this behavior.

Table 6- 5 Results of Polymer-Solvent systems using the LELAC model

Polymer-solvent	MW	ΔH_a (kJ/mol)	K_0	LELAC AAD%
PIB-butane	1,660,000	-0.891	1.481	0.94
PIB-pentane	1,660,000	-0.545	0.936	0.74
PIB-hexane	1,660,000	-0.314	0.779	1.49
PE-ethylene	108,000	-0.256	0.323	2.03
PE-propylene	108,000	-0.155	0.212	2.34
PS- butane	9,000	-1.413	0.813	2.56
PS- pentane	9,000	-1.016	0.695	2.09

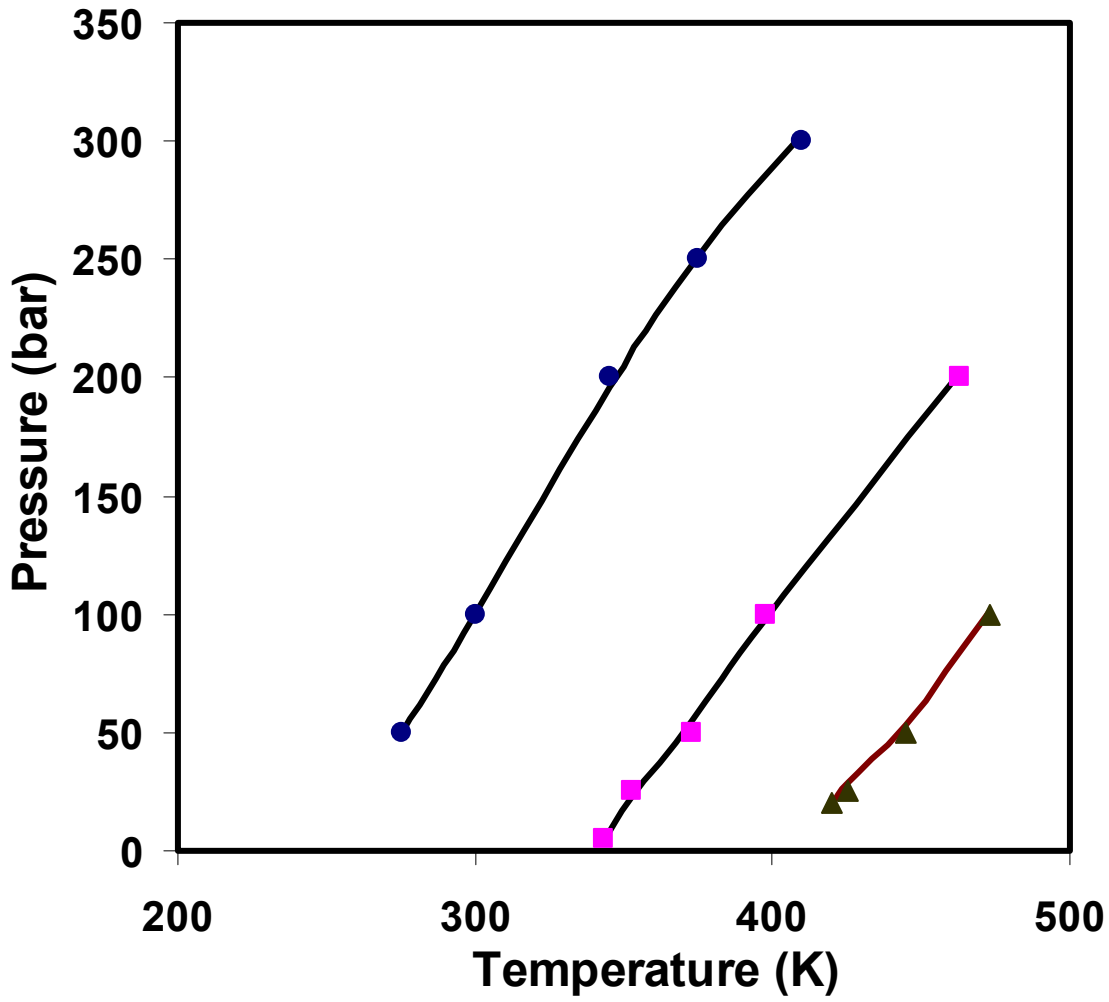

Figure 6- 9 Cloud point curves of PIB (MW=1,660,000) in various alkane solvents. The solid lines represent LELAC calculations with ΔH_a=-0.891 kJ/mol, and K_0=1.481 for PIB-butane, ΔH_a=-0.545 kJ/mol, and K_0=0.936 for PIB-pentane and ΔH_a=-0.314 kJ/mol, and K_0=0.779 for PIB-hexane. The circle, squares and triangles are experimental values for PIB systems with butane, pentane and hexane respectively (Zeman *et al*., 1972).

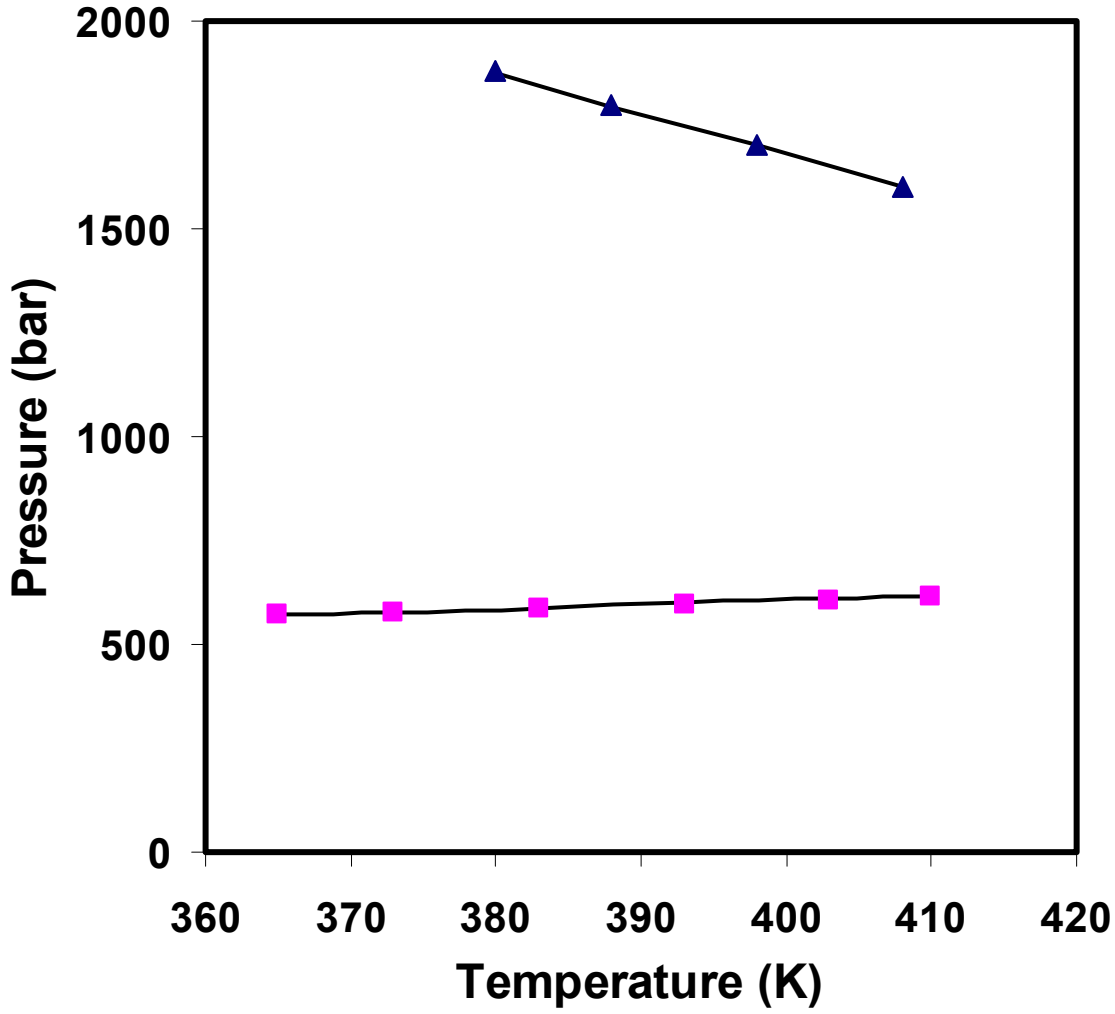

Figure 6- 10 Cloud point curves of PE (MW=108,000) in various solvents. The solid lines represent LELAC calculations with ΔH_a=-0.256 kJ/mol, and K_0=0.323 for PE-ethylene, ΔH_a=-0.155 kJ/mol, and K_0=0.212 for PE-propylene. The triangles and squares are experimental values for PE systems with ethylene and propylene respectively (Hasch *et al.*, 1993).

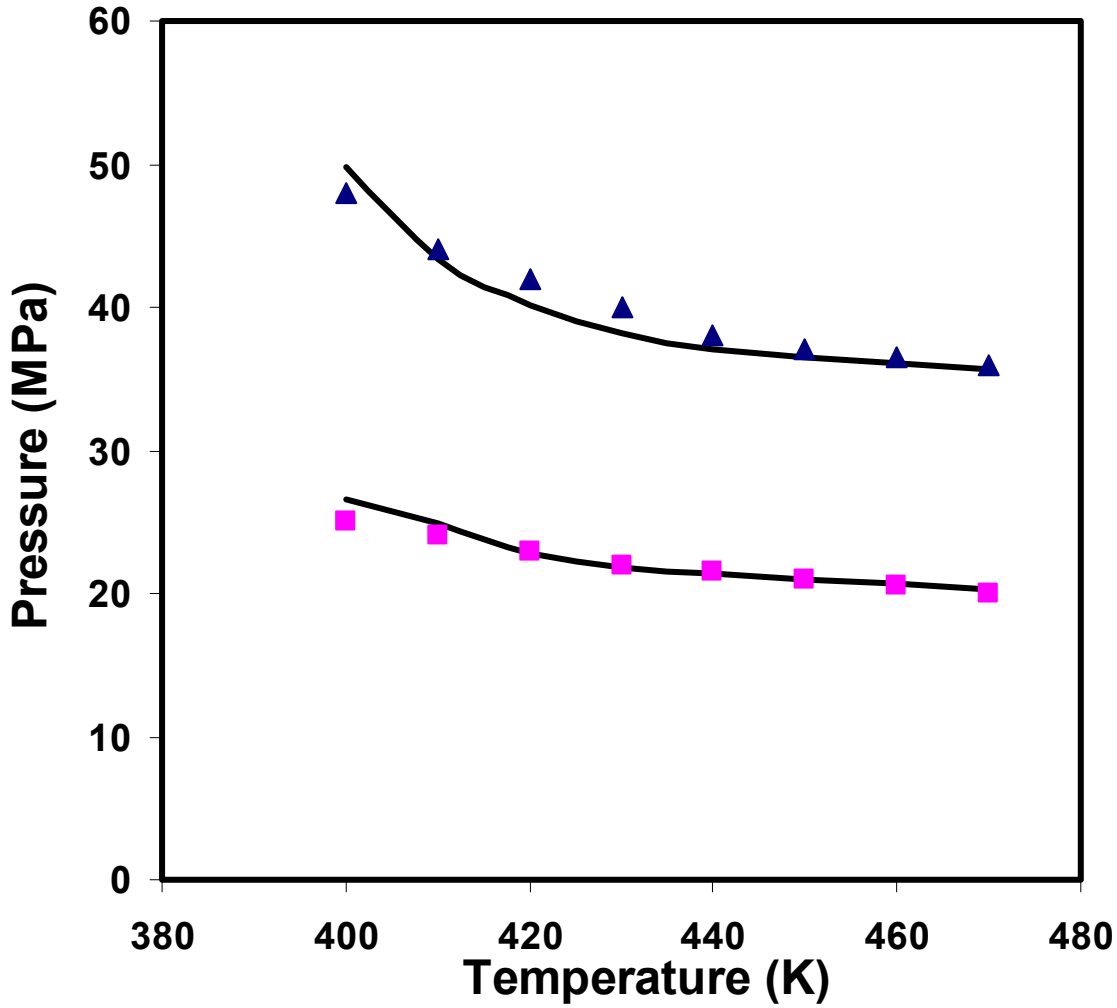

Figure 6- 11 Cloud point curves of PS (MW=9,000) in various solvents. The solid lines represent LELAC calculations with ΔH_a=-1.413 kJ/mol, and K_0=0.813 for PS-butane, ΔH_a=-1.016 kJ/mol, and K_0=0.695 for PS-pentane. The triangles and squares are experimental values for PS systems with butane and pentane respectively (Kiran *et al.*, 1989).

Extrapolation and prediction of cloud point curves using the LELAC model

The extrapolative capability of the LELAC model was investigated by calculating cloud point curves at polymer concentrations other than the one used to obtain the adjustable parameter(s). The two activity equations were solved as described previously to obtain cloud point pressures and "heavy" phase concentrations, at fixed values of the temperature and "light" phase concentration. Figure 6-12 through 6-14 present cloud point calculations at different concentrations for PMA-CO_2, PBMA-CO_2 and PS-Butane systems. The cloud point pressures increase with temperature at a fixed concentration, and the curve shifts upwards when the concentration of the polymer is increased. This is because higher pressures are needed for CO_2 to dissolve more polymer, as the concentration of the polymer is increased from 1 wt. % to 5%. This difference in pressure can be as large as 200- 300 bar depending on the temperature of the system and other factors such as free volume. Also, it is clear that a minimum pressure must be attained before the polymer is appreciably soluble in CO_2. This minimum can range from 200 bar up to 1000 bar, according to these calculations.

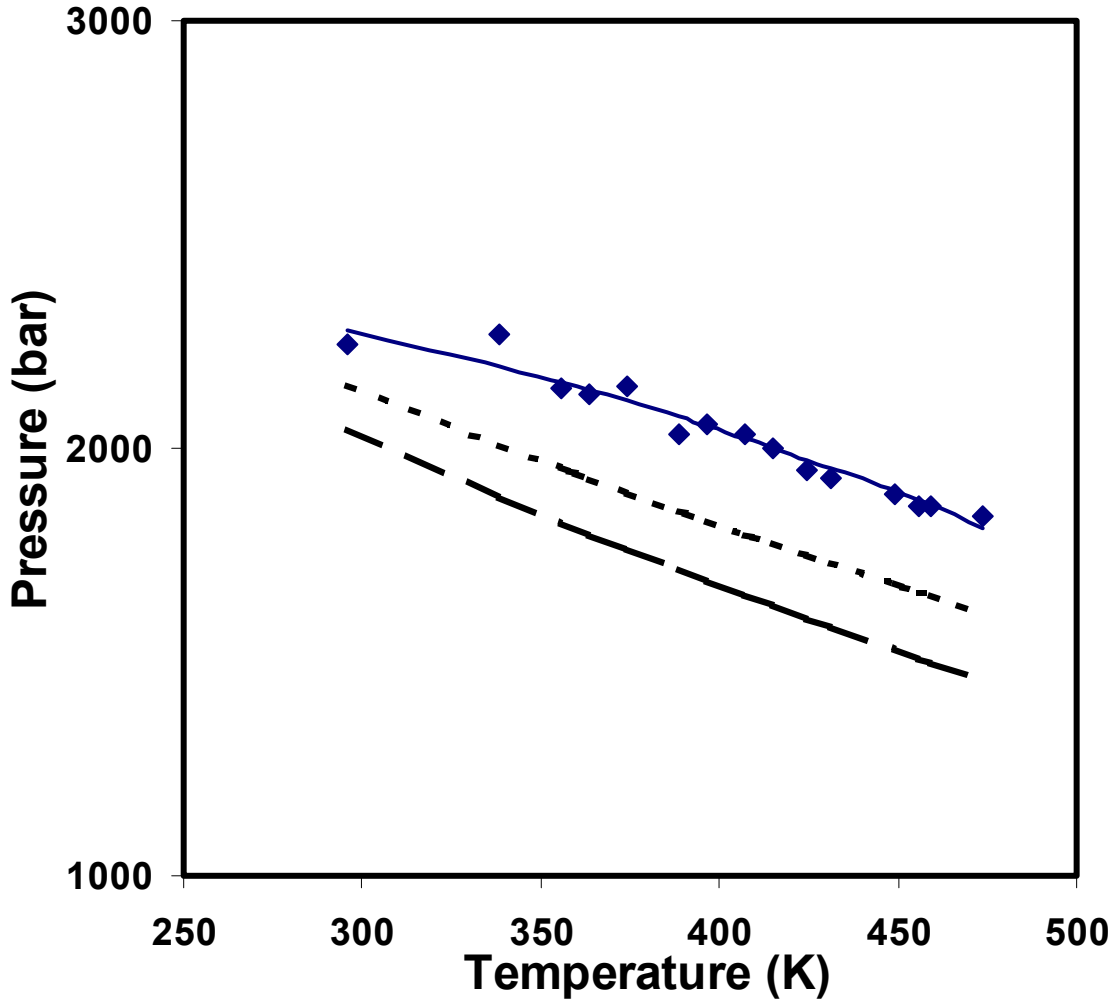

Figure 6- 12 LELAC prediction of PMA-CO_2 cloud point curves at different polymer compositions. The solid, dashed and broken lines represent LELAC calculations at polymer concentrations of 5, 3, and 1 wt %, respectively. The squares are experimental values at a polymer concentration of 5 wt. % (McHugh *et al.*, 1996).

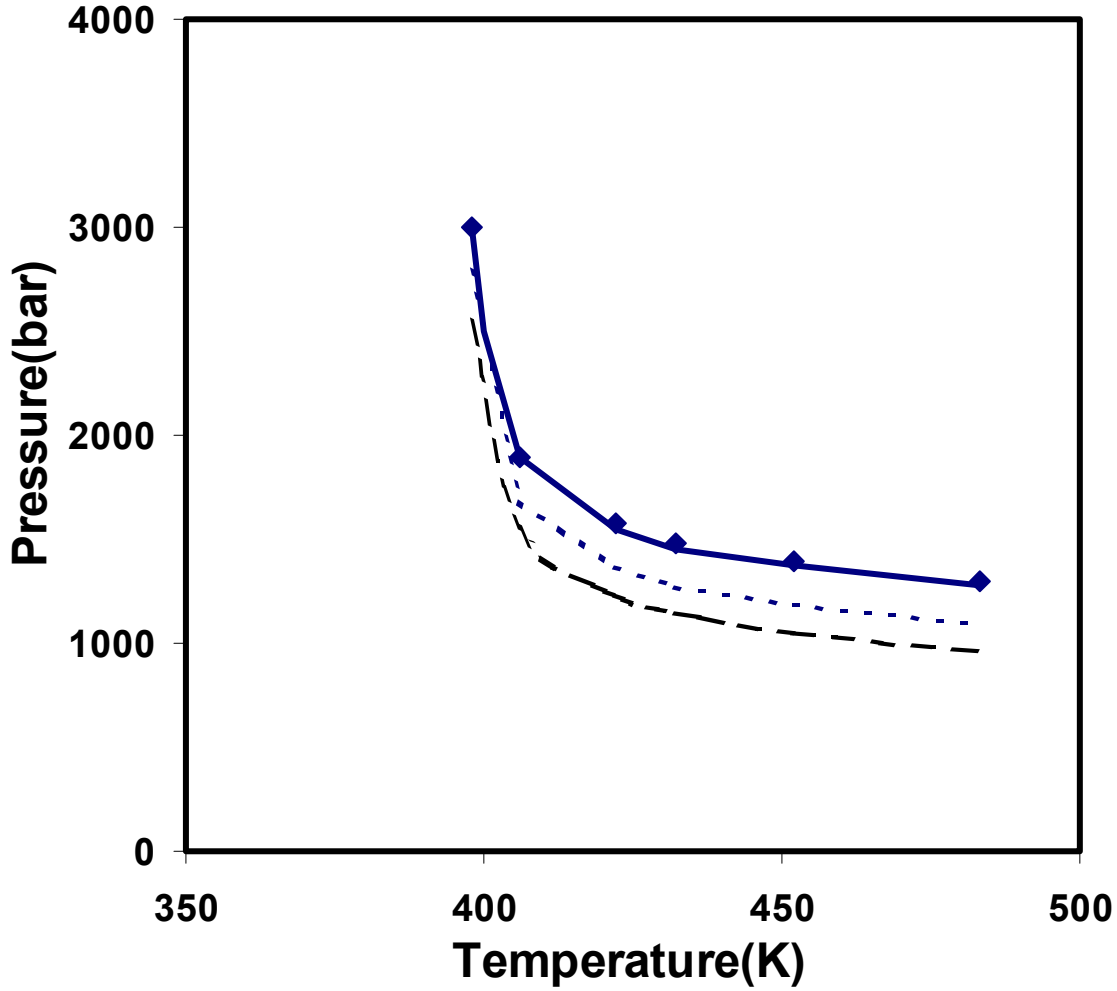

Figure 6- 13 LELAC predictions of PBMA-CO_2 cloud point curves at different polymer compositions. The solid, dashed and broken lines represent LELAC calculations at polymer concentrations of 5, 3, and 1 wt %, respectively. The squares are experimental values at 5 wt. % (McHugh *et al.*, 1996).

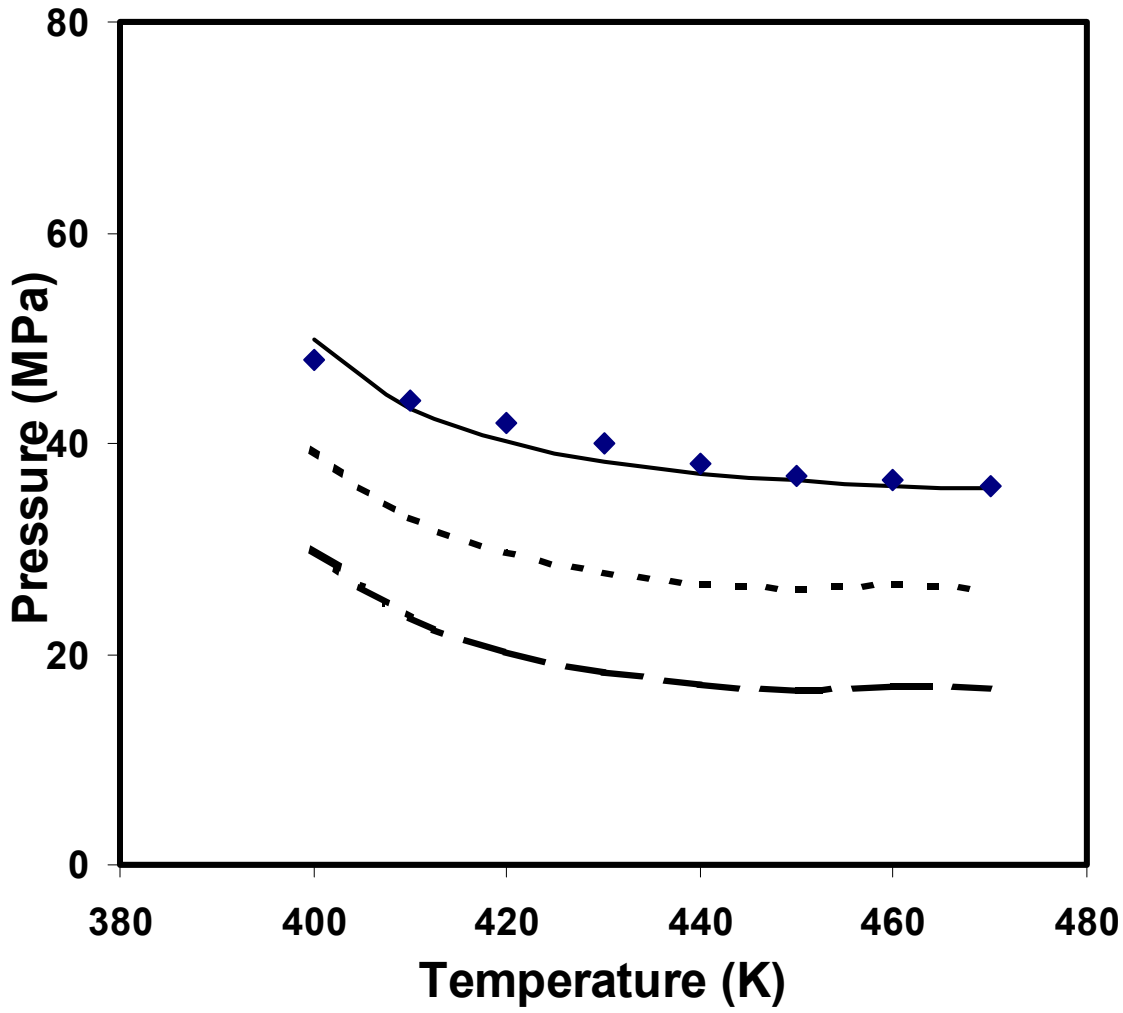

Figure 6- 14 LELAC prediction of PS-butane cloud point curves at different polymer compositions. The solid, dashed and broken lines represent LELAC calculations at 5, 3, and 1 wt %, respectively. The squares are experimental values at 5 wt. % (Kiran *et al.*, 1989).

The LELAC model was also used to plot pressure- composition and temperature-composition curves, since the composition in the second phase is also obtained in the calculations described above. In addition, the second and the third derivatives of the Gibbs energy of mixing were equated to zero at a given temperature (equations 4- 11 and 4- 12) to calculate the critical pressure and critical concentration at that temperature (UCST or LCST). Thus, demixing curves at constant temperatures (isotherm) were generated. This is equivalent to taking constant temperature cuts of the P-T loci. Figures 6- 15 through 6- 17 show the predicted pressure-composition curves for several systems. Table 6-5 presents the calculated critical pressures and the critical concentrations for these systems at specified temperatures. The region above each curve denotes a single phase region. As the temperature is increased, the region of miscibility increases as shown in these figures.

Temperature-composition diagrams were also obtained using an analogous procedure. Figure 6-18 shows the predicted temperature-composition curves for the PMA- CO_2 system. The region below each curve denotes the two-phase region at the indicated pressure. Complete miscibility is achieved upon increasing the temperature and the system exhibits UCST behavior at these pressures.

Table 6- 6 Predicted critical points of Polymer systems using the LELAC model

Polymer-Solvent	MW	Temperature (K)	Critical Pressure (bar)	Critical Polymer Concentration (wt.%)
PMA- CO_2	31,000	373.15	2153.21	12.3
PMA- CO_2	31,000	423.15	2001.23	10.7
PMA- CO_2	31,000	473.15	1877.12	10.5
PBMA- CO_2	100,000	398.15	3070.59	9.4
PBMA- CO_2	100,000	423.15	1621.34	8.9
PBMA- CO_2	100,000	473.15	1383.12	8.7
PS-Butane	9,000	423.15	406.28	14.1
PS-Butane	9,000	448.15	381.25	13.2
PS-Butane	9,000	473.15	370.17	12.4

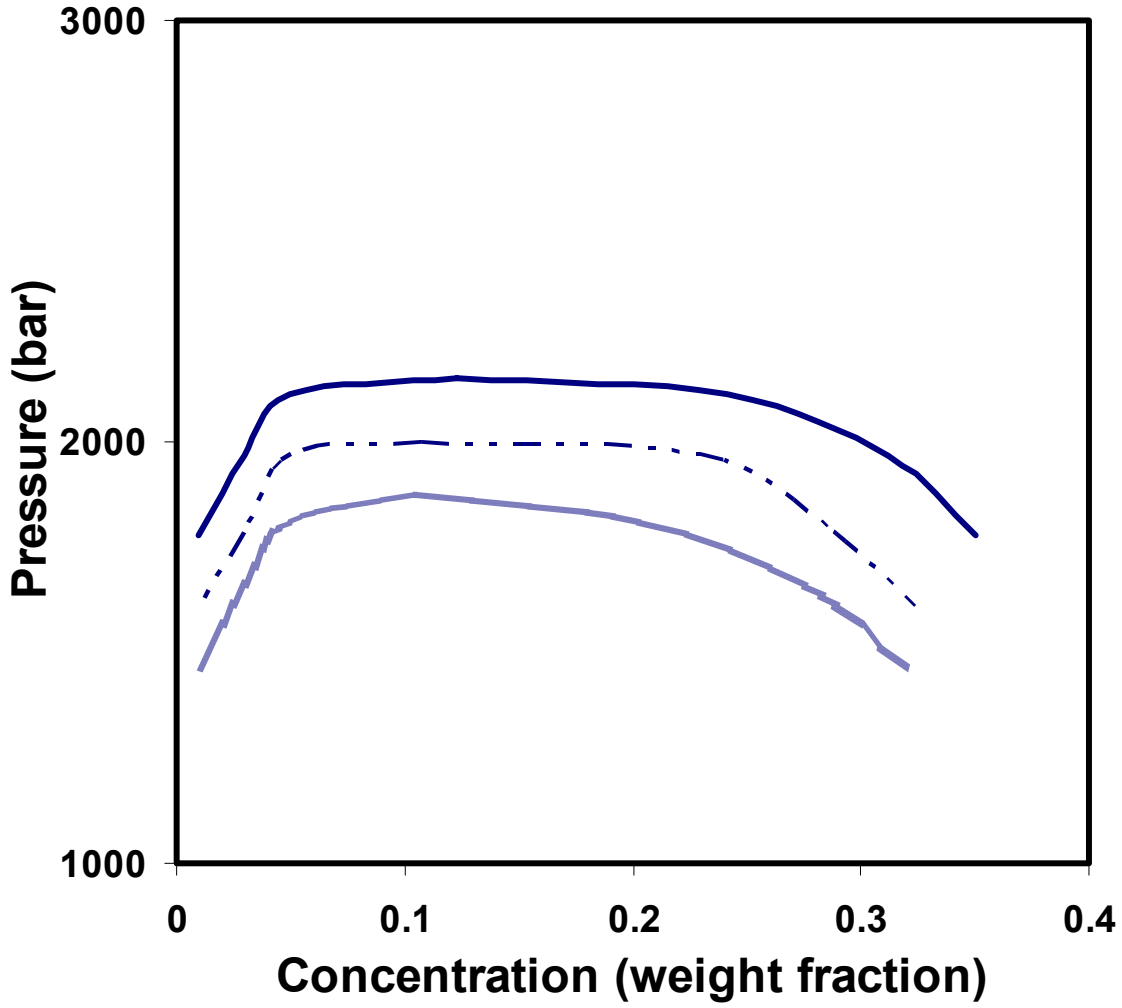

Figure 6- 15 LELAC prediction of PMA-CO_2 pressure- composition curves at different temperatures. The solid, dashed and broken lines represent calculations at 373.15, 423.15 and 473.15 K, respectively.

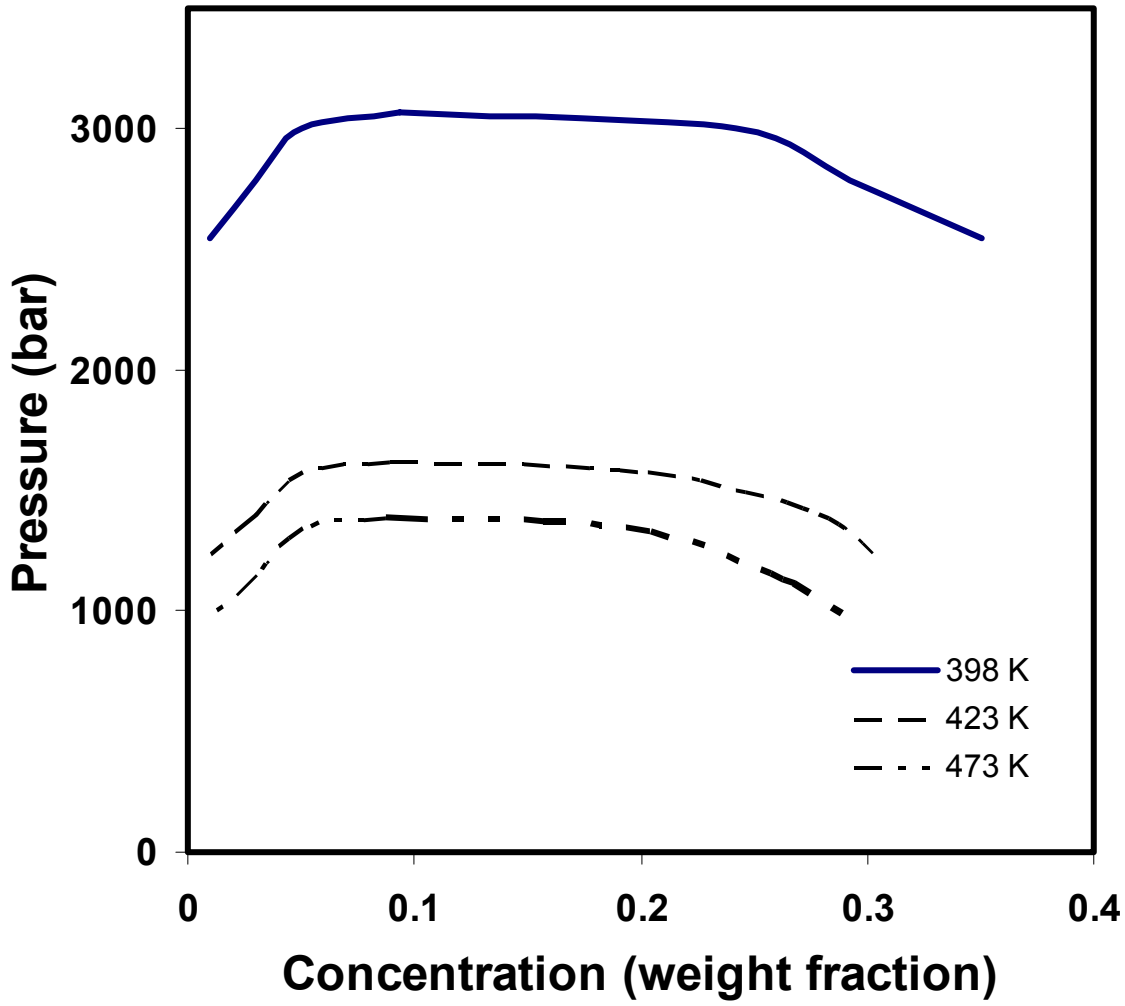

Figure 6- 16 LELAC prediction of PBMA-CO_2 pressure-composition curves at different temperatures. The solid, dashed and broken lines represent LELAC calculations at 398.15, 423.15 and 473.15 K, respectively.

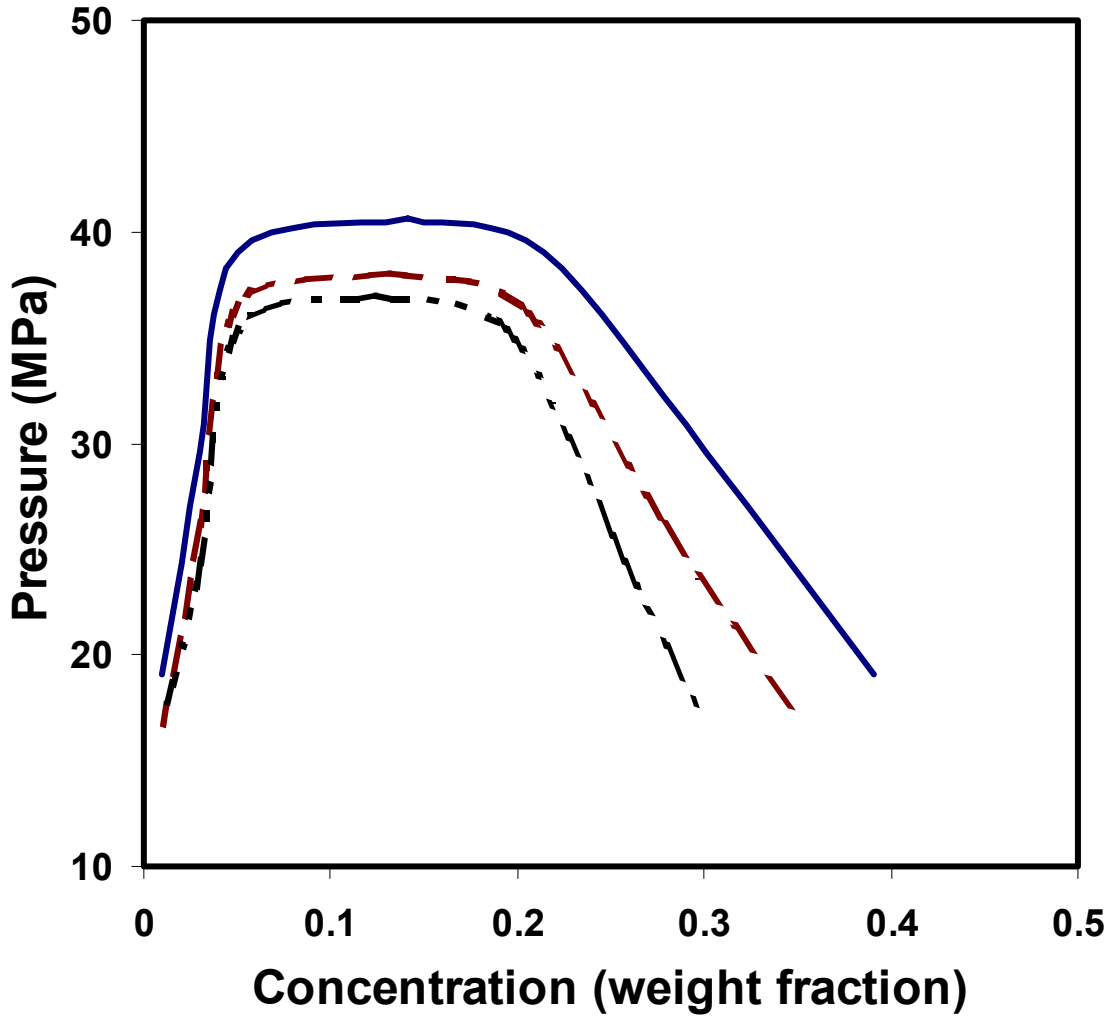

Figure 6- 17 LELAC prediction of PS-butane pressure-composition curves at different temperatures. The solid, dashed and broken lines represent LELAC calculations at 423.15 K, 448.15 K and 473.15 K, respectively.

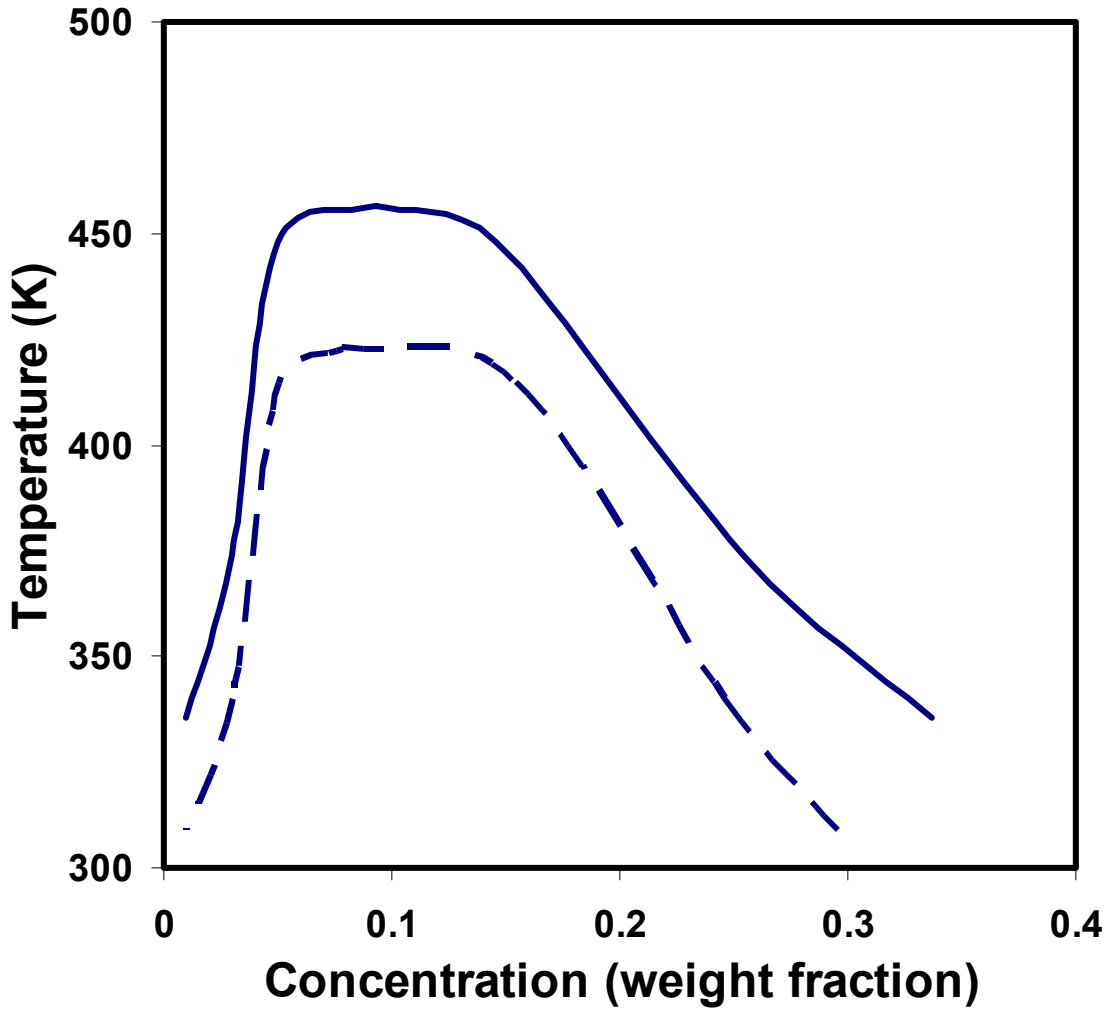

Figure 6- 18 LELAC prediction of PMA-CO_2 temperature-composition curves at different pressures. The solid and the dashed lines represent LELAC calculations at 1900 and 2000 bar, respectively.

Prediction of sorption behavior using the LELAC model

The solubility of CO_2 in polymers can also be predicted using the LELAC model and the parameters obtained by fitting cloud point curves. The results of such calculations and comparisons with experimental data in the case of PVAc-CO_2 and PBMA-CO_2 are presented in Figure 6- 19 and Figure 6- 20, respectively. It should be added here that the solubility of PVAc and PBMA in CO_2 is negligible at the conditions of the sorption measurements, which means that the fluid phase in equilibrium with the polymer phase is pure CO_2. This assumption is validated by cloud point data, which imply that much higher pressures are needed to obtain significant polymer solubility in CO_2. Equations (4-17) and (4- 18) can therefore be used to calculate the solubility of CO_2 in the polymer. Figures 6- 19 and 6- 20 show reasonable agreement between predicted values (since no adjustable parameters are used in the calculations) and experimental sorption data (error in the range 5 - 20%).

The model also predicts the correct trends in the sorption isotherms. In both systems, sorption increases almost linearly with pressure up to approximately 5 MPa. Above 5 MPa, sorption of CO_2 into the polymer increases more slowly and may reach a limiting value at very high pressures. The calculations imply limiting values of 30-35 wt.% in the case of PVAc- CO_2 and 20-25 wt.% in the case of PBMA-CO_2 at 313.15 K. The calculations also confirm that the sorption of CO_2 into the polymers decreases with increasing temperature, as do the limiting values. This is a result of a decrease in the density of carbon dioxide as it becomes more gas-like with increasing temperature. This makes it less soluble in the polymer as the temperature increases. The LELAC model correctly predicts this trend.

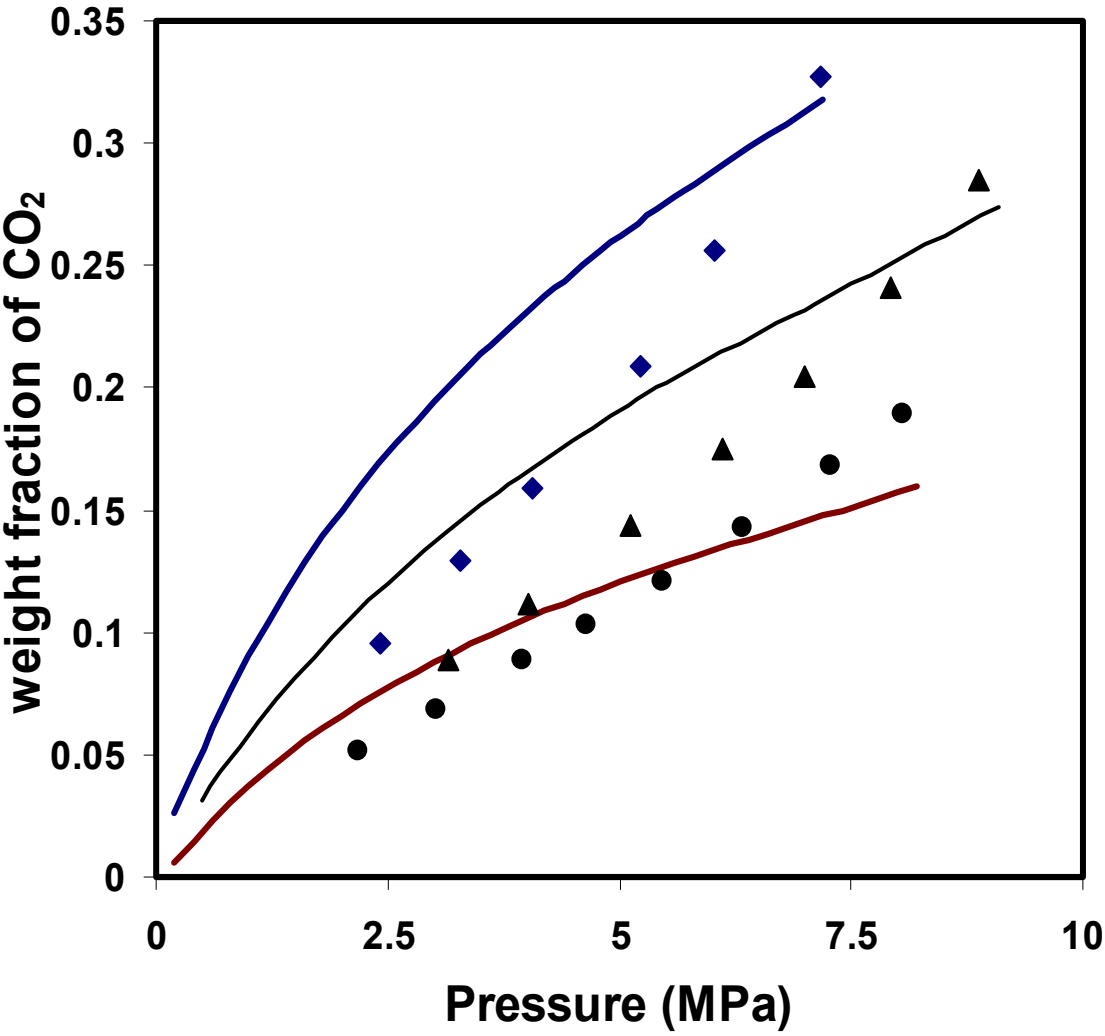

Figure 6- 19 Sorption predictions for PVAc (MW=100,000)-CO_2 systems. The squares, triangles and circles represent experimental sorption data at 313.15 K, 333.15 K, and 353.15 K respectively (Zhong *et al.*, 1997). The lines represent predictions using the LELAC model.

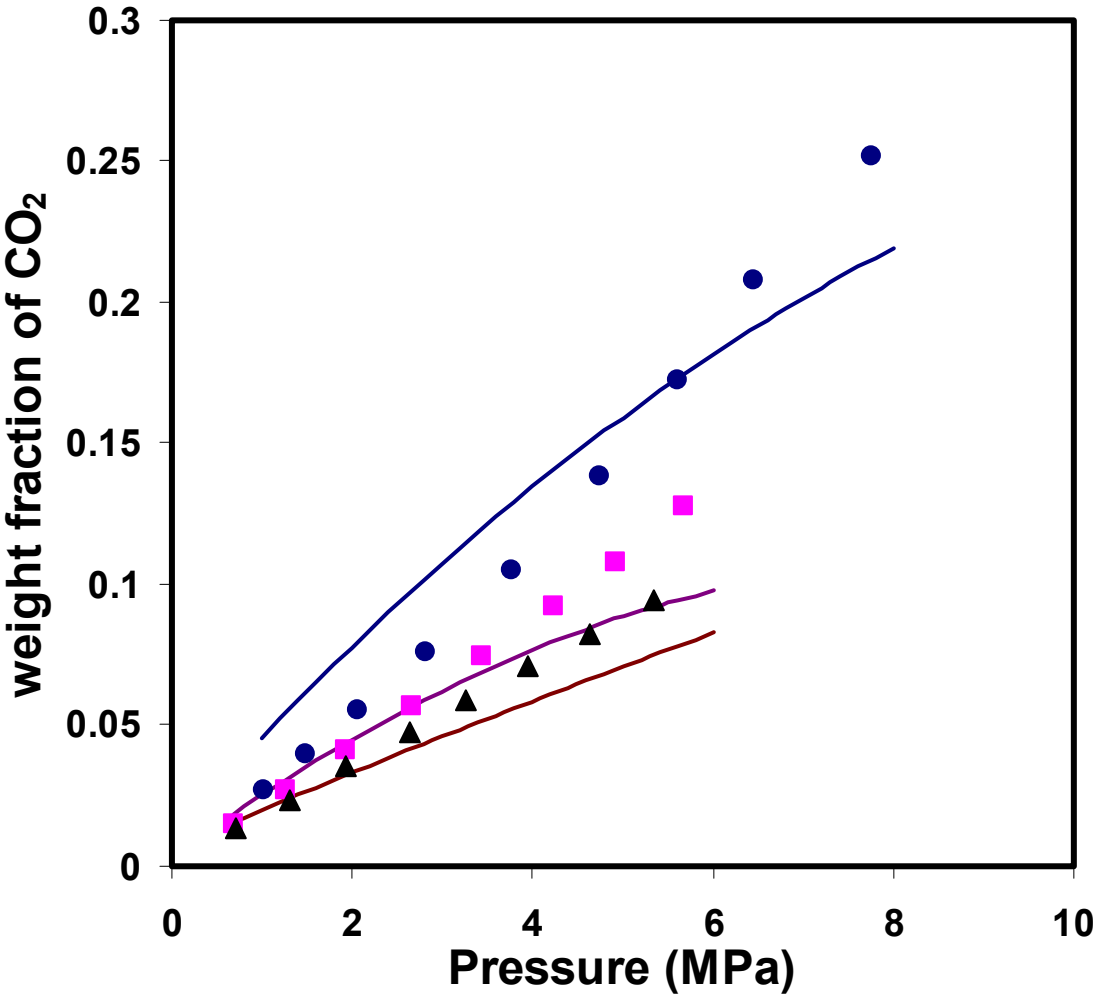

Figure 6- 20 Sorption predictions for PBMA (MW= 100,000)-CO_2 systems. The dots, squares and triangles represent experimental sorption data at 313.15 K, 333.15 K, and 353.15 K respectively (Zhong *et al.*, 1997). The lines represent predictions using the LELAC model.

Prediction of cloud point curves using parameters obtained from sorption data

The calculations described above used the LELAC model with parameters obtained by fitting cloud point data to predict the sorption of CO_2 into the polymer. Results of calculations using the LELAC model with parameters obtained from sorption data to predict cloud point curves are presented below.

Figure 6- 21 represents the experimental and calculated sorption curve for PBMA- CO_2 system at 333.15 K where the molecular weight of PBMA is 100,000 g/mol. The interaction energy ΔH_α in this system was estimated to be ~ 4 kJ/mol from FT-IR spectra, and K_0 was used as an adjustable parameter in fitting sorption data. As seen in the figure, the data were fitted with an average error of 1.2 % using only one adjustable parameter. Figure 6- 22 shows that similar results are obtained in the case of PVAc-CO_2 using one adjustable parameter. The errors in this case were 1.9%. The error values and the fitted parameters for these systems are tabulated in Table 6- 6. Predicted cloud point curves (using no adjustable parameters) are shown in Figures 6- 23 and 6- 24 at polymer concentrations of 5 wt. %. The results are in reasonable agreement with experimental data in both cases, with errors in the range 7- 18 %. Thus, different types of data may be used to obtain the one or two adjustable parameters. However the values of K_0 obtained using the forward and the inverse procedure are different. This might be due to several factors. The values of the parameters ΔH_α and K_0 have not been varying through the calculations since they are independent of temperature and pressure conditions. However, the difference in both procedures in a way implies that these parameters might be weakly dependent on temperature. Another reason might be that there are more data available for sorption than for cloud points. Additionally, conditions where the systems are

correlated by both procedures are quite different. The cloud points are at much higher pressures and temperatures. These might have a profound effect on the system parameters and the quality of the fitting where relatively higher errors are observed in the cloud point correlations at high pressure. Nevertheless, agreement is quite satisfactory.

Table 6- 7 Sorption correlations of Polymer-CO_2 systems using the LELAC model

Polymer	MW	Pressure range (bar)	Concentration range (wt.%)	ΔH_a (kJ/mol)	K_0	LELAC AAD%
PBMA	100,000	6.91-56.80	1.48-12.8	-3.8015	3.417	1.23
PVAc	100,000	24.1-71.8	9.53-32.70	-3.9003	7.162	1.86

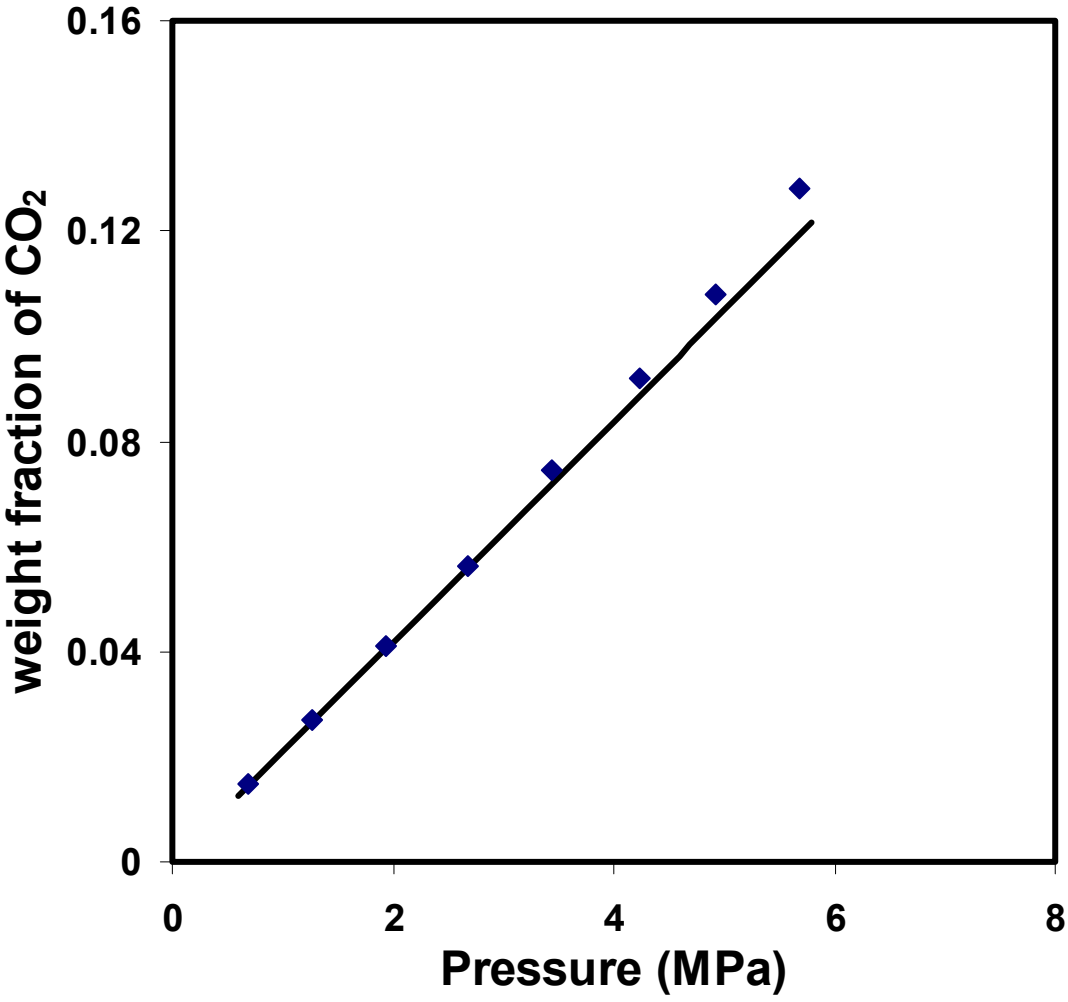

Figure 6- 21 Calculated sorption isotherms in PBMA (MW=100,000)-CO_2 systems. The squares represent experimental sorption data at 333.15 K (Zhong *et al.*, 1997). The curve represents LELAC calculations with ΔH_a=-3.8015 kJ/mol, and K_0=3.417.

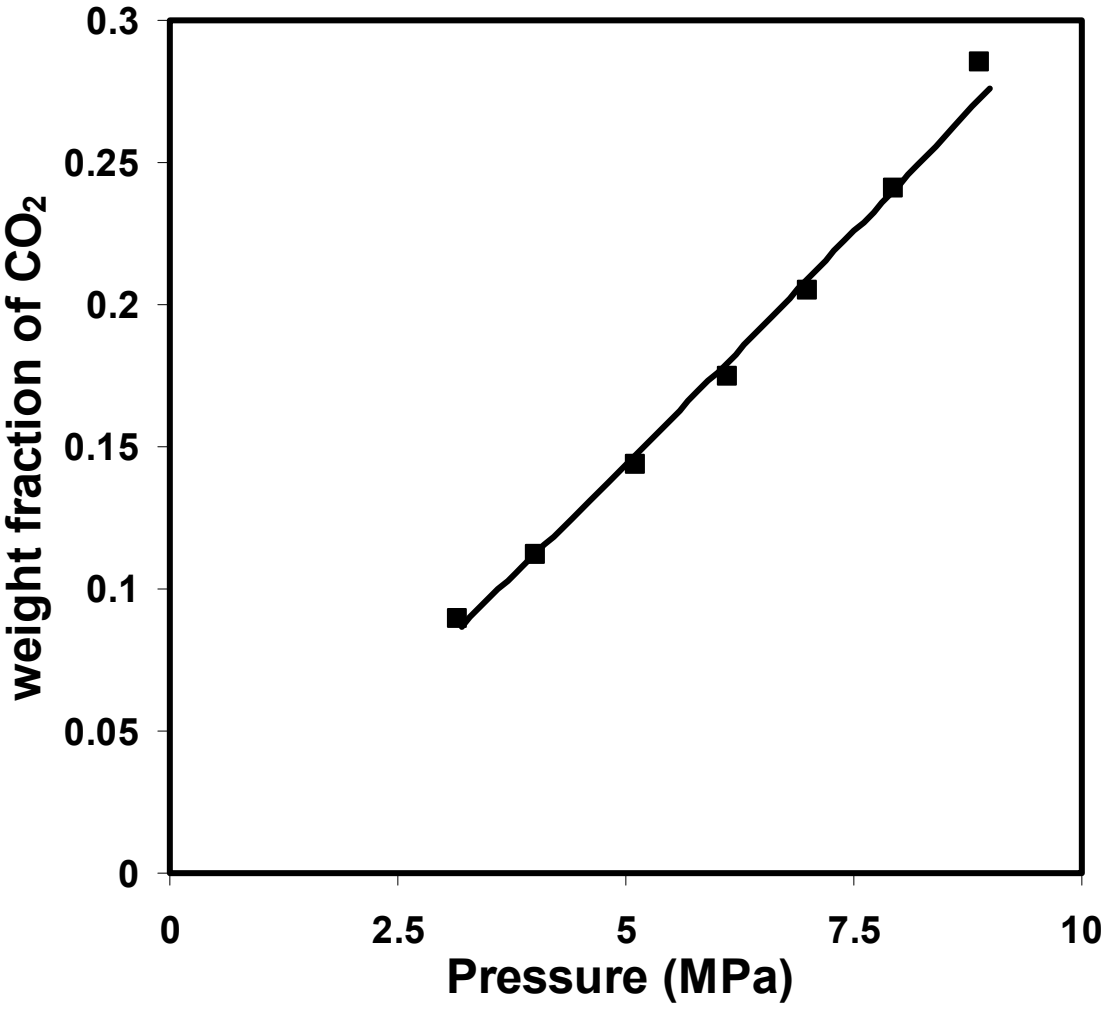

Figure 6- 22 Calculated sorption isotherms in PVAc (MW=100,000)-CO_2 systems. The squares represent experimental sorption data at 333.15 K (Zhong *et al.*, 1997). The curve represents LELAC calculations with ΔH_a=-3.9003 kJ/mol, and K_0=7.162.

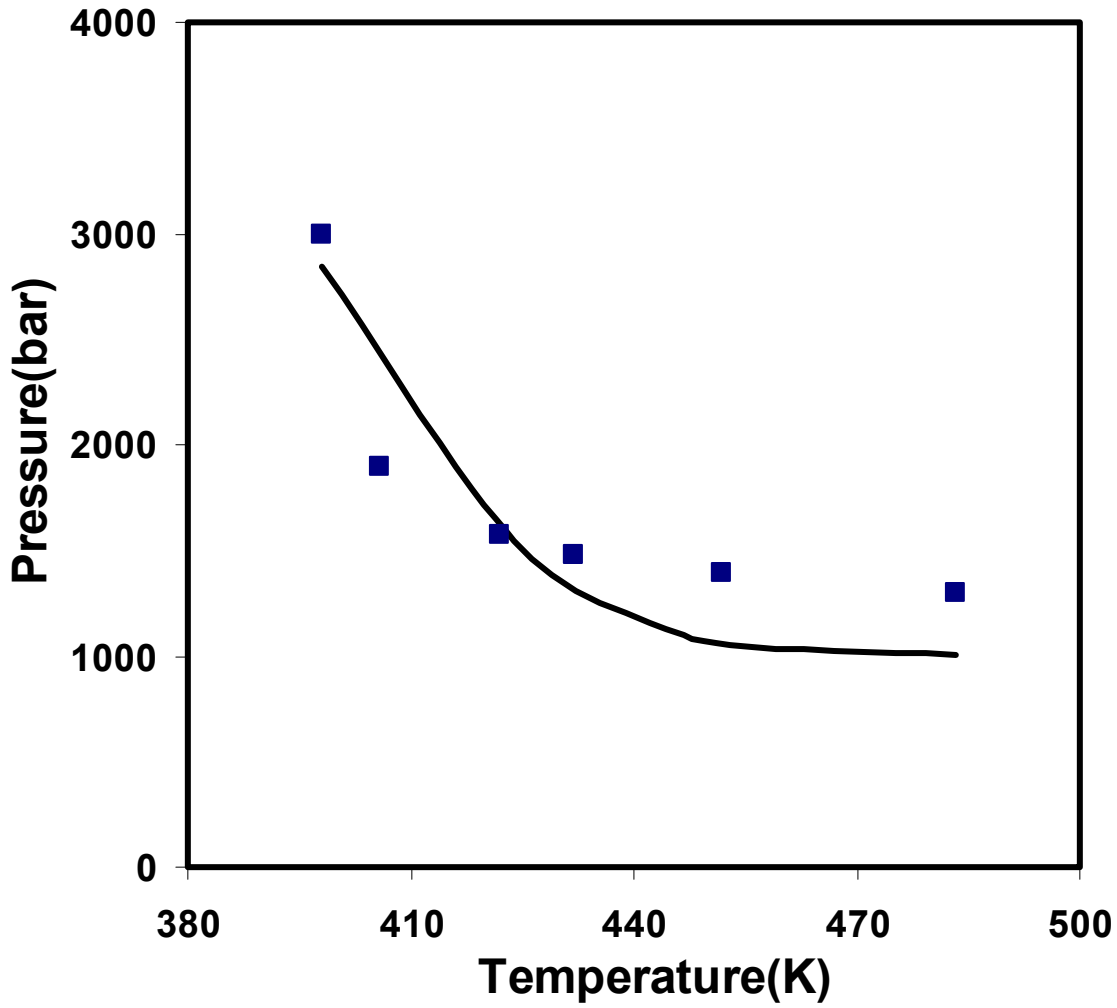

Figure 6- 23 Cloud point curve prediction in PBMA (MW= 100,000)-CO_2 systems. The squares represent experimental sorption data at 5 wt. % polymer concentration. (McHugh *et al.*, 1996). The lines represent predictions using the LELAC model.

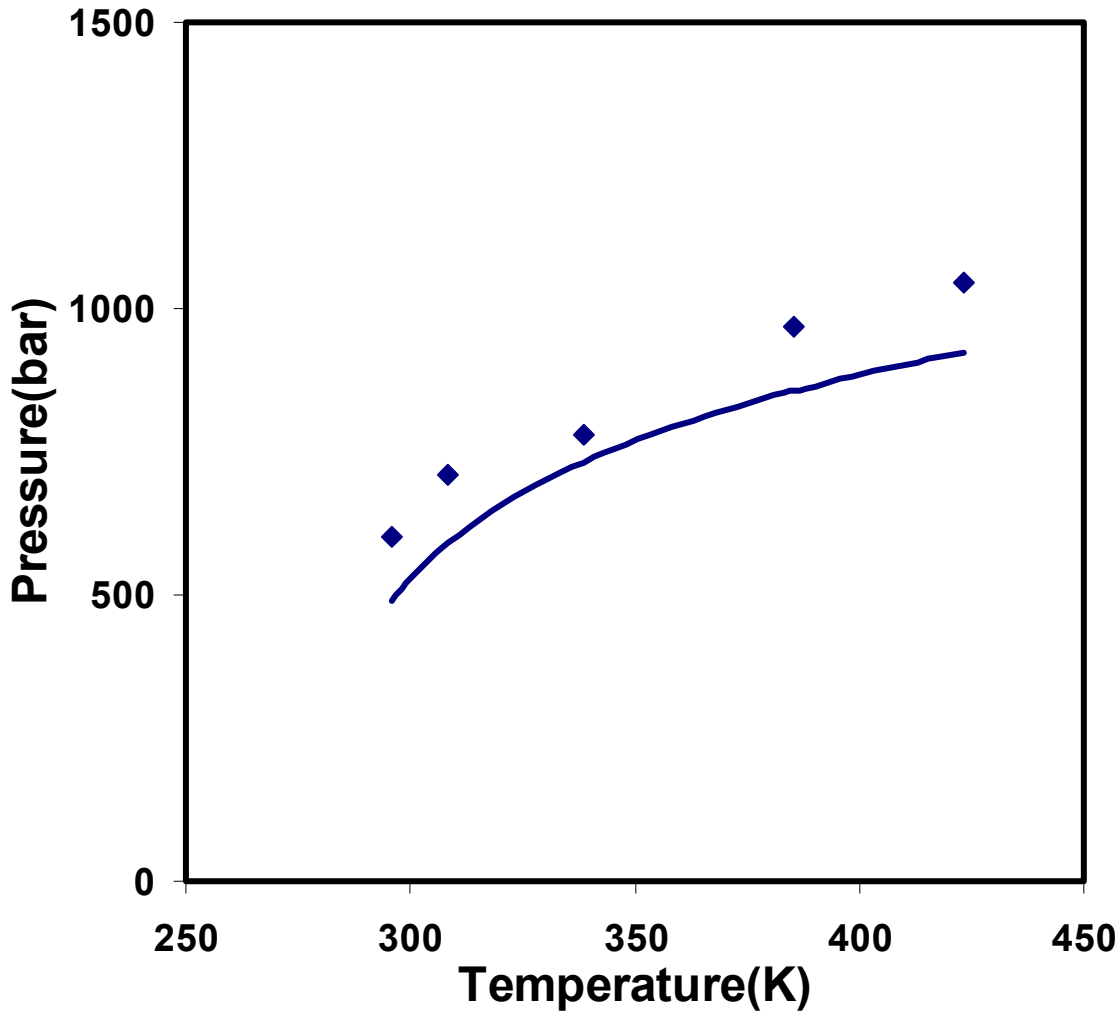

Figure 6- 24 Cloud point curve prediction in PVAc (MW= 125,000)-CO_2 systems. The squares represent experimental sorption data at 5 wt. % polymer concentration. (McHugh *et al.*, 1996). The lines represent predictions using the LELAC model.

Summary of Results

Cloud point curves in seven polymer - CO_2 systems have been correlated using the LELAC model with one or two adjustable parameters. Good agreement with experimental data was obtained (average errors between experimental and calculated values of 1.3%). Indeed, the LELAC model was better able to fit data with one or two adjustable parameters than the SAFT equation (3.6% error) with two adjustable parameters.

The ability to dissolve polymers in CO_2 is very temperature dependent since polar interactions scale with inverse temperature (McHugh and Krukonis, 1994). Energies of interaction therefore play an important role in determining the phase behavior of polymer solutions. This has been demonstrated via spectroscopy and in the LELAC model. These interactions result in complex formation between the polymer segment and the solvent leading to a reduction in the entropy of mixing if compared with a completely random, non-associating solution, as shown in Figure 6- 25 where the entropy of mixing for PMA-CO_2 is lower than the other polymer- CO_2 systems since it has stronger interactions. The modeling results confirm that CO_2 is able to distinguish differences in polymer architecture as shown in the case of polyacrylates. Polyacrylates with different backbone structures show distinct cloud point phase behavior and these differences are also apparent in the magnitude of the model parameters. Chemical architecture is also related to the polymer free volume which plays a role in solubility phenomena. This is again clearly observed in the family of acrylates where the stiffer the polymer chain, the more difficult it is to dissolve the polymer in supercritical CO_2, resulting in cloud points at high

pressure. As discussed previously, the trend of the fitted parameters and the magnitude of the variable used in LELAC model agree with these observations.

Polymer systems not employing CO_2 as the solvent were also correlated using the LELAC model with two fitted parameters. Once again, the results were in good agreement with the experimental data. It is very clear that the quality of the solvent along with molecular weight, temperature, and pressure plays an important in determining the miscibility of the system.

The LELAC model was also used to predict cloud point curves at concentrations other than the one used to obtain the adjustable parameters. Finally, pressure-composition and temperature- composition curves were constructed via the above calculations. These can be very helpful in terms of determining the phase behavior of these systems at the conditions investigated. Using these graphs, the solubility of the polymer and the solvent in each phase can be determined at a desired temperature and pressure.

The predictive capability of the model was also investigated when the solubilities of CO_2 in polymers were calculated using fitted parameters from cloud point data. The model predicts a limiting value for the carbon dioxide sorption, which is consistent with experimental information.

Finally, sorption data were correlated using LELAC model and the fitted parameter(s) used to predict cloud point curves in PBMA-CO_2 and PVAc-CO_2. Results were satisfactory with average errors in the range 7- 18%. However, the values of the fitted parameters are different from the parameters obtained in the inverse procedure. However, predicted values are still satisfactory. This alternative procedure provides the

model a great deal of flexibility in terms of making use of the limited data in most cases and predicting different set of data using the information from the data available.

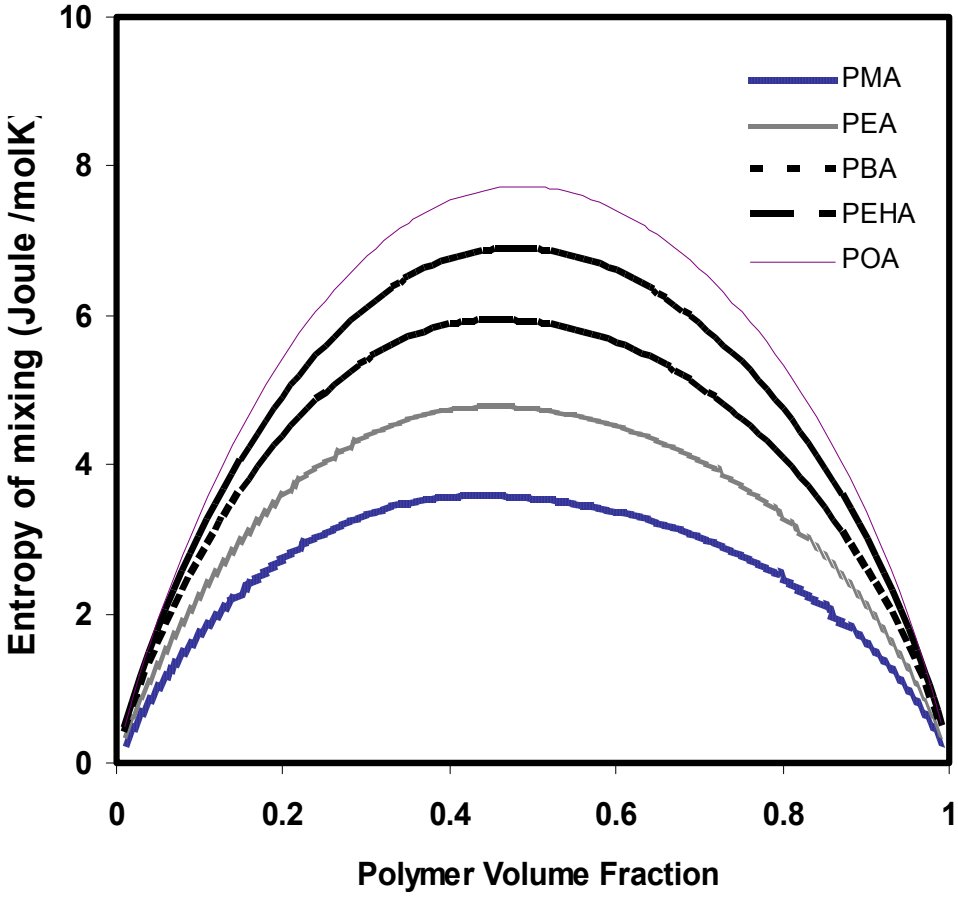

Figure 6- 25 Effect of association on entropy of mixing in polyacrylate – CO_2 systems.

CHAPTER 7

CORRELATION OF POLYMER-SUPERCRITICAL CO_2 PHASE BEHAVIOR USING SANCHEZ-LACOMBE EOS

The widely used Sanchez-Lacombe (SL) lattice fluid equation of state generally provides a satisfactory description of polymer phase behavior as discussed in Chapter 2. Two types of polymer- gas phase equilibrium can be correlated using this equation of state – cloud point curves (when a small amount of polymer dissolves completely in a gas phase) and swelling data (when a small amount of gas dissolves in the polymer).

As outlined in Chapter 3, the SL lattice fluid equation of state is given by:

$$\tilde{\rho}^2 + \tilde{P} + \tilde{T}\left[ln(1-\tilde{\rho}) + \left(1 - \frac{1}{r}\right)\tilde{\rho} \right] = 0 \qquad \textbf{(7- 1)}$$

where $\tilde{\rho}$, $\tilde{T}$, and $\tilde{P}$ are the reduced density, temperature, and pressure, and *r* represents a characteristic chain length. The reduced variables are defined as follows:

$$\tilde{T} = \frac{T}{T^*} = \frac{kT}{\varepsilon^*}; \quad \tilde{P} = \frac{P}{P^*} = P\frac{v^*}{\varepsilon^*}; \quad \tilde{\rho} = \frac{\rho}{\rho^*} = \rho\frac{rv^*}{M} \qquad \textbf{(7- 2)}$$

where T^*, P^* , and ρ^* are the characteristic temperature, pressure, and density, respectively; ε^* is the characteristic interaction energy, v^* is the volume of a lattice site, and M is the molecular weight of the fluid.

For equilibrium between a polymer and a supercritical phase:

$$\frac{\mu_i^{\mathrm{f}}}{kT} = \frac{\mu_i^{\mathrm{p}}}{kT} \tag{7- 3}$$

where the superscript *f* indicates the fluid phase, the superscript *p* indicates the polymer phase, and the subscript *i* refers to the solvent, or polymer. According to the SL EOS, the chemical potential of species *i* is

$$\begin{aligned}\frac{\mu_i^{\mathrm{LF}}}{kT} = \ln\phi_i + \left(1-\frac{r_i}{r}\right) + r_i\tilde{\rho}\left(\sum_{j=1}^{n}\phi_j\chi_{ij} - \sum_{j=1}^{n}\sum_{k=j+1}^{n}\phi_j\phi_k\chi_{jk}\right) + \\ r_i\left[\frac{\tilde{P}\tilde{v}}{\tilde{T}}\left(\frac{2}{v^*}\sum_{j=1}^{n}\phi_j v_{ij}^* - 1\right) - \frac{\tilde{\rho}}{\tilde{T}_i} + (\tilde{v}-1)\ln(1-\tilde{\rho}) + \frac{1}{r_i}\ln\tilde{\rho}\right]\end{aligned} \tag{7- 4}$$

where χ_{ij} is the Flory-Huggins interaction term

$$\chi_{ij} = \frac{\left(\varepsilon_{ii}^* + \varepsilon_{jj}^* - 2\varepsilon_{ij}^*\right)}{kT} \tag{7- 5}$$

The mole fraction y_i, weight fraction w_i, and molar concentration C_i of a component in the lattice are expressed in terms of the site fraction of the component by

$$y_i = \Phi_i \frac{r}{r_i}; \quad w_i = \Phi_i \frac{r}{r_i}\frac{M_i}{M}; \quad C_i = \Phi_i \frac{r}{r_i}\frac{\tilde{\rho}\rho^*}{M} \qquad \textbf{(7- 6)}$$

where M_i is the molecular weight of the species.

Pure-component parameters, T^*, P^*, and ρ^* are obtained by fitting saturated liquid density and vapor pressure data over an extended range up to the critical temperature for the solvent and by fitting PVT data for the polymer. Compilations of characteristic parameters for polymers and low molecular weight substances can be found in the work of Sanchez and Lacombe (1976, 1977). Rogers (1993) has compiled PVT data for a large number of polymers and some copolymers and these data can also be used to regress pure-component parameters.

In this study, the SL EOS is used to correlate phase behavior in systems also investigated using the LELAC model – namely PBMA-CO_2 and PVAc-CO_2, because swelling and cloud point data are available for these mixtures. Polymer-CO_2 systems that exhibit weak association were also investigated in order to compare the performance of the SL EOS for weakly associating systems.

Polymer Swelling with Supercritical CO_2

The SL EOS results of swelling calculations are tabulated in Table 7-1. It can be seen from the table that the model is able to correlate the experimental data very well, within an average error of 3.2 % using one adjustable parameter.

Table 7- 1 Error analysis for Polymer-CO_2 swelling correlations of SL model.

Polymer	Temperature range (K)	Pressure range (bar)	SL EOS AAD%
PMMA	314.95-341.15	10 - 250	0.95
PBMA	313.15-353.15	0 - 80	1.42
PVAc	313.15-353.15	20 - 90	2.25
PS	373.15-453.15	0-200	5.26
Silicon Rubber	308.15	0-60	3.02

Figure 7-1 shows the results obtained in the case of PMMA-CO_2 at 314.95 K, 331.25 K and 341.15 K. It should be noted that negative values of the binary parameter k_{ij} were obtained in this system, indicating strong specific interactions between PMMA and CO_2. The binary parameter decreased with temperature, in agreement with the behavior of specific interactions which also decrease with increasing temperature.

The model is also successful in correlating swelling in the systems PBMA-CO_2 and PVAc-CO_2, as shown in Figure 7-2 and 7-3. Calculated values were in good agreement with experimental data over a wide temperature range (313 K - 353 K) in both systems. At the higher temperatures, the calculations indicate that swelling reaches a maximum value. This may be due to a glass transition that limits the amount of CO_2 incorporated in the polymer phase. Negative values of k_{ij} are obtained due to the fact these polymers are known to interact with CO_2, described in Chapter 5.

Figure 7-4 shows the results for silicon rubber-CO_2 with an interaction parameter of 0.047. Experimental data reported by Fleming and Koros (1986) are also shown in the figure. Fleming and Koros indicated that the silicon rubber was cross-linked to a small extent, although this was neglected in the calculations. As shown in the figure, agreement

with experiment is satisfactory. Note that the interaction parameter is positive for this nonpolar system.

Figure 7-5 shows the calculated sorption isotherms of CO_2 - PS at several temperatures with a positive interaction parameter of 0.088 at 373.15 K and changing with temperature. Interaction of the polymer with CO_2 is not expected as shown in Chapter 5 since the polarity of PS is really low to form any association complex. Solubility of CO_2 increases almost linearly with pressure. The solubility decreases with increasing temperature, as has been observed in many gas-polymer systems, and solute-solvent systems in the case of gases such as helium, hydrogen, nitrogen and oxygen.

To summarize, the SL EOS is able to correlate swelling behavior of weakly as well as strongly associating systems with one adjustable parameter. However, this adjustable parameter varies with temperature for best results.

Cloud Point Curves in Polymer – CO_2 Systems (Solubility of polymers in Supercritical CO_2)

Cloud point curves were also calculated for the systems cited in the previous section. Figure 7-6 and 7-7 show SL EOS calculations of cloud point curves in PVAc – CO_2 and PBMA - CO_2 at a polymer concentration of approximately 5 wt % polymer. As seen in the figures, a quantitative representation of cloud point curve is not possible and the trends of the experimental data are not captured by the model although the adjustable parameter has been allowed to vary with temperature. Possible reasons for this poor estimation lie in the assumptions made in the formulation of the model. In the derivation of the SL model, molecules and holes are randomly distributed on the lattice. This

assumption is not valid when specific interactions exist between molecules. These specific interactions also create complexes between the polymer and CO_2 molecules, which are not taken into account by the model. These molecular orientations in the solutions have been neglected which result in the mismatch between the experimental data and estimations. As a result, it is not too surprising that the SL EOS does a poor job in modeling these systems involving polar polymers.

One way to add specific interactions to the SL EOS is to use a quasi-chemical approach to decompose the partition function into associative and non-associative parts. The partition function for association can be determined by calculating the number of ways that interaction bonds are distributed within the system. However, the approach is very complex and may not justify the effort when models such LELAC and SAFT are available and have proved successful in correlating phase equilibria.

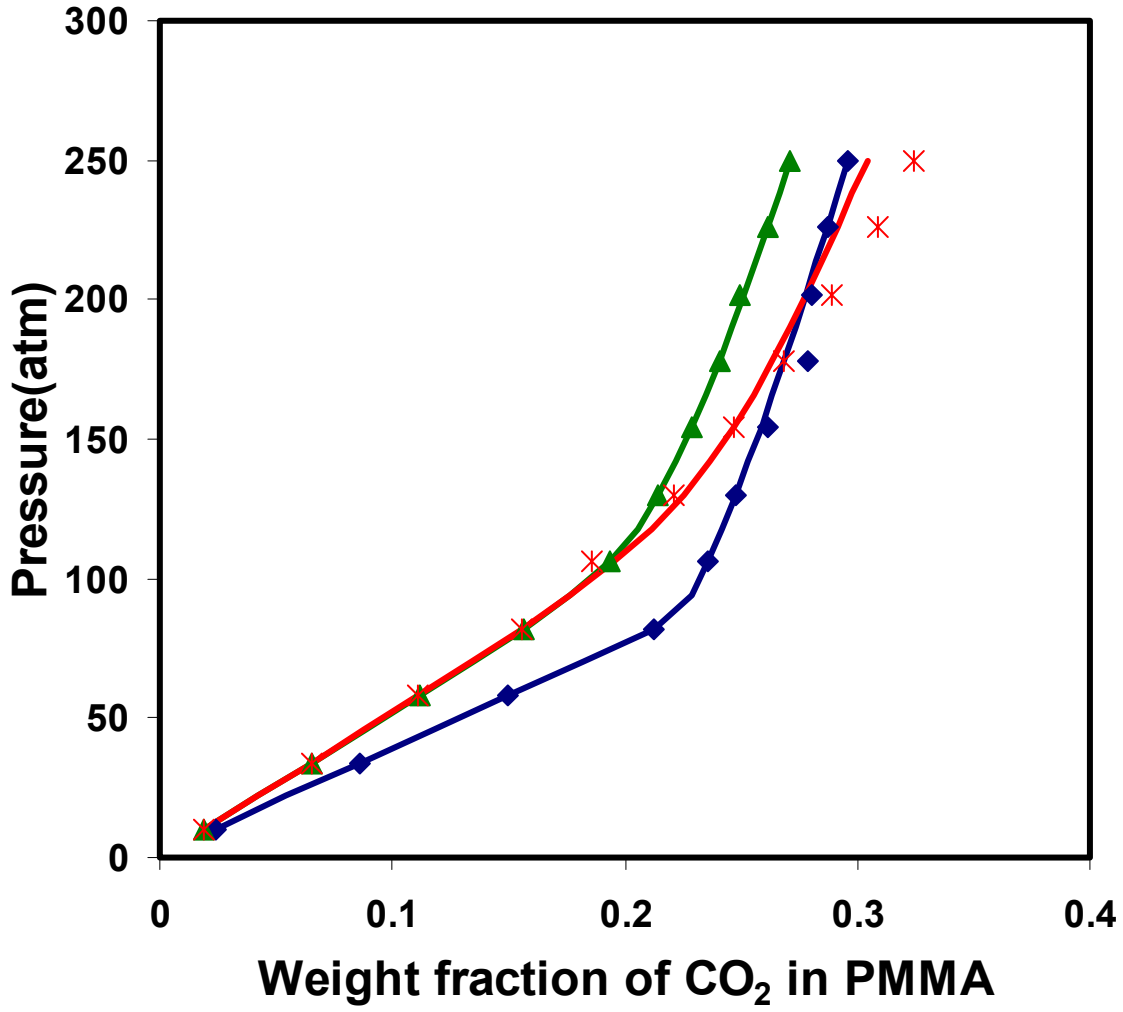

Figure 7- 1 Experimental and calculated sorption isotherms in the PMMA – CO_2 system. Experimental data from McHugh *et al.*, (1988). The solid lines represent the calculations using the SL EOS with δ_{ij}=–0.001 at 314.95 K, δ_{ij}=–0.004 at 331.25 K, and δ_{ij}=–0.019 at 341.15 K, respectively. The points are experimental values at 314.95 K (◊), at 331.25 K (Δ), at 341.15 K(*).

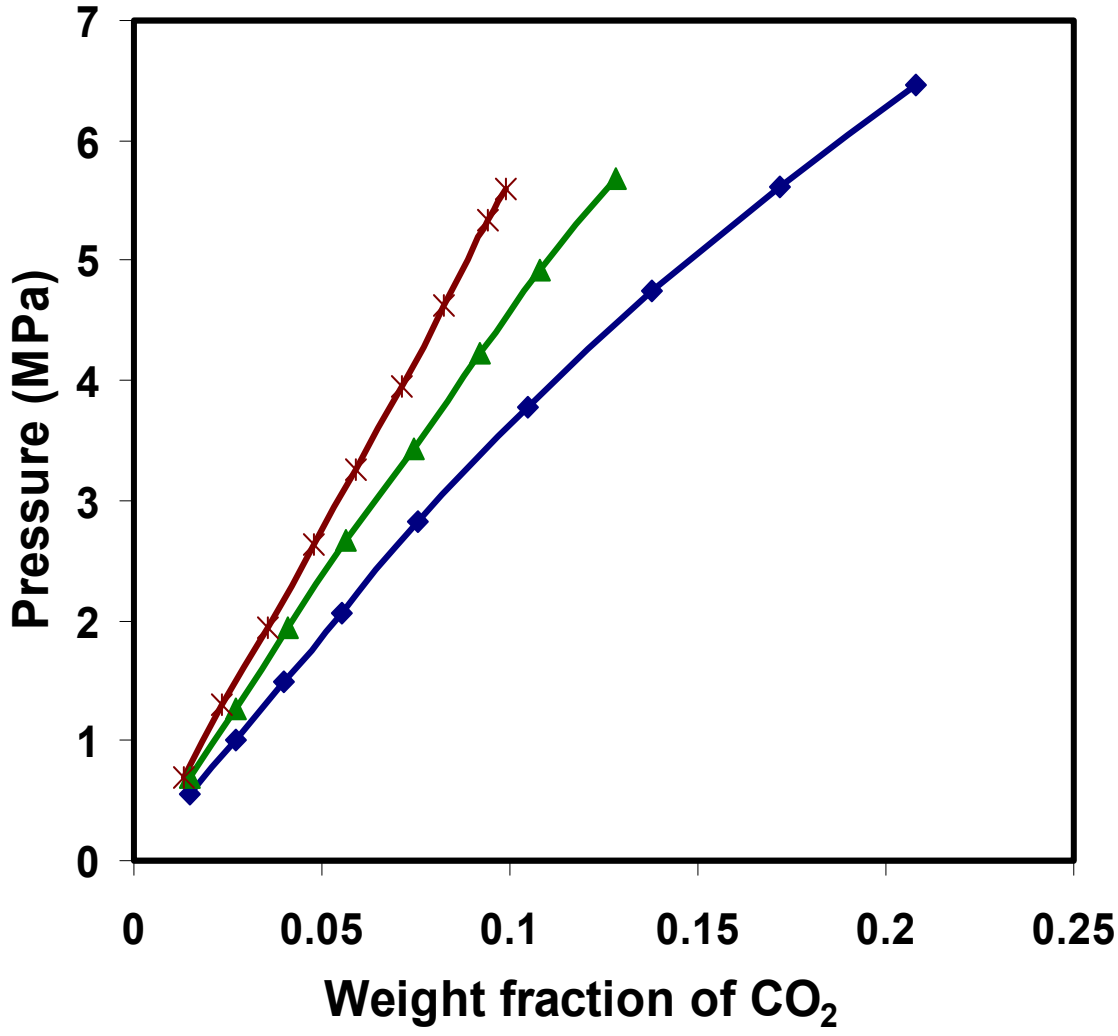

Figure 7- 2 Experimental and calculated sorption isotherms in the PBMA – CO_2 system. Experimental data from Zhong *et al.*, (1997). The solid lines represent the calculations using the SL EOS with δ_{ij}=–0.015 at 313.15 K, δ_{ij}=–0.026 at 333.15 K, and δ_{ij}=–0.043 at 353.15 K, respectively. The points are experimental values at 313.15 K (◊), at 333.15 K (Δ), at 353.15 K (*).

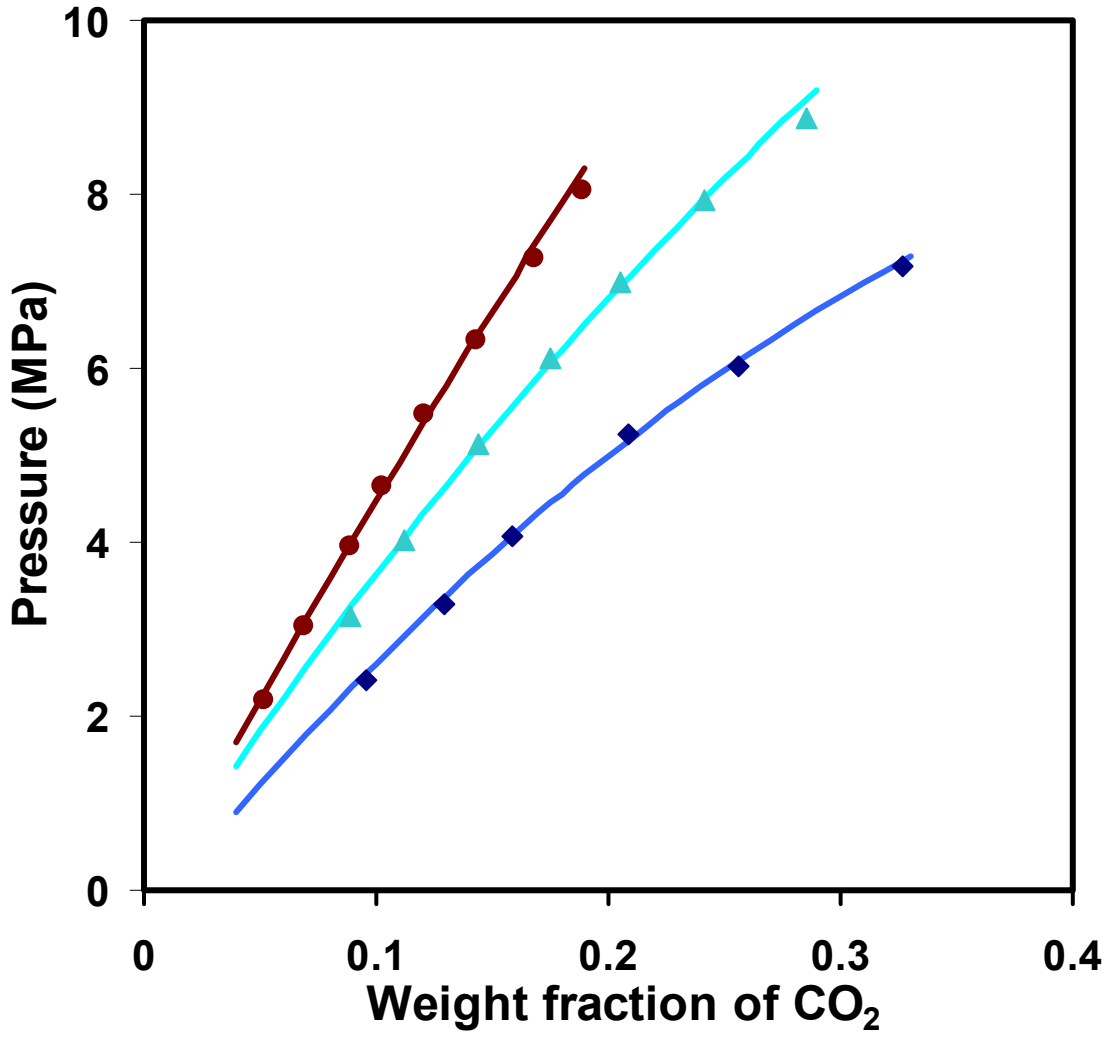

Figure 7- 3 Experimental and calculated sorption isotherms in the PVAc – CO_2 system. Experimental data from Zhong *et al.*, (1997). The solid lines represent the calculations using the SL EOS with δ_{ij}=–0.097 at 313.15 K, δ_{ij}=–0.102 at 333.15 K, and δ_{ij}=–0.125 at 353.15 K, respectively. The points are experimental values at 313.15 K (◊), at 333.15 K (Δ), at 353.15 K (o).

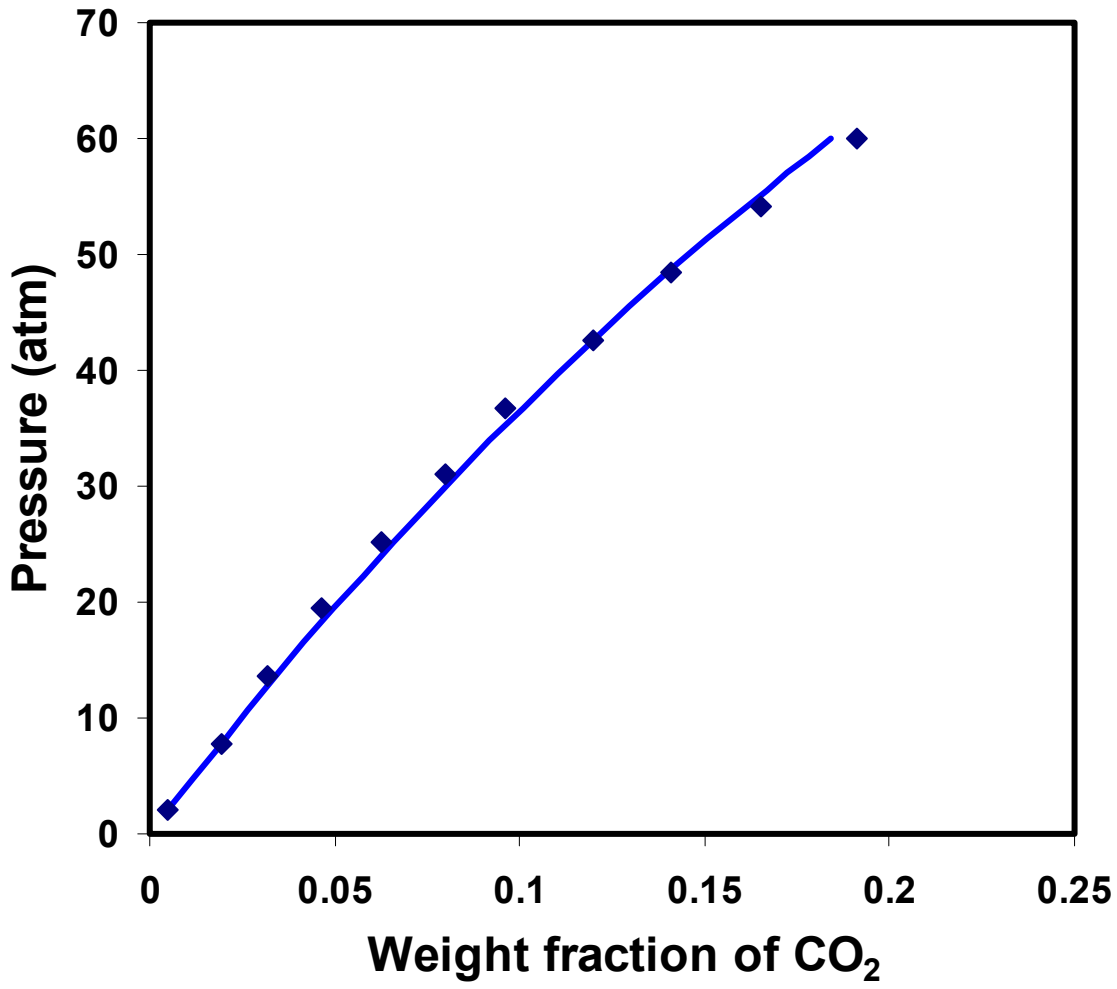

Figure 7- 4 Experimental and calculated sorption isotherms in the Silicone Rubber – CO_2 system. Experimental data from Fleming and Koros (1988). The solid line represents the calculations using the SL EOS with δ_{ij}=0.047 at 308.15 K. The points are experimental values at 308.15 K (◊).

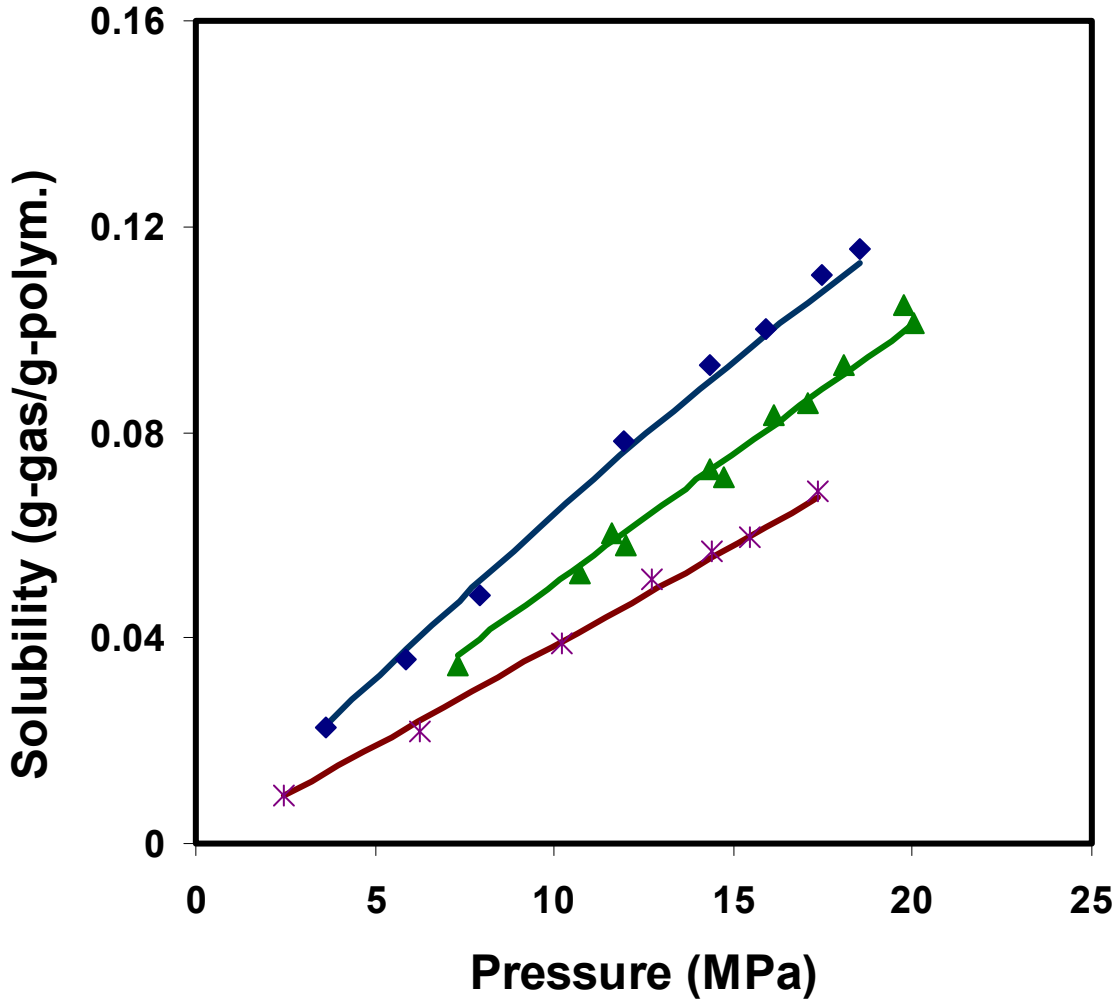

Figure 7- 5 Experimental and calculated sorption isotherms in the PS – CO_2 system. Experimental data from Sato *et al.*, (1996). The solid lines represent the calculations using the SL EOS with δ_{ij}=0.088 at 373.15 K, δ_{ij}=0.117 at 413.15 K, and δ_{ij}=0.132 at 453.15 K, respectively. The points are experimental values at 373.15 K (◊), at 413.15 K (Δ), at 453.15 K (*).

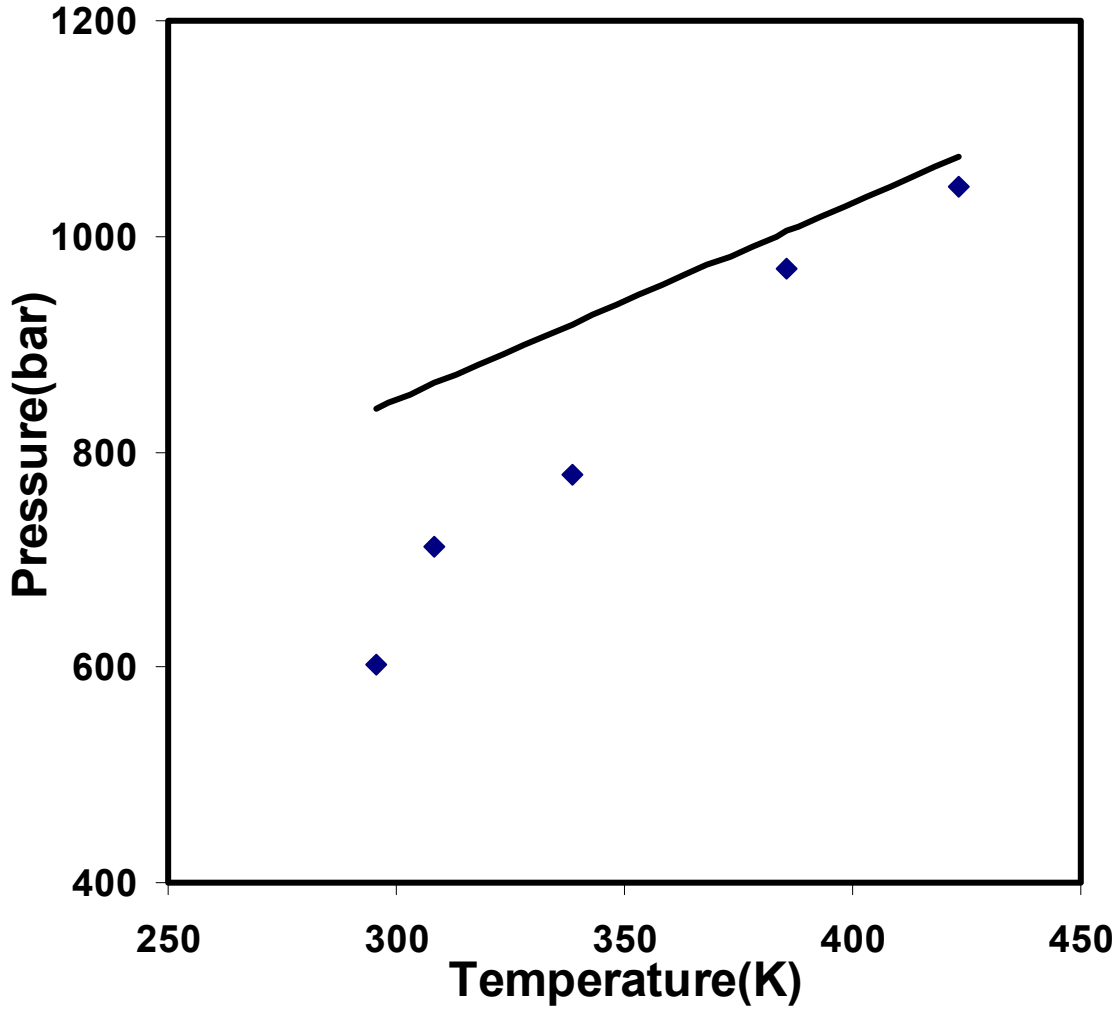

Figure 7- 6 Experimental and calculated cloud point curves in the PVAc – CO_2 system. Experimental data from McHugh *et al.*, (1996). The polymer solubility is approximately 5 wt%. The solid lines represent the SL EOS calculations with δ_{ij}=-0.097 at 313.15 K . The adjustable parameter changes with temperature with the relationship δ_{ij}=0.39258-0.0015632×T. The points are the experimental values.

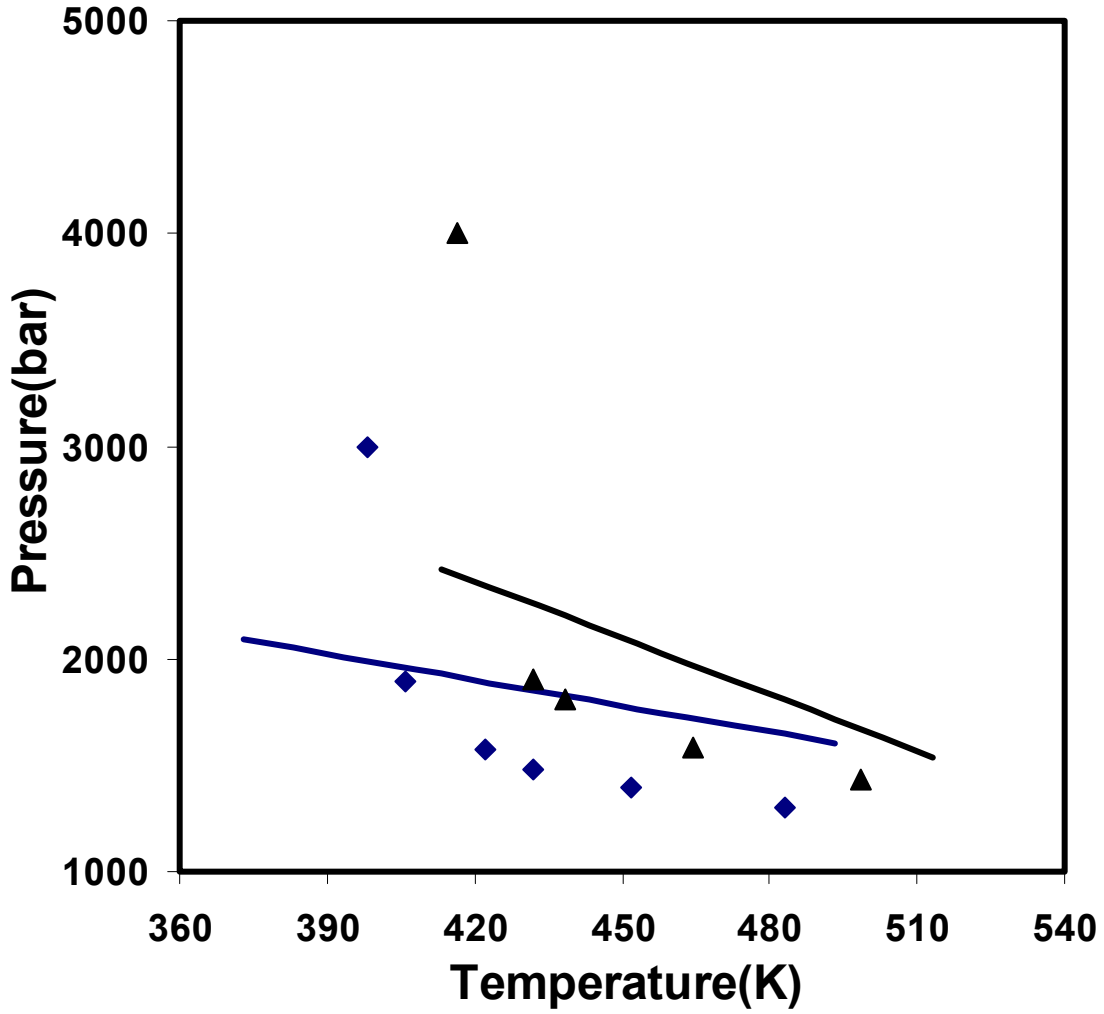

Figure 7- 7 Experimental and calculated point curves in PBMA-CO_2 system at different molecular weights of 100,000 and 320,000. Experimental data from McHugh *et al.*, 1996. The polymer solubility is approximately 5 wt%. The solid lines represent the SL EOS calculations with δ_{ij}=-0.026 at 393.15 K for PBMA 100,000 and δ_{ij}=-0.049 at 393.15 K for PBMA 320,000. The adjustable parameter changes with temperature with the relationship. δ_{ij}=0.17959-0.001564×T for PBMA100,000 and . δ_{ij}=0.19458-0.000627×T for PBMA 320,000. The points are the experimental values at MW=100,000(◊) and at MW=320,000(Δ).

CHAPTER 8

CONCLUSIONS AND RECOMMENDATIONS

Conclusions

The overall goal of this work was to develop a new model for calculating the phase behavior of polymer-CO_2 solutions in which there is association between the polymer and CO_2 molecules. Such a model should contain a minimum number of adjustable parameters and, as far as possible, the parameters should be obtained from independent measurements.

In this work, a new model has been proposed that extends the gART-L model for associating polymer solutions at high pressure. The resulting LELAC model contains three parameters (the association ratio, the association energy, and the dispersion energy) that must be obtained from independent measurements, or by fitting data. The association ratio was assumed to be 1 in this work, because the components in the systems investigated are capable of interacting only one way with each other. However, it is possible to obtain this ratio, as well as the association energy, via spectroscopy or molecular modeling. The dispersion energy was obtained via the solubility parameter of the non-polar analog of the polymer. The third parameter was obtained by fitting data.

Cloud point curves in PVAc - CO_2 and PBMA - CO_2 systems were calculated using the LELAC model. Good quantitative agreement with experiment was obtained using the association energy from FTIR spectra and one adjustable parameter. Cloud points of solutions containing a family of polyacrylates were also calculated. Two

adjustable parameters were used for these mixtures and, once again, good agreement was obtained with experimental data, with errors around 1%. The calculations also showed that the absolute values of the association energy and the equilibrium constant decreased as the length of alkyl side chain on the polymer molecule is increased. This can be attributed to shielding of the interaction sites by the alkyl chain. LELAC calculations were also compared with SAFT calculations, and the new model was found to be somewhat better in most cases.

Additionally, the LELAC model has been used to investigate its predictive capabilities when the solubilities of CO_2 in polymers were calculated using fitted parameters from cloud point data. The model predicts a limiting value for the carbon dioxide sorption, which is consistent with experimental information.

Finally, sorption data were correlated using LELAC model and the fitted parameter(s) used to predict cloud point curves in PBMA-CO_2 and PVAc-CO_2. Results were satisfactory with average errors in the range 7- 18%. However, the values of the fitted parameters are different from the parameters obtained when cloud point data are fitted.

FT-IR Spectroscopy was used to identify polymers that associate with CO_2 in terms of Lewis acid-base interactions. LELAC parameters were obtained via shifts in FT-IR band frequencies. These experiments also showed that PVC and CO_2 interact in a quite different way from other polymer – CO_2 interactions. A new mechanism for this interaction was proposed. This type of mechanism could shed some light on the phase behavior of PVC - CO_2 and also stimulate further work on the nature of this interaction in other polymer -CO_2 systems.

In the last part of this thesis, the Sanchez-Lacombe EOS was used to correlate cloud points and swelling behavior of polymers in supercritical CO_2. The SL EOS was successful in correlating high pressure swelling data with one fitted parameter. However, similar success was not achieved in cloud point calculations even though the interaction parameter was allowed to vary with temperature and molecular weight of the polymer. This suggests that the SL EOS is not a good model for systems with association.

Recommendations

One of the assumptions of the LELAC model is that the binding ratio in solute-solvent complexes is unity. This may not be true for systems containing multi functional groups. Spectroscopic techniques or rigorous molecular modeling methodologies can provide more appropriate estimates of this binding ratio. A binding ratio that is not unity also requires modification of the lattice formulation, especially in cases where a given solvent is bound to more than one segment.

In addition, in macromolecular systems, the molecular weight distribution plays an important role in phase equilibria. A system with a broad molecular weight distribution can no longer be treated as a pseudo binary system with respect to phase separation temperatures. Different molecular weight fractions can potentially have different equilibrium constants for association. Also, the solubility can be affected to a large extent by the molecular weight. This can be clearly seen in the difference of solubilities of oligomers and polymers in supercritical fluids (McHugh and Krukonis, 1994).

There remain a number of questions and unexplored opportunities in the area of modeling polymer solution phase behavior using this associative model. First, *in-situ* Fourier Transform Infra-Red (FT-IR) spectroscopy offers the ability to measure short path-lengths, thus allowing CO_2 to be studied without interference from large water absorbances. The main drawback of in-situ FT-IR spectroscopy is the absorptivity effect that can cause problems with quantitative analysis in some cases. Other types of spectroscopic techniques, such as NMR and UV-Vis can be employed to obtain both the association energy and equilibrium constant.

Fluoropolymers have been shown to exhibit a significant affinity for CO_2 (De Simone *et al.,* 1994). FT-IR spectral effects such as band shifts and shapes might yield quantitative data on CO_2-fluoropolymer interactions. An enhanced understanding of the affinity of fluoropolymers for CO_2 and estimation of the fluoropolymer solubilities would aid in effective utilization of technologies related to these systems.

The analysis presented in this work can be extended to a solute/binary solvent system by accounting for the different characteristics of association of two solvents. Different association characteristics of the two solvents in a binary solvent system can be incorporated in the lattice model by assigning different equilibrium constants to each solute-solvent association. This can be applied to co-solvents used in supercritical polymer solutions, where co-solvent is added to the binary system to enhance the solubility (McHugh and Krukonis, 1994).

Another important type of estimation that can be done with this model is the calculation of copolymer phase equilibria. The model can be formulated to account for different kinds of monomer units interacting with the solvent. There is an extensive

compilation of data in the literature for copolymer solutions which can be used for these modeling studies. The model developed in the study cannot be directly applied to polymer blends, but has to be modified substantially to take into account the connectivity of the associated and unassociated segments.

A separate area of academic and industrial interest that may also benefit from this approach is supercritical CO_2 assisted impregnation, e.g. incorporation of drugs into polymers for biological applications. In this work, the model has been used to correlate the solubilities of polymer in supercritical CO_2. On the other hand, the solubilities of CO_2 in polymers can be calculated to investigate the feasibility of using supercritical CO_2 as a swelling agent and for doping polymers with different solutes such as drugs. In addition, the effects of process conditions, partitioning of the solute between polymer and the fluid phases and interactions among the various components can be investigated to optimize the doping process.

APPENDIX A

DETAILED DESCRIPTION OF THE HIGH PRESSURE CELL

Following are detailed descriptions of the high-pressure cells utilized in this work. All of these cells are constructed from 308L or 316 stainless steel. Flanges connecting two steel components are sealed with 1/24" thick lead which has been cleaned with dilute acid to prevent contamination of the experimental fluid. These flanges must be retightened after initial pressurization, and should be checked every 7-10 days of use. The windows of optical cells are sealed with a soft metal o-ring such as indium. The seal is made by slowly increasing the pressure of the cell and allowing this force to compress the window into the soft metal. The window material can be quartz, sapphire, or IR-transparent salts such as BaF_2 or ZnSe. If indium is used as the sealing material, the cells are limited to approximately 353 K operation without a significant reduction in pressure rating. Other metals such as silver, lead, and gold have also been installed to ease this limitation. Dimensions in the figures are inches.

High-pressure batch vessels were utilized throughout the course of this research for a number of applications including investigations of polymer-CO_2 interactions (Chapter 5). Figures A-1 and A-2 show the dimensions of the bottom and top sections of one such two-piece batch vessel. These vessels were easily sealed using a lead gasket and 5/16"-18 steel bolts. The two AF2 1/8" ports allow easy connection of high-pressure tubing. Temperature was maintained by submerging the sealed vessel in a water bath for experiments between ambient and 353 K, and placing in an oven for experiments between 313 and 373 K. These batch vessels were tested and used for pressures up to 150 bar for temperatures between ambient and 353 K.

The optical cell shown in Figures A-3 and A-4 was also utilized for studying the effects of CO_2 on the PMMA and other polymers. This cell was equipped with ZnSe windows allowing it to be used over the complete mid-IR spectral region (4000 – 400 cm^{-1}). The path length was ~ 4 mm which reduced interference due to dense fluid absorbances when monitoring polymer or dye spectra. Temperature was maintained by three ¼" cartridge heaters connected to a control device. This cell was pressure tested and used up to 150 bars for temperatures less than 353 K.

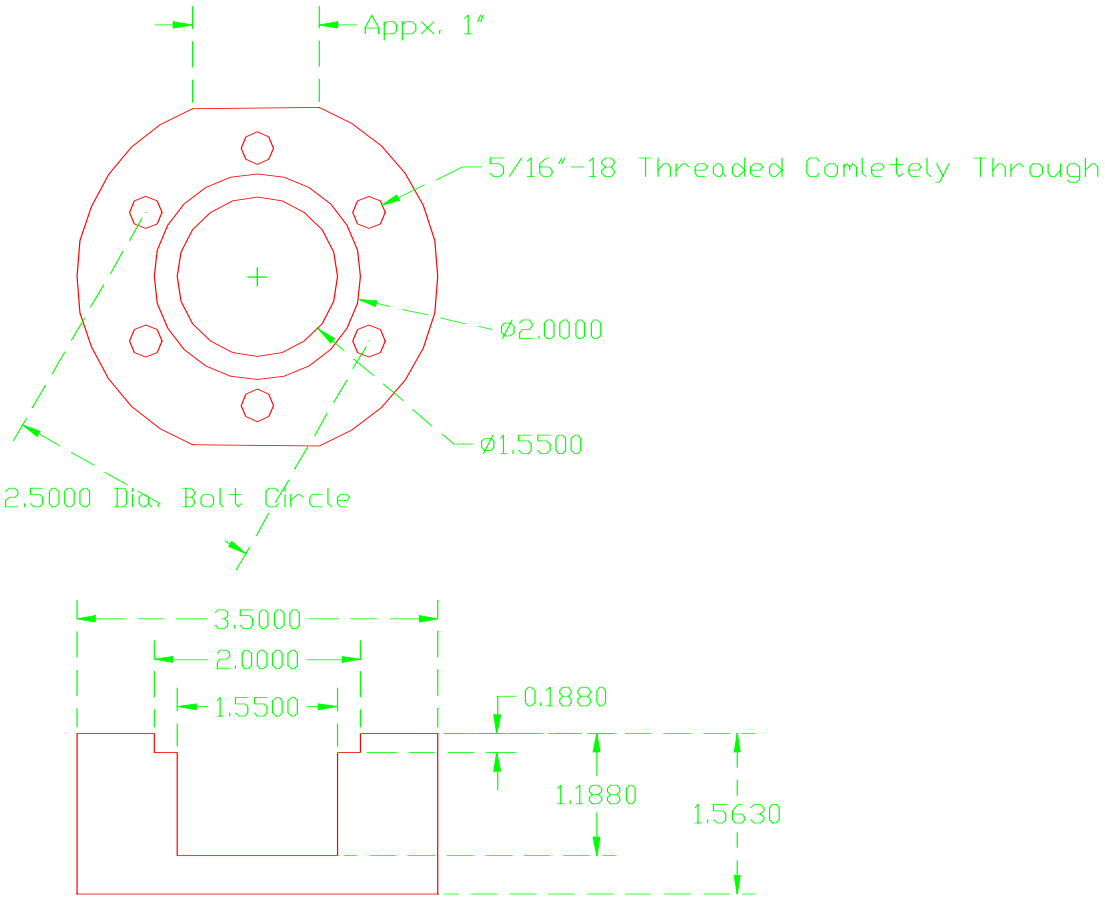

Figure A-1.Dimensions of high-pressure batch vessels – bottom section. Permission for the drawings A-1 through A-12 is obtained from Dr. Eckert and Dr. Brown of Specialty Separations Center.

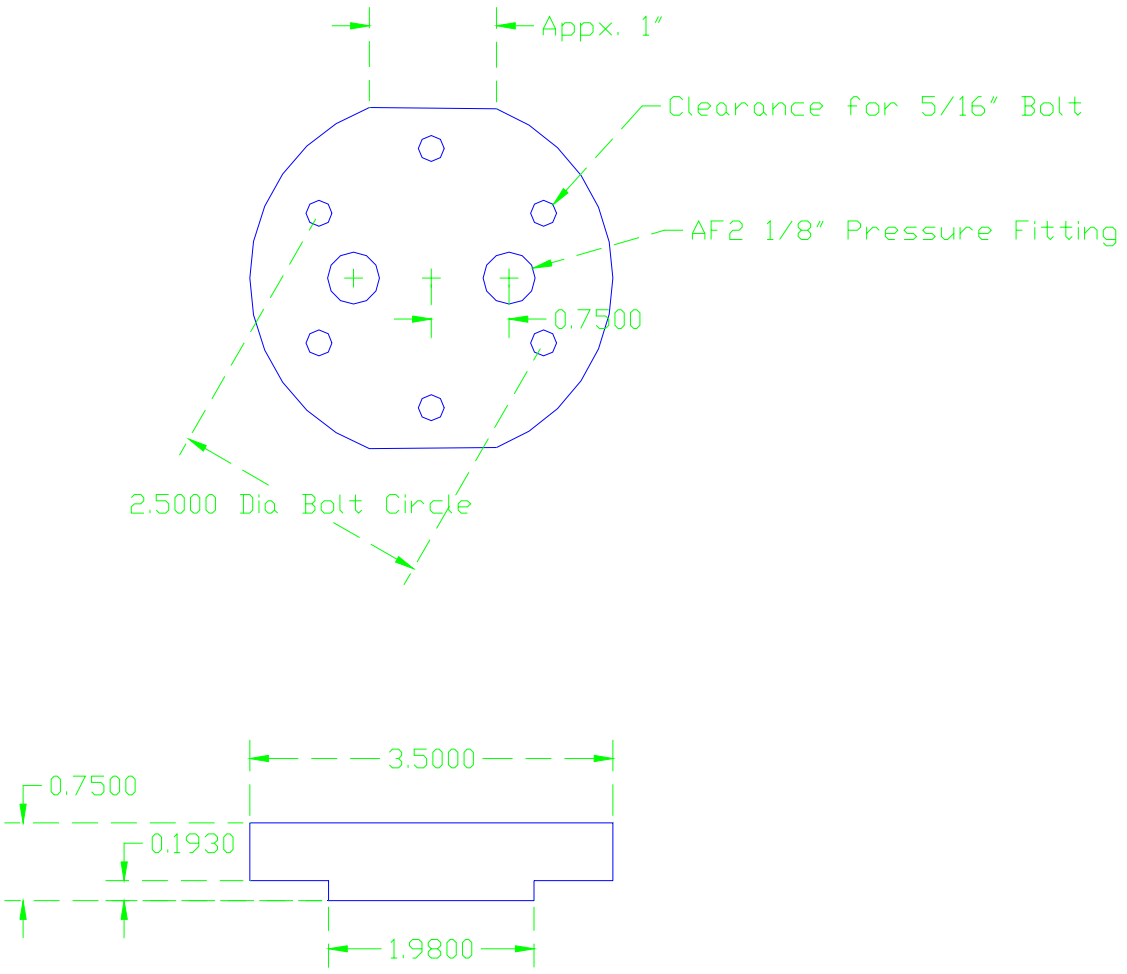

Figure A-2.Dimensions of high-pressure batch vessels – top section.

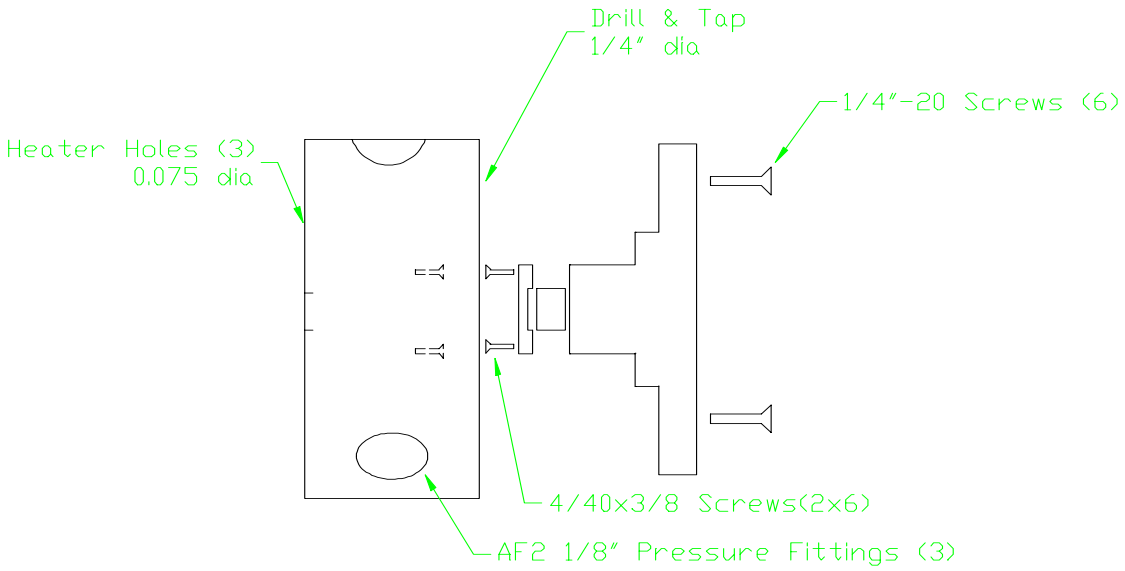

Figure A-3 Side view of single optical path high pressure cell 1 – short path length.

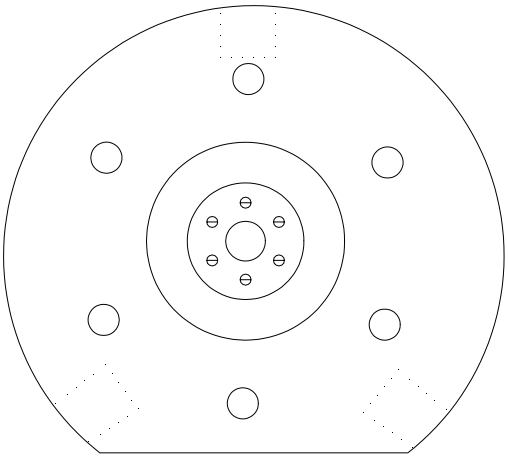

Figure A-4 Front view of single optical path high pressure cell 1 – short path length.

Also, another high-pressure cell utilized for the CO_2 interaction experiments (Chapter 5) was based on the original design of Kazarian *et al.*,(1996) and West (1997). The path length of their original cell was modified by changing window holders, along with replacing the ZnSe windows with BaF_2 windows. In addition two similar cells were constructed and utilized throughout this research. The path length of these cells could be adjusted from ~ 2 mm to over 6 cm by changing the window holders. Thus, a cell could be assembled having a short path length to observe a polymer phase (the short path length reduces the amount of surrounding fluid phase in the optical path) and a long path length to observe the fluid phase. Figures A-5 through A-11 present the dimensions of the parallel path cells utilized in this work. These figures are reproduced from West (1997) with the permission of Professor C.A. Eckert. The dual parallel path cells were pressure tested and used up to 150 bars for temperatures less than 333 K.

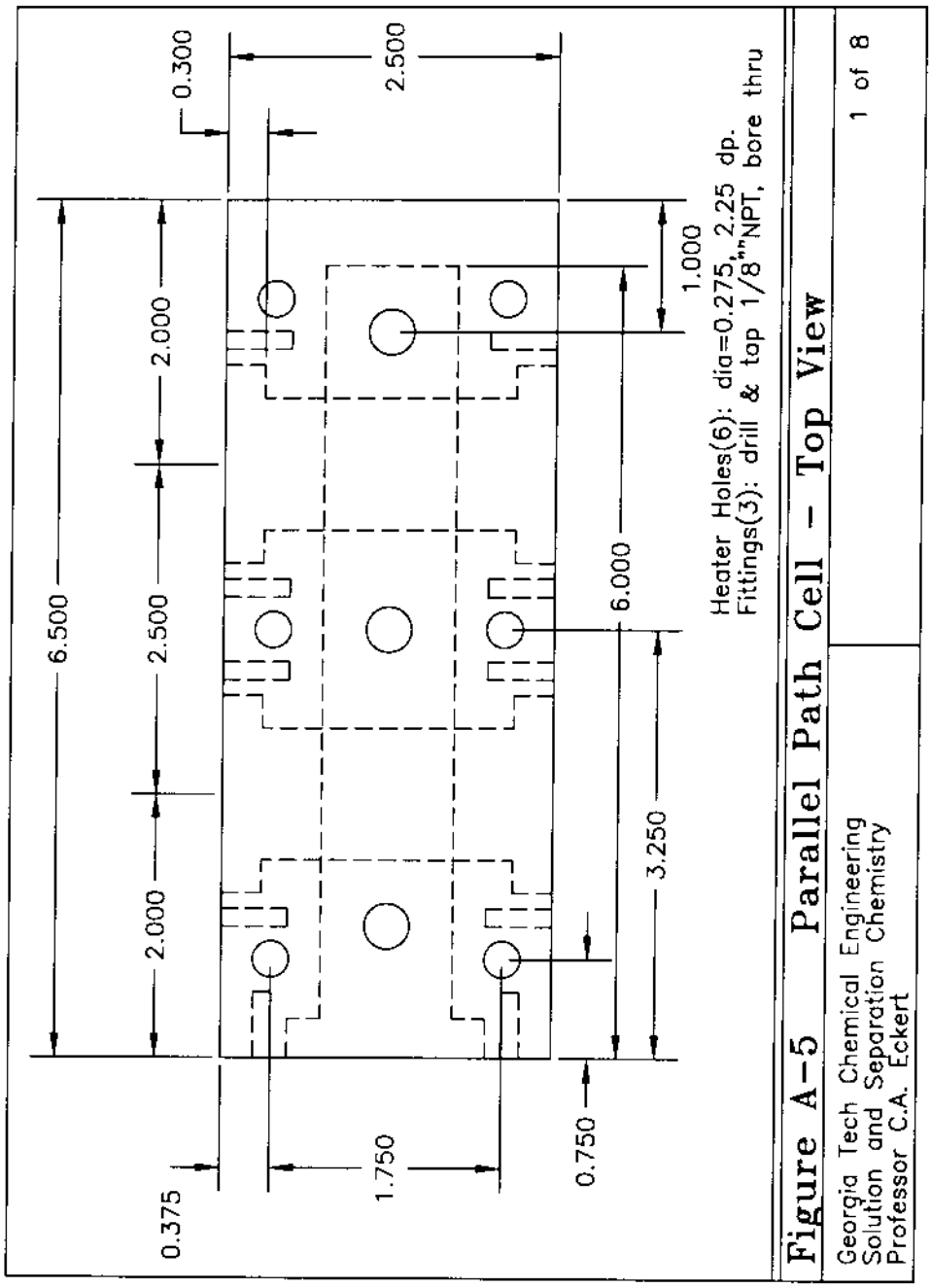

(Reproduced with the permission of Professor C.A. Eckert.)

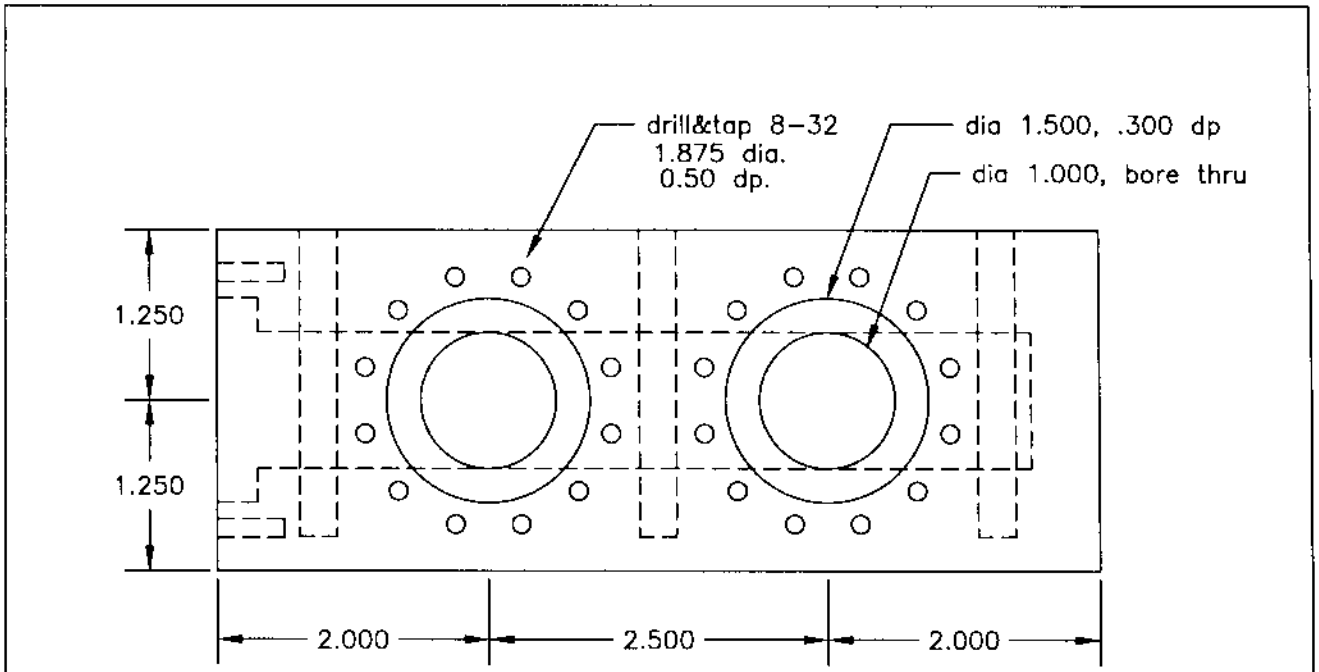

Figure A-6 Parallel Path Cell - Front View

Georgia Tech Chemical Engineering
Solution and Separation Chemistry
Professor C.A. Eckert

2 of 8

Rev History:

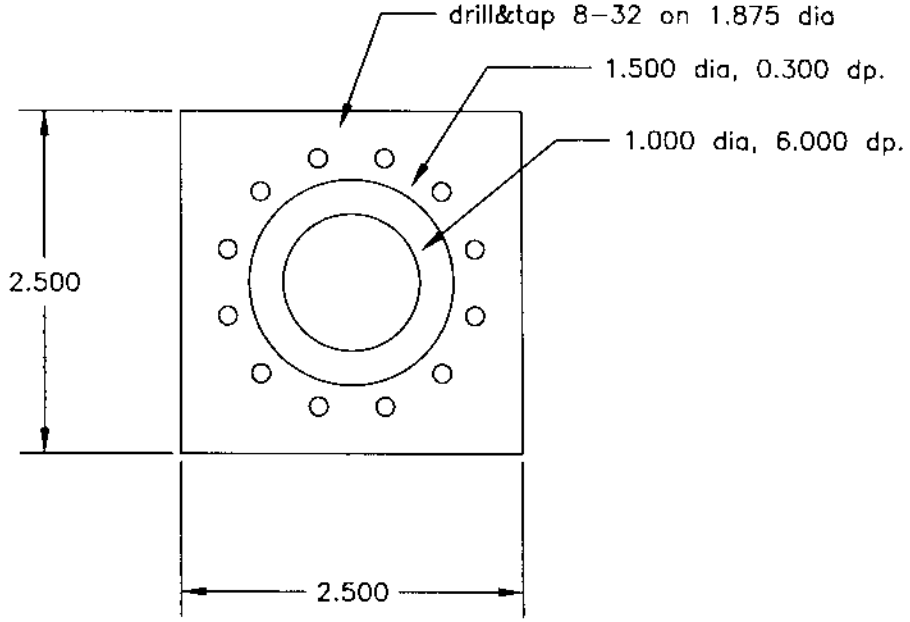

Figure A-7 Parallel Path Cell - Side View

Georgia Tech Chemical Engineering
Solution and Separation Chemistry
Professor C.A. Eckert

3 of 8

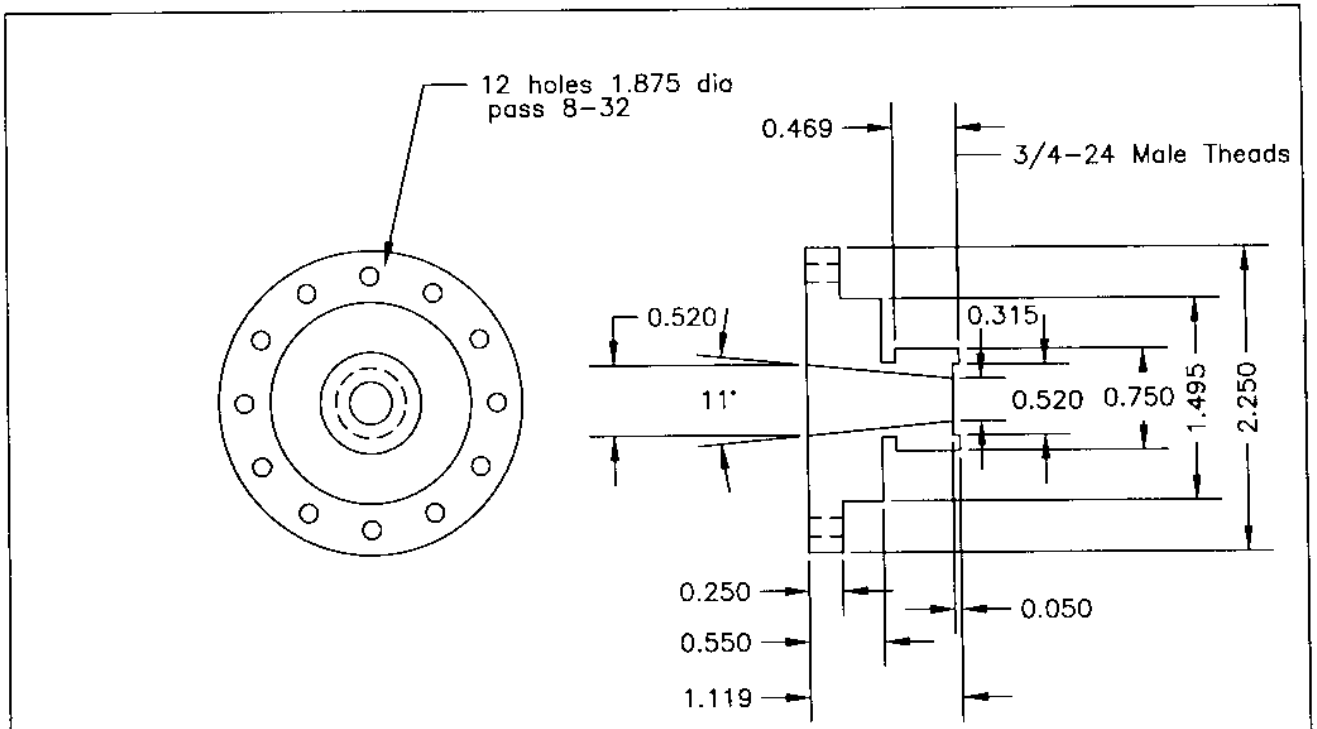

Figure A-8 Parallel Path Cell - 1.0 cm Window Holder

Georgia Tech Chemical Engineering
Solution and Separation Chemistry
Professor C.A. Eckert

4 of 8

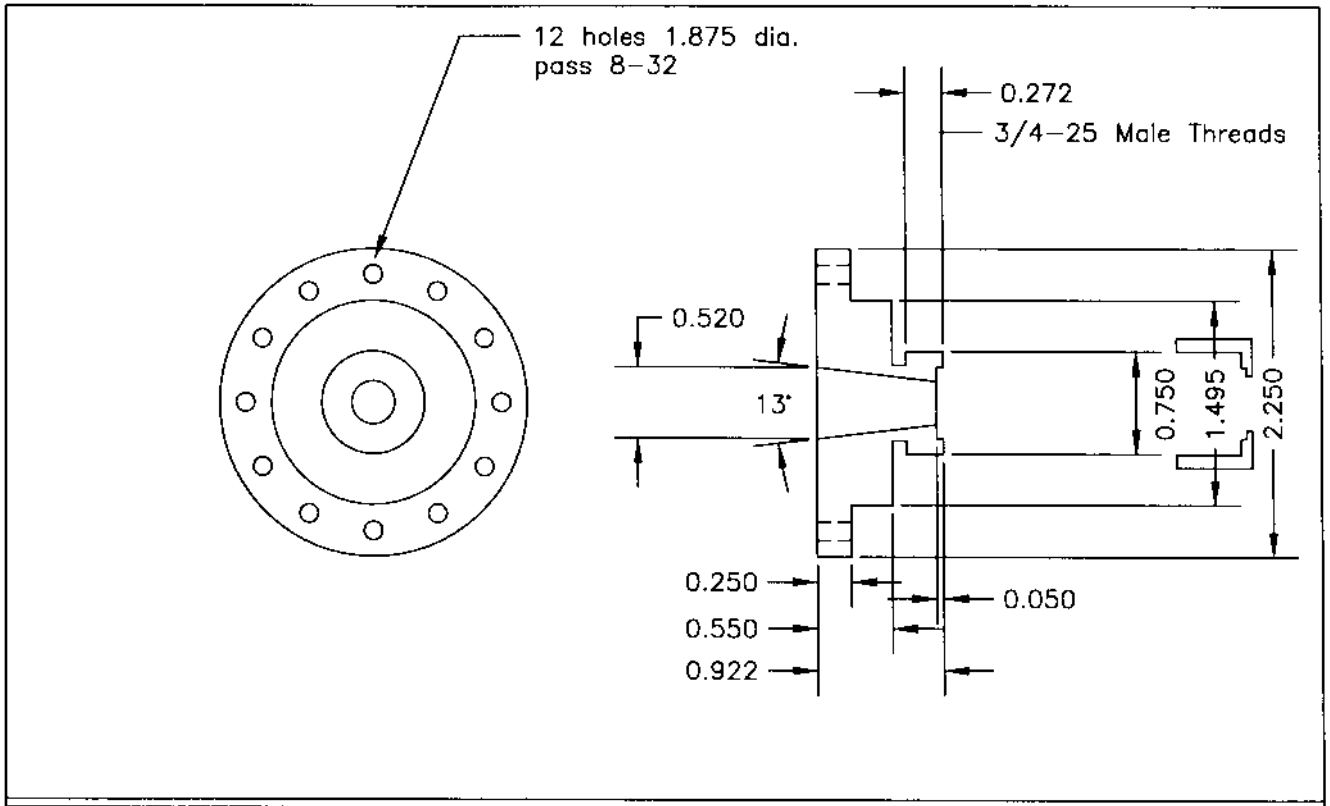

Figure A-9 Parallel Path Cell - 2.0 cm Window Holder

Georgia Tech Chemical Engineering
Solution and Separation Chemistry
Professor C.A. Eckert

5 of 8

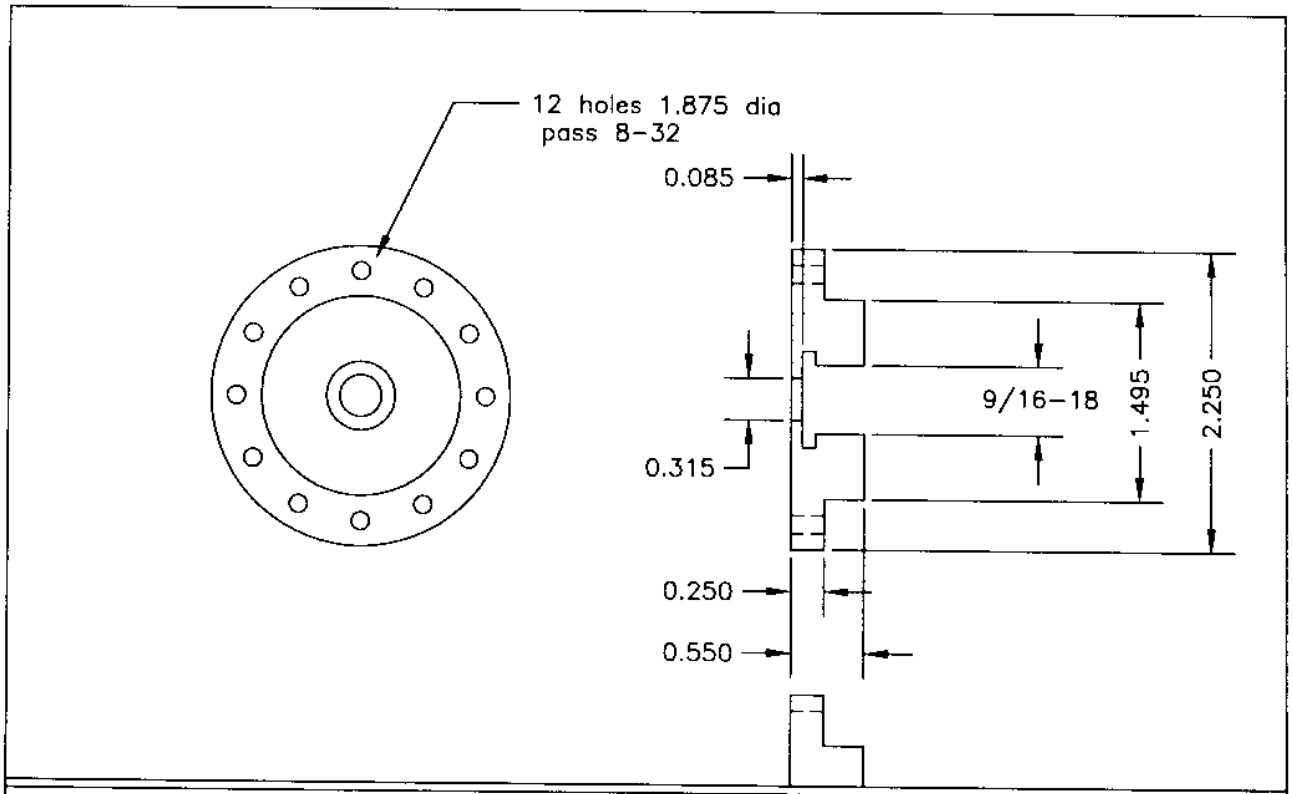

Figure A-10 Parallel Path Cell - 6.0 cm Window Holder

Georgia Tech Chemical Engineering
Solution and Separation Chemistry
Professor C.A. Eckert

6 of 8

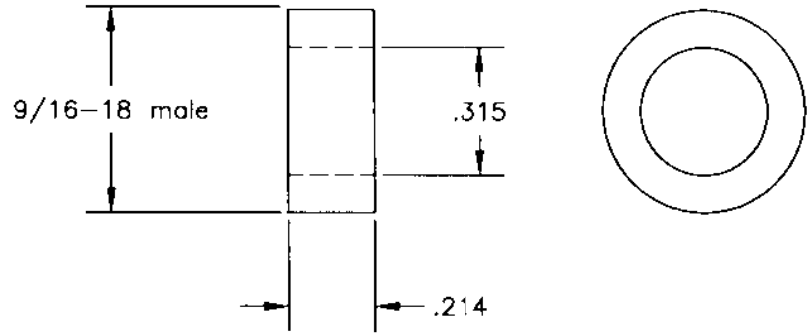

Figure A–11 Parallel Path Cell – 6 cm Window Nut

Georgia Tech Chemical Engineering
Solution and Separation Chemistry
Professor C.A. Eckert

7 of 8

APPENDIX B

EXTENSION OF PENG- ROBINSON CUBIC EQUATION OF STATE TO POLYMER SOLUTIONS

In this section, the Peng-Robinson EOS is extended to polymer solutions. The Peng-Robinson (PR) EOS is:

$$P = \frac{RT}{v-b} - \frac{a}{v(v+b)+b(v-b)} \qquad \textbf{(B- 1)}$$

The modified volume dependence of this equation compared to the previous equations resulted in improved saturated liquid volume predictions. The value of Z_c calculated with this equation, 0.307, is much closer to the experimental value for many substances. The PR EOS is the most widely-used equation for phase equilibrium, particularly in the petroleum industry for which it was developed. It is also considered fairly accurate for systems containing large molecules, such as n-alkanes having more then twenty carbon atoms and polymer solutions.

A convenient way to account for the compressibility effects in polymer–solvent mixtures is to use an EOS. They are powerful tools for investigating thermodynamic properties and phase behavior of pure fluids and their mixtures. There are many well-tested EOS for fluid mixtures of conventional solvents. For the mixtures of polymers with the solvents, however, problems persist. Efforts to represent conventional systems with these EOS have not always been very successful; indeed some of these models perform

less successfully than cubic EOS in this regard (Xiong and Kiran, 1994). This may be a handicap when these models are used for vapor–liquid equilibrium (VLE) of the polymer–solvent mixtures. In such cases, little or no polymer is present in the vapor phase and the solvent compressibility plays an important role in the phase behavior. Consequently, a strong incentive exists to extend the conventional EOS developed for small molecules to polymers. Recently, several extensions of cubic EOS to polymer–solvent mixtures were proposed (Kontogeorgis *et al.*, 1994; Kalospiros and Tassios, 1995; Zhong and Masuoka, 1996; Bertucco and Mio, 1996).

In extending a cubic EOS to polymers, it is important to keep the end-user in mind. Successful equations will eventually find their way into commercial design software. They will be used by a variety of engineers from various backgrounds, and it is unrealistic to expect all users to be experts in the area. This makes the EOS developer's task a particularly challenging one. The EOS must be mathematically robust and not highly sensitive to small variations in model input parameters. The model constants/parameters must be easily understandable and accessible in literature, and in their absence, there must be reasonable ways to estimate them. Preferably, the EOS input parameters for polymers should be related to commonly measured properties of polymers. In this section, we present a simple empirical way to extend cubic EOS to describe polymer–solvent mixtures.

There are two basic issues in extending cubic EOS to polymers and their mixtures. The first issue is the description of the pure component EOS parameters, a and b, for polymers. To obtain these parameters, various techniques have been suggested (Kontogeorgis *et al.,* 1994; Xiong and Kiran, 1994; Orbey and Sandler, 1994; Kalospiros

and Tassios, 1995; Zhong and Masuoka, 1996; Bertucco and Mio, 1996). There are four conditions to be satisfied in selecting pure component parameters of a cubic EOS for a polymer. First, the polymer is non-volatile and, thus, it should not exhibit any pure component vapor pressure. If oligomers exist in the mixture, a very low vapor pressure may be considered for them. Alternatively, the user may assign critical properties for oligomers and have them treated as conventional components. The second point is that the EOS should accommodate melt densities of the polymers. Third, the values of *a* and *b* should reflect basic polymer characteristics, such as degree of polymerization and polydispersity. This is important because experimental data show that these characteristics of the polymer directly affect the VLE of polymer–solvent mixture. Fourth point, somewhat connected to the third, is that necessary input parameters to evaluate *a* and *b* should be easily accessible and physically meaningful.

The second issue in extending cubic EOS to polymers is the selection of mixing rules for the EOS parameters. The classical mixing rules of van der Waals have been tested (Kontogeorgis *et al*., 1994) for polymer–solvent mixtures. It was observed that in order to fit the experimental data, some unrealistic values are necessary for the binary interaction parameters (parameters like -46.94 were reported for the van der Waals-type mixing rule for the polyisobutylene (PIB)–pentane binary mixture) (Kontogeorgis *et al*., 1994). This poses a problem, since for multicomponent systems, some of these parameters may be missing and estimates may be needed. If widely varying unrealistic values are required for the binary interaction parameters that would make the estimation of missing parameters very difficult. On the other hand, the mixing rules that combine excess free energy models with the EOS appear particularly suitable for the polymer–

solvent mixtures, for example, the mixing rule by Kalospiros and Tassios (1995) for VLE of polymer solutions relatively has been successful. In this study, the energy *a* and co-volume *b* parameters of the pure polymer in the PR EOS $\frac{a}{MW}$ and $\frac{b}{MW}$ are evaluated by fitting the available *PVT* data with a single set of $\frac{a}{MW}$ and $\frac{b}{MW}$ parameters for all MWs. The source of the required *PVT* data is the Tait equation, with the parameter values proposed by Rodgers (1993). Zhong and Masuoka (1998) used a similar approach but their parameters were MW-dependent. Parameter values for several polymers, along with the percent absolute average error in volume (ΔV) AAD%, are presented in Table B-1. Very satisfactory results are obtained, which are as expected better than those of the aforementioned methods.

For the solvent component of the polymer systems, the parameters in this study are determined from:

$$a = 0.45724 \frac{(RT_C)^2}{P_C} \alpha(T_R) \qquad \textbf{(B- 2)}$$

$$b = 0.0778 \frac{RT_C}{P_C} \qquad \textbf{(B- 3)}$$

where T_c and P_c are the pure compound critical temperature and pressure respectively, obtained from Daubert and Danner (1990). For the quantity of $\alpha(T_R)$, two cases can be distinguished depending on the polarity of the solvent.

For non-polar compounds, the $\alpha(T_R)$ is related to the acentric factor ω:

$$\alpha(T_R) = \left[1 + m\left(1 - \sqrt{T}_R\right)\right]^2 \qquad \textbf{(B- 4)}$$

$$m = 0.384401 + 1.52276\omega - 0.213808\omega^2 + 0.034616\omega^3 - 0.001976\omega^4 \qquad \textbf{(B- 5)}$$

It is proposed by Magoulas and Tassios (1990) and provides better prediction. For polar compounds, the Mathias-Copeman (1983) expression is used:

$$\alpha(T_R) = \left[1 + C_1\left(1 - \sqrt{T}_R\right) + C_2\left(1 - \sqrt{T}_R\right)^2 + C_3\left(1 - \sqrt{T}_R\right)^3\right]^2 \qquad \textbf{(B- 6)}$$

where the values of C_1, C_2 and C_3 are evaluated by fitting the pure compound vapor pressure data obtained from the correlation of Daubert and Danner (1990).

Mixing rules

In order to describe the mixtures in phase equilibrium predictions, mixing rules are required to calculate the mixture constants in an EOS. The following are the most popular and widely-used equations. Several existing mixing rules were adopted to test the capability of the PR EOS for correlating phase equilibria in polymer solutions. The first one is the conventional van der Waals one-fluid mixing rule with one adjustable parameter (vdW1):

$$a = \sum\sum x_i x_j a_{ij} \qquad \textbf{(B- 7)}$$

$$b = \sum x_i b_i \qquad \textbf{(B- 8)}$$

$$a_{ij} = \sqrt{a_i a_j}\left(1 - k_{ij}\right) \qquad \textbf{(B- 9)}$$

Equations B-7, B-8 and B-9, have been used by Kontogeorgis *et al.* (1994) to correlate VLE of polymer solutions with the vdW EOS. As very large k_{ij} was obtained, a modified expression for a_{ij} was used to replace B-9 in order to make the k_{ij} have an appropriate value for polymer solutions.

$$a_{ij} = \sqrt{a_i a_j}\,\frac{\left(b_i + b_j\right)/2}{\sqrt{b_i b_j}}\left(1 - k_{ij}\right) \qquad \textbf{(B- 10)}$$

The equations B-7, B-8, and B-10 constitute the vdW1 mixing rule. The capability of this mixing rule was tested by correlating high pressure gas solubilities in molten polymers in this work.

The second one is the conventional two-parameter van der Waals one-fluid mixing rule (vdW2):

$$b = \sum\sum x_i x_j b_{ij} \qquad \textbf{(B- 11)}$$

$$b_{ij} = \frac{b_i + b_j}{2}\left(1 - \ell_{ij}\right) \qquad \textbf{(B- 12)}$$

Equation B-8, B-9, B-11, B-12 and B-13 constitute the vdW2 mixing rule used in this work. Obviously, if l_{ij} is set to be 0, the vdW2 reduces to the vdW1. Therefore, the value of l_{ij} can present the deviation from the linear combination for b.

The following mixing rule was proposed by Rasmussen *et al.* (1987) to correlate VLE of polymer solutions with cubic EOSs;

$$\frac{a}{b} = \sum x_i \frac{a_i}{b_i} \qquad \textbf{(B- 13)}$$

Equation B-13 was derived based on the assumption that the excess Helmholtz free energy from a two-parameter cubic EOS is zero at infinite pressure (Zhong and Masuoka, 1996). The previous work shows that it is more appropriate than 6-19 for polymer solutions. This is reasonable considering that the asymmetry for a_i/b_i of the components is smaller than that for the b_i for highly asymmetric systems such as polymer–solvent systems.

Wong-Sandler Mixing Rule

This mixing rule has been used extensively for correlating vapor-liquid equilibrium. In this approach, a and b parameters in a mixture are determined in such a way that while the low-density quadratic composition dependence of the second virial coefficient is satisfied, the excess Helmholtz Energy at infinite pressure from the

equation of state is also equal to that of an appropriately chosen liquid activity coefficient model. The mixing rule for a two parameter cubic equation is:

$$b_m = \frac{Q}{1 - DD} \tag{B- 14}$$

$$\frac{a_m}{RT} = Q\frac{DD}{1 - DD} \tag{B- 15}$$

$$Q = \sum\sum x_i x_j \left(b - \frac{a}{RT} \right)_{ij} \tag{B- 16}$$

with

$$\left(b - \frac{a}{RT} \right)_{ij} = \frac{1}{2}\left[\left(b_i - \frac{a_i}{RT} \right) + \left(b_j - \frac{a_j}{RT} \right) \right]\left(1 - k_{ij} \right) \tag{B- 17}$$

and

$$Q = \sum\sum x_i x_j \left(b - \frac{a}{RT} \right)_{ij} + \frac{A_E}{cRT} \tag{B- 18}$$

where c is a constant equal to $\left(1/\sqrt{2}\right)\ln\left(\sqrt{2} - 1\right)$ for the PR equation used in the study, and A_E is any suitable molar excess Helmholtz at infinite pressure or equivalently an excess Gibbs energy model at low pressure. This has the advantage of incorporating

excess energy models into equations of state in a theoretically correct way and it can be used for the very accurate correlation and or prediction of VLE for highly nonideal mixtures. For this work, the Flory-Huggins model has been chosen which includes two contributions to the thermodynamics of binary polymer solutions, entropy of athermal mixing due to size difference between the species and an enthalpy of mixing due to difference of the intermolecular forces, as

$$\frac{A_E}{RT} = x_1 \, ln \frac{\Phi_1}{x_1} + x_2 \, ln \frac{\Phi_2}{x_2} + \chi \Phi_1 \Phi_2 \left(x_1 + x_2 r \right) \qquad \textbf{(B- 19)}$$

Here, χ is the Flory interaction parameter, Φ is the volume fraction, and r is the number of solvent-size segments that make up the polymer which is approximated by the hard-core volumes.

Since the Flory-Huggins model is developed using a rigid, incompressible lattice, a PVT equation of state cannot be derived from it. However, the Wong-Sandler mixing rule provides a way of combining the Flory-Huggins model with an equation of state when the Helmholtz energies from the EOS and Flory-Huggins theory are equated as infinite pressure (the volume terms are replaced by the hard-core volume b).With the selection of the PR EOS and Wong-Sandler mixing rule, the fugacity coefficient of a species i in a homogeneous binary mixture is (Wong and Sandler, 1992):

$$ln\phi_i = -ln\left[\frac{P(v-b)}{RT}\right] + \frac{1}{b_m}\left(\frac{\partial n b_m}{\partial n_i}\right)\left(\frac{Pv}{RT} - 1\right) + \frac{1}{2\sqrt{2}}\left(\frac{a_m}{RTb_m}\right)$$
$$\left[\frac{1}{a_m}\left(\frac{1}{n}\left(\frac{\partial n^2 a_m}{\partial n_i}\right)\right) - \frac{1}{b_m}\left(\frac{\partial n b_m}{\partial n_i}\right)\right] ln\left[\frac{v + b_m\left(1-\sqrt{2}\right)}{v + b_m\left(1+\sqrt{2}\right)}\right] \quad \textbf{(B- 20)}$$

The partial derivatives of a_m and b_m are:

$$\frac{\partial n b_m}{\partial n_i} = \frac{1}{(1 - DD)}\left(\frac{1}{n}\frac{\partial n^2 Q}{\partial n_i}\right) - \frac{Q}{(1 - DD)^2}\left(1 - \frac{\partial nD}{\partial n_i}\right) \quad \textbf{(B- 21)}$$

$$\frac{1}{RT}\left(\frac{\partial n^2 a_m}{\partial n_i}\right) = DD\frac{\partial n b_m}{\partial n_i} + b_m\frac{\partial nDD}{\partial n_i} \quad \textbf{(B- 22)}$$

with the partial derivatives of Q and DD given by:

$$\frac{1}{n}\left(\frac{\partial n^2 Q}{\partial n_i}\right) = 2\sum x_j\left(b - \frac{a}{RT}\right)_{ij} \quad \textbf{(B- 23)}$$

and

$$\frac{\partial nDD}{\partial n_i} = \frac{a_i}{b_i RT} + \frac{ln\,\gamma_i}{C} \quad \textbf{(B- 24)}$$

The activity coefficient expressions for the Flory-Huggins models are:

$$ln\gamma_1 = ln\frac{\Phi_1}{x_1} + \left(1 - \frac{1}{r}\right)\Phi_2 + \chi\Phi_2^2 \qquad \textbf{(B- 25)}$$

and

$$ln\gamma_2 = ln\frac{\Phi_2}{x_2} + (1 - r)\Phi_1 + \chi\Phi_1^2 r \qquad \textbf{(B- 26)}$$

Zhong and Masuoka Mixing Rule

Zhong and Masuoka (1996) came up with a new mixing rule for extending cubic EOS to polymer solutions, refining the work done by Wong-Sandler. Actually, the only difference between this mixing rule and the Wong-Sandler one is the absence of excess Helmholtz energy at infinite pressure, A_{∞}^{E}, which was set equal to zero in this case. This mixing rule has been proven to be better in correlating polymer solution phase behavior.

$$\frac{a_m}{RT} = Q\frac{DD}{1 - DD} \qquad \textbf{(B- 27)}$$

$$b_m = \frac{Q}{1 - DD} \qquad \textbf{(B- 28)}$$

where:

$$Q = \sum\sum x_i x_j \left(b - \frac{a}{RT}\right)_{ij} \qquad \textbf{(B- 29)}$$

$$Q = \sum\sum x_i x_j \left(b - \frac{a}{RT} \right)_{ij} \qquad \textbf{(B- 30)}$$

and

$$\left(b - \frac{a}{RT} \right)_{ij} = \frac{1}{2}\left[\left(b_i - \frac{a_i}{RT} \right) + \left(b_j - \frac{a_j}{RT} \right) \right] \left(1 - k_{ij} \right) \qquad \textbf{(B- 31)}$$

Summary of Results

VLE of Concentrated polymer solutions in conventional solvents

For this work, various systems are selected which have been studied in the literature (Orbey and Sandler, 1994) including PS-chloroform, PIB-cyclohexane/n-pentane/ benzene, PS-MEK,.PPO-Benzene, and PE-benzene. For these systems, Wong-Sandler mixing rule has been used and the parameters are given in each figure. The results are shown in Figures B-1 to B-5. In all cases, it was possible to obtain excellent correlations of the VLE data for these systems with the Peng-Robinson equation of state combined with the Flory-Huggins model.

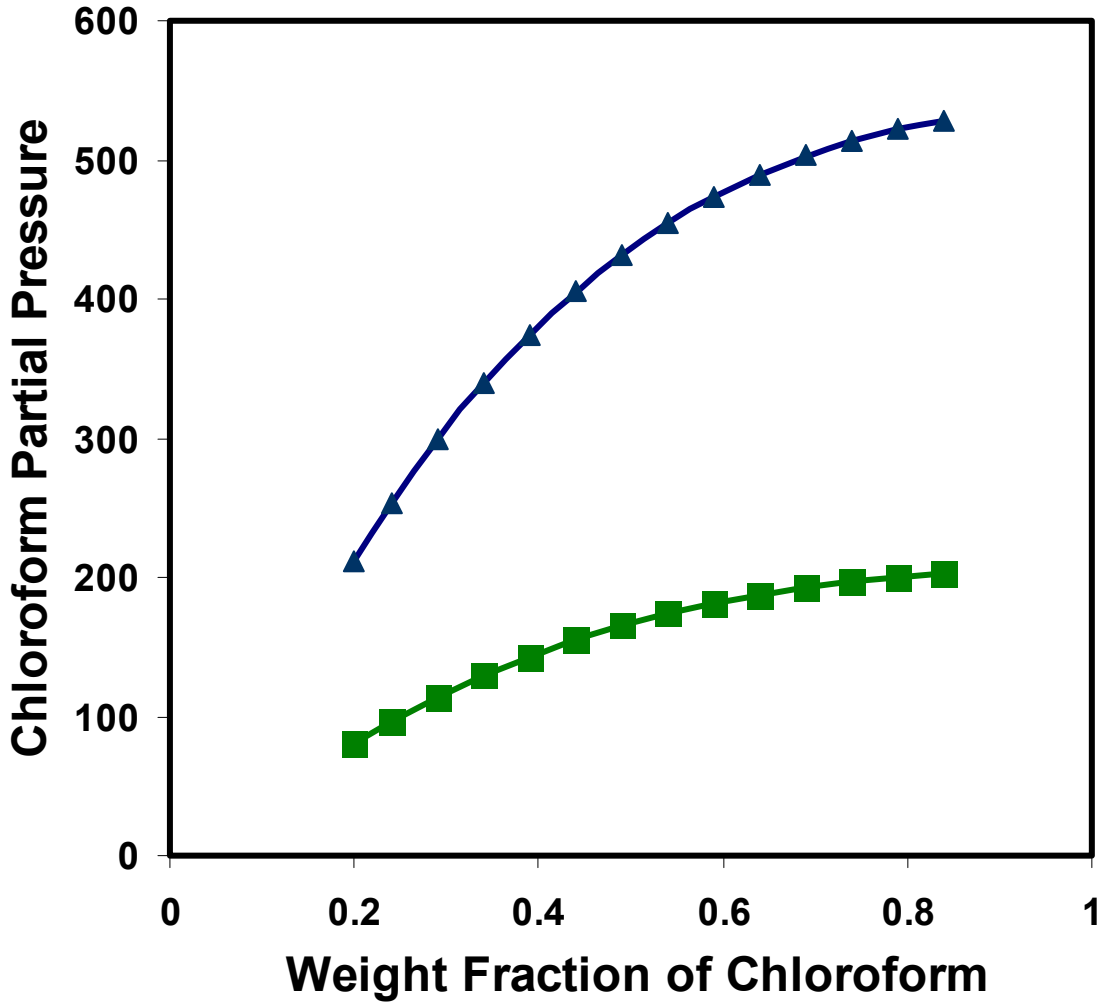

Figure B- 1 Partial Pressure of chloroform in polystyrene (MW=290,000). Squares and triangles represent experimental data (Bawn and Wajid, 1956) at 298.15 and 323.15 K respectively. The lines represent the PR EOS correlation with r=3,635, χ=0.19, k_{ij}=0.84.

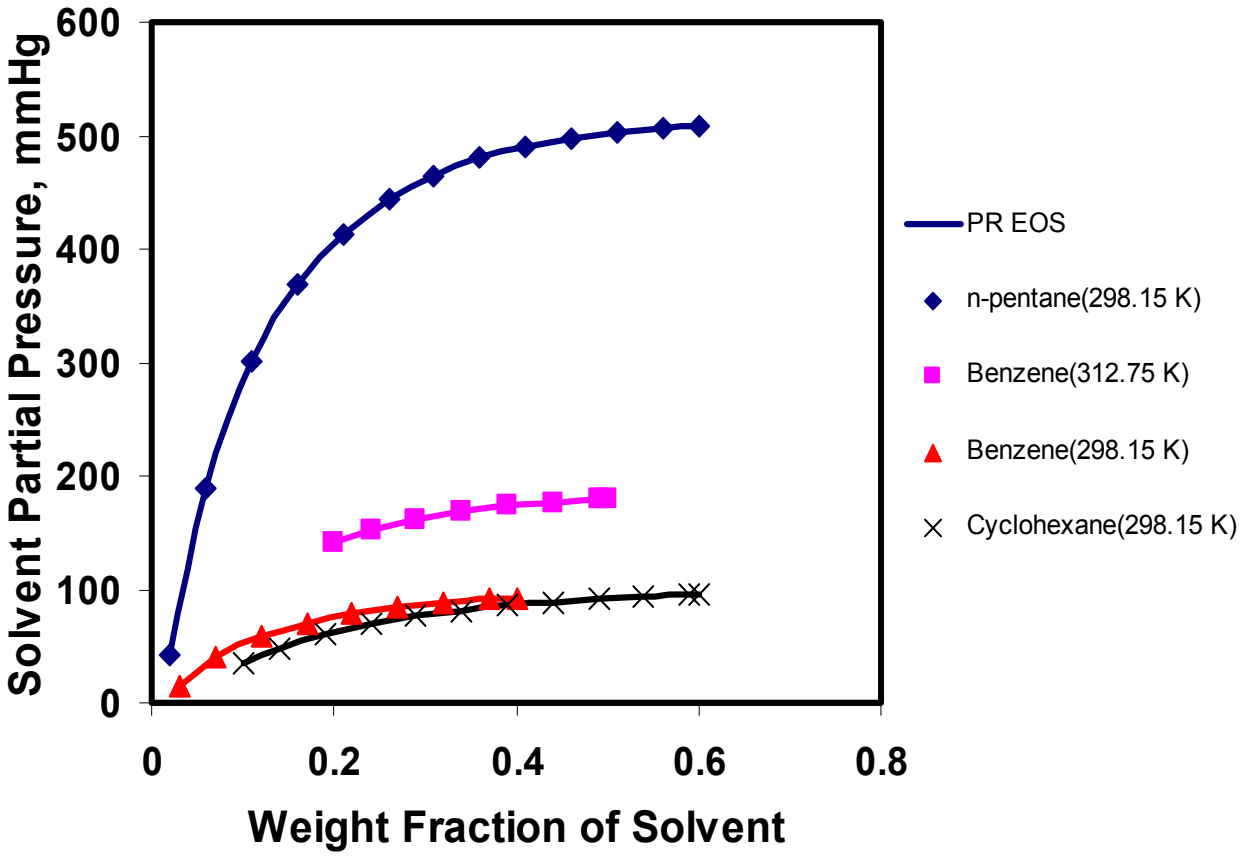

Figure B- 2 Partial Pressure of various solvents in polyisobutylene (MW=40,000) (a)Experimental data (Eichinger and Flory, 1968) for cyclohexane in PIB at 298.15 K and correlated with r=442.3, χ=0.46, k_{ij}=0.91.(b) Experimental data (Eichinger and Flory, 1968) for n-pentane in PIB at 298.15 K and correlated with r=445, χ=0.61, k_{ij}=0.96. (c) Experimental data (Eichinger and Flory, 1968) for benzene in PIB at 298.15 K and 312.75 K and correlated with r=547, χ=0.80, k_{ij}=0.97.

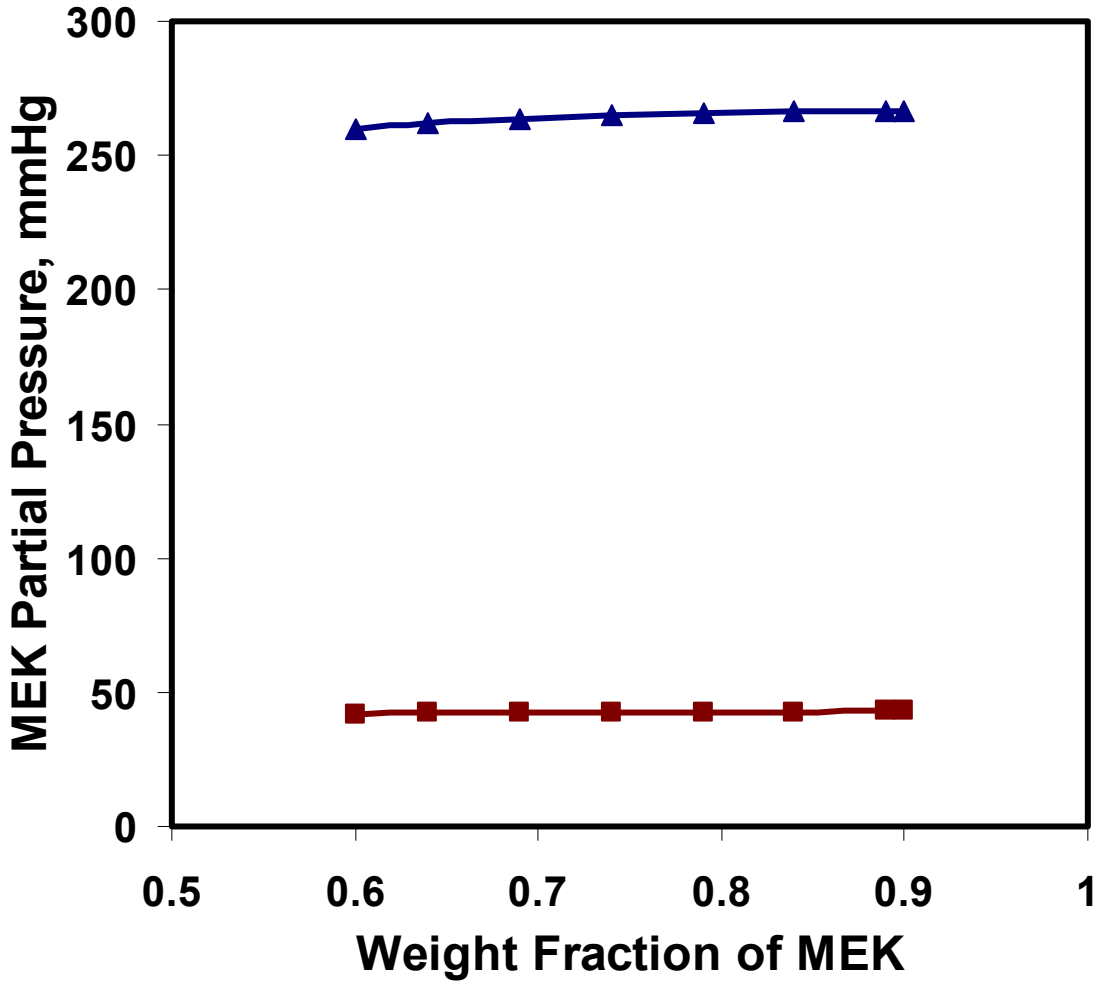

Figure B- 3 Partial pressure of methyl ethyl ketone in polystyrene (MW=97,200) Squares and triangles represent experimental data (Flory and Hoecker, 1971) at 283.15 and 323.15 K respectively. The lines represent the PR EOS correlation with r=1,140, χ=0.56, k_{ij}=0.49.

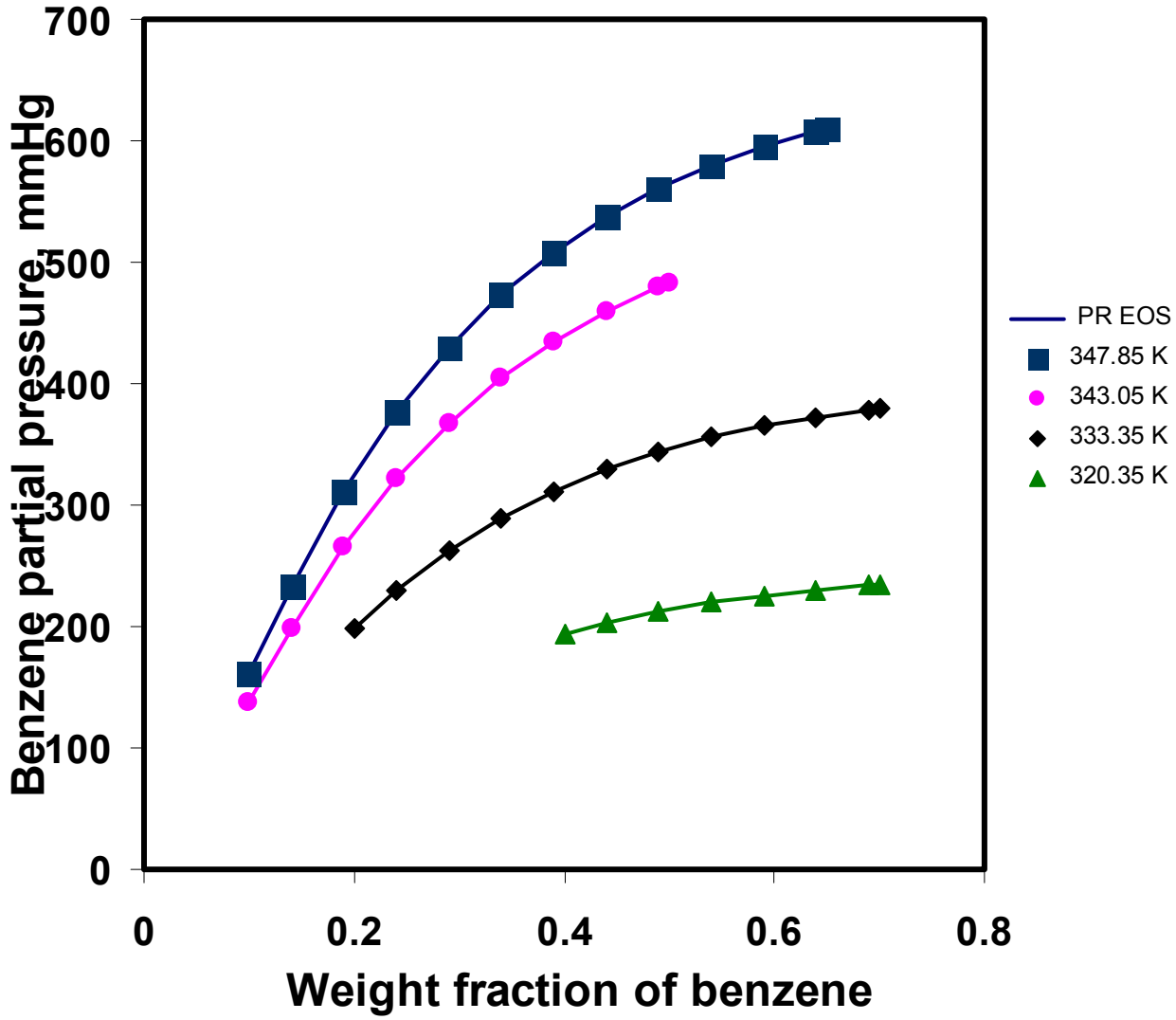

Figure B- 4 Partial Pressure of benzene in polyproylene oxide (MW=500,000) Experimental data (Booth and Devoy, 1971) and correlated with r=1,140, χ=0.56, k_{ij}=0.49.

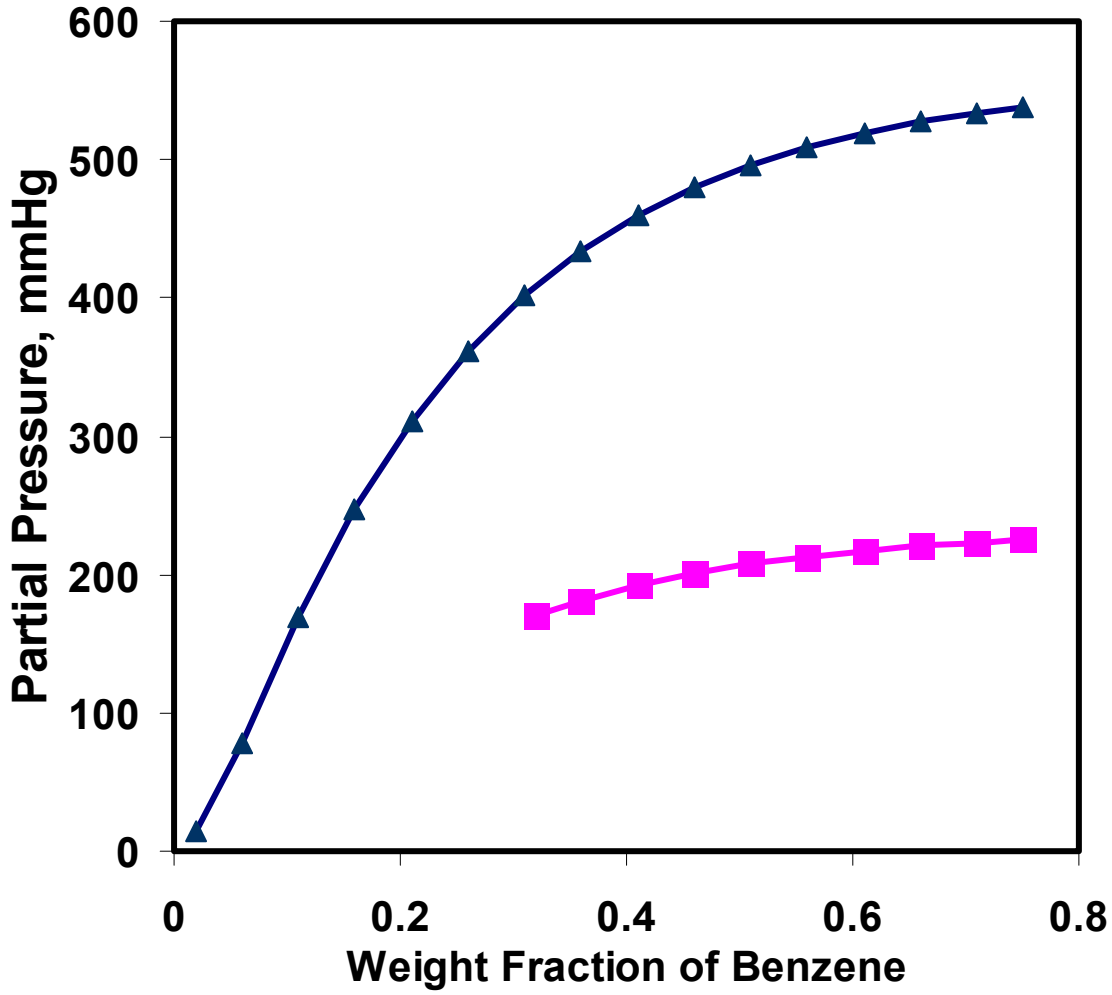

Figure B- 5 Partial Pressure of benzene in polyethylene oxide (MW=5,700) Squares and triangles represent experimental data (Bawn and Wajid, 1956) at 318.95 and 343.15 K respectively. The lines represent PR EOS correlation with r=61.4, χ=0.21, k_{ij}=0.78.

The systems have been calculated with different mixing rules and bubble point pressure calculations were done using vdW2 and Zhong-Masuoka mixing rule (simplified version of Wong-Sandler). The results are represented in Figure B-6 to B-8. Very satisfactory results are obtained with all mixing and combining rules, with typical errors for non-polar solvents of 2-3% and a little higher for polar ones shown in Table B-2. Additionally, other polymer systems have been correlated using the vdW1 and Wong-Sandler mixing rule as shown in Figure B-9 to B-11. Wong-Sandler seems to give better results in representing the properties of polymeric solutions. This can be explained by the size difference between the polymer and the solvent; one parameter is not sufficient to describe this disparity. As a conclusion of this section, VLE of polymer solutions has been correlated using cubic equation of state with a high accuracy. Wong-Sandler, Zhong-Masuoka and vdW2 mixing rules have all demonstrated their ability to describe long chain phase behavior. Advantages of this approach are that it extends the cubic equation of state to polymer -solvent systems in a simple fashion by including free volume effect in the excess Gibbs energy. This will allow for accurate interapolation and extrapolation of existing experimental data.

Table B- 1 PR EOS parameters of the polymers investigated in this study.

Polymer	T range (K)	P range (bar)	a/MW/10^6	b/MW	AAE% in V
HDPE	413.15-476.15	0-1960	1.2808	1.2066	2.77
LDPE	394.15-448.15	0-1960	1.3739	1.1991	2.62
PS	388.15-469.15	0-2000	1.3154	0.9549	2.17
PVAc	308.15-373.15	0-800	1.8473	0.8428	1.38
PMMA	387.15-432.15	0-2000	1.2775	0.8407	1.77
PIB	326.15-383.15	0-1000	2.3074	1.0882	1.40
PEO	361.15-497.15	0-685	2.2783	0.9497	2.48
PDMS	298.15-343.15	0-1000	1.0220	0.9968	2.10
i-PP	443.15-570.15	0-1960	1.2924	1.2444	3.65

A(cm^6bar/mol^2) and b (cm^3/mol)

$$AAE\% = \sum \text{abs} \frac{\frac{\left(V_{cal} - V_{exp}\right)}{V_{exp}}}{NP} \times 100$$

Table B- 2 Overall correlation results for representative polymer-solvent systems.

			Overall AAD%	
Polymer	Solvent	T range (K)	VdW	Zhong-Masuoka
PIB	n-C6	298-338	2.07	2.37
PIB	Benzene	298-338	3.81	3.07
PVAc	Benzene	303-333	5.40	3.56

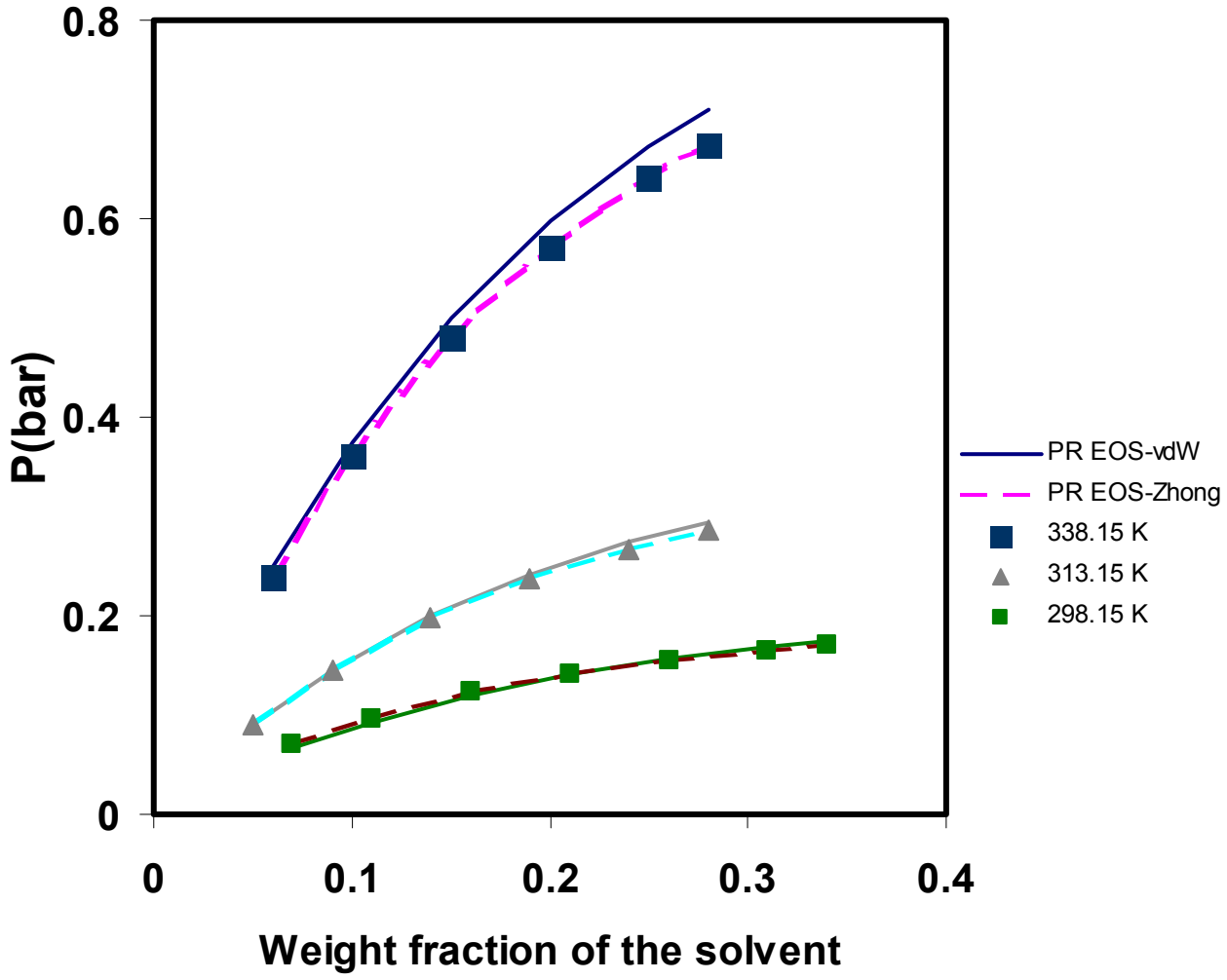

Figure B- 6 Correlation of bubble point pressure for the system PIB-nC6 at 298.15, 313.15, 338.15 K Experimental data (Wen *et al*., 1991). For 298.15/ 313.15 / 338.15 K, vdW k_{ij}= 0.620/ 0.627/ 0.640, Zhong k_{ij}=0.917/ 0.917/ 0.922; χ=1.068/ 1.112/ 1.083 respectively.

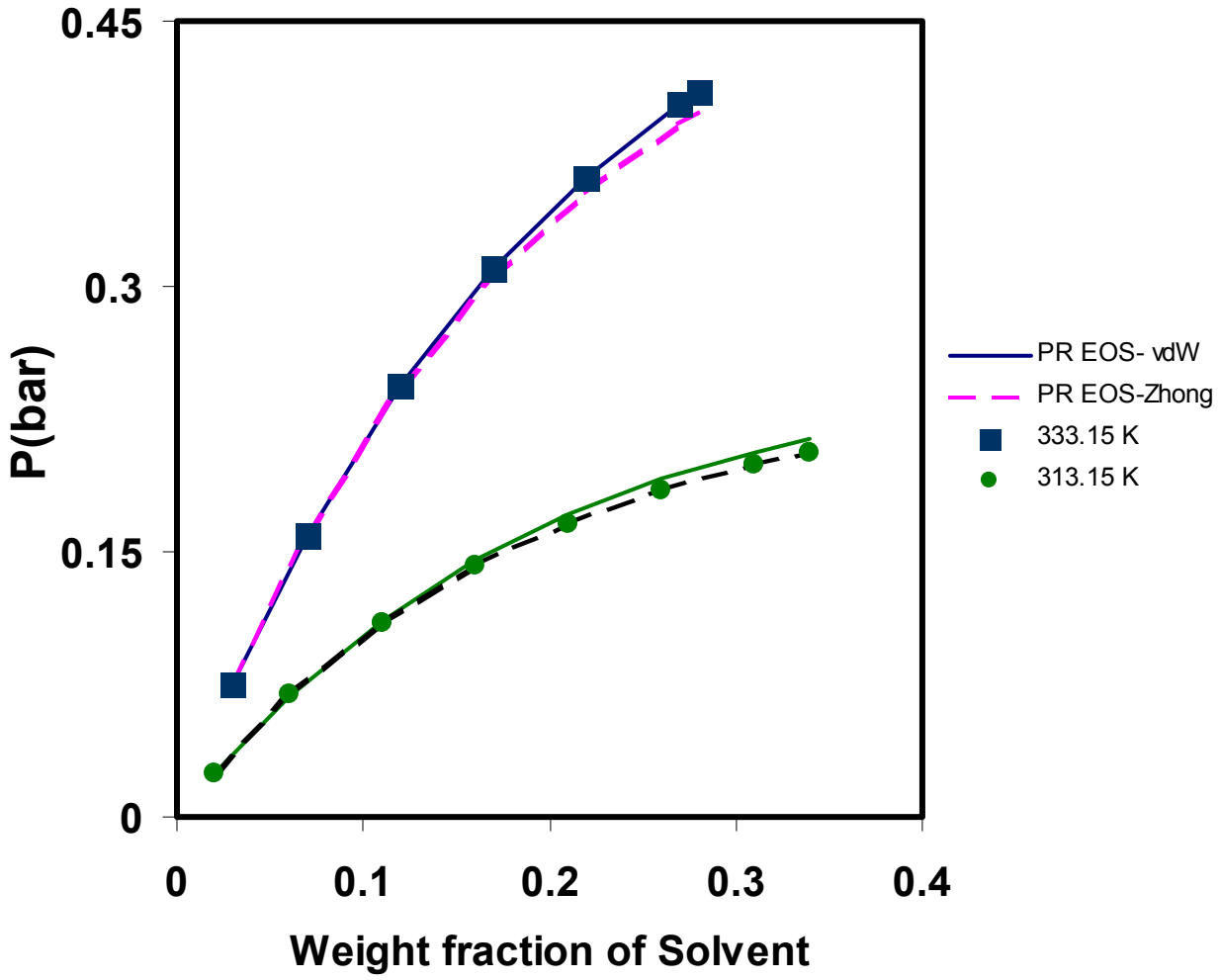

Figure B- 7 Correlation of bubble point pressure for the system PVAc-benzene at 313.15 K and 333.15 K. Experimental data (Wen *et al.*, 1991). For 313.15/ 333.15 K, vdW k_{ij}= 0.612/ 0.619, Zhong k_{ij}=0.909/ 0.910; χ=0.667/ 0.652 respectively.

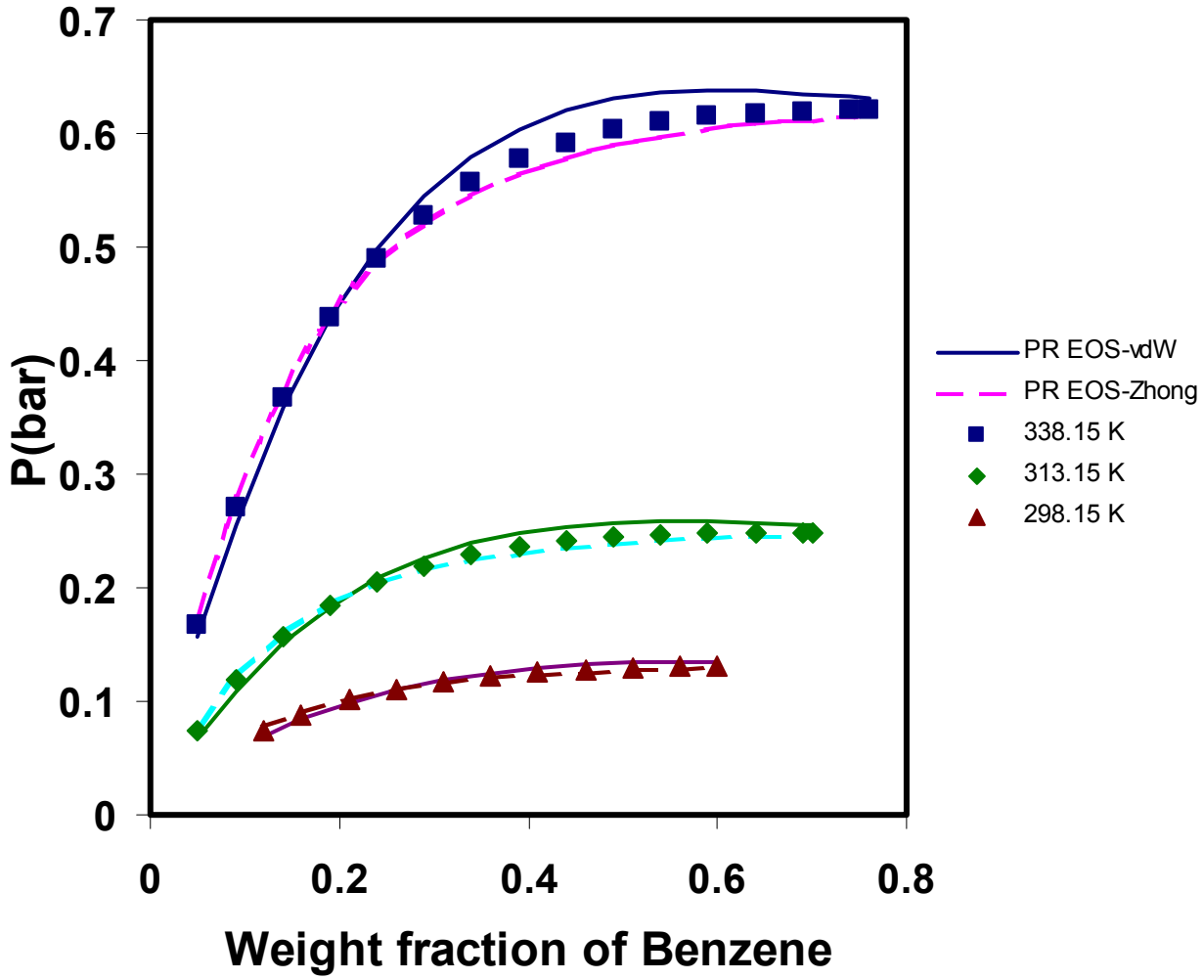

Figure B- 8 Correlation of bubble point pressure for the system PIB-benzene at 298.15, 313.15 and 338.15 K Experimental data (Wen *et al.*, 1991). For 298.15/ 313.15 / 338.15 K, vdW k_{ij}= 0.613/ 0.624/ 0.634, Zhong k_{ij}=0.946/ 0.949/ 0.944; χ=1.047/ 1.080/ 1.034 respectively.

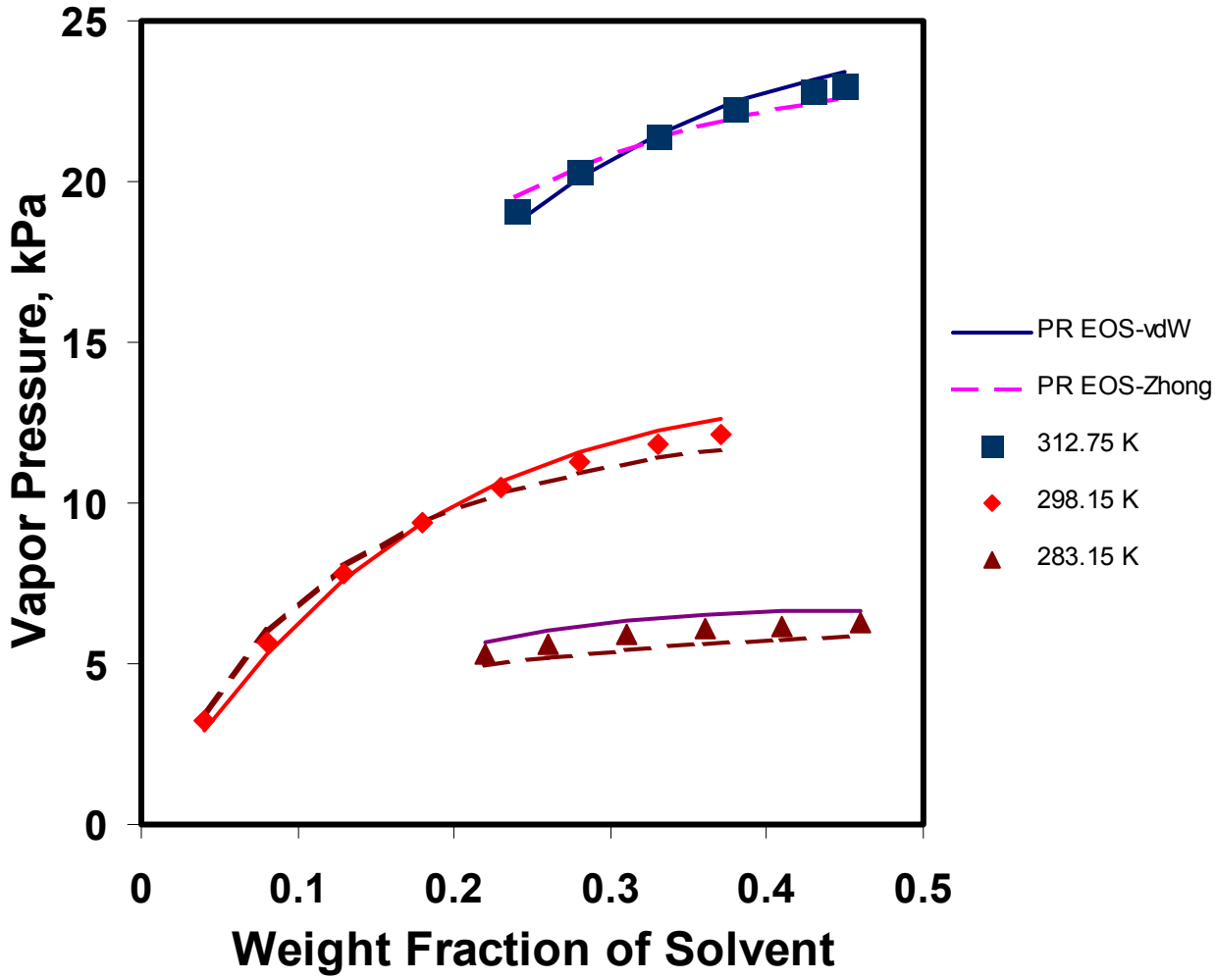

Figure B- 9 Experimental (Eichinger and Flory, 1968) and calculated vapor pressure versus weight fraction of the solvent for the system PIB(MW=40,000)-Benzene.

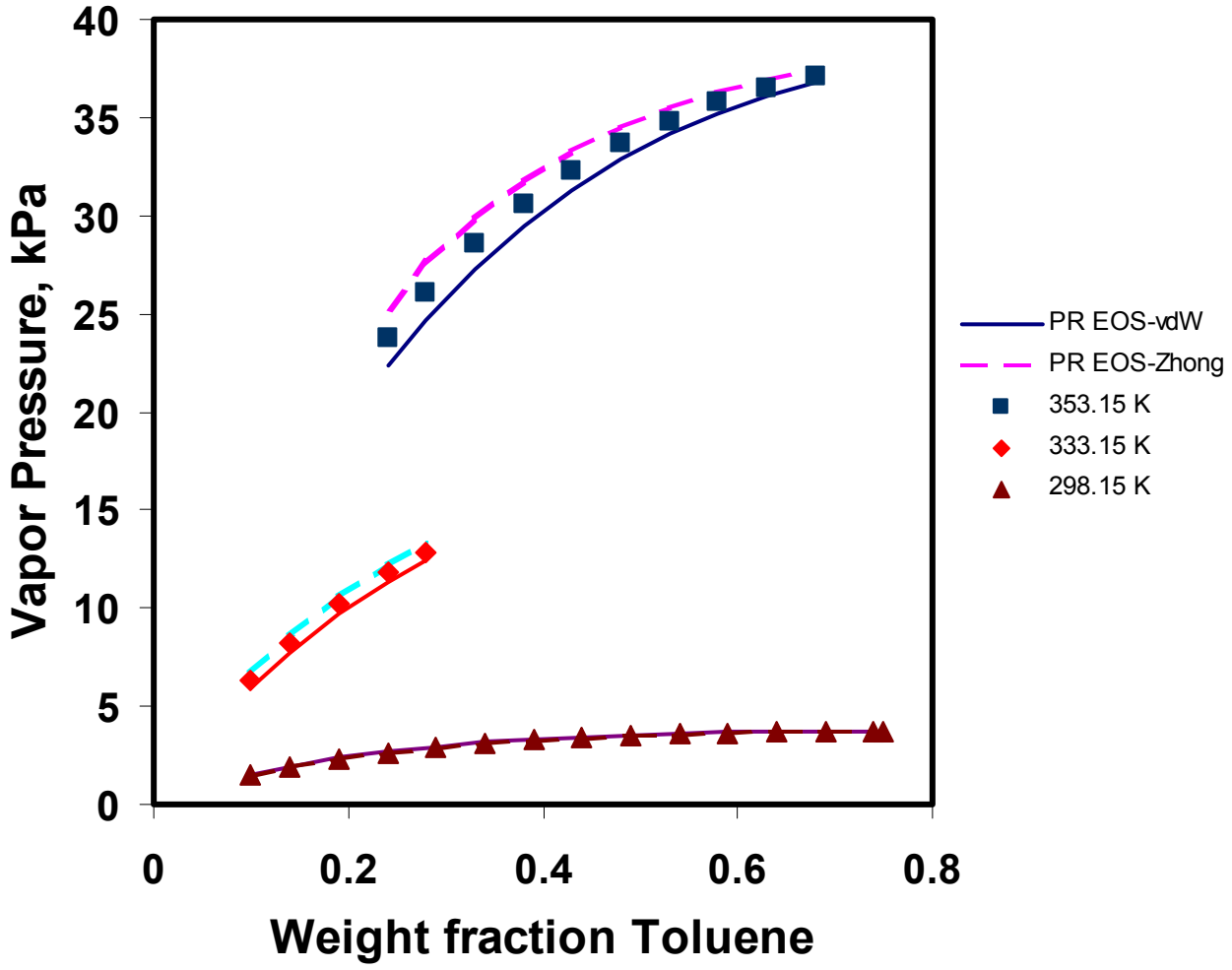

Figure B- 10 Experimental (Bawn *et al.*,1950) and calculated vapor pressure versus weight fraction of the solvent for the system PS(MW=290,000)-Toluene.

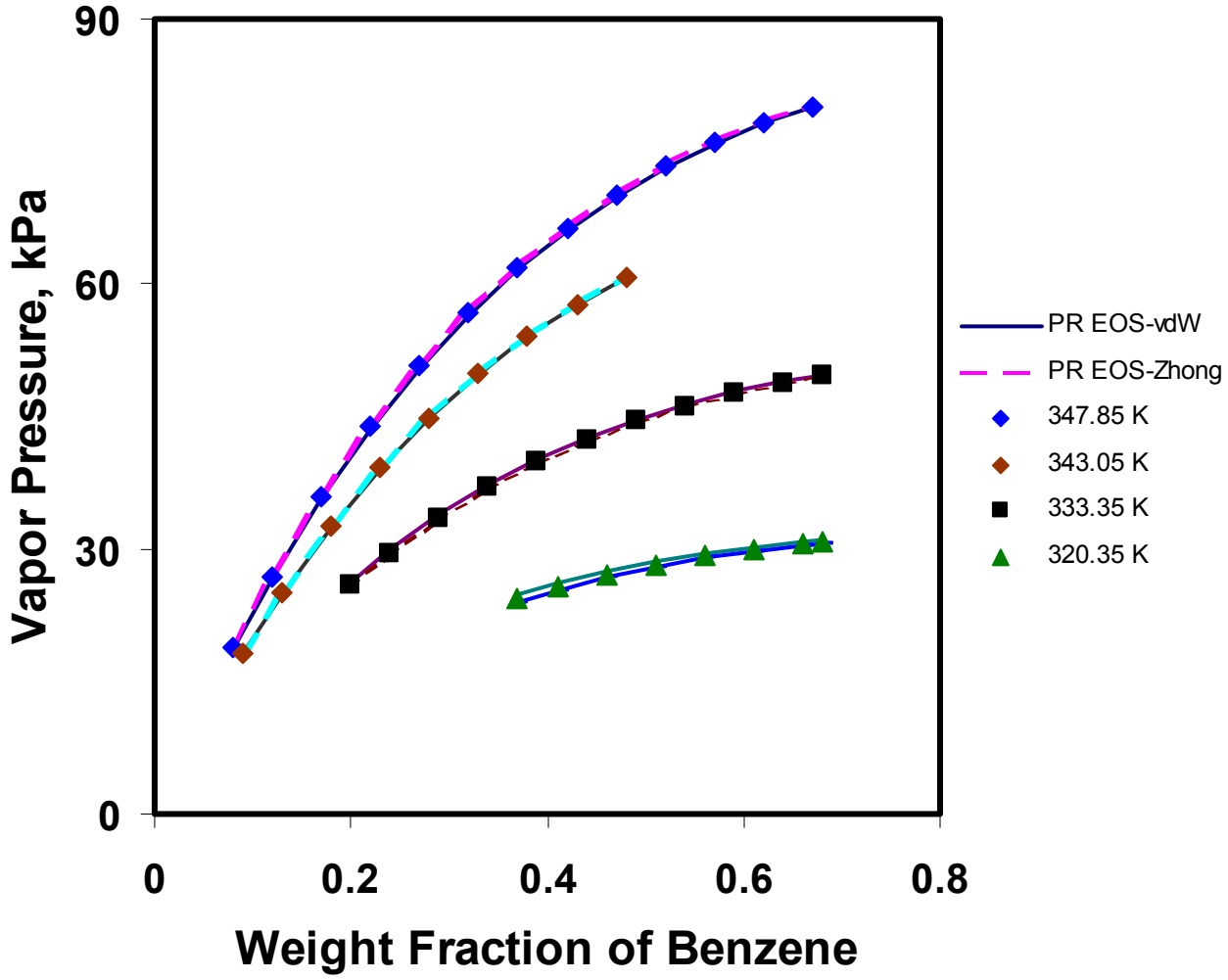

Figure B- 11 Experimental (Booth and Devoy, 1971) and calculated vapor pressure versus weight fraction of the solvent for the system PPO(MW=500,000)-Benzene.

Correlation of Polymer Swelling with Supercritical Fluids

The solubility of a gas in an amorphous polymer is an important consideration in membrane and polymer processes. For instance, the efficacy of a membrane that is used for gas mixture separation is dependent on the solubility of the various species in the membrane. Another application that can utilize the gas solubilities is the swelling of the solid polymer matrix with a high pressure gas that can aid in the deposition of temperature sensitive materials into the polymer. The supercritical fluid swells the polymer and thus, allows the substance to migrate into the polymer matrix. These substances can be anything from pharmaceutical drugs to pest control agents (Mc Hugh and Krukonis, 1994). Swelling of the polymer effectively increases the diffusion coefficient of the heavy dopant by several orders of magnitude, and thus, allows it to be transported into the polymer within a reasonable time. Also, these phenomena can be utilized effectively in stripping the polymer of impurities, including entrapped solvent, residual catalyst, or low molecular oligomers by contacting with a high pressure gas.

For any polymer-gas process which operates at high pressure, it is often necessary to be able to predict the solubility of the gas in the polymer. In this section, Peng-Robinson cubic equation of state is used for modeling this phenomenon. Several systems have been correlated using PR EOS and are shown in Figures B-12 to B-16. Zhong and Masuoka mixing rule has been used for these systems. The adjustable parameters were obtained by fitting the experimental solubility at constant temperature. It has been observed that vdw1 is not capable of applying PR EOS to gas solubilities in polymers. On the other hand, Zhong-Masuoka mixing rule gives greatly improved and acceptable

correlations, it has been shown that this mixing rule is suitable for high pressure polymer-gas systems, especially if the pressure range is wide. However, it should be noted that the correlations are not as accurate as SL EOS when compared with experimental data. The calculated curve tails off high pressure; this discrepancy might be due to SL EOS being more capable of correlating linear behavior for swelling where cubic EOS is not accurate at higher concentrations. Thus, it can be concluded that swelling behavior can be predicted with SL EOS with higher accuracy. However, there are some cases cubic EOS is comparable with some systems with non-polar polymers.

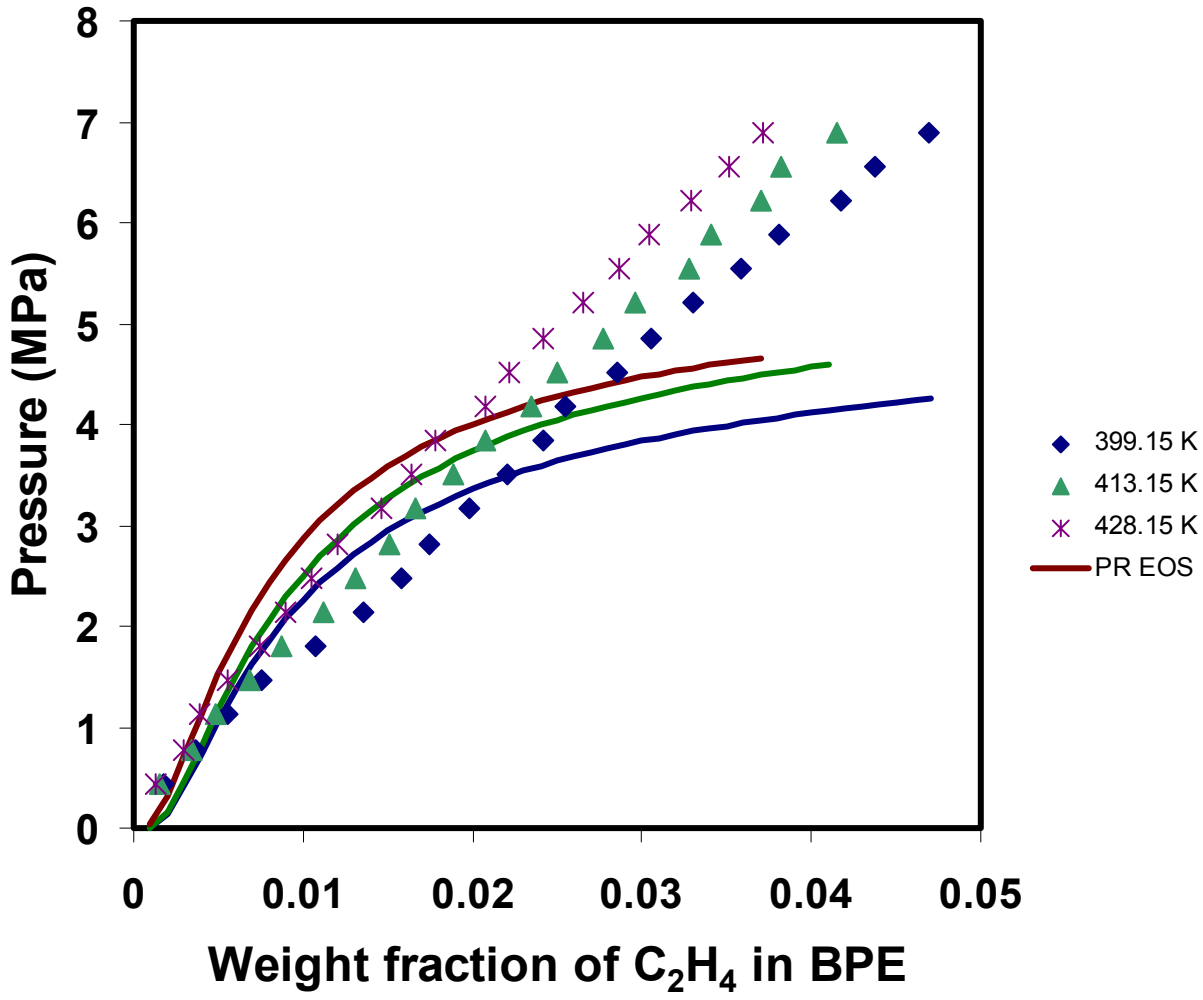

Figure B- 12 Comparison of the experimental and calculated ethylene solubility isotherm by Peng-Robinson cubic EOS for the etyhlene-Polyetyhlene at 399.15, 413.15 and 428.15 K. Experimental data from Zhong and Masuoka, 1998 and correlated with k_{ij}=0.083 ,0.206 and 0.319 respectively.

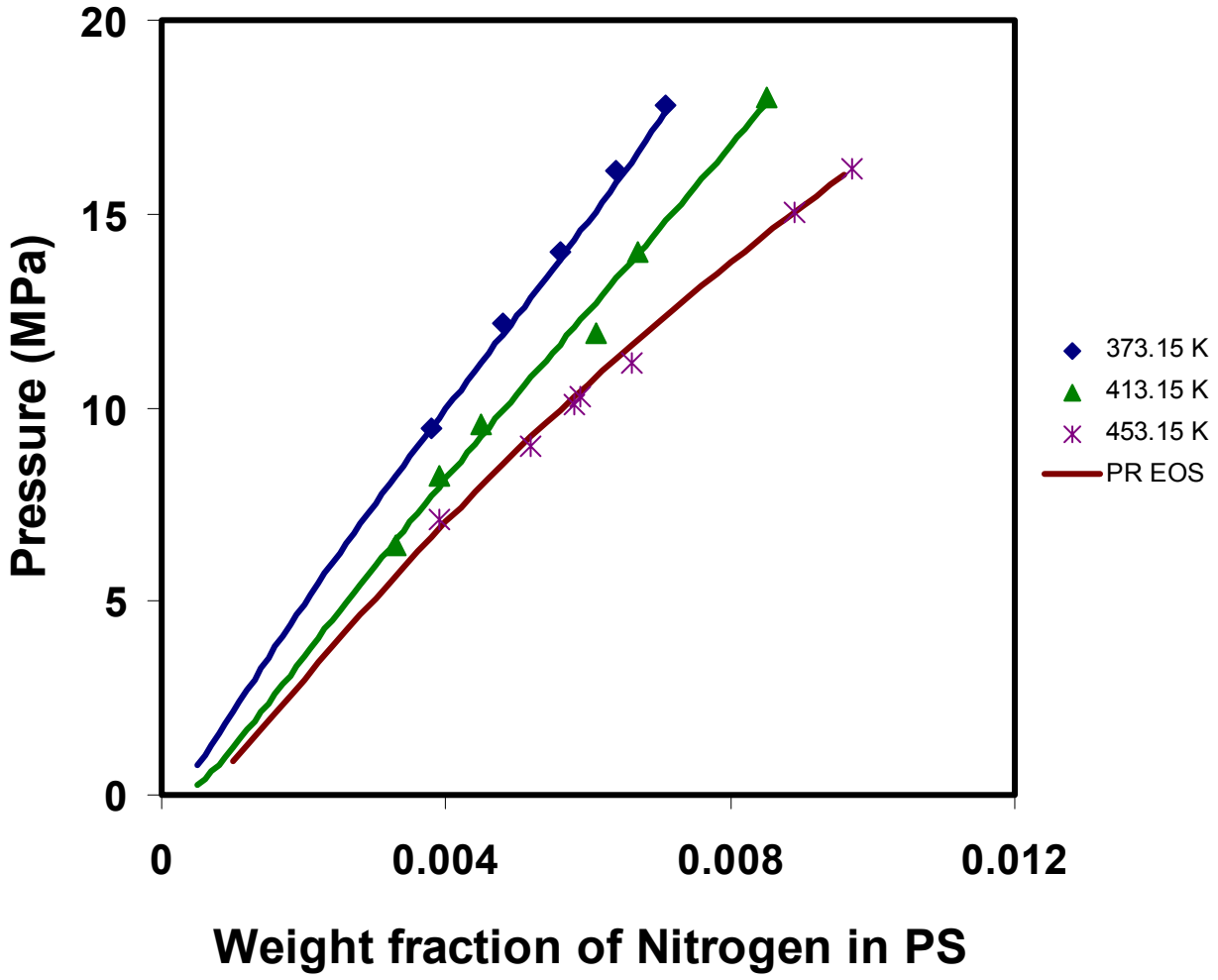

Figure B- 13 Comparison of the experimental and calculated nitrogen solubility isotherm by Peng-Robinson cubic EOS for the nitrogen-polystyrene at 373.15, 413.15 and 453.15 K. Experimental data from Zhong and Masuoka, 1998 and correlated with k_{ij}=0.907 ,0.915 and 0.922 respectively.

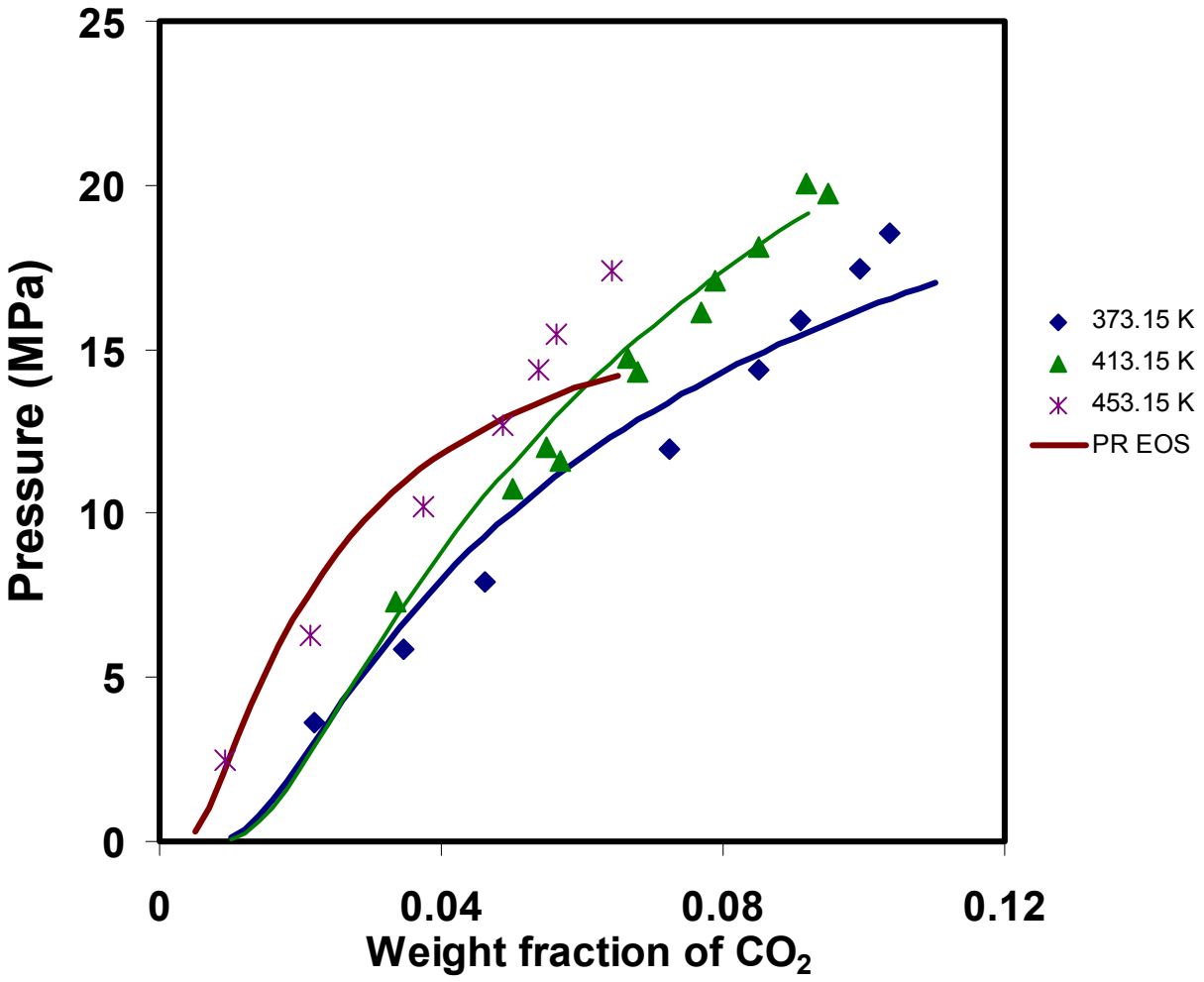

Figure B- 14 Comparison of the experimental and calculated carbon dioxide solubility isotherm by Peng-Robinson cubic EOS for the carbon dioxide-polystyrene at 373.15, 413.15 and 453.15 K. Experimental data from Zhong and Masuoka„ 1998 and correlated with k_{ij}=0.237 ,0.471 and 0.632 respectively.

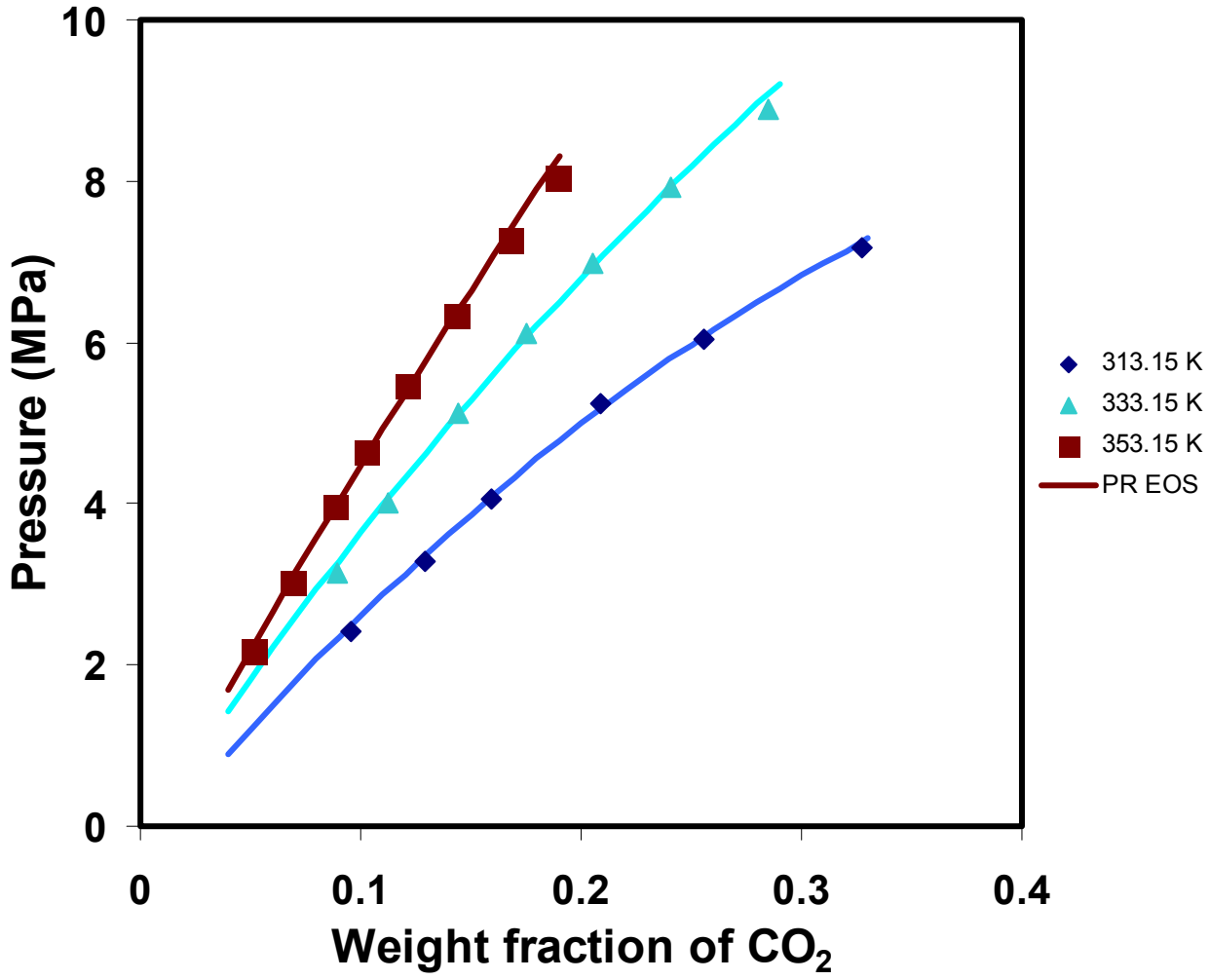

Figure B- 15 Comparison of the experimental and calculated carbon dioxide solubility isotherm by Peng-Robinson cubic EOS for the carbon dioxide-polyvinylacetate at 313.15, 333.15 and 353.15 K. Experimental data from Zhong and Masuoka, 1998 and correlated with k_{ij}=0.956 ,0.960 and 0.962 respectively.

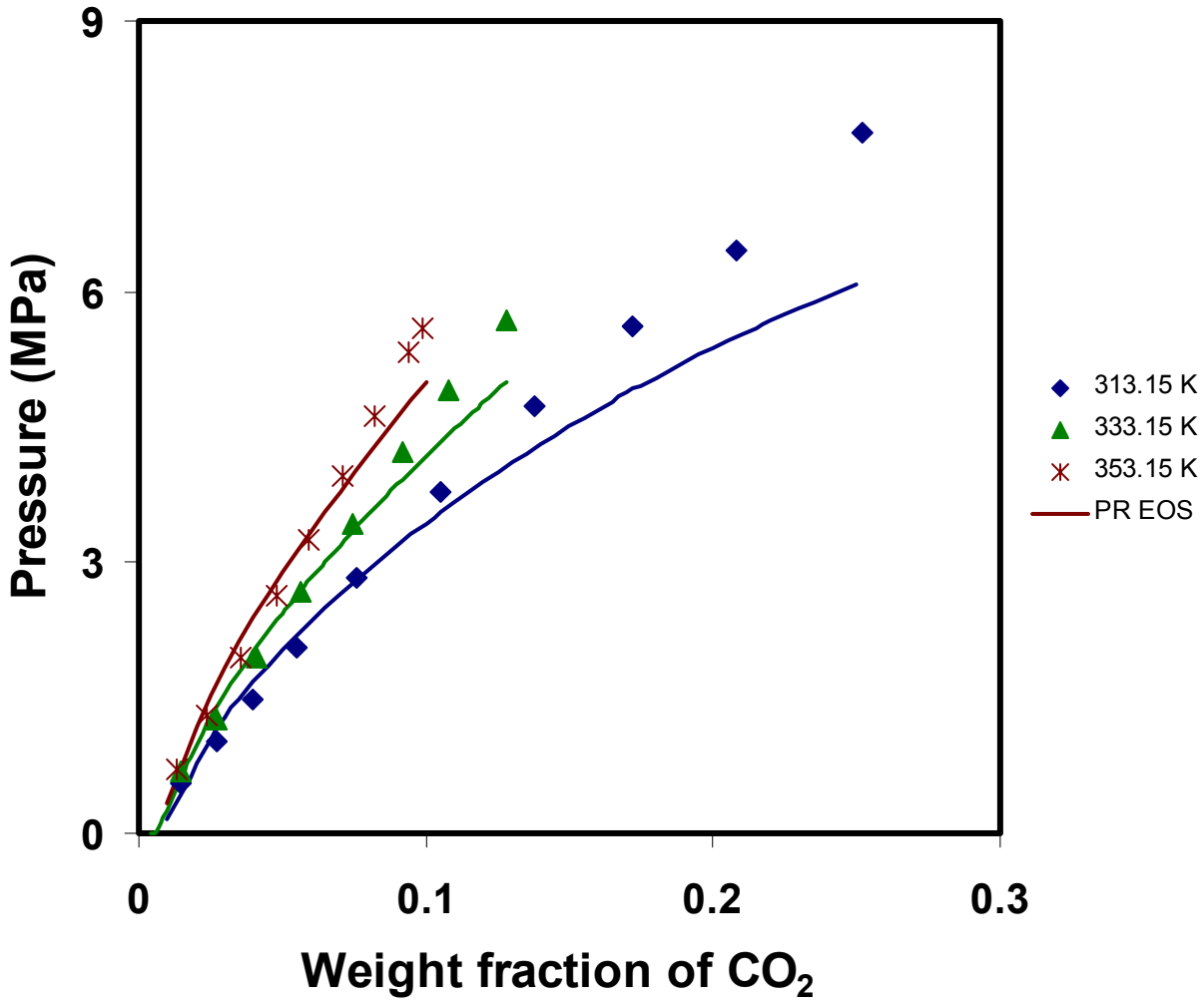

Figure B- 16 Comparison of the experimental and calculated carbon dioxide solubility isotherm by Peng-Robinson cubic EOS for the carbon dioxide-polybutylmethacrylate at 313.15, 333.15 and 353.15 K. Experimental data from Zhong and Masuoka„ 1998 and correlated with k_{ij}=0.964 ,0.964 and 0.966 respectively.

Pressure Induced Phase Separation (PIPS) of Polymers in Supercritical Fluids

More than 30 million tons of various polymers are produced yearly in United States which finds use in diverse applications ranging from common households to toys, to highly specialized materials used in electronics, or those used for medical applications (Anon, 1995). Among these various commodity polymers, polyethylene, polypropylene, and Polyvinyl chloride, polyesters and phenolics are produced in the greatest amounts. Especially, polyethylene in different forms (low and high density PE) alone amount to more than one third of the yearly polymer production.

It is important to note that supercritical fluid processing does not mean extreme pressures. In fact, many fluids become supercritical at relatively low pressures, typically under 100 bars (Life, 1990) and relatively lower temperatures. For example, the critical temperature for carbon dioxide, pentane and toluene are 31 and 196.7 and 318.6°C where their critical pressures are around 80 bars. These solvents in supercritical conditions can be used in different specific applications in a extremely large areas such polymer (a) formation, (b) purification (c) fractionation (d) property modification and processing and (e) recycling and recovery. For all these applications, the fundamental information that is needed is clearly centered around those factors that influence miscibility and phase separation of polymers in supercritical fluids at high pressures.

The following are the key factors that determine the miscibility of the polymers in a given fluid system: Polymer type, Molecular weight and molecular weight distribution, Nature of the solvent, Polymer concentration, Temperature, Pressure. The essentials features of pressure-induced phase separation are described in Figure B-17, which is a

pressure composition phase diagram showing the binodal and spinodal boundaries, and the stable and metastable, and unstable regions. This is an idealized diagram, where for real solutions, because polymers display polydispersity, the binodal and spinodal curves do not necessarily merge at the maximum of binodal, but rather shifted to higher concentrations. The regions between the binodal and spinodal are metastable, where solutions in these regions are stable to small fluctuations in compositions, but for large fluctuations undergo demixing. Inside the spinodal envelope, all fluctuations result in a increase of Gibbs energy, and as a result, the solutions are unstable and demixing is spontaneous.

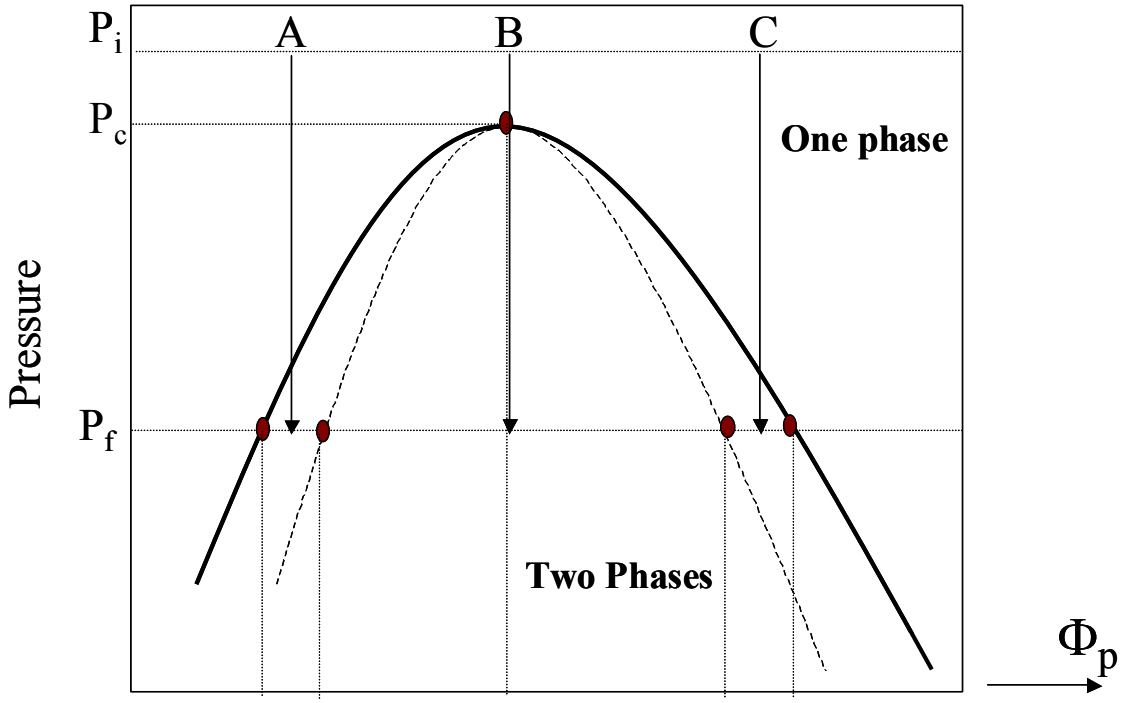

Figure B- 17 Schematic illustration pressure induced phase separation, which in this case, upper critical solution pressure has been presented.

In this section, the results predicted from PR EOS+vdW2 and SL EOS have been compared with each other and the experimental data (Kiran *et al.*, 1993) for polyethylene solutions in n-pentane.

Initial calculations were carried out on binodals to generate P-x diagrams for the polymer samples with different molecular weights ranging from 2150 to 420000 at a temperature 460 K is illustrated in Figure B-18 and B-19. The relation of UCSP can be observed very clearly. The characteristic parameters are used for SL EOS and $A^* = \frac{a_2}{MW * 10^6}$ and interaction parameters for vdW2 mixing rule, K_1 and K_2 are fitted for PR EOS. For cubic EOS, it is observed that $\frac{b_2}{MW}$ remains the same (1.25). However, A* has a regular trend when plotted against MW with R^2=0.9972. SL EOS calculations showed significant deviation from the experimental (cloud point) data and could not be improved by adjusting the binary interaction parameter δ_{12}. The binary interaction parameter for systems in these figure ranged 0 to 0.0175. PR EOS tends to perform than SL EOS although they have the same number of fitted parameters. Using the literature values for the characteristic temperature parameter leads to poor SL EOS predictions, even when these values is adjusted for SL EOS as shown in the figure, PR EOS tends to conform better with the experimental data.

To generate P-T curves, either the demixing pressures at certain temperature or the demixing temperature at certain pressure must be calculated. For example, to determine the demixing temperature at a specific temperature and a specific pressure, an initial temperature is assumed and then the iterations are continued until the composition

(which corresponds to binodal) matches the composition corresponding the isopleth under consideration. Figure B-20 and B-21 show two examples of the demixing pressures of polyethylene of molecular weight of 16,400 and 108,000 in n-pentane solution at different temperatures covering the concentration range from 1 to 15%. The predictions of both EOS have been compared with the experimental data. The prediction deviations are within 1 MPa for both models. The polyethylene-n-pentane system in Figures B-22 and B-23 all show LCST behavior at pressures of 5 and 10 MPa. The temperature coefficient of pressure $\left(\frac{\partial P}{\partial T}\right)_c$ is positive and the two phase regions are entered upon increasing the temperature. This is illustrated explicitly in these figures, where the predictions for binodal points for both models as well as experimental data are included.

The model calculations give results comparable with each other and the experimental observations. At a fixed pressure of 5 and 10 MPa, calculated values of LCST moves, in accordance with the experimental values, to lower temperatures with increasing molecular weight of the polymer sample. This phenomenon can be explained due to free volume differences. LCST is often explained in terms of an unfavorable entropy effect which in non-polar polymer-solvent systems arises from the difference between the free volume of the polymer and the solvent. At a given pressure, when the temperature is increased, the solvent molecules undergo an expansion towards a larger free volume state, but find themselves confined within the matrix. As the critical temperature is approached, the free volume difference becomes very large, leading to decreased entropy of mixing and phase separation. The difference in free volume is expected to become larger as the molecular weight becomes higher, thus shifting the phase separation to lower temperatures. The free volume of the solvent decreases much

faster than that of the polymer when increasing the pressure and that decreases the free volume difference. This causes phase separation not to occur until the high temperatures to have sufficient difference in the free volume.

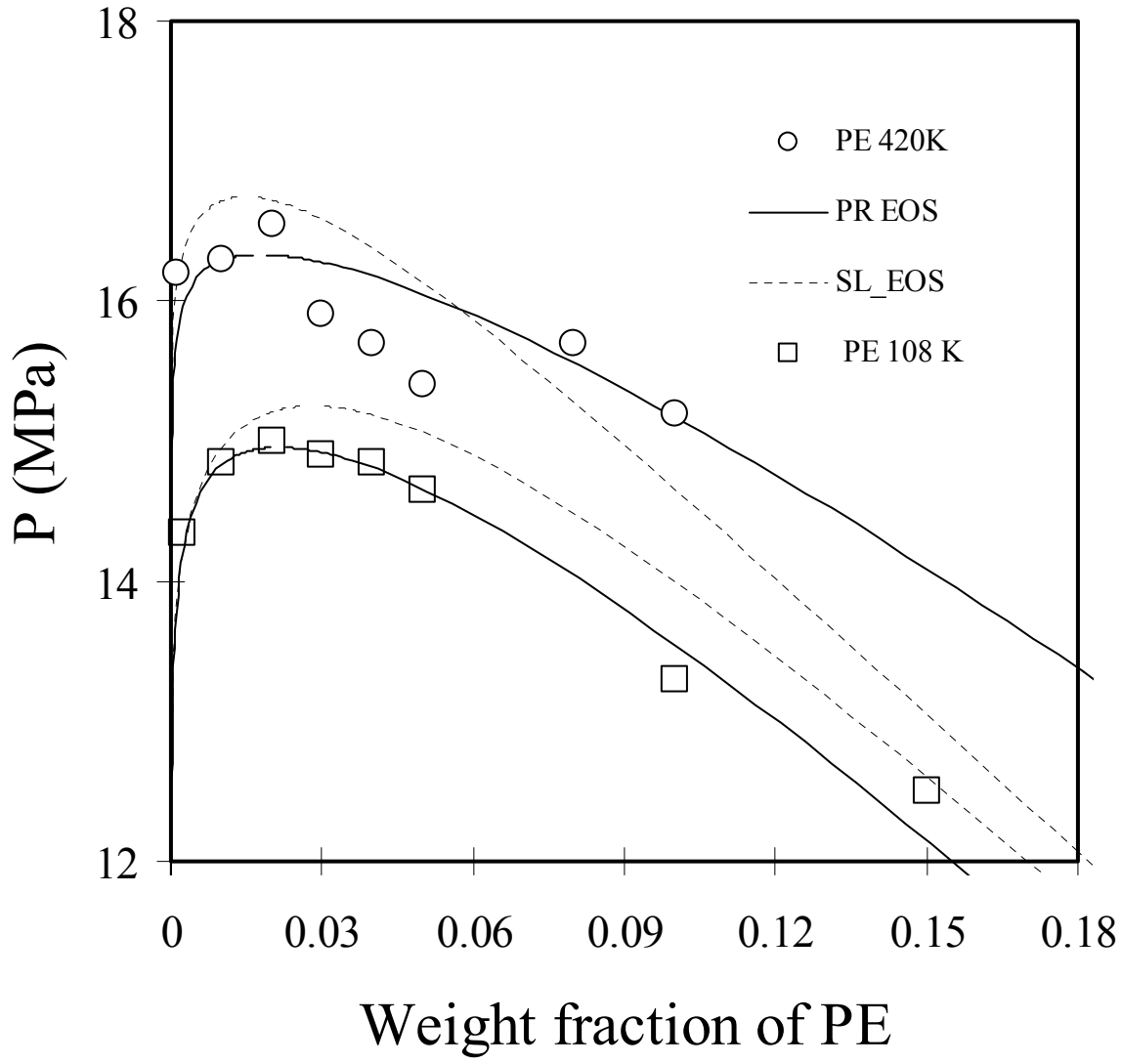

Figure B- 18 Comparison of experimental and predicted demixing pressures for poylethylene of molecular weights 108,000 and 420,000 in n-pentane. Our prediction with Peng-Robinson cubic EOS: For PE 420,000 A*=3.2, K_1=0.80, K_2=0.87. For PE108,000 A*=2.6, K_1=0.69, K_2=0.81 respectively.

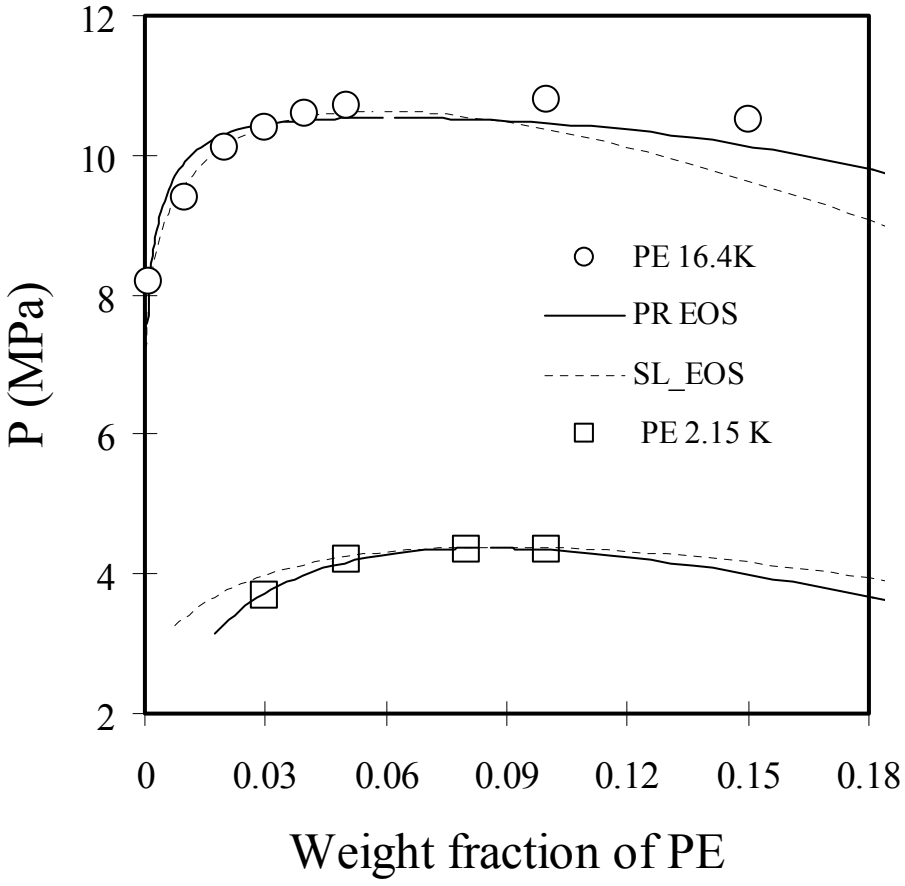

Figure B- 19 Comparison of experimental and predicted demixing pressures for poylethylene of molecular weights 16,400 and 2,150 in n-pentane. Our prediction with Peng-Robinson cubic EOS: For PE 16,400 A*=1.0, K_1=0.65, K_2=0.84. For PE 2,150 A*=0.7, K_1=0.32, K_2=0.62 respectively.

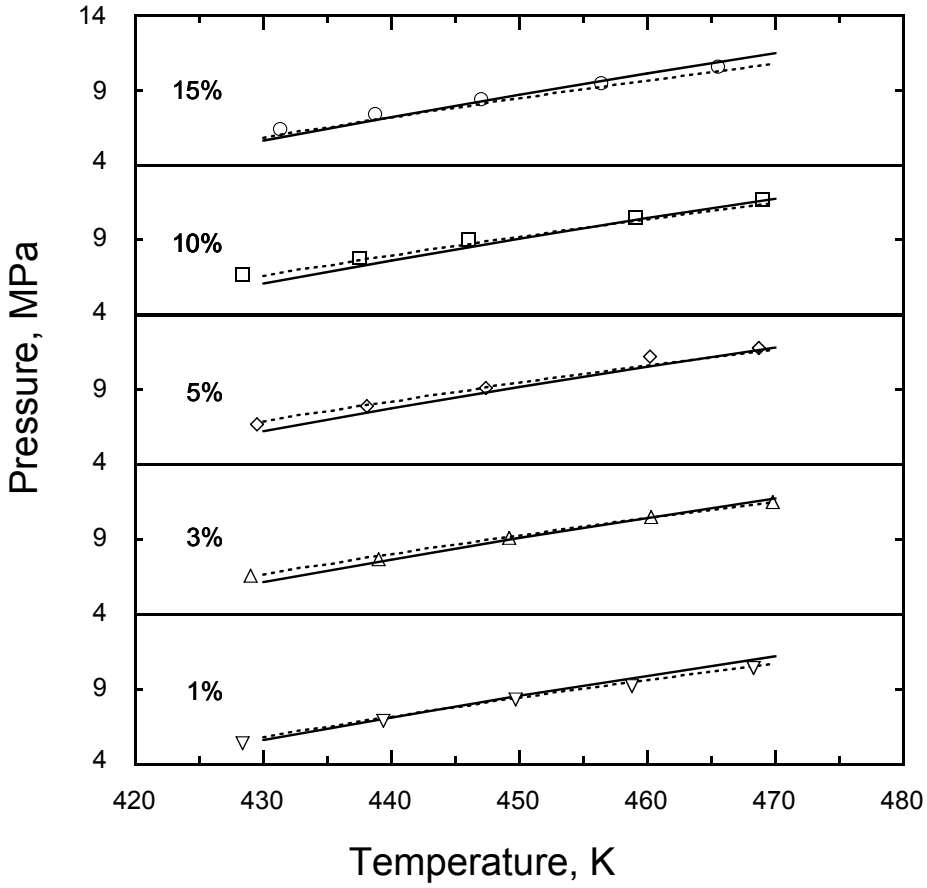

Figure B- 20 Demixing Pressures for PE 16,400 in n-pentane. The symbols are experimental points, the solid lines are calculated by Peng-Robinson EOS and dashed lines are calculated by Sanchez-Lacombe EOS.

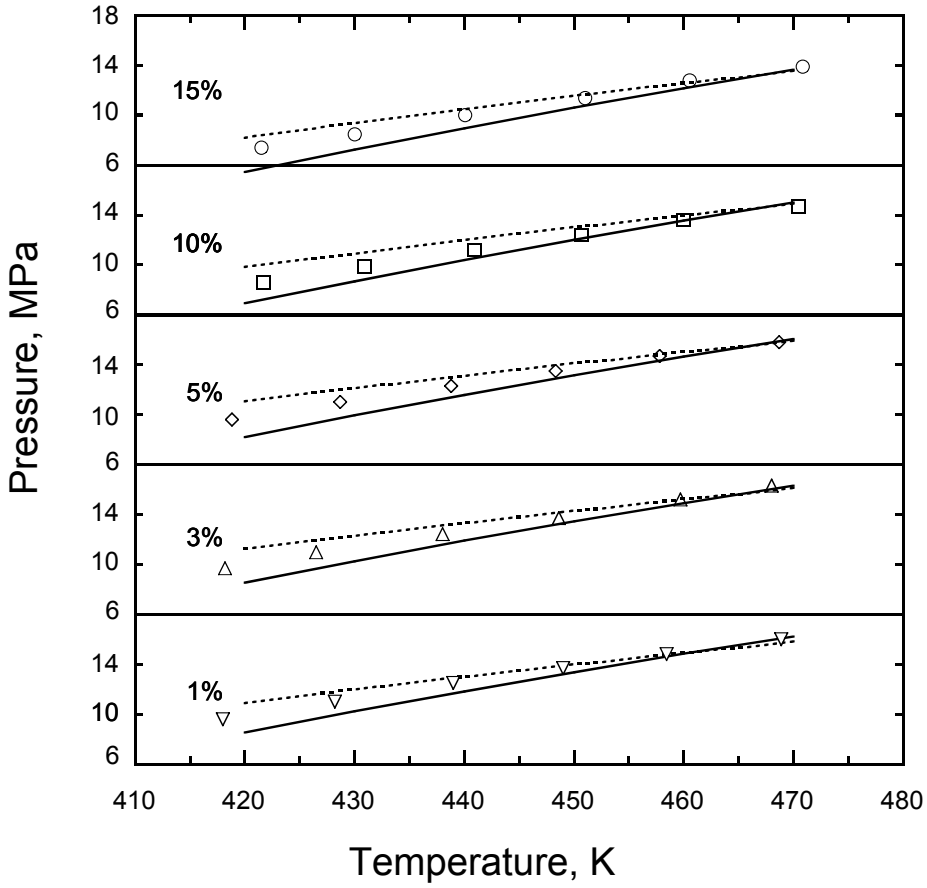

Figure B- 21 Demixing Pressures for PE 108,000 in n-pentane.
The symbols are experimental points, the solid lines are calculated by Peng-Robinson EOS and dashed lines are calculated by Sanchez-Lacombe EOS.

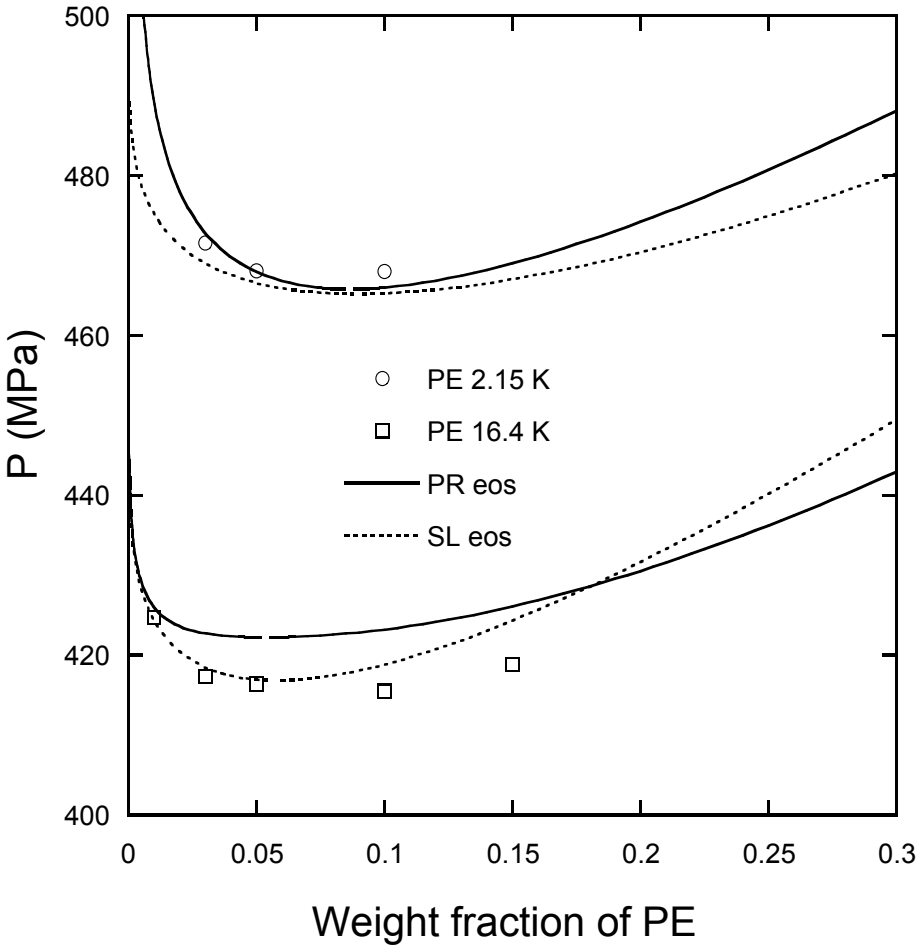

Figure B- 22 Variation of demixing temperatures of PE solutions with polymer concentration and molecular weight at 5Mpa in n-pentane .

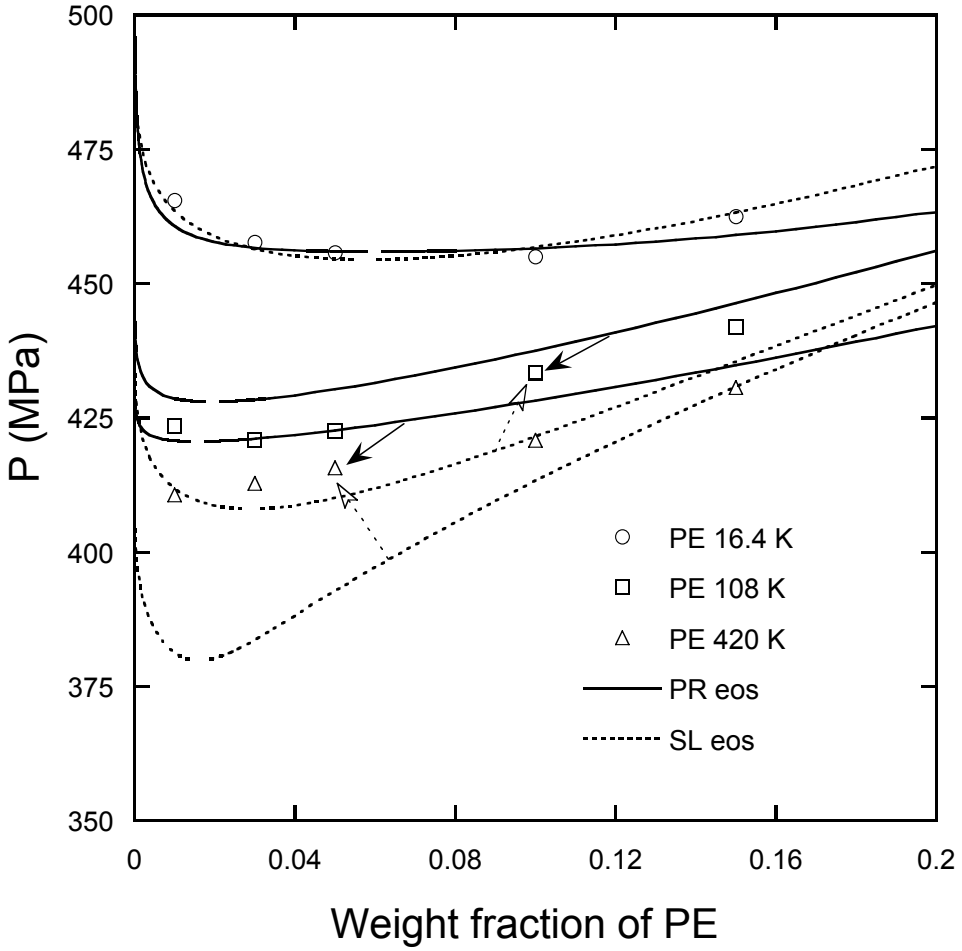

Figure B- 23 Variation of demixing temperatures of PE solutions with polymer concentration and molecular weight at 10Mpa in n-pentane.

REFERENCES

Adamsky, F. A.; Beckman, E. J. *Macromolecules*, 27(1), 312, 1994.

Akki, R. *Morphological Implications of Phase Transitions in Polymer Solutions: Inferences from Polyacrylonitrile-based solutions*, Ph.D. Dissertation, Georgia Institute of Technology, Atlanta, GA, 1996.

Alder, B.J.; Young, D.A.; Mark, M.A. *Journal of Chemical Physics*, 56, 3013, 1972.

Anon, *Modern Plastics*, 72(1), 63, 1995.

Armeniades, C.D.; Baer, E. *Introduction to Polymer Science and Technology:* Chapter 6; Kaufman and Falcetta, Eds.; John Wiley and Sons: New York, 1977.

Barker, J.A.; Henderson, D. *Journal of Chemical Physics,* 47,4714,1967.

Barton, S.W.; Dris, G. *Polym. Material Science and Engineering,* 74, 226,1996.

Bawn, C. E. H.; Freeman, R. F. J.; Kamaliddin, A. R. *Transactions of the Faraday Society*, 46, 677, 1950.

Bawn, C. E. H.; Wajid, M. A. *Transactions of the Faraday Society,* 52, 1658, 1956.

Beckman, E.J.; Hoefling, T.A.; Enick, R.M. *Journal of Physical Chemistry* 95(19), 7127, 1991.

Bell, R. J.*, 'Introductory Fourier Transform Spectroscopy'*, Academic Press, New York, 1972.

Belopolskaya, T. V.; Trapeznikova, O. N. *Vysokomol Soedin* ,13, 1119, 1971.

Berens, A.R.; Huvard, G.S.; Korsmeyer, R.W.; Kunig, F.W. *Journal of Applied Polymer Science*, 46(2), 231, 1992.

Bertucco A.; Mio, C. *Fluid Phase Equilibria* **,**117(1-2), 18, 1996.

Booth, C.; Devoy, C.J. *Polymer*, 12(5), 311, 1971.

Briscoe, B.J.; Thomas, P.S. *Tribology Transactions.* 38(2), 382, 1995.

Chapman, W. G.; Gubbins, K. E.; Jackson, G.; Radosz, M. *Industrial and Engineering Chemistry Reearch* 29(8), 1709,1990.

Chapman, B. R.; Gochanour, C.R.; Paulaitis, M.E. *Macromolecules*, 29, 5635, 1996.

Chee, C. K. *Materials World,* 5(11), 658, 1997.

Chen, S.J.; Radosz, M. *Macromolecules*, 25,3089, 1992.

Chiou, J.S.; Barlow, J.W.; Paul, D.R. *Journal of Applied. Polymer Science,* 30, 2633, 1985.

Clark, M. R.; DeSimone, J. M. *Macromolecules* ,28, 3002,1995.

Coleman, M. M.; Pehlert, G. J.; Yang X.; Stallman J.B.; Painter, P.C. *Macromolecules*, 37(21), 4753, 1996.

Cooper, A. I.; Kazarian, S. G.; Poliakoff, M. *Chemical Physics Letters* 206, 175,1993.

Condo, P.D.; Johnston, K.P. *Macromolecule*s, 25: 6730,1992.

Daneshvar, M.; Gulari, E. *ACS Symposium Series 406*, ed. By Johnston K.P.; Penninger J.M.L., chapter 6, 1989.

Danner, R. P.; Daubert, T. E. *Physical and Thermodynamic Properties of Pure Compounds: Data Compilation*, Hemisphere Publishing Corp., New York, NY,1990.

Dee, G.T.; Walsh, D.J. *Macromolecules*, v 21, 811,1988.

DeSimone, J.M.; Zihibin, G.; Elsbernd, C.S. *Science*, 257,945, 1992.

DeSimone, J.M.; Maury, E.E.; Combes, J.R.; Menceloglu, Y.Z.; McClain, J.B.; Romack, T.J. *Science*,265, 356, 1994.

DeSimone, J.M.; Adamsky F.A. *Macromolecules*, 28,912, 1995.

Dobrowolski, J. C.; Jamroz, M. H. *Journal of Moecular Structures* ,275, 211, 1992.

Eichinger, B.E.; Flory, P.J. *Macromolecules*, 5,1285, 1968.

Ehrlich, P. *Journal Polymer Science*, Part A, v 3, 131, 1965.

Finck, U.;Wohlfarth, C.;Heuer, T. *Berlin. Bunsen-Gas,Physical Chemistry,* 96,179, 1992.

Fleming, G. K.; Koros, W. J. *Macromolecules* 19(8), 2285, 1986.

Fleyfel, F.; Devlin, J. P. *Journal of Physical Chemistry* ,95, 3811, 1991.

Flory, P.J. *Journal of Chemical Physics*, 10,51,1942.

Flory, P. J.; Orwoll, R. A.; Vrij, A. *Journal of American Chemical Society*, 86, 3507,1964.

Flory, P. J.; Hoecker, H. *Transactions of the Faraday Society*, 67(8), 2258, 1971.

Fowkes, F. M.; Tischler, D. O.; Wolfe, J. A.; Lannigan, L. A.; Ademu-John, C. M.; Halliwell, M. J. *Journal of Polymer Science, Part A: Polymer Chemistry*, *22*, 547, 1984.

Fredenslund, A.; Jones, R. L.; Prausnitz, J.M. *AICHE Journal*, 21,1086, 1975.

Frushour, B. Private Communications, Monsanto Company, 1997.

George, S.; Nair, P.D. *Journal of Applied Polymer Science* 73, 10,1949, 1999.

Goel, S.K.; Beckman E. J. *Polymer*, 33, 3502, 1992.

Goel, S.K.; Beckman E. J. *Polymer*, 34, 1410, 1993.

Gregg, C.J.; Stein, F. P.; Radosz, M. *Macromolecules,* 27, 4972, 1994.

Guggenheim, E.A. *Mixtures*, Clarendon Press, Oxford, 1952.

Gupta, R.B.; Brinkley, R.L. *AICHE Journal,* 44, 1, 207, 1998.

Hasch, B.M.; Lee, S-H.; McHugh, M.A.; Watkins, J.J.;Krukonis, V.J. *Polymer*, 34,2554, 1993.

Hasch, B. M.; McHugh, M. A. *Journal of Polymer Science, Part B: Polymer Physics*, 33(4), 715, 1995.

Hasch, B. M.; Lee, S-H.; McHugh, M. A. *Journal of Applied Polymer Science* 59(7), 1107, 1996.

Havriliak, S.; Roman, N. *Polymer* , 7, 387, 1966.

Hildebrand, J. H.; Scott, R. L. *The Solubility of Nonelectrolytes*, Reinhold, NY, 1950.

Hildebrand, J.H.; Prausnitz, J.M.; Scott, R.L. *Regular and Related Solutions*, Van Nostrand Reinhold Company, New York, 1970.

Hirose, T.; Mizoguchi, K.; Kamiya, Y. *Journal of Polymer Science, Part B: Polymer Physics*., 24, 2197, 1986.

Holtz, J.H.; Asher, S.A. *Nature*, 389, 829, 1997.

Huang, S.H.; Radosz, M. *Industrial Engineering and Chemistry Research*, 29, 2284, 1990.

Huggins, M.L. *Journal of Physical Chemistry* ,9, 440, 1941.

Hyatt, J.A. *Journal of Organic Chemistry,* 49,5097, 1984.

Irani, C.A.; Cozewith, J. *Journal of Applied Polymer Science*, 31, 1879, 1986.

Iwai, Y.; Arai, Y. *Journal of Japanese Petroleum Institute*, 34,416, 1991.

Jessop, P. G.; Ikariya, T.; Noyori, R. *Chemical Reviews* ,95, 259,1995.

Joesten, M.D.; Schaad, L. J. *Hydrogen Bonding*, Marcel Dekker, NY, 1974.

Kalospiros, N.S.; Tassios, D.P. *Industrial Engineering and Chemistry Research* 34, 2117, 1995.

Kamiya, Y.; Mizoguchi, K.; Terada, K.; Fujiwara Y. ; Wang, J. S-. *Macromolecules,* 31,472,1998.

Kato, S.; Tsujita, T.; Yoshimizu, H.; Kinoshita, T.; Higgins, J.S. *Polymer,* 38,2807, 1997.

Kazarian, S. G.; Jobling, M.; Poliakoff, M. *Mendeleev Communications*, 148,1993.

Kazarian, S.G.; Vincent, M. F.; Bright, F. V.; Liotta, C. L.; Eckert, C. A. *Journal of the American Chemical Society* 118, 1729, 1996.

Kazarian, S.G.; Vincent, M.F.; Eckert, C.A. *Review of Scientific Instruments*, 67, 1586, 1996.

Kiran, E.; Zhuang, W.; Sen, Y.L. *Journal of Applied. Polymer Science,* 47, 895, 1993.

Kiran, E.; Saraf, P.; Sen, Y.L. *International Journal of Thermophysics,* Vol. 10, No.2,437-446, 1989.

Kontogeorgis, M.G.; Fredenslund, A.; Economou, I.G.; Tassios, D.P. *AIChE Journal* **,**40, 1711, 1994.

Krukonis, V.J., *Journal of Polymer News*, 11, 7, 1985.

Kuenen, J.P.; Robson, W.G. *Philosophy Magazine, 5th ser.* V48, 180,1899.

Langer, R. *Polymer and Material Science Engineering*, 66, 232, 1992.

Liau, I.S.; McHugh, M.A. "High Pressure Solid Polymer-Supercritical Fluid Phase Behavior", *Supercritical Fluid Technology*, Elsevier Science Publishers, Amsterdam, 1985.

Lee, J.; Prochazka, F.; Urry, D.W.; Macosko, C.W., *American Chemical Society Polymer Preparation. Division Polymer Chemistry.* ACS, 40, 2,214,1999.

Lee, J.W.; Park, M.W.; Bae, H.K. *Fluid Phase Equilibria*, 173, 277, 2000.

Lee, M.; Tzoganakis, C.; Park, C.B. *Polymer Science and Engineering* 38,1112, 1998.

Life, D.R.(ed.), Handbook of Chemistry and Physics, 71st ed., CRC press: Baco Raton, Chapter 6. 48, 1990.

Liphard, K.G.; Schneider, G.M. *Journal of Chemical Thermodynamics,* v 7, 805, 1975.

Magoulas, K.; Tassios, D. *Fluid Phase Equilibria*, 56, 119, 1990.

Mark, H.F. *Encyclopedia of Polymer Science and Technology, Volumes 5-8, Part 2*, Wiley and Sons Ltd., 2003.

Mathias, P.M.; Copeman, T.W. *Fluid Phase Equilibria*, 13, 91, 1983.

Mawson, S.; Johnston, K. P.; Combes, J. R.; DeSimone, J. M. *Macromolecules*, 28, 3182,1995.

McClellan A.K.; McHugh, M.A. *Journal of Polymer Science and Engineering*, v 25, 1088, 1985.

McHugh, M.A.;Guckes, T.L. *Macromolecules*, v 18, 674, 1985.

McHugh, M. A.;Kiszka, M. B.; Meilchen, M. A.*Journal of Applied Polymer Science*, 36(3), 583, 1988.

McHugh, M. A.; Krukonis, V. J. *Encyclopedia of Polymer Science and Engineering,* John Wiley & Sons, Inc., New York, 1989.

McHugh, M. A; Krukonis, V. J. *Supercritical Fluid Extraction: Principles and Practice,* 2nd edition, Butterworths-Heinemann, Boston, 1994.

McHugh, M.A.; Rindfleisch, F.; DiNoia, T.P. *Journal of Physical Chemistry,* 100, 15581, 1996.

McHugh, M. A.; Lora, M.; Rindfleisch, F. J*ournal of Applied Polymer Science*, 73(10), 1979, 1999.

Meilchen, M. A.; Hasch, B. M.; McHugh, M. A., *Macromolecules*, 24, 4874,1991.

Mokdad, A.; Dubault, A.; Monnerie, L. *Journal of Polymer Scence., Part B: Polymer Physics*, 34, 2723, 1996.

Moore, W.R.; Russel, J. *Journal of Polymer Science*, 8 ,63, 1955.

Moore, W.R.; Tidswell, *B.M. Makromolekuler Chemie,* 81, 1, 1965.

Moore, W.R. *Journal of Polymer Science, Part C*, 16,571, 1967.

Nagai, H. *Journal of Applied Polymer Science* 7, 1697,1963.

Nandel, F. S.; Jain, D. V. S. *Indian Journal of Chemistry* ,23A, 543, 1984.

Ng, H.J.; Robinson, D. B. *Journal of Chemical and Engineering Data*, 23(4), 325, 1978.

Nxumalo, L. M.; Ford, T. A.; Cox, A. *J. Theoretical Chemistry* 307, 153, 1994.

Oishi, T.; Prausnitz, J.M.; *Industrial Engineering Chemistry Process Design and Development*, 17,333, 1978.

Orbey N.; Sandler, S.I. *AIChE Journal*, 40, pp. 1203, 1994.

Ozhono, M., Iwai Y; Arai, Y. *Journal of Chemical Engineering Japan*, 17, 550, 1984.

Painter, P.C.; Park, Y.; Coleman, M.M. *Macromolecules*, 22, 2, 570, 1989.

Painter, P.C.; Graf, J.; Coleman, M.M. *Macromolecules*, 92, 10, 6166, 1990.

Painter, P.C.; Hu, Y.; Coleman, M.M. *Macromolecule*s, 32, 6, 2055, 1999.

Panayiotou, C.P.; Vera, J.H. *Polymer Journal*, 14, 681, 1982.

Panayiotou, C.P.; Sanchez, I. C. .*Journal of Physical Chemistry*, 95, 10090, 1991.

Patel, N.C.; Teja ,A.S. *Chemical Engineering Science*, v.37, N 3, p.463-473, 1982.

Paulaitis, M.E.; Mackay M.E. *Industrial and. Engineering Chemistry. Fundamentals.* Vol 18, No.2, 149,1979.

Peng, D.Y.; Robinson, D.B. *Industrial and. Engineering Chemistry. Fundamentals* 15,59, 1976.

Pernecker, T.; Kennedy, J. P. *Polymer Bulletin*, 32, 537, 1994.

Poliakoff, M.; Howdle, S. M.; Kazarian, S. G. *Angewante. Chemie, Internation Edition English* 34, 1275, 1995.

Prausnitz, J.M.; Shair, F.H., *AICHE Journal*, 7,682,1961.

Prausnitz, J.M. *Molecular Thermodynamics of Fluid-Phase Equilibria*, Prentice-Hall, Englewood Cliffs, N.J., 1969.

Prausnitz, J.M.; Lichtenthaler, R.N.; deAzevedo, E.G., *Molecular Thermodynamics of Fluid-Phase Equilibria*, 2nd ed., Prentice-Hall, Englewood Cliffs, N.J.,1986.

Prausnitz, J.M.; Lichtenthaler, R.N.; deAzevedo, E.G., *Molecular Thermodynamics of Fluid-Phase Equilibria*, 3rd ed., Prentice-Hall, Englewood Cliffs, N.J.,1999.

Prigogine, I. "The molecular theory of Solutions", Interscience, New York, 1957.

Quinn, R.; Appleby, J. B.; Pez, G. P. *Journal of American Chemical Society.* ,117, 329, 1995.

Rasmussen, P.; Holten-Andersen, J.; Fredenslund, A. *Industrial Engineering Chemistry and Research,* 26, 1382, 1987.

Rodgers, P.A. *Journal of Applied Polymer Science* v48, n 6, 1061, 1993.

Rowlinson, J.A.; Swinton, F. L. *Liquids and Liquid Mixtures,* 3rd edition, Ch. 6, Boston: Butterworth and Co. Ltd., 1982.

Rudolf, B.;Kressler, J.;Shinomai, K.;Ougizawa, T.; Inoue, T. *Acta Polymer* ,46,312,1995.

Sanchez, I. C.; Lacombe, R.H. *Journal of Physical Chemistry*, 80, 2352, 1976.

Sanchez, I.C.; Lacombe, R.H. *Journal of .Polymer Science.Polymer Letters Edition,* v 15, 71,1977.

Sato, Y.; Yurugi, M.; Fujiwara, K.; Takishima, S.; Masuoka, H. *Fluid Phase Equilibria,* 125, 129, 1996.

Schneider, G.M. *Advanced Chemical Physics*, v 17, 1, 1970.

Schreinemakers, F.A.H*., Z.Physical Chemistry.(Leipzig),* 23, 417, 1897.

Schweizer, K.S.; Curro, J.G. *Advanced Polymer Science*, 113, 319, 1994.

Scott, R.L.; van Konynenburg, P.B. *Discussions of Faraday Society* v 49, 87, 1970.

Shah, V. M.; Hardy, B. J.; Stern, S. A. *Journal of Polymer Science, Part B: Polymer Physics* ,31, 313, 1993.

Shenoy, S.L.; Painter, P. C.; Coleman, M.M. *Polyme. Preparation Division Polymer Chemistry American Chemical Society*, 31, 1, 539, 1990.

Shieh, Y. T.; Su, J. H.; Mannivannan, G.; Lee, P. H. C.; Sawan, S. P.; Spall, W. D. *Journal of Applied Polymer Science*, 59, 695, 1996.

Shild, H.G.; Tirrel, D.A. *Journal Physical Chemistry,* 94, 4352, 1990.

Shild, H.G.; Muthukumar, M.; Tirrel, D.A. *Macromolecules*, 24,948, 1991.

Shild, H.G. *Progressive Polymer Science,* 17,163, 1992.

Shim, J. J.; Johnston, K. P. *AIChE Journal* 35, 1097,1989.

Sigman, M.E.; Lindley, S.M.; Leffler, J.E. *Journal of .American Chemical Society*, 107, 1471, 1985.

Staverman, A. J.; *Rec, Trav. Chim. Pays-Bas*., 69,163, 1950.

Street, W.B. *Chemical Engineering at Supercritical Fluid Conditions,* ed. Paulaitis, M.E.; Penninger, J.M.L.; Gray, R.D.; Davidson, P. Ann Arbor, MI: An Arbor Science, 1983.

Sukhadia, T. *Prediction of phase equilibrium in solution: a associative reformulation of thermodynamic theories of solutions,* Ph.D. Dissertation, Georgia Institute of Technology, Atlanta, GA, 1999.

Sun, S. F. *Physical Chemistry of Macromolecules*; John Wiley and Sons: New York, 1994.

Tait, P. G. "*Physics and Chemistry of the Voyage HMS Challenger*", Vol II, Part IV., S.P.L.XI., 1888.

Todd, D.B.; Elgin, J.C. *AICHE Journal,* v 1, 20, 1955.

Tuminello, W. H.; Dee, G. T.; McHugh, M. A. *Macromolecules*, 28, 1506,1995.

Van Pelt, A.; Peters, C. J.; De Swaan Arons, J. *Journal of Chemical Physics*, 95(10), 7569, 1991.

Variankaval, N. *Structure and thermodynamics of associating solutions : prediction of phase equilibrium*, Ph.D. Dissertation, Georgia Institute of Technology, Atlanta, GA, 2001.

Veystman, B. A. *Journal of Physical Chemistry*, 94, 8499, 1990.

Vieth, W. R. *Diffusion In and Through Polymers, Principles and Applications*; Hanser Werlag: Munich, 1991.

Vincent, M. F.; Kazarian, S. G.; Eckert, C. A. *AIChE Journal* ,40, 1838,1997.

Wang, W.C.V.; Kramer, E.J.; Sachse, W.H. *Journal of Polymer Science. Part B: Polymer Physics*, 20, 1371, 1982.

Webb, K. F. *Formation of Electrically Conducting Polymer Blends Using Supercritical Carbon Dioxide*, M.S. Thesis, Georgia Institute of Technology, 1998.

Wen, H.; Elbro, H.S.; Alessi, P. Polymer Solution Data Collection Part I: Vapor-Liquid equilibrium, DECHEMA Chemistry data series, DECHEMA, Frankfurt, 1991.

Wertheim, M.S.; *Journal of Statistical Physics*, 42, 19, 1984.

West, B.L. "*Partioning of Solutes between Supercritical CO_2 and Polymer Phases*", PhD Thesis, Georgia Institute of Technology, 1997.

Wissinger, R. G.; Paulaitis, M. E. *Journal Polymer Science, Part B:Polymer Physics*, 25, 2497, 1987.

Wissinger, R. G.; Paulaitis, M. E. *Journal Polymer Science, Part B:Polymer Physics* 29, 631, 1991.

Wong, D.S.H.;Sandler, S.I. *AICHE Journal,* 38, 671,1992.

Xiong, Y.; Kiran, E. *Polymer* 35, 4408, 1994.

Xiong, Y.; Kiran, E. *Journal of Applied Polymer Science* ,53 , 1179, 1994.

Xiong, Y.; Kiran, E. *Polymer*, 36, 4817, 1995.

Yilgor, I.; McGrath, J.E.; Krukonis, V.J. *Journal of Polymer Bulletin.,* 12, 499, 1984.

Yiling, T.; Michelberger, T.; Frank, E.U. *Journal of Chemical Thermodynamics* v 23, 105, 1991.

Zeman, L.; Patterson, D. *Journal of Physical Chemistry*, 76, 1214, 1972.

Zerda, T.W.; Song, X; Jonas, J. *Journal of Applied Spectroscopy,* 40,1194 ,1986.

Zhang, Y.; Gangwani, K. K.; Lemert, R. M. *Journal of Supercritical Fluids*, 11, 115, 1997.

Zhong C.; Masuoka, H. *Fluid Phase Equilibria,* 123, 59, 1996.

Zhong, C.; Masuoka, H. *Fluid Phase Equilibria*, 144(1-2), 49, 1998.

VITA

Ibrahim Ali Ozkan was born in Adana, Turkey in 1976. He graduated from Tarsus American High School (formerly St. Paul's Institute) in Spring 1994, and received his bachelor in Chemical Engineering from Bosphorus University in Spring 1998. He started his graduate career in the fall of that year in University of Hartford where he received his Masters of Science in Environmental Engineering and also his MBA degree through the dual-degree program in Summer 2000. Then he moved to Atlanta and started his doctoral research under the direction of Dr. Amyn S. Teja at Georgia Institute of Technology.